

เซ็นเซอร์ทางเคมีที่มีควิโนนและกรดโพรนิกเป็นองค์ประกอบและสมบัติการเกิดสารประกอบ
เชิงซ้อน



นางสาวเมธินี จามกระโทก

ศูนย์วิทยทรัพยากร

วิทยานิพนธ์นี้เป็นส่วนหนึ่งของการศึกษาตามหลักสูตรปริญญาวิทยาศาสตรดุษฎีบัณฑิต

สาขาวิชาเคมี ภาควิชาเคมี

คณะวิทยาศาสตร์ จุฬาลงกรณ์มหาวิทยาลัย

ปีการศึกษา 2552

ลิขสิทธิ์ของจุฬาลงกรณ์มหาวิทยาลัย

CHEMOSENSORS BASED ON QUINONE AND BORONIC ACID
AND THEIR COMPLEXATION PROPERTIES



Miss Matinee Jamkratoke

ศูนย์วิทยทรัพยากร

A Dissertation Submitted in Partial Fulfillment of the Requirements
for the Degree of Doctor of Philosophy Program in Chemistry
Department of Chemistry
Faculty of Science
Chulalongkorn University
Academic Year 2009

Copyright of Chulalongkorn University

Thesis Title CHEMOSENSORS BASED ON QUINONE AND BORONIC
ACID AND THEIR COMPLEXATION PROPERTIES
By Miss Matinee Jamkratoke
Field of Study Chemistry
Thesis Advisor Associate Professor Thawatchai Tuntulani, Ph. D.
Thesis Co-Advisor Assistant Professor Boosayarat Tomapatanaget, Ph. D.

Accepted by the Faculty of Science, Chulalongkorn University in Partial
Fulfillment of the Requirements for the Doctoral Degree

S. Hannongbua
..... Dean of the Faculty of Science
(Professor Supot Hannongbua, Dr.rer.nat)

THESIS COMMITTEE

Sirirat Kokpol
..... Chairman
(Associate Professor Sirirat Kokpol, Ph.D.)

T. Tuntulani
..... Thesis Advisor
(Associate Professor Thawatchai Tuntulani, Ph.D.)

B. Tomapatanaget
..... Thesis Co-Advisor
(Assistant Professor Boosayarat Tomapatanaget, Ph.D.)

N. Muangsin
..... Examiner
(Associate Professor Nongnuj Muangsin, Ph.D.)

Mongkol Sukwattanasitt
..... Examiner
(Associate Professor Mongkol Sukwattanasitt, Ph.D.)

Tienthong Thongpanchang
..... External Examiner
(Assistant Professor Tienthong Thongpanchang, Ph.D.)

เมธีณี จามกระโทก : เซ็นเซอร์ทางเคมีที่มีควิโนนและกรดโบโรนิกเป็นองค์ประกอบและสมบัติการเกิดสารประกอบเชิงซ้อน. (CHEMOSENSORS BASED ON QUINONE AND BORONIC ACID AND THEIR COMPLEXATION PROPERTIES) อ.ที่ปรึกษาวิทยานิพนธ์หลัก : รศ. ดร. ธวัชชัย ต้นจตุลानी, อ.ที่ปรึกษาวิทยานิพนธ์ร่วม : ผศ. ดร. บุญยรัตน์ ธรรมพัฒน์กิจ, 164 หน้า.

สังเคราะห์เซ็นเซอร์ชนิด เอ-ดี-เอ ที่เป็นอนุพันธ์ของเนฟโทควิโนนอิมิดาโซลและกรดโบโรนิก 6 ชนิด ได้แก่ อนุพันธ์โปรโตรเนตเตด *o*-HNQB *m*-HNQB และ *p*-HNQB และอนุพันธ์เมทิลเลเตด *o*-MNQB *m*-MNQB และ *p*-MNQB แล้วศึกษาสมบัติการเกิดสารเชิงซ้อนกับแอนไอออนชนิดต่างๆ โดยใช้เทคนิคฟลูออเรสเซนซ์สเปกโตรโฟโตเมทรี พบว่าในเซ็นเซอร์ที่เป็นอนุพันธ์โปรโตรเนตเตดทุกชนิดจะเกิดการลดลงของสัญญาณฟลูออเรสเซนซ์ที่ $\lambda_{\text{emiss}} = 554$ นาโนเมตร จากการสูญเสียโปรตรอนเมื่อเติมแอนไอออนที่เป็นเบส เช่น F^- AcO^- และ CN^- การลดลงของสัญญาณฟลูออเรสเซนซ์นี้เกิดผ่านกระบวนการย้อนกลับของการถ่ายโอนอิเล็กตรอนชักนำโดยแสง (PET) ศึกษาสมบัติการจับกับแอนไอออนของอนุพันธ์เมทิลเลเตด ในตัวทำละลาย 4 ระบบ ได้แก่ ไดเมทิลซัลฟอกไซด์ สารละลายผสมของน้ำกับไดเมทิลซัลฟอกไซด์ (1:1) สารละลายผสมของบัฟเฟอร์ HEPES ที่ pH 7.4 กับไดเมทิลซัลฟอกไซด์ (1:1) และซีเทปไมเซลล์ พบว่าจะเกิดอิมิชันแบนด์ใหม่ที่ 460 นาโนเมตร เมื่อเติม CN^- F^- และ OH^- ซึ่งจะเกี่ยวข้องกับการเปลี่ยนแปลงของประสิทธิภาพการเกิดการถ่ายโอนประจุภายใน โมเลกุลอันเกิดจากการเปลี่ยนแปลงไฮบริดไดส์ของโบรอนจาก sp^2 เป็น sp^3 โดยในระบบไดเมทิลซัลฟอกไซด์ เซ็นเซอร์ *p*-MNQB จะตอบสนองต่อ F^- ในขณะที่ในระบบเอเคเวียสเซ็นเซอร์ *m*-MNQB และ *p*-MNQB จะตอบสนองเฉพาะ CN^- ในระบบซีเทปไมเซลล์เซ็นเซอร์ *m*-MNQB และ *p*-MNQB จะแสดงลักษณะที่คิของการเป็นตัวตรวจวัดชนิดฟลูออเรสเซนซ์สำหรับไซยาไนด์ ในน้ำที่ความเข้มข้นระดับไมโครโมลาร์ในเชิงของความจำเพาะเจาะจงและขีดต่ำสุดของการตรวจวัด

สังเคราะห์เซ็นเซอร์ที่เป็นอนุพันธ์ของแอนทราควิโนนอิมิดาโซลและกรดโบโรนิก 2 ชนิด คือ HAQB และ MAQB แล้วศึกษาสมบัติการจับกับน้ำตาลโมโนซัคคาไรด์โดยใช้เทคนิคฟลูออเรสเซนซ์สเปกโตรโฟโตเมทรีพบว่า ที่ pH 8.5 แนวโน้มของการจับกับน้ำตาลโมโนซัคคาไรด์ของเซ็นเซอร์ทั้งสอง คือ ดี-ฟรุคโตส > ดี-กาแลคโตส > ดี-แมนโนส > ดี-กลูโคส

ภาควิชา.....เคมี..... ลายมือชื่อนิสิต.....เมธีณี จามกระโทก
สาขาวิชา.....เคมี..... ลายมือชื่อ อ.ที่ปรึกษาวิทยานิพนธ์หลัก.....ศ.ดร.ศ.ดร.ต้นจตุลानी
ปีการศึกษา.....2552..... ลายมือชื่อ อ.ที่ปรึกษาวิทยานิพนธ์ร่วม.....บุญยรัตน์ ธรรมพัฒน์

4873888923 : MAJOR CHEMISTRY

KEYWORDS: BORONIC ACID / QUINONE IMIDAZOLE / CHEMOSENSOR

MATINEE JAMKRATOKE : CHEMOSENSORS BASED ON QUINONE AND BORONIC ACID AND THEIR COMPLEXATION PROPERTIES. THESIS

ADVISOR : ASSOC. PROF. THAWATCHAI TUNTULANI, Ph. D., THESIS CO-

ADVISOR : ASST. PROF BOOSAYARAT TOMAPATANAGET, Ph. D., 164 pp.

Six A-D-A sensors containing naphthoquinone imidazole boronic acid were synthesized including protonated derivatives, *o*-HNQB, *m*-HNQB and *p*-HNQB and methylated derivatives, *o*-MNQB, *m*-MNQB and *p*-MNQB. Complexation properties of all sensors were studied by fluorescence spectrophotometry. All protonated sensors showed quenching of fluorescence intensity at $\lambda_{\text{emiss}} = 554 \text{ nm}$ due to an inverse PET character upon the deprotonation by basic anions such as F^- , OAC^- and CN^- . Anion binding properties of methylated sensors were carried out in four solvent systems: DMSO, DMSO:H₂O (1:1), DMSO:HEPES pH 7.4 (1:1) and CTAB micelles. The appearance of a new emission band at 460 nm was observed in the presence of F^- , CN^- and OH^- corresponding to the disturbance of an ICT efficiency of the sensor upon changes in hybridization changes at the boron center from sp^2 to sp^3 . In the DMSO system, *p*-MNQB preferred binding F^- whereas in aqueous solution *m*-MNQB and *p*-MNQB showed the selectivity toward CN^- . In the CTAB micellar system, *m*-MNQB and *p*-MNQB showed promising characteristics of fluorescence probes in term of selectivity and limit of detection for micromolar cyanide detection in water.

Two anthraquinone imidazole boronic based sensors, HAQB and MAQB were synthesized. The saccharide binding properties were studied using fluorescence spectrophotometry. At pH 8.5, affinity trends of both sensors were D-fructose > D-galactose > D-mannose > D-glucose.

Department : Chemistry

Field of Study : Chemistry

Academic Year : 2009

Student's Signature : *Matinee Jamkratoke*

Advisor's Signature : *ท. ทนต์ลณี*

Co-Advisor's Signature : *B. Boosayarat*

ACKNOWLEDGEMENTS

I wish to express my deepest appreciation to my advisor Assoc. Prof. Dr. Thawatchai Tuntulani and Asst. Prof. Dr. Boosayarat Tomapatanaget for their guidance, kindnesses, suggestions and supports throughout my Ph. D. career. I would like to thank Assoc. Prof. Dr. Vithaya Ruangpornvitsuti for assistance in computational studies. In addition, I wish to thank Assoc. Prof. Dr. Sirirat Kokpol, Assoc. Prof. Dr. Mongkol Sukwattanasinitt, Assoc. Prof. Dr. Nongnuj Muangsin and Asst. Prof. Dr. Tienthong Thongpanchang for their valuable comments and suggestions as thesis committee and thesis examiner. Furthermore, I wish to thank Prof. Dr. Bradley D. Smith at University of Notre Dame who gave me a great opportunity to join his group.

I would like to acknowledge the financial support from the Thailand Research Fund and the Commission on Higher Education through the Royal Golden Jubilee Ph.D. Program (Grant No. PHD/0049/2550). I wish to thank many organizations for supporting namely, the National Nanotechnology Center and the Center for Petroleum, Petrochemicals, and Advanced Materials. In addition, this accomplishment could not occur without the support from Chulalongkorn University and Burapha University. Special thanks are due to all members of the Supramolecular Chemistry Research Unit at Department of Chemistry, Chulalongkorn University for their encouragement and supports.

Finally, I would like to express my deepest gratitude to my parent and my sisters, for their love, care, kindness, encouragement and other supports throughout my life.

ศูนย์วิจัยทรัพยากร
จุฬาลงกรณ์มหาวิทยาลัย

CONTENTS

	Page
ABSTRACT (IN THAI)	iv
ABSTRACT (IN ENGLISH)	v
ACKNOWLEDGEMENTS	vi
CONTENTS	vii
LIST OF TABLES	xiii
LIST OF FIGURES	xv
LIST OF SCHEMES	xxvi
LIST OF ABBREVIATIONS	xxvii

CHAPTER I INTRODUCTION

1.1 Supramoleclar chemistry and sensing applications.....	1
1.2 Designing concepts for anion sensors.....	2
1.3 Literature review for cyanide sensors.....	3
1.3.1 Non-covalent based cyanide sensors.....	4
1.3.2 Cyanide sensors using displacement methods.....	6
1.3.3 Chemodosimeters for cyanide.....	6
1.3.3.1 C-C bond formation based sensors.....	7
1.3.3.2 C-S bond formation based sensors.....	10
1.3.3.3 C-B bond formation based sensors.....	11
1.4 Literature reviews of boronic based sensors for saccharides and their derivatives.....	13
1.4.1 Fluorescence sensors for saccharide based on photoinduced electron transfer (PET).....	14
1.4.2 Fluorescence sensors for saccharide based on intramolecular charge transfer (ICT).....	16
1.5 Objective and scope of this dissertation	19

CHAPTER II EXPERIMENTAL

2.1 Synthesis of boronic based receptors.....	20
2.1.1 Analytical measurements and materials.....	20
2.1.2 Experimental procedure.....	21

2.1.2.1	Preparation of propane-1,3-dilyl-fomylboronate (1a-c).....	21
2.1.2.2	Preparation of 2,3-diaminonaphthalene-1,4-dione (3).....	22
2.1.2.3	Preparation of 2-(1,3,2-dioxaborinan-2-yl)phenyl - 1H-naphtho[2,3-d]imidazole-4,9-dione (4a-c)....	23
2.1.2.4	Preparation of (4,9-dioxo-4,9-dihydro-1H-naphtho [2,3-d]imidazol-2-yl)phenylboronic acid (<i>o</i> - HNQB , <i>m</i> - HNQB and <i>p</i> - HNQB).....	25
2.1.2.5	Preparation of 4-(1-methyl-4,9-dioxo-4,9-dihydro- 1H-naphtho[2,3-d]imidazol-2-yl) phenylboronic acid (<i>o</i> - MNQB , <i>m</i> - MNQB and <i>p</i> - MNQB).....	27
2.1.2.6	Preparation of 1-methyl-2-phenyl-1H-naphtho [2,3-d]imidazole-4,9-dione, 7b	29
2.1.2.7	Preparation 2-(4-(1,3,2-dioxaborinan-2-yl)phenyl) -3H-anthra[1,2-d]imidazole-6,11-dione, 8	30
2.1.2.8	Preparation 4-(6,11-dioxo-6,11-dihydro-3H-anthra [1,2-d]imidazol-2-yl)phenylboronic acid, HAQB ..	31
2.1.2.9	Preparation of 4-(3-methyl-6,11-dioxo-6,11-dihy dro-3H-anthra[1,2-d]imidazol-2-yl)phenyl boronic acid, MAQB	32
2.2	The complexation studies of the protonated and methylated naphthoquinone imidazole based sensors.....	33
2.2.1	The complexation studies of the protonated sensors, <i>o</i> - HNQB , <i>m</i> - HNQB and <i>p</i> - HNQB	33
2.2.1.1	The complexation studies of sensors using ¹ H-NMR techniques.....	33
2.2.1.2	The complexation studies of sensors using UV- Vis spectroscopic techniques.....	33
2.2.1.3	The complexation studies of the sensor using fluorescence titration experiments.....	34

2.2.2	The complexation studies of the methylated sensors, <i>o</i> -MNQB, <i>m</i> -MNQB and <i>p</i> -MNQB.....	35
2.2.2.1	The complexation studies of sensors using NMR techniques.....	35
2.2.2.2	The complexation studies using fluorescence spectrophotometry in DMSO.....	35
2.2.2.3	The complexation studies by fluorescence spectrophotometry mixture of 1:1; DMSO:H ₂ O and 1:1; DMSO: HEPES buffer pH 7.4.....	37
2.2.3	The cyanide complexation studies of the methylated sensors, <i>o</i> -MNQB, <i>m</i> -MNQB and <i>p</i> -MNQB in micellar systems using fluorescence spectrophotometry.....	38
2.2.3.1	Fluorescence measurements for the optimizing condition of the micellar system.....	38
2.2.3.2	Fluorescence measurement for screening test of anions in optimum condition of the micellar system.....	41
2.2.3.3	Fluorescence titration procedure of sensor with CN ⁻ in optimum condition of the micellar system..	41
2.3	The complexation studies of anthraquinone imidazole boronic acid based sensors, HAQB and MAQB with monosaccharides.....	43
2.3.1	The pH dependent experiments.....	43
2.3.2	The stoichiometric determination by Job's method.....	44
2.3.3	The complexation studies of sensors with sugars using fluorescence titration.....	45
2.4	Determinations of quantum yield	47

CHAPTER III RESULTS AND DISCUSSIONS

3.1	Design and synthesis of quinone boronic-based receptors.....	48
3.2	Design and synthesis of anthraquinone imidazole boronic acid based receptors HAQB and MAQB.....	55

	Page
3.3 Complexation properties of the protonated naphthoquinone sensors <i>o</i>-HNQB , <i>m</i>-HNQB and <i>p</i>-HNQB	59
3.3.1 Photophysical properties of the protonated sensors.....	59
3.3.2 The complexation studies of sensors <i>o</i>-HNQB , <i>m</i>-HNQB and <i>p</i>-HNQB with various anions using spectrophotometry	60
3.3.3 The complexation studies of sensors <i>o</i>-HNQB , <i>m</i>-HNQB and <i>p</i>-HNQB using ¹ H-NMR spectroscopy.....	65
3.3.4 Applications of sensors <i>o</i>-HNQB , <i>m</i>-HNQB and <i>p</i>-HNQB as a CN ⁻ naked eye sensor in DMSO:H ₂ O mixture.....	69
3.3.5 Applications of sensors <i>o</i>-HNQB , <i>m</i>-HNQB and <i>p</i>-HNQB as fluorescence anion sensors.....	72
3.4 The complexation studies of methylated naphthoquinone imidazole based sensors <i>o</i>-MNQB , <i>m</i>-MNQB and <i>p</i>-MNQB	73
3.4.1 Photophysical properties of the methylated sensors.....	73
3.4.2 The complexation studies of sensors, <i>o</i>-MNQB , <i>m</i>-MNQB and <i>p</i>-MNQB using fluorescence spectrometry.....	75
3.4.2.1 Complexation properties of sensors <i>o</i>-MNQB , <i>m</i>-MNQB and <i>p</i>-MNQB using fluorescence spectrophotometry in DMSO system.....	75
3.4.2.2 The complexation studies of sensors <i>o</i>-MNQB , <i>m</i>-MNQB and <i>p</i>-MNQB using fluorescence spectrophotometry in DMSO:H ₂ O system.....	77
3.4.2.3 The complexation studies of sensors, <i>o</i>-MNQB , <i>m</i>-MNQB and <i>p</i>-MNQB by fluorescence spectrophotometry in DMSO:H ₂ O system in the presence of HEPES as buffering reagent.....	81
3.4.3 The complexation studies of the sensors, <i>o</i>-MNQB , <i>m</i>-MNQB , and <i>p</i>-MNQB using fluorescence spectrophotometry in aqueous micellar systems.....	85

3.4.3.1	The micellar optimum condition for the cyanide complexation studies of the sensors <i>o</i>-MNQB , <i>m</i>-MNQB and <i>p</i>-MNQB by fluorescent spectrophotometry.....	85
3.4.3.2	Selectivity and sensitivity of the sensor in the optimal micellar system.....	90
3.4.3.3	The evaluations of stability constants for tricyano-substitution complexes of the sensors in optimum condition of the CTAB micellar system.....	92
3.4.3.4	Calculated structures of the methylated sensors and their <i>tri</i> -cyano adducts using density functions theory (DFT).....	97
3.4.3.5	Analytical applications of the sensor in the CTAB micellar system for micromolar cyanide detection in water.....	99
3.4.4	The electronic properties of the anionic adducts of the sensors.....	101
3.4.4.1	¹ H-NMR spectroscopy of fluoride and cyanide adducts of the sensors.....	101
3.4.4.2	¹⁹ F-NMR spectroscopy of fluoride adducts of sensors.....	103
3.4.4.3	Electrochemical studies of the sensors in the presence of cyanide in the mixture of DMSO:H ₂ O system.....	105
3.5	The sensing properties of the anthraquinone sensors towards monosaccharides.....	106
3.5.1	Photophysical properties of the anthraquinone sensors, HAQB and MAQB	107
3.5.2	The complexation studies of the anthraquinone sensors, HAQB and MAQB towards several monosaccharides using fluorescence spectrophotometry.....	108

3.5.3 The correlation of ionization state of the boron center and fluorescence properties of sensor MAQB	115
--	-----

CHAPTER IV CONCLUSIONS

4.1 Naphthoquinone imidazolidione boronic acid based fluorescence sensor for cyanide detection in water.....	119
4.2 Anthraquinone imidazolidione boronic acid based sensor for fluorescence saccharide detection.....	122
4.3 Suggestion for future works.....	123

REFERENCES	124
-------------------------	-----

APPENDIX	139
-----------------------	-----

VITAE	164
--------------------	-----


 ศูนย์วิทยทรัพยากร
 จุฬาลงกรณ์มหาวิทยาลัย

LIST OF TABLES

		Page
Table 2.1	Volume of the stock solution of CTAB (1.25×10^{-2} mol/L) and the final concentration of CTAB in 5.0 mL.....	39
Table 2.2	Volume of sensor (5×10^{-4} mol/L) and CTAB (1.25×10^{-2} mol/L) in the stock solution and the final concentration of sensor and CTAB in 5.0 mL of 1:4 ethanol:H ₂ O.....	40
Table 2.3	Volume of KCN stock solution (2.5×10^{-4} mol/L) and final concentration of CN ⁻ in 5.0 mL of 1:4 ethanol:H ₂ O.....	42
Table 2.4	Mole fraction and volume of sensor (5×10^{-5} mol/L) and saccharide stock solution (5×10^{-5} mol/L) for Job's plot method..	45
Table 2.5	Volume of the saccharide stock solution (0.25 mol/L) and the final concentration of saccharide in 5.0 mL.....	46
Table 3.1	Photophysical properties of the protonated sensors in DMSO.....	59
Table 3.2	Photophysical properties of methylated sensors in DMSO.....	74
Table 3.3	Overall stability constants for tri-substituted cyanide complex of <i>o</i> -MNQB, <i>m</i> -MNQB and <i>p</i> -MNQB in CTAB micellar condition (5×10^{-5} mol/L of sensors, 5×10^{-3} mol/L of CTAB in 1:4 ethanol:H ₂ O)	95
Table 3.4	NBO charges of segments of <i>o</i> -MNQB, <i>m</i> -MNQB and <i>p</i> -MNQB and of <i>o</i> -MNQB(CN) ₃ ⁻ , <i>m</i> -MNQB(CN) ₃ ⁻ and <i>p</i> -MNQB(CN) ₃ ⁻ derived from the B3LYP/6-31+G(d) computations.....	98
Table 3.5	Analytical characteristics of <i>m</i> -MNQB and <i>p</i> -MNQB sensors (5×10^{-5} mol/L of sensors, 5×10^{-3} mol/L of CTAB in 1:4 ethanol:H ₂ O)	99
Table 3.6	Photophysical properties of HAQB and MAQB in DMSO and EtOH.....	107
Table 3.7	Stability constants (K_s) of complexes HAQB and MAQB and different monosaccharides at pH 8.5 in 40% ethanol: sodium borate buffer and in 20% ethanol: sodium borate buffer, respectively.....	112

Table 3.8	Equilibrium percentages of <i>syn</i> -periplanar anomeric hydroxyl pair of furanose form in D ₂ O of simple monosaccharides	114
Table 3.9	Fluorescence enhancement values (FE) at 560 nm of MAQB in presence of 50 mM of various saccharides at pH 4-12.....	116
Table A.1.	Relative energies (ΔE_{rel}) of <i>o</i> - MNQB , <i>m</i> - MNQB and <i>p</i> - MNQB and of <i>o</i> - MNQB(CN)₃⁻ , <i>m</i> - MNQB(CN)₃⁻ and <i>p</i> - MNQB(CN)₃⁻ computed at the B3LYP/6-31+G(d) level.....	154
Table A.2	Cartesian coordinates (in angstrom) of <i>o</i> - MNQB	155
Table A.3	Cartesian coordinates (in angstrom) of <i>o</i> - MNQB(CN)₃⁻	156
Table A.4	Cartesian coordinates (in angstrom) of <i>m</i> - MNQB	158
Table A.5	Cartesian coordinates (in angstrom) of <i>m</i> - MNQB(CN)₃⁻	159
Table A.6	Cartesian coordinates (in angstrom) of <i>p</i> - MNQB	161
Table A.7	Cartesian coordinates (in angstrom) of <i>p</i> - MNQB (CN)₃⁻	162



 ศูนย์วิจัยทรัพยากร
 จุฬาลงกรณ์มหาวิทยาลัย

LIST OF FIGURES

		Page
Figure 1.1	Structures of hydrogen bonding based sensors 1 , 2 , and 3 for cyanide.....	4
Figure 1.2	Structures of ditopic sensors 4a , 4b , 5a and 5b	5
Figure 1.3	Structures of organic reagents for cyanide detection by Cu-displacement.....	6
Figure 1.4	Structures of C-C bond formation based sensors using intramolecular hydrogen bond stabilization concept and the plausible mechanism of signal moderation by cyanide binding of sensor 8	7
Figure 1.5	A) structures of C-C bond formation based sensors using carbonyl activation concept and b) the plausible mechanism of signal moderation by cyanide binding of sensor 11	8
Figure 1.6	Structure of sensor 12	8
Figure 1.7	Reaction of calix[4]pyrrole-based sensor 13 with cyanide.....	9
Figure 1.8	Mechanism of the reaction of sensor 14 with cyanide.....	9
Figure 1.9	Structures of sensors 15 and 16	10
Figure 1.10	Structures of sensor 17	10
Figure 1.11	Structures of subphthalocyanine dyes derivatives employed as cyanide probes.....	11
Figure 1.12	Structure of BODIPY-borane sensor 20 as a cyanide probe.....	11
Figure 1.13	Structures of the <i>para</i> sensos 21 and the <i>ortho</i> sensors 22	12
Figure 1.14	Structures of sensor 23 and mechanism of fluorescence enhancement of sensors upon cyanide binding.....	12
Figure 1.15	Illustration of anthracene-based photoinduced electron transfer system of sensor 24	15
Figure 1.16	Structure of the sensor 25 and esterification causing an increasing of fluorescence intensity.....	15
Figure 1.17	Structure of the sensor 26 and a thermodynamic structure of 1:1 complex of sensor 26 with furanose form of D-glucose.....	16

	Page
Figure 1.18 Structure of the sensor 27	16
Figure 1.19 Structure of ICT based sensor 28	17
Figure 1.20 Structures of ICT based sensors 29-32	18
Figure 1.21 Structures of fluorescence sensors 33-36 of Wang Lab.....	18
Figure 1.22 Structures of designed receptors based on quinone and boronic acid.	19
Figure 3.1 ¹ H-NMR (400 MHz, DMSO- <i>d</i> ₆) spectra of a) 4a , b) 4b and c) 4c	52
Figure 3.2 ¹ H-NMR spectra (400 MHz, DMSO- <i>d</i> ₆) of a) <i>o</i> - HNQB , b) <i>m</i> - HNQB and c) <i>p</i> - HNQB	53
Figure 3.3 ¹ H NMR spectra of (400 MHz, DMSO- <i>d</i> ₆) a) <i>o</i> - MNQB , b) <i>m</i> - MNQB and c) <i>p</i> - MNQB	54
Figure 3.4 ¹ H-NMR spectra (400 MHz) of a) 8 in CDCl ₃ , b) HANQB in DMSO- <i>d</i> ₆ and c) MAQB in DMSO- <i>d</i> ₆	57
Figure 3.5 ¹ H-H NOESY NMR of MAQB (500 MHz) in DMSO- <i>d</i> ₆	58
Figure 3.6 Absorption and emission spectra ($\lambda_{\text{excite}} = 344$ nm) of <i>o</i> - HNQB , <i>m</i> - HNQB (5×10^{-4} mol/L) and <i>p</i> - HNQB (2.5×10^{-4} mol/L) in DMSO.....	60
Figure 3.7 Color changes observed upon the addition of 30 equivalents anions into the DMSO solution of <i>p</i> - HNQB (3×10^{-4} mol/L).....	61
Figure 3.8 Absorption spectra of a) <i>o</i> - HNQB , b) <i>m</i> - HNQB and c) <i>p</i> - HNQB in the presence of 30 equivalents of various anions in DMSO (3×10^{-4} mol/L of sensors).....	61
Figure 3.9 Absorption spectra (left) and absorption response at 464 nm (right) toward various anions 0-7 equivalents (A/A_{∞}) of a) <i>o</i> - HNQB , b) <i>m</i> - HNQB and c) <i>p</i> - HNQB upon addition of CsF in DMSO (3×10^{-3} mol/L of sensor in DMSO)	63
Figure 3.10 Absorption spectra and color changes of control compound <i>p</i> - MNBQ in the presence of various anions in DMSO (3×10^{-4} mol/L of the sensor in DMSO)	64

Figure 3.11	¹ H-NMR spectra (400 MHz) of <i>o</i> - HNBQ upon the addition of 7.0 and 1.1 equiv. of tetrabutylammonium salt of basic anion, F ⁻ , AcO ⁻ , CN ⁻ , BzO ⁻ and OH ⁻ in DMSO (3x10 ⁻³ mol/L of sensors in DMSO- <i>d</i> ₆)	66
Figure 3.12	¹ H-NMR spectra (400 MHz) of <i>m</i> - HNBQ upon the addition of 7.0 and 1.1 equiv. of tetrabutylammonium salt of basic anions, F ⁻ , AcO ⁻ , CN ⁻ , BzO ⁻ and OH ⁻ in DMSO (3x10 ⁻³ mol/L of sensors in DMSO- <i>d</i> ₆)... ..	67
Figure 3.13	¹ H-NMR spectra (400 MHz) of <i>p</i> - HNBQ upon a addition of 7.0 and 1.1 equiv. of tetrabutylammonium salt of basic anions, F ⁻ , AcO ⁻ , CN ⁻ , BzO ⁻ and OH ⁻ in DMSO (3x10 ⁻³ mol/L of sensors in DMSO- <i>d</i> ₆)	68
Figure 3.14	UV-Vis spectra and color change of <i>p</i> - HNQB in presence of anions in 1:1 H ₂ O:DMSO (3x10 ⁻⁴ mol/L of <i>p</i> - HNQB in presence of 5.0 equiv. anions)	70
Figure 3.15	Fluorescence spectra of protonated receptors (left) at different aliquots of CsF (0-7 equivs) and fluorescence responses (I ₀ /I at 554 nm) (right) upon the addition of 0-7 equiv. of various anions; CsF, KAcO, KBzO and KCN in DMSO, a) <i>o</i> - HNBQ , b) <i>m</i> - HNBQ and c) <i>p</i> - HNBQ (3x10 ⁻⁴ mol/L of sensors in DMSO).....	71
Figure 3.16	Absorption and emission spectra of <i>o</i> - MNQB , <i>m</i> - MNQB and <i>p</i> - MNQB in DMSO (3x10 ⁻⁴ mol/L)	74
Figure 3.17	Fluorescence spectral change of <i>p</i> - MNQB (3x10 ⁻⁴ mol/L) in the presence of 500 equivalents of potassium salt for CN ⁻ and AcO ⁻ in DMSO and tetrabutylammonium salt for F ⁻	75
Figure 3.18	Fluorescence spectra (left) and fluorescence response (I/I ₀ at 460 nm) (right) of <i>p</i> - MNQB (3x10 ⁻⁴ mol/L) in the presence of 0-1500 equivalents of tetrabutylammonium fluoride in DMSO..	76
Figure 3.19	Fluorescence responses (I/I ₀ at 460 nm) of <i>p</i> - MNQB (3x10 ⁻⁴ mol/L) in the presence of 100 equivalent of tetrabutylammonium fluoride in DMSO at various times (0-320 minutes).....	77

Figure 3.20	Fluorescence spectral changes of a) <i>o</i> -MNQB, b) <i>m</i> -MNQB c) <i>p</i> -MNQB and d) control compound 7b in presence of 100 equiv of potassium salt of anions (5×10^{-5} mol/L of receptor in 0.1 mol/L NaCl 1:1, H ₂ O:DMSO)	78
Figure 3.21	Fluorescence response ($I-I_0$ at 460 nm) of <i>o</i> -MNQB, <i>m</i> -MNQB and <i>p</i> -MNQB and control compound 7b in the presence of 100 equiv potassium salt of anions (5×10^{-5} mol/L of receptor in 0.1 mol/L NaCl 1:1, H ₂ O:DMSO)	79
Figure 3.22	A) showed fluorescence spectra changes of <i>m</i> -HNBQ (5×10^{-5} mol/L) upon the addition of 0-500 equivalents of KCN and right panel b) showed fluorescence responses at 460 nm (I/I_0) of <i>o</i> -HNBQ, <i>m</i> -HNBQ and <i>p</i> -HNBQ in the presence of 0-500 equivalents) of KCN in 0.1 mol/L NaCl 1:1, H ₂ O:DMSO (5×10^{-5} mol/L of sensors)	80
Figure 3.23	Fluorescence responses at 460 nm (I/I_0) of <i>m</i> -HNBQ in the presence of 0-100 equivalents of KCN and KOH in 0.1 mol/L NaCl 1:1, H ₂ O:DMSO (5×10^{-5} mol/L of sensors).....	81
Figure 3.24	A) fluorescence response ($I-I_0$ at 460 nm) of <i>o</i> -MNQB, <i>m</i> - MNQB and <i>p</i> -MNQB in the presence of 500 equivalents of potassium salts of anions and b) Fluorescence responses upon irradiated with UV-lamp (256 nm) of solutions of 3b (left), 3b + CN ⁻ (middle) and 3b + F ⁻ (right) (5×10^{-5} mol/L of receptor in 0.1 mol/L NaCl in 50% HEPES pH 7.4: DMSO)	82
Figure 3.25	A) Fluorescence spectra of <i>m</i> -MNQB with increasing of cyanide concentration (5×10^{-5} mol/L of receptor in HEPES buffer pH 7.4, 0.1 mol/L NaCl, 50% H ₂ O:DMSO) and b) fluorescence response ($I-I_0$ at 460 nm) of <i>o</i> -MNQB, <i>m</i> -MNQB and <i>p</i> -MNQB with increasing of cyanide concentration.....	83
Figure 3.26	The ESI mass spectrum of <i>p</i> -MNQB in the presence of 500 equiv. of KCN in HEPES buffer pH 7.4, 0.1 mol/L NaCl, 50% H ₂ O:DMSO.....	84

Figure 3.27	Fluorescence spectra of <i>m</i> -MNQB and <i>m</i> -MNQB + 50 μ M KCN with various types of surfactants (5×10^{-5} mol/L of <i>m</i> -MNQB, 5×10^{-3} mol/L of surfactant in 1:4 of ethanol:H ₂ O)....	86
Figure 3.28	The proposed model of the reaction of sensors and cyanide in the CTAB micellar system.....	87
Figure 3.29	Fluorescence responses of <i>m</i> -MNQB and <i>m</i> -MNQB + 50 μ M KCN with various types of cationic surfactants (5×10^{-5} mol/L of <i>m</i> -MNQB, 5×10^{-3} mol/L of surfactant in 1:4 ethanol:H ₂ O)...	88
Figure 3.30	Fluorescence response ($I-I_0$) of <i>m</i> -MNQB (5×10^{-5} mol/L) + 50 μ M KCN in various concentration of CTAB and CMC of CTAB in 10% ethanol:H ₂ O shown as gray area.....	88
Figure 3.31	Fluorescence responses of <i>m</i> -MNQB + 25 μ M KCN and <i>p</i> -MNQB + 25 μ M KCN with various concentration of sensors (100 equivalents of CTAB compared to sensors in 1:4 ethanol:H ₂ O).....	89
Figure 3.32	Fluorescence responses ($I-I_0$ at 460 nm) of <i>m</i> -MNQB and <i>p</i> -MNQB in the CTAB micellar system in the presence of 50 μ M (1 equiv.) of various anions (5×10^{-5} mol/L of sensors, 5×10^{-3} mol/L of CTAB in 1:4 ethanol:H ₂ O) and fluorescence response of <i>m</i> -MNQB and <i>p</i> -MNQB in DMSO:H ₂ O system with 25 mM (500 equivalents) of various anions (5×10^{-5} mol/L of receptor in 0.1 mol/L of NaCl in 50% HEPES pH 7.4:DMSO)..	90
Figure 3.33	Fluorescence response (I/I_0 at 460 nm) of <i>o</i> -MNQB, <i>m</i> -MNQB and <i>p</i> -MNQB with 0.25 mM of cyanide mixing for 30 minutes in the DMSO:H ₂ O system (5×10^{-5} mol/L of sensor in 0.1 mol/L of NaCl in 50% HEPES pH 7.4:DMSO) and in the micellar system (5×10^{-5} mol/L of sensors, 5×10^{-3} mol/L of CTAB in 1:4 ethanol:H ₂ O).....	91

Figure 3.34	Fluorescence titration spectra (left) and the fluorescence titration curves (right) of a) <i>o</i> -MNQB, b) <i>m</i> -MNQB and c) <i>p</i> -MNQB upon the addition of cyanide ion in CTAB micellar system (5×10^{-5} mol/L of sensors, 5×10^{-3} mol/L of CTAB in 1:4 ethanol:H ₂ O).....	93
Figure 3.35	B3LYP/6-31+G(d) optimized structures of (a) <i>o</i> -MNQB (left), <i>o</i> -MNQB-CN ₃ ⁻ (right), (b) <i>m</i> -MNQB (left), <i>m</i> -MNQB-CN ₃ ⁻ (right) and (c) <i>p</i> -MNQB (left), <i>p</i> -MNQB -CN ₃ ⁻ (right).....	96
Figure 3.36	Calibration curves of cyanide 2.5-40 μM, 2.5-15 μM and 20-40 μM for (a) <i>m</i> -MNQB and (b) <i>p</i> -MNQB in optimum condition (5.0×10^{-5} mol/L of sensors; 5.0×10^{-3} mol/L CTAB in 1:4 ethanol in H ₂ O)	100
Figure 3.37	The ¹ H-NMR spectrum (400 MHz) of <i>o</i> -MNQB (0.001 mol/L) in presence of 10 equiv. of potassium cyanide and tetrabutyl ammonium fluoride in DMSO- <i>d</i> ₆	102
Figure 3.38	The ¹ H-NMR spectrum (400 MHz) of <i>m</i> -MNQB (0.005 mol/L) in presence of 10 equiv. of potassium cyanide and tetrabutyl ammonium fluoride in DMSO- <i>d</i> ₆	102
Figure 3.39	The ¹ H-NMR spectrum (400 MHz) of <i>p</i> -MNQB (0.001 mol/L) in presence of 10 equiv. of potassium cyanide and tetrabutyl ammonium fluoride in DMSO- <i>d</i> ₆	103
Figure 3.40	The ¹⁹ F-NMR spectrum (470 MHz) of <i>m</i> -MNQB in presence of 3 equiv. of tetrabutylammonium fluoride in DMSO- <i>d</i> ₆	104
Figure 3.41	The ¹⁹ F-NMR spectrum (470 MHz) of <i>m</i> -MNQB in presence of 3 equiv. of tetrabutylammonium fluoride in DMSO- <i>d</i> ₆	104
Figure 3.42	Cyclic voltammogram of sensors in the absence (solid line) and the presence 5 equivalent of KCN (dash line) (2×10^{-4} mol/L of sensor in 0.1 mol/L NaCl 1:1; H ₂ O:DMSO for <i>m</i> -MNQB, <i>p</i> -MNQB and control compound 7b , 1×10^{-4} mol/L for <i>o</i> -MNQB in 0.1 mol/L NaCl 1:1; H ₂ O:DMSO)	105

Figure 3.43	Structures of the anthraquinone imidazole boronic based sensors, HAQB and MAQB	106
Figure 3.44	Absorption and emission spectra of HAQB and MAQB (5×10^{-5} mol/L) in a) DMSO and b) EtOH.....	108
Figure 3.45	Fluorescence spectra of HAQB (5×10^{-5} mol/L in 40% ethanol:buffer) at pH 3-10 buffer and MAQB (5×10^{-5} mol/L in 20% ethanol: buffer) at pH 5-12 buffer (pH 3-5 : 0.2 mol/L phthalate-HCl buffer, pH 6-8 : 0.2 mol/L phosphate buffer, pH 8.5-10 : 0.2 mol/L sodium borate buffer, pH 11-12 : 0.2 mol/L phosphate-NaOH buffer)	109
Figure 3.46	pH-Dependent fluorescence response (I/I_{acid} at 555 nm) of HAQB (5×10^{-5} mol/L in 40% ethanol:buffer) at pH 3-10 buffer and MAQB (5×10^{-5} mol/L in 20% ethanol: buffer) at pH 5-12 (pH 3-5 : 0.2 mol/L phthalate-HCl buffer, pH 6-8 : 0.2 mol/L phosphate buffer, pH 8.5-10 : 0.2 mol/L sodium borate buffer, pH 11-12 : 0.2 mol/L phosphate-NaOH buffer)	110
Figure 3.47	Job's plot for 1:1 complexes of a) HAQB and b) MAQB with D-fructose at pH 8.5 (5×10^{-5} mol/L in 40% EtOH:buffer pH 8.5 for HAQB and 5×10^{-5} mol/L in 20% EtOH:buffer pH 8.5 for MAQB).....	110
Figure 3.48	Fluorescence spectra of a) HAQB (5×10^{-5} mol/L in 40% ethanol : buffer pH 8.5, $\lambda_{\text{ex}} = 410$ nm) and b) MAQB (5×10^{-5} mol/L in 20% ethanol: buffer pH 8.5, $\lambda_{\text{ex}} = 395$ nm)	111
Figure 3.49	Fluorescence response ($\Delta I/I_0$) at 600 nm of a) HAQB (5×10^{-5} mol/L in 40% ethanol:buffer pH 8.5) and b) at 560 nm of MAQB (5×10^{-5} mol/L in 20% ethanol: buffer pH 8.5) in the presence of 0-150 mM of various saccharides ; \square = D-fructose, \circ = D-galactose, ∇ = D-glucose, Δ = D-mannose	111

Figure 3.50	pH-Profiles of the fluorescence intensities 560 nm of MAQB (5×10^{-5} mol/L, 20%EtOH:buffer) in various pH (pH 3-5 : 0.2 mol/L phthalate-HCl buffer, pH 6-8 : 0.2 mol/L phosphate buffer, pH 8.5-10 : 0.2 mol/L sodium borate buffer, pH 11-12 : 0.2 mol/L phosphate-NaOH buffer)	115
Figure 3.51	pH-Profiles of the fluorescence intensities ratio at 587 nm and 555 nm (I_{587}/I_{555}) of MAQB in the absence (-□-) and the presence of 50 mM of sugars: D-fructose (-○-), D-galactose (-△-), D-glucose(-▽-) and D-mannose (-◇-) (5×10^{-5} mol/L in 20% EtOH in various buffer; pH 3-5 : 0.2 mol/L phthalate-HCl buffer, pH 6-8 : 0.2 mol/L phosphate buffer, pH 8.5-10 : 0.2 mol/L sodium borate buffer, pH 11-12 : 0.2 mol/L phosphate-NaOH buffer).....	117
Figure A.1	The $^1\text{H-NMR}$ spectrum (400 MHz) of 2-(5,5-dimethyl-1,3,2-dioxaborinan-2-yl)benzaldehyde (1a) in CDCl_3	136
Figure A.2	The $^1\text{H-NMR}$ spectrum (400 MHz) of 3-(1,3,2-dioxaborinan-2-yl)benzaldehyde (1b) in CDCl_3	136
Figure A.3	The $^1\text{H-NMR}$ spectrum (400 MHz) of 4-(1,3,2-dioxaborinan-2-yl)benzaldehyde (1c) in CDCl_3	137
Figure A.4	The $^1\text{H-NMR}$ spectrum (400 MHz) of diphthalimide naphthaquinone (2) in CDCl_3	137
Figure A.5	The $^1\text{H-NMR}$ spectrum (400 MHz) of 2,3-diaminonaphthalene-1,4-dione (3) in CDCl_3	138
Figure A.6	The $^1\text{H-NMR}$ spectrum (400 MHz) of 2-(2-(5,5-dimethyl-1,3,2-dioxaborinan-2-yl)phenyl)-1H-naphtho[2,3-d]imidazole-4,9-dione (4a) in $\text{DMSO-}d_6$	138
Figure A.7	The $^{13}\text{C-NMR}$ spectrum (100.6 MHz) of 2-(2-(5,5-dimethyl-1,3,2-dioxaborinan-2-yl)phenyl)-1H-naphtho[2,3-d]imidazole-4,9-dione (4a) in $\text{DMSO-}d_6$	139
Figure A.8	The $^1\text{H-NMR}$ spectrum (400 MHz) of 2-(3-(1,3,2-dioxaborinan-2-yl)phenyl)-1H-naphtho[2,3-d]imidazole-4,9-dione (4b) in $\text{DMSO-}d_6$	139

Figure A.9	The ^{13}C -NMR spectrum (100.6 MHz) of 2-(3-(1,3,2-dioxaborinan-2-yl)phenyl)-1H-naphtho[2,3-d]imidazole-4,9-dione (4b) in $\text{DMSO-}d_6$	140
Figure A.10	The ^1H -NMR spectrum (400 MHz) of 2-(4-(1,3,2-dioxaborinan-2-yl)phenyl)-1H-naphtho[2,3-d]imidazole-4,9-dione (4c) in $\text{DMSO-}d_6$	140
Figure A.11	The ^{13}C -NMR spectrum (100.6 MHz) of 2-(4-(1,3,2-dioxaborinan-2-yl)phenyl)-1H-naphtho[2,3-d]imidazole-4,9-dione (4c) in $\text{DMSO-}d_6$	141
Figure A.12	The ^1H -NMR spectrum (400 MHz) of 4,9-dioxo-4,9-dihydro-1H-naphtho[2,3-d]imidazol-2-yl)phenylboronic acid (<i>o</i>-HNQB) in $\text{DMSO-}d_6$	141
Figure A.13	The ^{13}C -NMR spectrum (100.6 MHz) of 4,9-dioxo-4,9-dihydro-1H-naphtho[2,3-d]imidazol-2-yl)phenylboronic acid (<i>o</i>-HNQB) in $\text{DMSO-}d_6$	142
Figure A.14	The ^1H -NMR spectrum (400 MHz) of 4,9-dioxo-4,9-dihydro-1H-naphtho[2,3-d]imidazol-2-yl)phenylboronic acid (<i>m</i>-HNQB) in $\text{DMSO-}d_6$	142
Figure A.15	The ^{13}C -NMR spectrum (100.6 MHz) of 4,9-dioxo-4,9-dihydro-1H-naphtho[2,3-d]imidazol-2-yl)phenylboronic acid (<i>m</i>-HNQB) in $\text{DMSO-}d_6$	143
Figure A.16	The ^1H -NMR spectrum (400 MHz) of 4,9-dioxo-4,9-dihydro-1H-naphtho[2,3-d]imidazol-2-yl)phenylboronic acid (<i>p</i>-HNQB) in $\text{DMSO-}d_6$	143
Figure A.17	The ^{13}C -NMR spectrum (100.6 MHz) of 4,9-dioxo-4,9-dihydro-1H-naphtho[2,3-d]imidazol-2-yl)phenylboronic acid (<i>p</i>-HNQB) in $\text{DMSO-}d_6$	144
Figure A.18	The ^1H -NMR spectrum (400 MHz) of 4-(1-methyl-4,9-dioxo-4,9-dihydro-1H-naphtho[2,3-d]imidazol-2-yl) phenylboronic acid (<i>o</i>-MNQB) in $\text{DMSO-}d_6$	144

Figure A.19	The ^{13}C -NMR spectrum (100.6 MHz) of 4-(1-methyl-4,9-dioxo-4,9-dihydro-1H-naphtho[2,3-d]imidazol-2-yl) phenylboronic acid (<i>o</i>-MNQB) in $\text{DMSO-}d_6$	145
Figure A.20	The ^1H -NMR spectrum (400 MHz) of 4-(1-methyl-4,9-dioxo-4,9-dihydro-1H-naphtho[2,3-d]imidazol-2-yl) phenylboronic acid (<i>m</i>-MNQB) in $\text{DMSO-}d_6$	145
Figure A.21	The ^{13}C -NMR spectrum (100.6 MHz) of 4-(1-methyl-4,9-dioxo-4,9-dihydro-1H-naphtho[2,3-d]imidazol-2-yl) phenylboronic acid (<i>m</i>-MNQB) in $\text{DMSO-}d_6$	146
Figure A.22	The ^1H -NMR spectrum (400 MHz) of 4-(1-methyl-4,9-dioxo-4,9-dihydro-1H-naphtho[2,3-d]imidazol-2-yl) phenylboronic acid (<i>p</i>-MNQB) in $\text{DMSO-}d_6$	146
Figure A.23	The ^{13}C -NMR spectrum (100.6 MHz) of 4-(1-methyl-4,9-dioxo-4,9-dihydro-1H-naphtho[2,3-d]imidazol-2-yl) phenylboronic acid (<i>p</i>-MNQB) in $\text{DMSO-}d_6$	147
Figure A.24	The ^1H -NMR spectrum (400 MHz) of 2-phenyl-1H-naphtho [2,3-d]imidazole-4,9-dione (7a) in $\text{DMSO-}d_6$	147
Figure A.25	The ^{13}C -NMR spectrum (100.6 MHz) of 2-phenyl-1H-naphtho[2,3-d]imidazole-4,9-dione (7a) in $\text{DMSO-}d_6$	148
Figure A.26	The ^1H -NMR spectrum (400 MHz) of 1-methyl-2-phenyl-1H-naphtho[2,3-d]imidazole-4,9-dione (7b) in $\text{DMSO-}d_6$	148
Figure A.27	The ^{13}C -NMR spectrum (100.6 MHz) of 1-methyl-2-phenyl-1H-naphtho[2,3-d]imidazole-4,9-dione (7b) in $\text{DMSO-}d_6$	149
Figure A.28	The ^1H -NMR spectrum (400 MHz) of 2-(4-(1,3,2-dioxaborinan-2-yl)phenyl)-3H-anthra[1,2-d]imidazole-6,11-dione (8) in CDCl_3	149
Figure A.29	The ^{13}C -NMR spectrum (100.6 MHz) of 2-(4-(1,3,2-dioxaborinan-2-yl)phenyl)-3H-anthra[1,2-d]imidazole-6,11-dione (8) in $\text{DMSO-}d_6$	150
Figure A.30	The ^1H -NMR spectrum (400 MHz) of 4-(6,11-dioxo-6,11-dihydro-3H-anthra[1,2-d]imidazol-2-yl)phenylboronic acid (HAQB) in $\text{DMSO-}d_6$	150

- Figure A.31** The ^{13}C -NMR spectrum (100.6 MHz) of 4-(6,11-dioxo-6,11-dihydro-3H-anthra[1,2-d]imidazol-2-yl)phenylboronic acid (**HAQB**) in DMSO-d_6 151
- Figure A.32** The ^1H -NMR spectrum (400 MHz) of 4-(3-methyl-6,11-dioxo-6,11-dihydro-3H-anthra[1,2-d]imidazol-2-yl)phenylboronic acid (**MAQB**) in DMSO-d_6 151
- Figure A.33** The ^{13}C -NMR spectrum (100.6 MHz) of 4-(3-methyl-6,11-dioxo-6,11-dihydro-3H-anthra[1,2-d]imidazol-2-yl)phenylboronic acid (**MAQB**) in DMSO-d_6 152
- Figure A.34** The UV-vis spectrum of diamionaphthoquinone 6×10^{-4} mol/L in DMSO..... 152
- Figure A.35** Fluorescence spectra of **MAQB** (5×10^{-5} mol/L in 20% ethanol: buffer) at pH 4-12 buffer in the presence of 50 mM a) D-fructose, b) D-galactose, c) D-mannose and d) D-glucose (pH 3-5 : 0.2 mol/L phthalate-HCl buffer, pH 6-8 : 0.2 mol/L phosphate buffer, pH 8.5-10 : 0.2 mol/L sodium borate buffer, pH 11-12 : 0.2 mol/L phosphate-NaOH buffer) 153

LIST OF SCHEMES

	Page
Scheme 1.1 Three approaches model for the anion sensor: a) binding site-signaling approach, b) displacement approach and chemodosimeter approach.....	2
Scheme 1.2 The equilibrium of boronic acid interacts with diol in aqueous media.	14
Scheme 3.1 Structures of designed receptors based on quinone imidazole and boronic acid.....	49
Scheme 3.2 Synthetic pathway of sensors <i>o</i> -HNBQ, <i>m</i> -HNBQ and <i>p</i> -HNQB and <i>o</i> -MNBQ, <i>m</i> -MNBQ and <i>p</i> -MNQB.....	50
Scheme 3.3 Synthetic pathway of sensors HAQB and MAQB.....	55
Scheme 3.4 Feasible frontiers orbital energy diagram for the protonated sensors which was represented as the inverse PET (photo induced electron transfer) upon the deprotonation by anions...	72
Scheme 3.5 Equilibrium of nucleophilic substitution on the boron center of the methylated sensors <i>o</i> -MNQB, <i>m</i> -MNQB and <i>p</i> -MNQB.....	73
Scheme 3.6 Equilibrium of tricyano-substituted of the methylated sensors <i>o</i> -MNQB, <i>m</i> -MNQB and <i>p</i> -MNQB.....	94
Scheme 3.7 The acid-conjugate base equilibrium for phenylboronic acid in water.....	108
Scheme 3.8 Association of fluorescence properties and ionization states of MAQB in the absence of sugar.....	116
Scheme 3.9 The model of signal transductions of MAQB upon the hybridization changes of boron center.....	117
Scheme 4.1 Structures of all synthesized sensors.....	119

LIST OF ABBREVIATIONS

°C	Degree Celsius
μL	Microliter
μM	Micromolar
¹³ C-NMR	Carbon nuclear magnetic resonance
¹⁹ F-NMR	Fluorine nuclear magnetic resonance
¹ H-NMR	Proton nuclear magnetic resonance
Å	Angstrom
AcO ⁻	Acetate
Anal. Calcd.	Analysis calculated
Br ⁻	Bromide
Bzo ⁻	Benzoate
Cl ⁻	Chloride
ClO ₄ ⁻	Perchlorate
CN ⁻	Cyanide
CTAB	Cetyltrimethylammonium bromide
DMAC	<i>N,N'</i> -Dimethylacetamide
DMF	Dimethylformamide
DMSO	Dimethylsulfoxide
DNA	Deoxyribonucleic acid
DTAB	Dodecyltrimethyl ammonium bromide
equiv.	Equivalent

F ⁻	Fluoride
g	Gram
h	Hour
H ₂ PO ₄ ⁻	Dihydrogen phosphate
HEPES	2-[4-(2-Hydroxyethyl)-1-piperazinyl]-propane-sulphonic acid
I ⁻	Iodide
ICT	Intramolecular charge transfer
<i>J</i>	Coupling constant
<i>K_s</i>	Stability constant
m/z	Mass per charge ratio
mg	Milligram
MHz	Megahertz
mL	Milliliter
mm	Millimeter
mmol	Millimole
nm	Nanometer
NMR	Nuclear magnetic resonance
NO ₃ ⁻	Nitrate
NOESY	Nuclear Overhauser Effect Spectroscopy
PET	Photoinduced electron transfer
ppm	Part per million
s, d, t, m	Splitting pattern of ¹ H-NMR (singlet, doublet, triplet, multiplet)
S ₀	Electronic ground state

S_1	Electronic excited state
SDS	Sodium dodecyl sulfate
TBAF	Tetrabutylammonium fluoride
THF	Tetrahydrofuran
TTAB	Tetradecyltrimethylammonium bromide
TX-100	Triton X-100
UV-Vis	Ultraviolet-Visible
v/v	volume per volume
δ	Chemical Shift
Φ_F	Fluorescence quantum yield
λ_{emiss}	Emission maxima
λ_{max}	Absorption maxima

ศูนย์วิจัยทรัพยากร
จุฬาลงกรณ์มหาวิทยาลัย

CHAPTER I

INTRODUCTION

1.1 Supramolecular chemistry and sensing applications

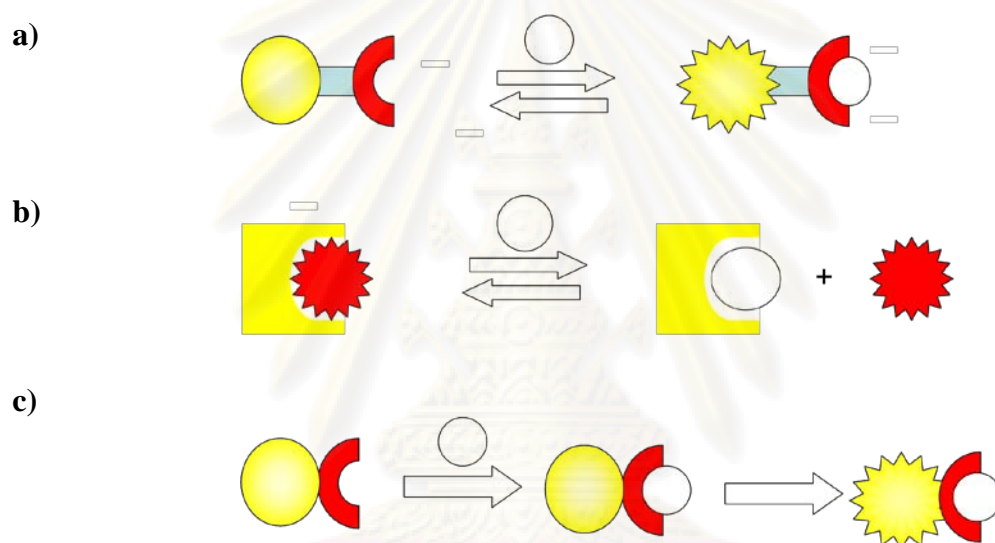
Supramolecular chemistry is a multi-disciplinary field of chemistry. Early definition was introduced by Lehn in 1978 as a chemistry beyond molecules. [1] Nowadays, supramolecular chemistry applications have pursued fruitfully in many fields such as the development of new materials, pharmaceuticals, chemosensors, and contrast agents for imaging applications *etc.* [1-5]

Molecular sensors or chemosensors are molecules which are capable to recognize and to give signals for specific analytes in the real time. Signaling is given by the cooperation of the basic function of the components such as a binding site and a signaling unit. Complementary interactions between a guest and a host binding site capably generate a physical signal change such as color, absorption, emission and redox properties corresponding to the recognition event. [3-5]

Molecular recognition is a process involved interactions between hosts and guests which do not define only binding event but this process requires the selectivity between the host and the guest. In physiological system, the perfect recognition of a receptor arises from the complementary matched of many factors such as electronic, geometry and polar of host and guest. [3-5] Considering on the signaling unit, optical signals based on the change of absorbance or fluorescence properties are the most frequently employed because of their simple applications using inexpensive instruments. On the one hand, the alternation changes of optical properties, particularly of color or emissions, can immediately reveal the recognition event. Especially fluorescence emissions allow sensors to have very high sensitivity. [6, 7]

1.2 Designing concepts for anion sensors [8-12]

According to a fundamental role of anions in a wide range of chemical and biological processes, many research groups have paid attentions to the development of an effective anion sensing system. It is well known that anions have larger size than cations and they are more subjected to solvation. Therefore, it is difficult to use a synthetic chemosensor in aqueous system. From the variety of synthetic sensors, optical sensors for anions were categorized in three types as shown in Scheme 1.1. [11, 12]



Scheme 1.1 Three approaches model for the anion sensor: a) binding site-signaling approach, b) displacement approach and chemodosimeter approach. [11, 12]

i) Binding site-signaling approach

Molecular recognition of binding site-signaling subunit approach or classical approach is relied on non-covalent interaction such as H-bonding and electrostatic interactions. Regarding to successful function in aqueous system, synthetic anion sensors in this approach must have sufficiently affinity for anions in water such as metal complexes coordination interactions and electrostatic interactions. [11]

ii) Displacement approach

This approach utilizes the displacing of guests into the binding pocket and releasing of the signaling subunit. The recognition event is observed by the recovery of spectroscopic signal of uncoordinated signaling subunit upon the displacement of the guest in the binding site. The displacement of the guest can take place only when an affinity of the signaling unit and a binding site is lower than that of the guest and the binding site. [11]

iii) Chemodosimeter approach

In this approach, the specific reaction between a host and an anion guest provide new species which has different optical properties from its original form. Because of the specific reaction of between hosts and guests, generally this approach offered desired characteristics of an anion sensor in water in term of selectivity and sensitivity. [12]

1.3 Literature reviews for cyanide sensors

Cyanide has long been known to be the most extremely toxic poison. Acute toxicity of cyanide is attributed to the effective binding to the active site of *cytochrome C oxidase* resulting in the disruption of electron transport chain. Many tissues that mainly depend on aerobic respiration such as brain, central nervous system, heart are acutely affected. [13, 17] Cyanide contaminated in surface water or environments are originated from many industries such as electroplating, plastic manufacturing, metal extraction, metallurgy and tanning. [14] The Environment Protection Agency (EPA) has set the maximum level for cyanide in drinking water at 0.2 ppm. [16] The LD₅₀ of hydrogen cyanide for adult have reported to be 1.0 mg/kg which were estimated from lethal dose for liquid contact. [14] Recent studies of fire victims and survivors of cyanide toxic have reported that survivors was found to have < 20 μM blood cyanide while victims was found to have 20-30 μM blood cyanide. [15, 16] Therefore, any techniques used to monitor cyanide to assure physiological safeguard must have detection ability down to micromolar level. In the field of supramolecular chemistry, the development of cyanide sensors has long been known

as the most attractive subject over the past ten years. [12] In this section, optical sensors for cyanide was classified into three groups as motioned previously.

1.3.1 Non-covalent based cyanide sensors

Cyanide sensors in this approach rely on non-covalent interactions between hosts and guests. Comparison to other anions, cyanide is not a good hydrogen bond acceptor due to delocalization of electron through the triple bond. [18, 19] Therefore, the hydrogen bonding based sensor for cyanide can function in a non-aqueous system only, and they have poor selectivity. [12] For example, Lee *et al.* [20] demonstrated that a luminescent rhenium(I) polypyridyl based sensor, **1**, served as artificial receptor for halide, cyanide and acetate in CH_2Cl_2 . This receptor showed the affinity trend of $\text{CN}^- > \text{F}^- > \text{I}^- > \text{Cl}^- \approx \text{Br}^- \approx \text{OAc}^- \gg \text{H}_2\text{PO}_4^- > \text{NO}_3^- > \text{ClO}_4^-$.

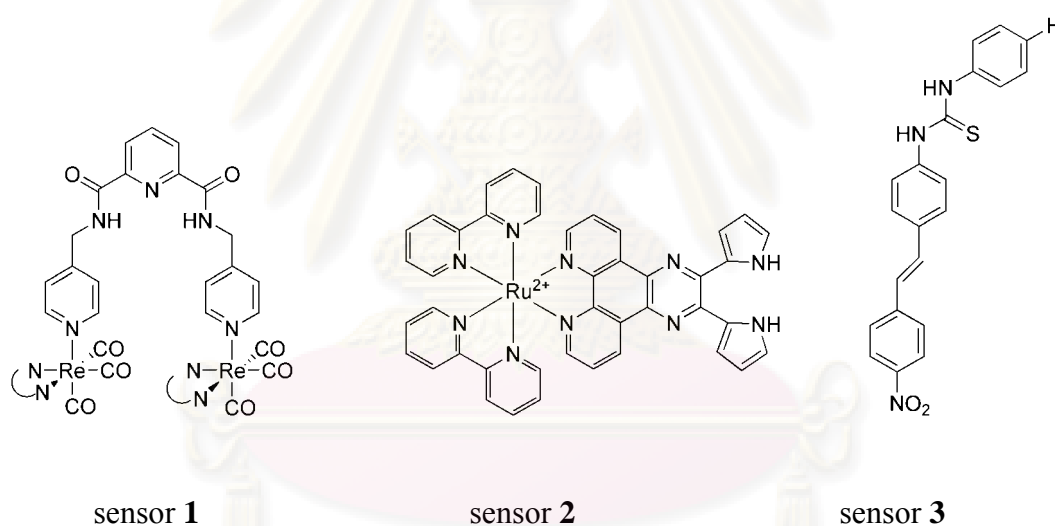


Figure 1.1 Structures of hydrogen bonding based sensors **1**, **2**, and **3** for cyanide.

Hydrogen bonding based sensor, **2** for cyanide were reported by Anzenbacher and Catellano *et al.* [21] It can serve as anion-induced luminescence lifetime-changes sensor for fluoride and cyanide in $\text{CH}_2\text{Cl}_2/\text{CH}_3\text{CN}$.

Recently, Vilar *et al.* [22] utilized azo-phenylthiourea sensor **3** for a chromogenic cyanide probes in methanol due to the deprotonation of thiourea NH groups. However, this sensor showed poor selectivity for cyanide in DMSO because they responded to other basic anions including fluoride, H_2PO_4^- and CH_3CO_2^- .

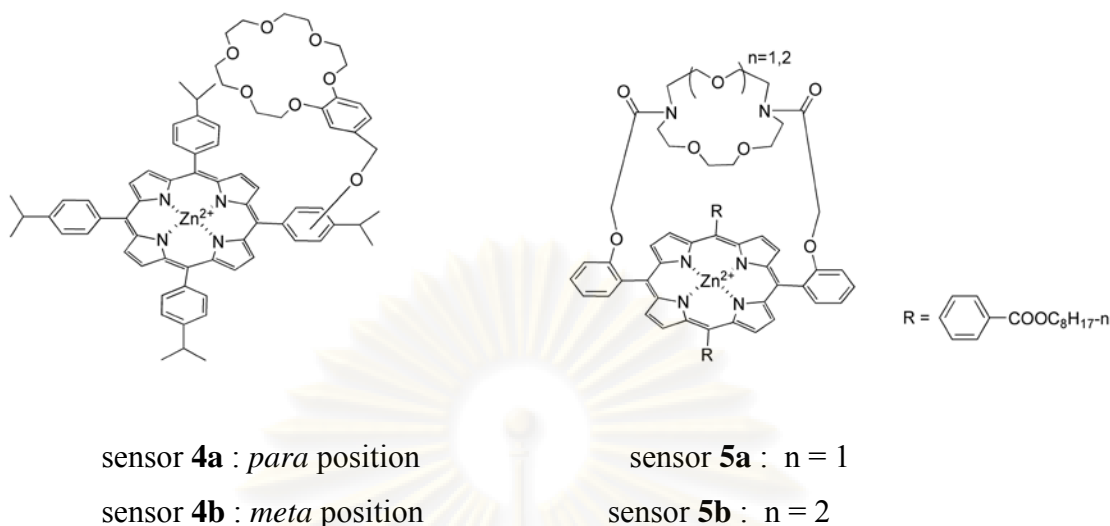


Figure 1.2 Structures of ditopic sensors **4a**, **4b**, **5a** and **5b**.

In addition, ditopic receptors possessing two metal sites (Figure 1.2) utilized the cooperative function of two metals for cyanide recognition. The first example was reported by Hong *et al.* [23] The authors reported that zinc-porphyrin crown ether based sensors, **4a** and **4b** acted as chromogenic sensors for cyanide in methanol. The cooperative of Zn^{2+} on porphyrin and Na^+ on crown ether served as the coordination site for cyanide ion. These sensors showed the color changes from original red of Zn-porphyrin to green in presence of cyanide ion. Selectivity of those sensors towards cyanide was attributed to the ditopic manner of cyanide binding whereas other anion binding relied on the monotopic fashion.

Ditopic Cyanide sensors **5a** and **5b** were synthesized and studied by Chen *et al.* [24] Sensors **5a** and **5b** utilized the variation of the azacrown ether site for selective recognition of sodium cyanide and potassium cyanide, respectively.

1.3.2 Cyanide sensors using displacement methods

Displacement methods for cyanide sensing are usually exploited high affinity of cyanide toward copper and cobalt for the sensing system. Li *et. al.* [25] prepared a new imidazole-functionalized polyfluorene **6** serving as sensitive and selective system for cyanide detection. The recovery of the fluorescence intensity of compound **6** which were completely quenched by Cu^{2+} was observed upon the addition of cyanide. Recently, Qin and Li *et al.* [26] utilized an old and inexpensive compound zircon, **7** (2-carboxy-2'-hydroxy-5'-sulfonylmarsyl-benzene) for a highly sensitive and selective cyanide chemosensor in water using Cu-displacement. This effort provided a limit of cyanide detection in water as low as 0.13 ppm.

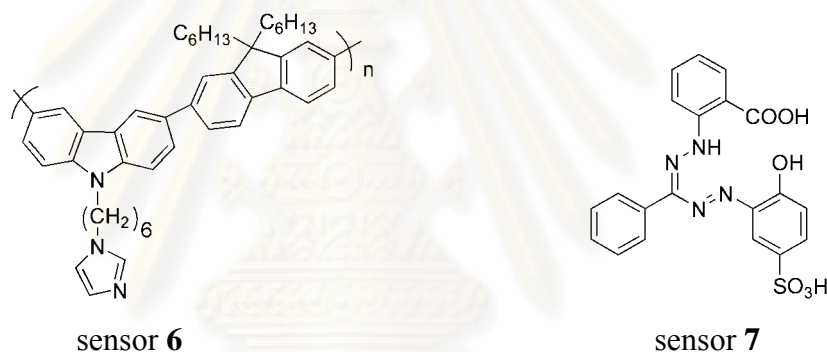


Figure 1.3 Structure of organic reagent for cyanide detection by Cu-displacement

1.3.3 Chemodosimeters for cyanide

Regarding to exceptional nucleophilicity of cyanide, chemodosimeters have long been considered for the development of cyanide detection especially in an aqueous system. Most of cyanide chemodosimeter probes are electrophilic organic reagents which undergo C-C bond [27-46] and C-S formation [47, 48] for cyanide sensing. Recently cyanide sensors using C-B formation have been reported by many research groups. [49-55]

1.3.3.1 C-C bond formation based sensors

Fluorometric method of cyanide detection based on specific reaction between cyanide and quinone derivatives were discovered in 1963. [27, 28] To date, a number of organic reagents such as oxazine, [41-43] derivative of BODIPY [34], dipyrrole carboxamide, [40] dicyanovinyl derivative [44], acridium [45] and squaraine [46] *etc.* were used as for cyanide probes by forming a new C-C bond upon cyanide recognition.

The first example of C-C bond formation based sensor is shown in Figure 14. The reaction center of the sensor possessed trifluoroacetyl-carboxanilide moiety which can be attacked by cyanide resulting in an intramolecular H-bonding stabilization of the anion-sensor adduct. [29-34]

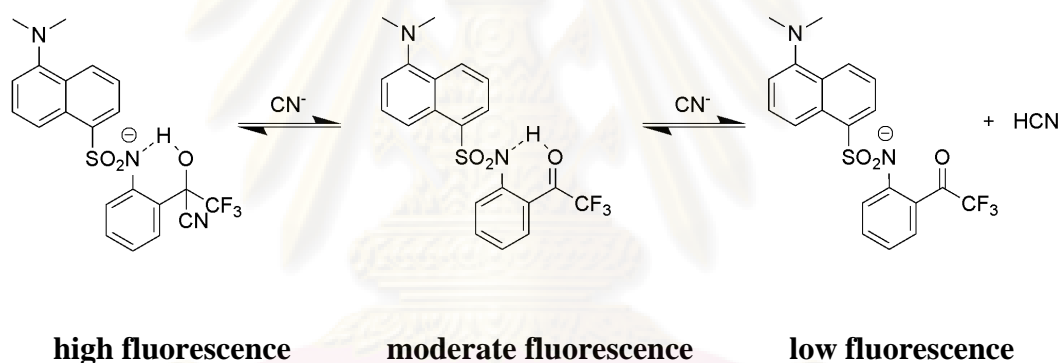


Figure 1.4 Structures of C-C bond formation based sensors using intramolecular hydrogen bond stabilization concept and the plausible mechanism of signal moderation by cyanide binding of sensor **8**.

Ahn *et al.* [31] reported that fluorescence signaling of anion binding for sensor **8** is modulated from quenching to enhancement by the intramolecular H-bonding stabilization of anion-ionophore adducts.

Besides the exceptional nucleophilicity of cyanide, sensors **9**, [35] **10** [36] and **11** [37] (Figure 1.5) utilized the nucleophilic attack of cyanide on carbonyl moiety which were activated by an appropriated location of hydroxy phenol group. For example sensor **11** showed the color change in DMSO upon the nucleophilic addition of cyanide. According to this concept, Yoon and Park *et al.* applied

fluorescein a ldehyde-based sensor which served as an “OFF–ON” cyanide fluorescence probes in living cells by incorporation into a microfluidic platform. [37]

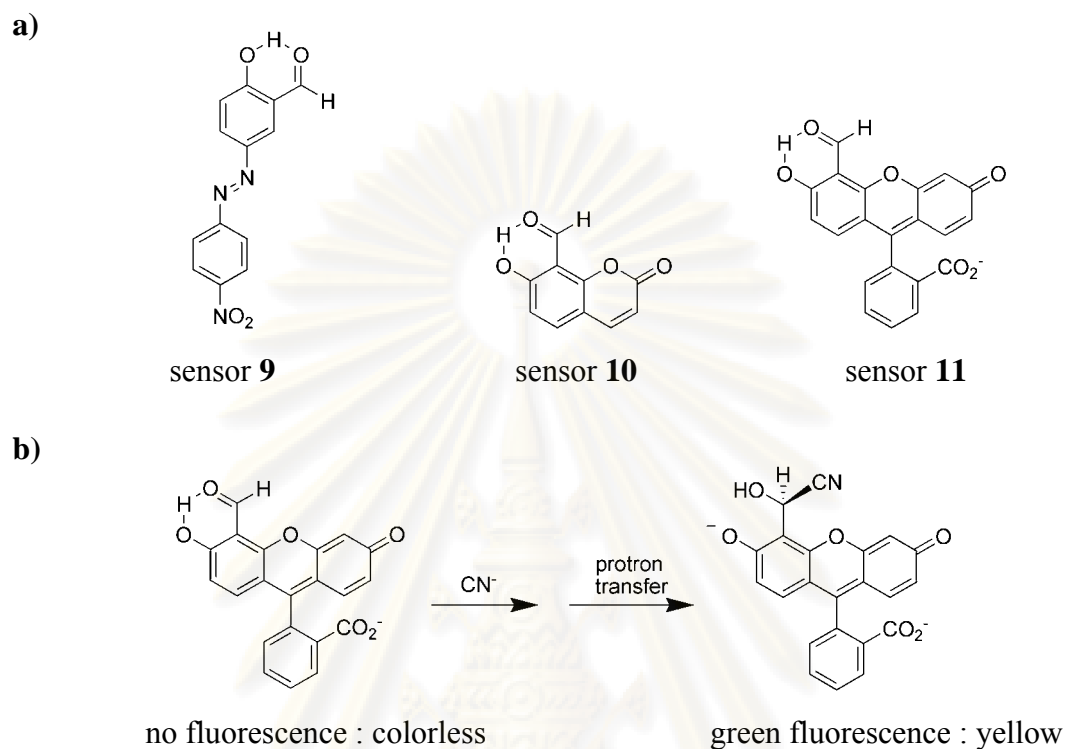


Figure 1.5 A) structures of C–C bond formation based sensor using carbonyl activation concept and b) the plausible mechanism of signal moderation by cyanide binding of sensor **11**

Recently, Sessler *et al.* [38, 39] have employed a benzil–cyanide reaction for the design of a colorimetric method for the cyanide detection. The nucleophilic addition of cyanide resulted in the fluorescence intensity and color changes of sensor **12** in methanol:H₂O. [38]

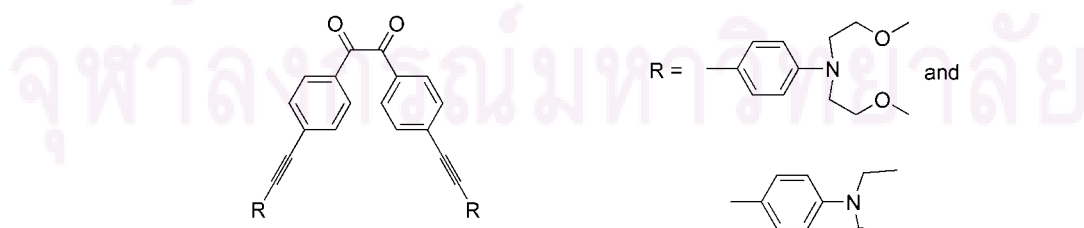


Figure 1.6 Structure of sensor **12**

Divinyl-cyano group was exploited as the active functional group for a nucleophilic attack by cyanide. Lee *et al.* [44] recently reported a new calix[4]pyrrole-based **13** for the cyanide selective indicator (Figure 1.7). Complete bleaching of the color of this sensor in the mixture of CH₃CN: DMSO upon the addition was attributed to the addition of cyanide on the vinyl site chain at the pyrrole moiety of the sensor.

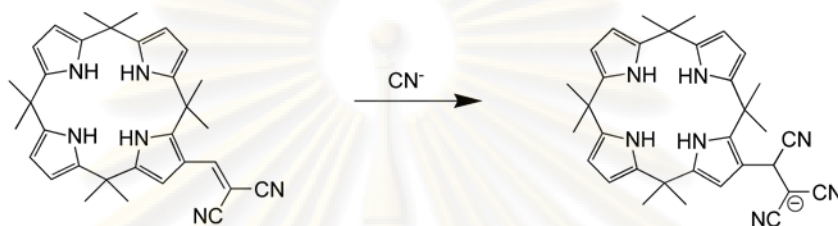


Figure 1.7 Reaction of calix[4]pyrrole-based sensor **13** with cyanide.

Tae *et al.* [45] reported a new cyanide selective chemodosimeter based on acridine salt, sensor **14**. This sensor took advantage of the nucleophilic addition of cyanide at the 9-position of the *N*-methylacridinium group resulting in adduct **14-I** which rapidly reacted with oxygen to give acridinone **14-II** as shown in Figure 1.8. The final adduct showed the fluorescence quenching as a function of cyanide concentration accompanying with the color change from orange to blue. Upon the addition of various anions in DMSO:H₂O (95:5), this sensor showed the selectivity toward cyanide with a limit of cyanide detection down to 1 μ M.

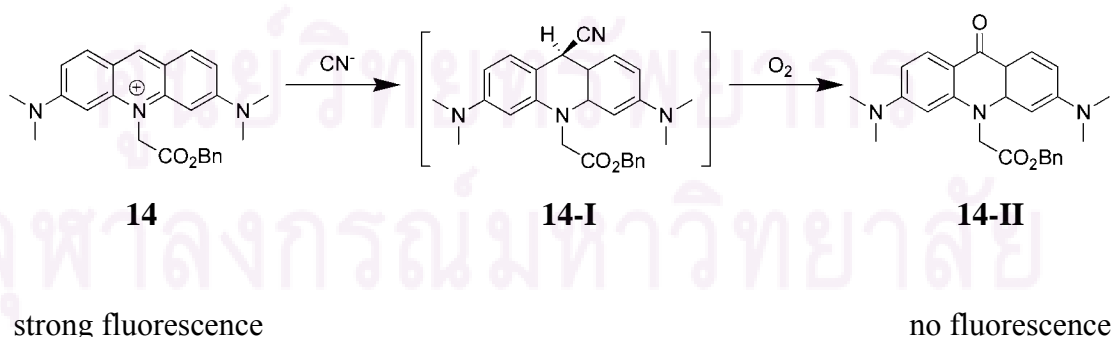


Figure 1.8 Mechanism of the reaction of sensor **14** with cyanide

Furthermore, C-C bond formation based sensors were obtained from many organic molecules which have electron deficiency center for cyanide attack such as squaraine **15**, [46] and croconium **16** [47] as displayed in Figure 1.9.

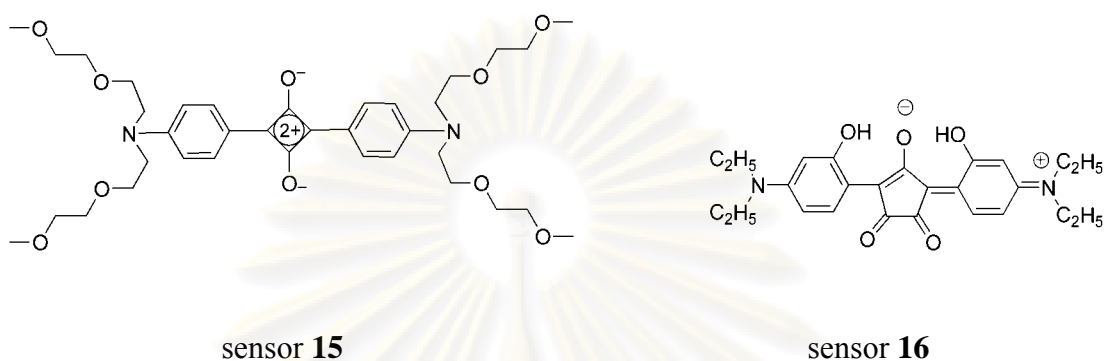


Figure 1.9 Structures of sensor **15** and **16**

1.3.3.2 C-S bond formation based sensors

Wang *et al.* [48] developed sensor **17** using cyanide attack on the benzothiadiazole ring sulfur for a quantitative system for micromolar cyanide detection as low as 26 ppb in DMF–H₂O (99 : 1, v/v). In addition, sensor **17** offered the capability of multiple signaling, including visible absorption, a high contrast change in color, and absorption and fluorescence spectral changes in the visible and NIR wavelength regions.

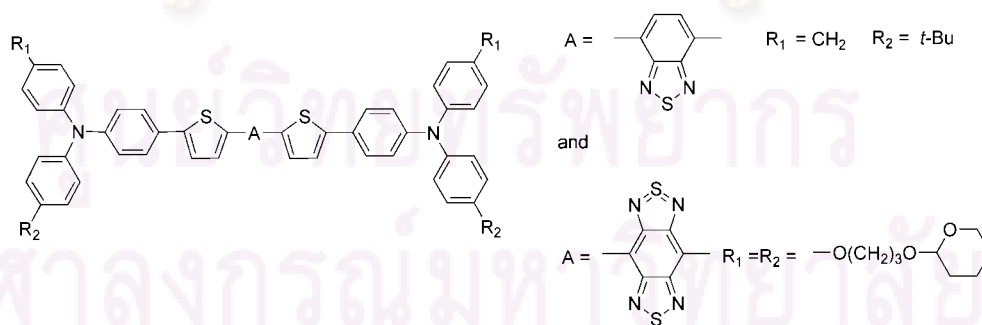


Figure 1.10 Structures of sensor **17**

1.3.3.3 C-B bond formation based sensors

Because of Lewis acid properties of sp^2 boron center [57], four groups of organo-boron compounds were dedicated for cyanide sensors including subphthalocyanine dye [49, 50], boron BODIPY derivative [51], cationic boron derivatives [52] and boronic acid derivatives. [53-56]

Martínez-Máñez *et al.* [49] reported the use of subphthalocyanine dye as ‘naked-eye’ sensor for cyanide detection. In 5% v/v aqueous acetonitrile solution, subphthalocyanine dye showed remarkably selective to cyanide over fluoride due to the relative nucleophilicity of fluoride and cyanide in this system. In addition, subphthalocyanine dye derivatives **19** [50] were also employed as selective colorimetric and fluorimetric cyanide probes.

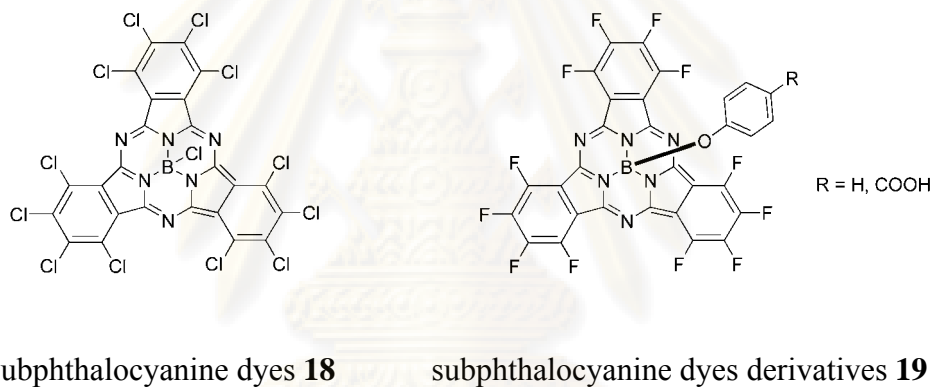


Figure 1.11 Structures of subphthalocyanine dyes derivatives as cyanide probes.

Recently, Do and Lee *et al.* [53] developed BODIPY dye as a donor segment coupling with borane for the preparation of boron-based sensor. The sensor **20** offered the 3-fold enhancement of fluorescence intensity upon cyanide binding due to the blocking of intramolecular charge transfer upon the cyanide binding at the boron on borane moiety.

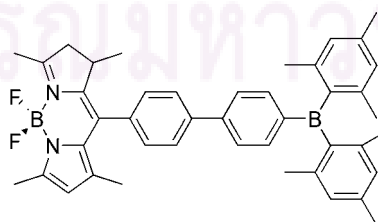


Figure 1.12 Structure of BODIPY-borane sensor **20** as a cyanide probes

Gabbai and Hudnall [54] developed cationic boranes receptors in *ortho* and *para* position of B-Mes as selective cyanide and fluoride probes in aqueous system. Favorable columbic effects in cationic borane increased in Lewis acid properties of boron resulting in strengthening of cyanide-receptor interactions. By the combination of steric and electronic effect, the selectivity of sensors can be tuned for cyanide for *para* sensors **21** and fluoride for *ortho* sensors **22** as shown in Figure 1.13.

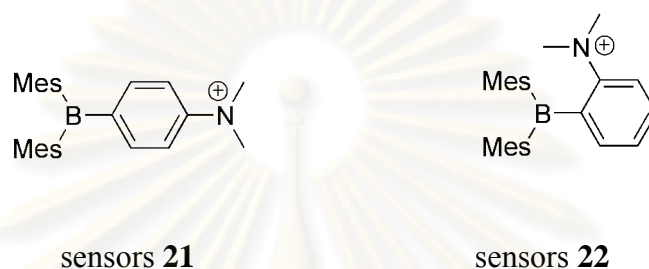


Figure 1.13 Structures of the *para* sensor **21** and the *ortho* sensor **22**

It is well known that boronic acid is widely used for binding site of the saccharide sensors. Geddes *et al.* extended the application of boronic acid to the binding site for cyanide. [53-56] New pyridinium boronic sensors **23** [56] can be used as powerful fluorescence sensors for cyanide in water with a detection limit down to 0.5 ppm. The interaction between anionic boron center and pyridinium upon cyanide binding reduced intramolecular charge transfer or ICT process from the amino group to the pyridinium nitrogen group resulting in the enhancement of fluorescence intensities at short wavelength as a function of cyanide concentrations.

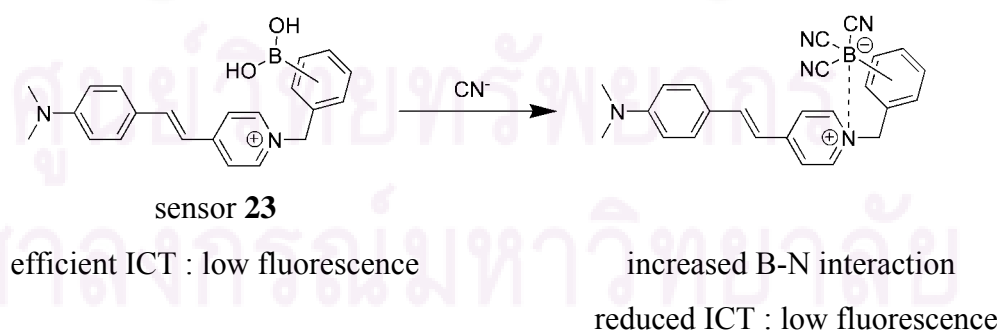


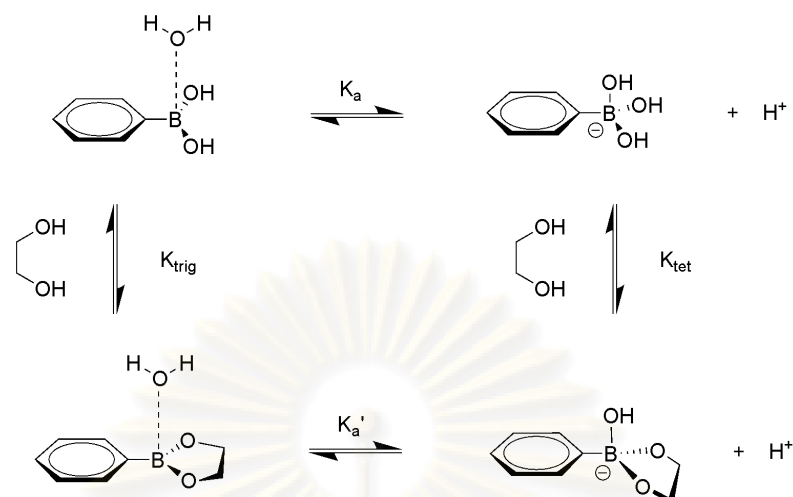
Figure 1.14 Structures of sensor **23** and mechanism of fluorescence enhancement of sensors upon cyanide binding

1.4 Literature reviews of boronic based sensors for saccharides and their derivatives

Saccharides and their derivatives play ubiquitous roles in many systems. They endow in many functions such as structural rigidity in the form of cellulose and energy storage in the form of starch and glycogen. [58, 59] For medical perspectives, the monitoring of D-glucose or simple monosaccharides is very important in the medical diagnosis. Therefore, the development of synthetic chemosensors for the recognition of saccharides and their derivatives has attracted chemist's attention since the last decade. [58]

In the last 20 years, boronic acid has been used as recognition site in a number of synthetic saccharide sensors and their derivatives. [5, 58-61] Diol of saccharide formed a tight complex with boronic acid as shown in Scheme 1.2. [62-66] Although, boronic acid and boronate anion reversibly interacted with diol of saccharide, experimental observation showed that the rate of this reaction was fastest in aqueous basic media at which the boron existed in tetrahedral anionic form ($k_{\text{tet}} > k_{\text{tri}} \cong 10^4$). Furthermore, the neutral boronic acid became more acidic upon binding, in other word the boronic ester was more acidic than boronic acid ($pK_a > pK_a'$). [62-66]

In many boronic sensing sensors, the saccharide recognition event is monitored using fluorescence spectrophotometry due to its superb sensitivity. A simple mechanism of boronic acid-saccharide fluorescence sensing system involved two factors: i) acid-base interactions of the boron group and amino group induced the spectral changes based on photoinduced electron transfer (PET) [5,59] and ii) differences between the electron-withdrawing and electron-donating properties of boronic group upon the binding induced spectral changes based on internal charge transfer (ICT). [61]



Scheme 1.2 The equilibrium of boronic acid interacts with diol in a aqueous media. [64]

1.4.1 Fluorescence sensors for saccharide based on photoinduced electron transfer (PET)

Basic strategy for designing PET based sensors is accomplished by connecting boronic acid and a fluorophore with a spacer containing tertiary amine in an appropriate position. The amine-boronic acid (N-B) interaction provides many advantages. This interaction decreased pK_a of boronic acid causing boronic acid to bind with diol at neutral pH with a fast reaction rate. Importantly, complexations of boronic acid with saccharides strengthen the N-B interactions and consequently disrupt the PET process resulting in intensification of the fluorescence intensity.[5,58]

The first fluorescence PET sensor **24** [67, 68] based on amine-boronic acid (N-B) modulation was reported by Shinkai and James *et al.* in 1994. As illustrated in Figure 1.15, the sensors utilized N-B interactions which were strengthened upon saccharide binding to inhibit PET process resulting in fluorescence enhancement of anthracene. According to the assistance of adjacent nitrogen atom, this sensor capably functioned in a large pH range in aqueous media upon the saccharide binding as low as pH 6.4.

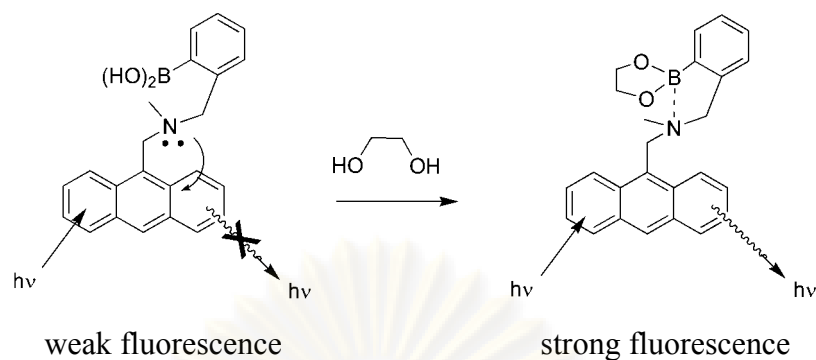


Figure 1.15 Illustration of anthracene-based photoinduced electron transfer system of sensor **24**

Recently, Mohr *et al.* [69] have demonstrated a new water-soluble fluorescence sensor based on naphthalimide and amino-phenyl boronic acid, sensor **25** (Figure 1.16). This sensor showed sensitivity in the mM range for saccharide detection in physiological pH.

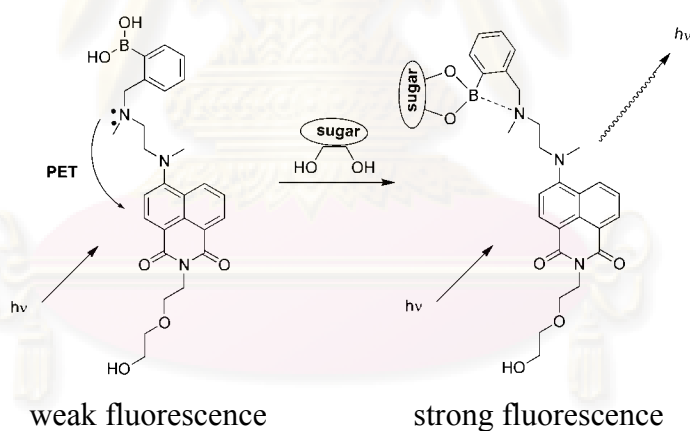


Figure 1.16 Structure of the sensor **25** and esterification causing an increasing of fluorescence intensity

The next generation of saccharide sensor **26** based on PET mechanisms was developed by Shinkai and James *et al.* (Figure 1.17). [70] This sensor composed of diboronic acid in order to improve selectivity for specific saccharides. Sensor **26** possessed a cleft-like structure that was particularly selective and sensitive to glucose. It was found that the diboronic initially bound with pyranose of D-glucose and then

the thermodynamic conversion of pyranose form to furanose form occurred slowly. [71]

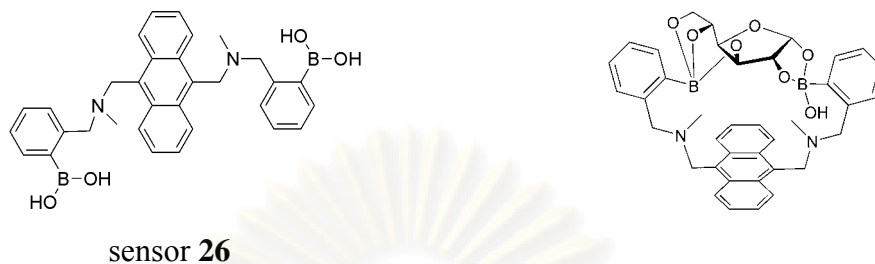


Figure 1.17 Structure of the sensor **26** and a thermodynamic structure of 1:1 complex of sensor **26** with furanose form of D-glucose.

Selectivity of fluorescence sensor in this class stemmed from the linker between two boronic groups providing the effective binding pocket for particular saccharide or their derivatives. Jame *et. el.* [72,73] demonstrated the sensor **27** containing a chiral center on the linker as a highly enantioselective, chemoselective, and sensitive fluorescence sensor for sugar acid such as tartaric acid.

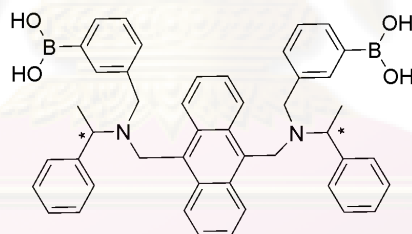


Figure 1.18 Structure of sensor **27**

1.4.2 Fluorescence sensors for saccharide based on intramolecular charge transfer (ICT)

In the application of chemosensor, interactions of guests toward acceptors or donor sites of ICT dyes induced changes in ICT efficiency of dyes resulting in changes in their optical properties. Due to the alternation between electron acceptor and electron donors of the boron center upon the hybridization change, this property caused boronic acid possibly to be ICT based sensors for saccharide.

The first generation of the ICT sensors was introduced by Shinkai as displayed in Figure 1.19. [74] Sensor **28** possessed stilbene scaffold as a large π -conjugative system and one of the terminal sites possessed boronic acid as a binding site for saccharide. The other terminal site possessed an amine group as an electron donor. This sensor showed the blue shift of emission spectra upon the changing of pH from high to low. This phenomenon was due to the loss of electron acceptor abilities of the boron upon hybridization changes from sp^2 of neutral form to sp^3 of an anionic form.

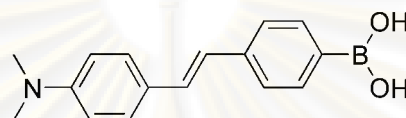


Figure 1.19 Structure of ICT based sensor **28**

Dicesare and Lakowicz *et al.* [75] developed systematic series of five different stilbene derivatives combining the boronic acid group in position 4 and donor or acceptor groups in position 4' as shown in Figure 1.20. In the case of sensor **28**, the loss of electron acceptability properties of the boron sensor upon the conversion of sp^2 to sp^3 hybridization was verified by changing of pH from low to high. This change induced a blue shift of about 50 nm and an increase of intensity in the emission spectrum due to the loss of charge transfer effect. This phenomenon was also observed by the addition of a saccharide.

Conversely, by the changing of pH from low to high sensor **33** showed a red shift of about 35 nm concomitant with a decreasing of fluorescence intensity. The fluorescence properties of this sensor was attributed to the hybridization changes of the boron allowing the ICT process possessed between the boron donor and the cyano acceptor. Furthermore, this phenomenon was also observed in the presence of saccharides. In addition, Dicesare and Lakowicz has prepared a number of analogous ICT system including chalcones, [76] oxazoline, [77] and BODIPY.[78]

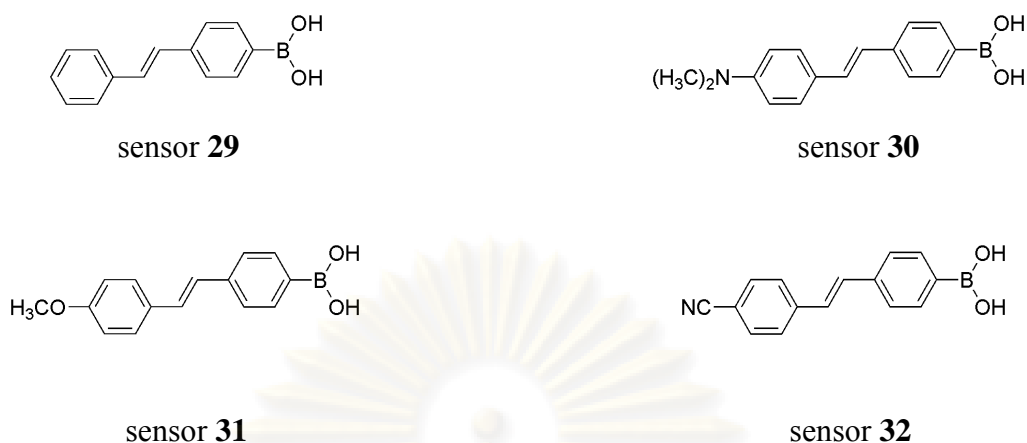


Figure 1.20 Structures of ICT based sensor **29-32**

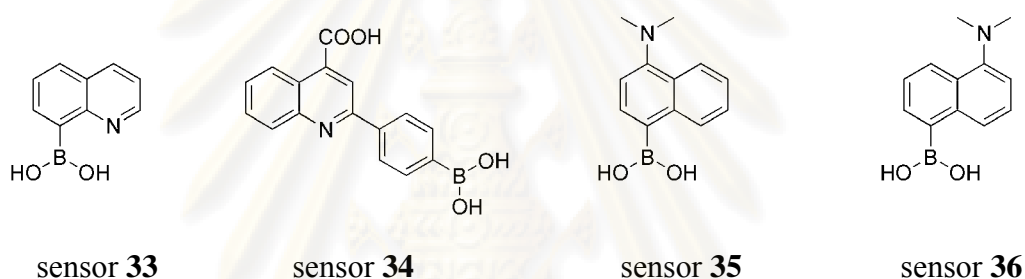


Figure 1.21 Structures of fluorescence sensors **33-36** of Wang Lab

As presented in Figure 1.21, Wang group has developed a number of simple naphthalene based sensors [79-81] for applications of boronolectins. Wang have been focused on water-soluble fluorescence boronic acid based sensors that showed more “biocompatible” properties such as long excitation/emission wavelength, high chemical/photophysical stability. The sensors in this group utilized the alternation of ICT efficiency to produce the changes in fluorescence spectra upon the saccharide binding. For example, sensor **35** [79] revealed the large fluorescence enhancement upon the addition of 50 mM fructose in aqueous phosphate buffer at pH 7.4. In this compound, the electron acceptor boron atom and electron-donating amino group were attached to the same aromatic ring which set up for intramolecular charge transfer resulting in low fluorescence intensities in the absence of sugar. Upon the ionization state change, the ICT state was turned “off” upon the binding with saccharide resulting in the increasing of fluorescence intensity. Conversely, ratiometric sensor **36** [79] which possessed boronic acid and amino group in different aromatic rings showed the

fluorescence intensity changes in the opposite direction at two wavelengths, 513 nm and 433 nm upon the addition of saccharide.

1.5 Objective and scope of this dissertation

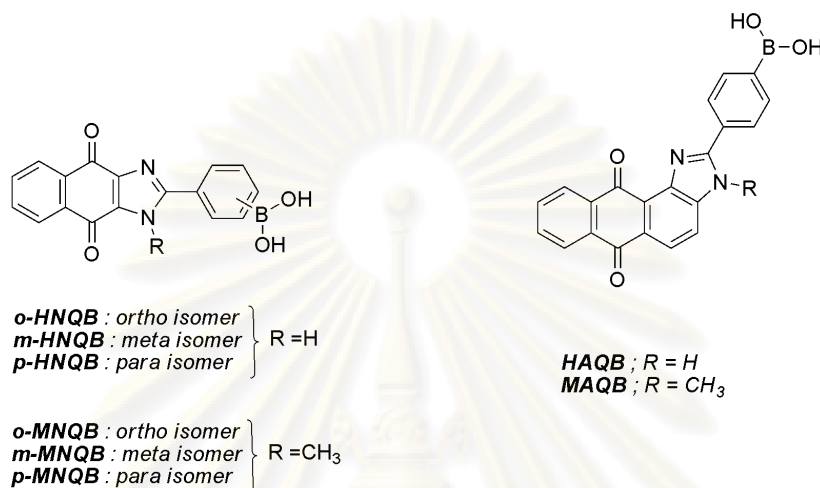


Figure 1.22 Structures of designed receptors based on quinone and boronic acid

An ultimate goal in this work is to develop effective fluorescence sensors for particular analytes especially anions and neutral guests. We intend to utilize moderate Lewis acid properties of boronic acid for the recognition in the aqueous sensing applications. Regarding to signaling output, this work focused on fluorescence spectrophotometry due to its high sensitivity. As displayed in Figure 1.22, eight target sensors were designed using acceptor-donor-acceptor (A-D-A) system by connecting quinone including naphthoquinone and anthraquinone with boronic acid using imidazole as spacer. Quinone coupling with imidazole groups was expected to be a main A-D system. Besides the main function of boronic acid as binding site, it was expected to be a complementary electron acceptor site.

The sensing properties of all synthesized compounds were evaluated using fluorescence spectrophotometry in DMSO, DMSO:H₂O and the micellar systems. Other techniques such as ¹H-NMR, ¹⁹F-NMR are also used to study properties of complexes. Moreover, computer calculations are also carried out to explain of signal transduction and the reactivity of the sensors.

CHAPTER II

EXPERIMENTAL

2.1 Synthesis of boronic based receptors

2.1.1 Analytical measurements and materials

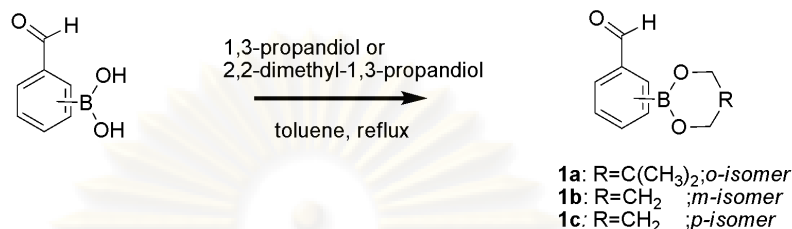
Nuclear Magnetic Resonance (NMR) spectra were recorded on a Varian Mercury Plus 400 NMR spectrometer. All chemical shifts were reported in part per million (ppm) using the residual proton or carbon signal in deuterated solvents as internal references. Elemental analysis was carried out on CHNS/O analyzer (Perkin Elmers PE2400 series II) by ignition combustion gas chromatography separated by frontal analysis and qualitative detected by thermal conductivity detector. MALDI-TOF mass spectra were carried out on Bruker Daltonics MALDI-TOF using 2-cyano-4-hydroxy cinnamic acid (CCA) as matrix.

All materials and solvents chemicals were purchased from Aldrich, Fluka and Merck as standard analytical grade, and were used without further purification. Commercial grade solvents such as dichloromethane, ethyl acetate, hexane, and methanol were purified by distillation. Anhydrous solvents such as acetonitrile and toluene were dried over CaH_2 and freshly distilled under nitrogen atmosphere. Thin-layer chromatography (TLC) was performed on silica gel plates (Kieselgel 60 F₂₅₄, 1 mm, Merck).

ศูนย์วิทยทรัพยากร
จุฬาลงกรณ์มหาวิทยาลัย

2.1.2 Experimental procedure

2.1.2.1 Preparation of propane-1,3-dilyl-fomylboronate (1a-c)



Into a two-neck round bottom flask equipped with a magnetic bar and a Dean-Stark equipment to remove water, corresponding formyl boronic acid (0.750 g, 5 mmol) and 2,2 -dimethyl-1,3-propanediol (0.520 g, 5 m mol) or 1,3 -propanediol (0.380 g, 5 m mol) were heated at reflux in toluene (100 m L) for 12 hours. Subsequently, the solvent was evaporated under reduced pressure to give a crude product as clear oil for *ortho* isomer, **1a**, and as a white solid for *meta* isomer, **1b**, and *para* isomer, **1c**, isomers. The crude product was used in the next step without purification.

Characterization data for 1a, 1b and 1c

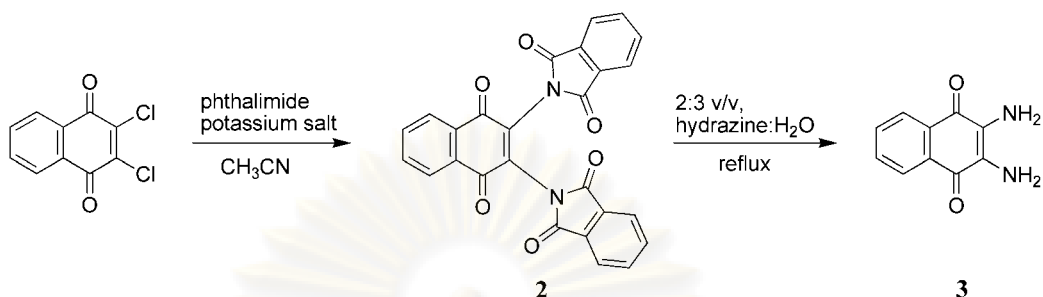
¹H NMR spectrum (400 MHz, CDCl₃) : δ (in ppm)

Compound 1a : δ = 10.46 (s, 1H, CHO), 7.92 (d, 1H, *J* = 8.0 Hz, ArH), 7.81 (d, 1H, *J* = 7.2 Hz, ArH), 7.55 (m, 2H, ArH), 3.82 (s, 4H, OCH₂), 1.08 (s, 6HC(CH₃)₂). (Figure A.1)

Compound 1b : δ = 10.04 (s, 1H, CHO), 8.30 (s, 1H, ArH), 8.06 (d, *J* = 7.6 Hz, 1H, ArH), 7.95 (d, *J* = 8.0 Hz, 1H, ArH), 7.51 (t, *J* = 7.5 Hz, 1H, ArH), 4.20 (t, *J* = 5.2 Hz, 4H, OCH₂), 2.10 (t, *J* = 5.6 Hz, 2H, OCH₂CH₂CH₂O). (Figure A.2)

Compound 1c : δ = 10.03 (s, 1H, CHO), 7.91-7.84 (dd, *J* = 2.6, 7.6 Hz, 2H, ArH), 4.18 (t, *J* = 5.2 Hz, 4H, OCH₂), 2.08 (t, *J* = 5.6 Hz, 2H, OCH₂CH₂CH₂O). (Figure A.3)

2.1.2.2 Preparation of 2,3-diaminonaphthalene-1,4-dione (**3**) [82]



Into a two-neck round bottom flask equipped with a magnetic bar, 2,3-dichloro-1,4-naphthoquinone (6.81 g, 30 mmol) and phthalimide potassium salt (11.11 g, 30 mmol) were stirred and heated at reflux in acetonitrile (75 mL) under nitrogen atmosphere for 12 hours to afford a yellow precipitate. The yellow precipitate was filtered and washed with 1:1 of H₂O:methanol to give diphthalimide naphthoquinone, **2** (8.961 g, 66%). Subsequently, the reduction of diphthalimide derivative was carried out in refluxing of 2:3 v/v hydrazine in water (45 mL) for 4 hours to give a deep purple precipitate. The precipitate was filtered and washed with water. The filtered was extracted with dichloromethane and washed with water. The organic layer was dried over sodium sulfate anhydrous, filtered and evaporated to dryness providing the product 2,3-diaminonaphthalene-1,4-dione. The collected product was dried *in vacuo* (**3**, 98%).

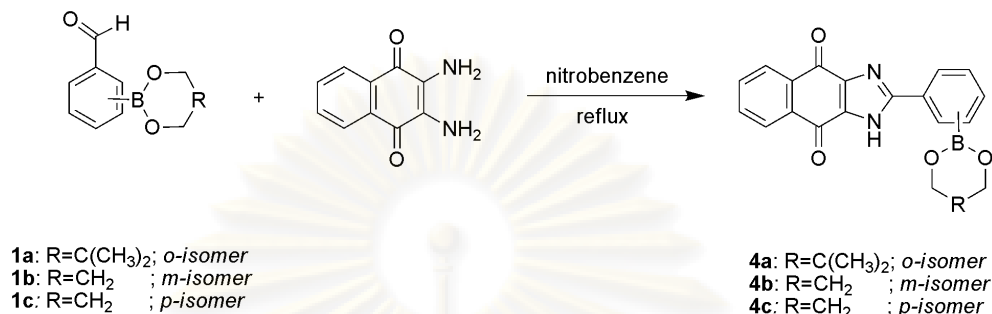
Characterization data for **2** and **3**

¹H NMR spectrum (400 MHz, CDCl₃): δ (in ppm)

Compound 2: δ = 8.23 (m, 2H, OCArH), 7.87 (m, 4H, NOCArH), 7.85 (m, 2H, ArH), 7.76 (m, 4H, ArH) (Figure A.4)

Compound 3: δ = 7.91 (dd, *J* = 3.2, 5.2 Hz, 2H, OCArH), 7.521 (dd, *J* = 3.2, 5.2 Hz, 2H, ArH) (Figure A.5)

2.1.2.3 Preparation of 2-(1,3,2-dioxaborinan-2-yl)phenyl)-1H-naphtho[2,3-d]imidazole-4,9-dione (**4a-c**) [83]



Into a two-neck round bottom flask equipped with a magnetic bar, the corresponding formyl phenylboronate ester (5 mmol) in nitrobenzene (25 mL) was added dropwise to a solution of 2,3-diamino-1,4-naphthoquinone (0.940 g, 5 mmol) in nitrobenzene (75 mL). The reaction mixture was slowly heated up to 150 °C for 12 h under nitrogen atmosphere. The solution was cooled to room temperature and then the precipitate was slowly formed. The precipitate was filtered and washed with diethylether to give a yellow solid of corresponding heterocyclic protecting products (**4a** 29%, **4b** 45% and **4c** 71%).

Characterization data for **4a**, **4b** and **4c**

Compound **4a** :

¹H NMR (400 MHz, DMSO-*d*₆) δ (in ppm):

δ = 14.40 (broad, 1H, **NH**), 8.12 (m, 3H, **ArH**), 7.84 (m, 2H, **ArH**), 7.47 (m, 3H, **ArH**), 3.74 (s, 4H, **OCH₂**), 1.06 (s, 6H, **C(CH₃)₂**) (Figure A.6)

¹³C-NMR (100.6 MHz, DMSO-*d*₆) δ (in ppm)

δ = 154.0, 134.3, 133.2, 131.7, 131.0, 130.1, 128.9, 126.7, 126.7, 125.9, 72.0, 31.7, 22.3 (Figure A.7)

Elemental Analysis: Anal. Calcd. for C₂₂H₁₉BN₂O₄: C, 68.42; H, 4.96; N, 7.25.

Found: C, 67.99; H, 4.82; N, 7.55.

EI-MS *m/z* for (M + 2H)⁺ = 387.15

Compound 4b :¹H-NMR (400 MHz, DMSO-*d*₆)

δ = 14.42 (s, 1H, NH), 8.57 (s, 1H, ArH), 8.26 (d, J = 7.6 Hz, 1H, ArH), 8.083 (m, 2H, ArH), 7.83 (m, 2H, ArH), 7.77 (d, J = 7.6 Hz, 1H, ArH), 7.50 (t, J = 7.2 Hz, 1H, ArH), 4.14 (t, J = 4.8 Hz, 4H, OCH₂), 2.02 (t, J = 5.2 Hz, 2H, OCH₂CH₂CH₂O) (Figure A.8)

¹³C-NMR (100.6 MHz, DMSO-*d*₆) δ (in ppm)

δ = 179.1, 166.7, 152.9, 136.6, 135.8, 135.8, 134.5, 134.4, 134.4, 134.4, 134.3, 134.3, 134.2, 134.2, 132.6, 129.2, 128.6, 128.2, 127.0, 126.9, 62.5, 27.3 (Figure A.9)

Elemental Analysis: Anal. Calcd. for C₂₂H₁₉BN₂O₄: C, 67.07; H, 4.22; N, 7.82.

Found: C, 66.96; H, 4.23; N, 7.88.

MALDI-TOF m/z for (M + 2H)⁺ = 359.64**Compound 4c :**¹H-NMR (400 MHz, DMSO-*d*₆) δ (in ppm)

δ = 14.39 (s, 1H, NH), 8.19 (d, J = 8.5 Hz, 2H, ArH), 8.09 (m, 2H, ArH), 7.49 (m, 2H, ArH), 7.78 (d, J = 8.0 Hz, 2H, ArH), 4.12 (t, J = 4.1 Hz, 4H, OCH₂), 2.01 (t, J = 5.2 Hz, 2H, OCH₂CH₂CH₂O). (Figure A.10)

¹³C-NMR (100.6 MHz, DMSO-*d*₆) δ (in ppm)

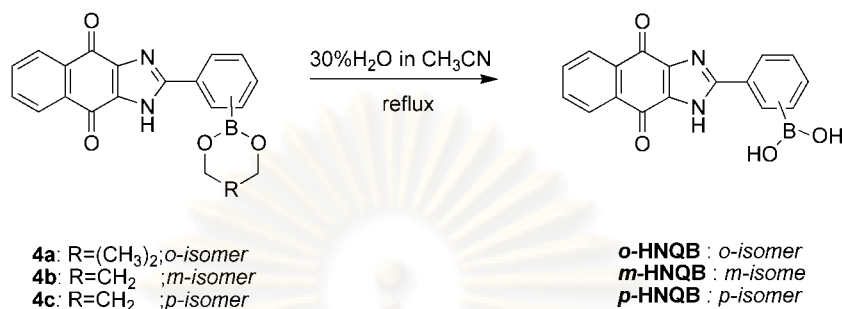
δ = 152.7, 134.4, 134.4, 134.3, 134.2, 130.7, 127.1, 126.4, 126.3, 62.0, 27.3. (Figure A.11)

Elemental Analysis: Anal. Calcd. for C₂₂H₁₉BN₂O₄: C, 67.07; H, 4.22; N, 7.82.

Found: C, 67.06; H, 4.59; N, 7.76.

MALDI-TOF m/z for (M + H)⁺ = 358.63

2.1.2.4 Preparation of (4,9-dioxo-4,9-dihydro-1H-naphtho[2,3-d]imidazol-2-yl)phenylboronic acid (*o*-HNQB, *m*-HNQB and *p*-HNQB)



Protecting groups of 2-(1,3,2-Dioxaborinan-2-yl)phenyl)-1H-naphtho[2,3-d]imidazole-4,9-dione (**4a**, **4b** or **4c**) (5 mmol) were removed by refluxing in 50 mL of 30% H₂O:CH₃CN. The yellow solid of product was filtered off and washed with diethylether to provide a desired product in a quantitative yield.

Characterization data for *o*-HNQB, *m*-HNQB and *p*-HNQB

Compound *o*-HNQB:

¹H-NMR (400 MHz, DMSO-*d*₆) δ (in ppm)

δ = 14.39 (s, 1H, NH), 8.97 (b, 1H, BOH), 8.21 (b, 1H, BOH), 8.09 (t, *J*_{H_z} = 8.1, 1H, ArH), 7.93 (d, *J*_{H_z} = 7.9, 2H, ArH), 7.85 (t, *J*_{H_z} = 7.8, 2H, ArH), 7.65 (d, *J*_{H_z} = 7.7, 1H, ArH), 7.48 (t, *J*_{H_z} = 7.5, 1H, ArH) (Figure A.12)

¹³C-NMR (100.6 MHz, DMSO-*d*₆) δ (in ppm)

δ = 154.93, 138.12, 138.10, 138.05, 134.57, 134.32, 133.03, 133.89, 129.81, 129.17, 128.27, 126.94 (Figure A.13)

Elemental Analysis: Anal. Calcd. for C₁₇H₁₁BN₂O₄: C, 64.19; H, 3.49; N, 8.81.

Found: C, 64.29; H, 3.41; N, 8.93.

MADI-TOF: *m/z* for (M + H)⁺ = 318.00

Compound *m*-HNQB:¹H-NMR (400 MHz, DMSO-*d*₆) δ (in ppm)

δ = 14.34 (s, 2H, **NH**), 8.67 (s, 2H, **BOH**), 8.25 (d, $J_{Hz} = 8.2$, 2H, **ArH**), 8.08 (t, $J_{Hz} = 8.1$, 2H, **ArH**), 7.94 (d, $J_{Hz} = 7.9$, 2H, **ArH**), 7.83 (d, $J_{Hz} = 7.8$, 2H, **ArH**), 7.51 (t, $J_{Hz} = 7.5$, 2H, **ArH**) (Figure A.14)

¹³C-NMR (100.6 MHz, DMSO-*d*₆) δ (in ppm)

δ = 179.01, 175.93, 153.30, 136.60, 135.76, 135.57, 135.51, 134.42, 134.27, 133.52, 133.22, 128.67, 128.47, 128.39, 128.14, 126.89, 126.84, 126.82, 126.79, 126.75, 126.72, 126.69, 126.64, 126.50 (Figure A.15)

Elemental Analysis: Anal. Calcd. for C₁₇H₁₁BN₂O₄: C, 64.19; H, 3.49; N, 8.81.

Found : C, 64.27; H, 3.49; N, 8.94.

MADI-TOF : m/z for (M+2H)⁺ = 319.0**Compound *p*-HNQB :**¹H-NMR (400 MHz, DMSO-*d*₆) δ (in ppm)

δ = 14.34 (s, 2H, **NH**), 8.22 (s, 2H, **BOH**), 8.19 (d, $J_{Hz} = 8.2$, 2H, **ArH**), 8.10 (t, $J_{Hz} = 8.1$, 2H, **ArH**), 7.93 (d, $J_{Hz} = 7.9$, 2H, **ArH**), 7.84 (d, $J_{Hz} = 7.8$, 2H, **ArH**). (Figure A.16)

¹³C-NMR (100.6 MHz, DMSO-*d*₆) δ (in ppm)

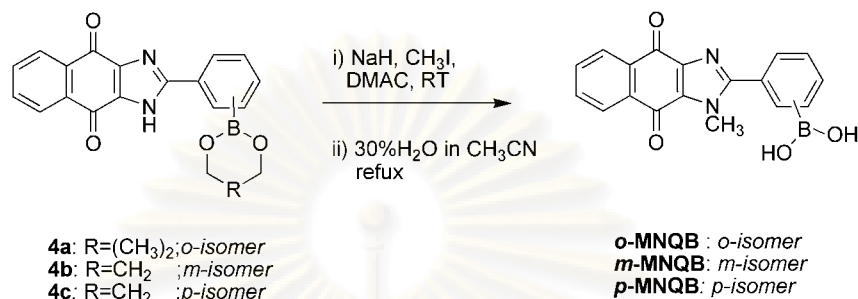
δ = 152.86, 135.22, 135.17, 135.13, 135.01, 134.29, 134.22, 133.26, 133.20, 130.22, 126.86, 126.82, 126.71, 126.30, 126.23, 126.21, 126.14 (Figure A.17)

Elemental Analysis: Anal. Calcd. for C₁₇H₁₁BN₂O₄: C, 64.19; H, 3.49; N, 8.81.

Found : C, 63.60; H, 3.85; N, 8.66.

MADI-TOF: m/z for (M+2H)⁺ = 319.0

2.1.2.5 Preparation of 4-(1-methyl-4,9-dioxo-4,9-dihydro-1H-naphtho [2,3-d]imidazol-2-yl) phenylboronic acid (*o*-MNQB, *m*-MNQB and *p*-MNQB)



2-(1,3,2-Dioxaborinan-2-yl)phenyl)-1H-naphtho[2,3-d]imidazole-4,9-dione (**4a**, **4b** or **4c**) (5 mmol) and NaH (0.132 g, 5.5 mmol) were charged with 25 mL of *N,N*-dimethylacetamide under nitrogen. Methyl iodide (343 μ L, 5.5 mmol) was added to the reaction mixture via micro syringe. The reaction mixture was stirred at room temperature for 2 days. The solvent was removed under vacuum to give the solid of methylated products. The protecting group was removed by refluxing in 30% H₂O:CH₃CN. The solution was filtered and washed with diethylether to give yellow solids of desired products. (*o*-MNQB 20%, *m*-MNQB 40% and *p*-MNQB 35%).

Characterization data for *o*-MNQB, *m*-MNQB and *p*-MNQB

Compound *o*-MNQB :

¹H-NMR (400 MHz, DMSO-*d*₆) δ (in ppm)

δ = 8.11 (m, 2H, ArH), 8.01 (s, 2H, BOH), 7.87 (m, 2H, ArH), 7.77 (m, 1H, ArH), 7.54 (m, 3H, ArH), 3.84 (s, 3H, NCH₃). (Figure A.18)

¹³C-NMR (100.6 MHz, DMSO-*d*₆) (in ppm)

δ = 178.9, 174.4, 157.0, 142.6, 134.6, 134.5, 134.4, 133.1, 132.7, 129.8, 129.6, 126.8, 126.6, 34.3. (Figure A.19)

Elemental Analysis: Anal. Calcd. for: C₁₈H₁₃BN₂O₄ : C, 65.10; H, 3.95; N, 8.43.

Found: C, 65.27; H, 3.98; N, 8.48.

MADI-TOF: m/z for (M + 3H)⁺ = 334.66.

Compound *m*-MNQB :¹H-NMR (400 MHz, DMSO-*d*₆) δ (in ppm)

δ = 8.29 (s, 2H, BOH), 8.21 (s, 1H, ArH), 8.09(d, *J* = 8.1 Hz, 2H, ArH),
 7.99(d, *J* = 8.0 Hz, 2H, ArH), 7.86 (t, *J* = 7.5, 1H, ArH), 7.86 (d, *J* = 7.8, 1H, ArH),
 7.56 (t, *J* = 7.5, 1H, ArH), 4.06 (s, 3H, NCH₃). (Figure A.20)

¹³C-NMR (100.6 MHz, DMSO-*d*₆) δ (in ppm)

δ = 178.9, 176.4, 154.9, 143.0, 136.5, 135.5, 134.5, 134.3, 133.8, 133.3, 132.9,
 131.3, 128.3, 127.8, 126.8, 126.6, 34.8. (Figure A.21)

Elemental Analysis: Anal. Calcd. for: C₁₈H₁₃BN₂O₄ : C, 65.10; H, 3.95; N, 8.43.

Found : C, 65.28; H, 3.90; N, 8.48.

MADI-TOF : m/z for (M)⁺ = 331.60.**Compound *p*-MNQB:**¹H-NMR (400 MHz, DMSO-*d*₆) δ (in ppm)

δ = 8.23 (s, 2H, BOH), 8.09 (t, *J* = 8.0 Hz, 2H, ArH), 7.98 (d, *J* = 8.0 Hz,
 2H, ArH), 7.86 (t, *J* = 7.8, 2H, ArH), 7.78 (d, *J* = 7.76, 2H, ArH), 4.08 (s, 3H, NCH₃).
 (Figure A.22)

¹³C-NMR (100.6 MHz, DMSO-*d*₆) δ (in ppm)

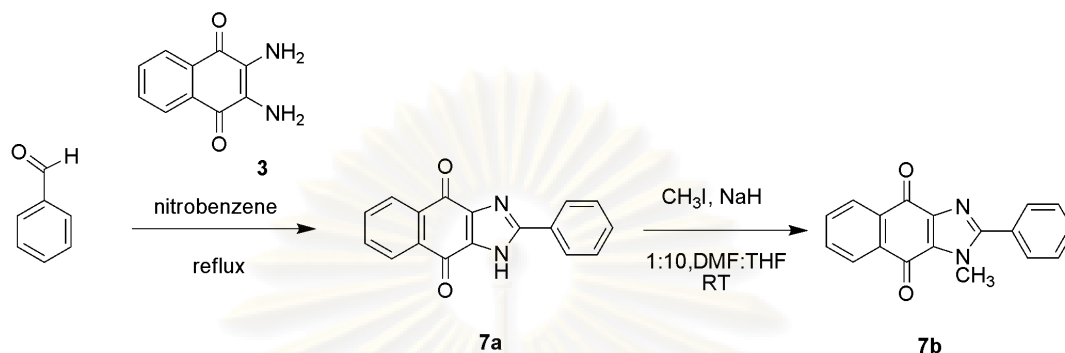
δ = 178.8, 176.4, 154.5, 143.0, 134.7, 134.5, 134.3, 133.8, 133.3, 132.8, 129.9,
 128.7, 126.8, 126.6, 34.8 (Figure A.23)

Elemental Analysis: Anal. Calcd. for: C₁₈H₁₃BN₂O₄ : C, 65.10; H, 3.95; N, 8.43.

Found : C, 65.07; H, 3.90; N, 8.56.

MADI-TOF: m/z for (M + H)⁺ = 332.39.

2.1.2.6 Preparation of 1-methyl-2-phenyl-1H-naphtho[2,3-d]imidazole-4,9-dione, **7b**



Benzaldehyde (0.212 g, 2 mmol) in nitrobenzene (20 mL) was added dropwise to a solution of 2,3-diamino-1,4-naphthoquinone (0.376 g, 2 mmol) in nitrobenzene (20 mL). The reaction mixture was heated at 150 °C and stirred for 12 hours under nitrogen atmosphere. The solution was cooled to room temperature and then the brown precipitation slowly formed. The precipitate was filtered and washed with diethylether to obtain 2-phenyl-1H-naphtho[2,3-d]imidazole-4,9-dione, **7a**. Compound **7a** (0.274 g, 1.0 mmol) and NaH (34 mg, 1.5 mmol) were stirred in 30 mL of 1:10; DMF:THF. Subsequently, methyl iodide (77 μL , 1.5 mmol) was added to the reaction mixture via a micro syringe. The reaction mixture was stirred at room temperature for 1 day. The solvent was removed under vacuum to give the solid of methyl protected product **7b** as bright yellow solid in 94% yield.

Characterization data for **7a** and **7b**

Compound **7a**:

$^1\text{H-NMR}$ (400 MHz, $\text{DMSO-}d_6$)

δ = 8.20 (m, 2H, ArH), 8.07 (m, 2H, ArH), 7.76 (m, 2H, ArH), 7.76 (m, 3H, ArH) (Figure A.24)

Compound **7b**:

$^1\text{H-NMR}$ (400 MHz, $\text{DMSO-}d_6$)

δ = 8.05 (m, 2H, ArH), 7.82 (m, 4H, ArH), 7.58 (m, 3H, ArH), 4.03 (s, 3H, NCH_3). (Figure A.25)

^{13}C -NMR (100.6 MHz, $\text{DMSO-}d_6$)

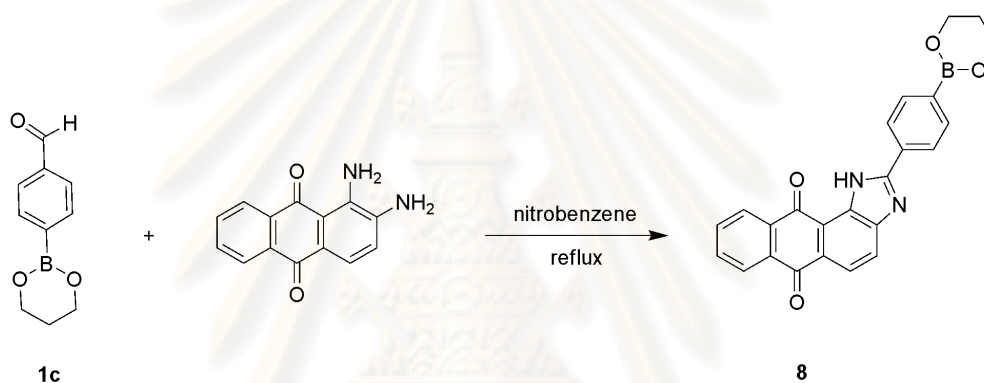
$\delta = 178.8, 176.4, 154.5, 142.9, 134.5, 134.3, 133.7, 133.2, 132.8, 130.9, 129.8, 129.3, 128.6, 126.8, 126.6, 34.7$ (Figure A.25)

Elemental Analysis: Anal. Calcd. for: $\text{C}_{18}\text{H}_{12}\text{N}_2\text{O}_2$: C, 74.99; H, 4.20; N, 9.72.

Found: C, 74.96; H, 4.14; N, 9.79

MADI-TOF: m/z for $(\text{M} + 2\text{H})^+ = 274.56$

2.1.2.7 Preparation 2-(4-(1,3,2-dioxaborinan-2-yl)phenyl)-3H-anthra[1,2-d]imidazole-6,11-dione, **8**



Into a two-neck round bottom flask equipped with a magnetic bar, the corresponding 4-formyl phenylboronate ester (5 mmol) in nitrobenzene (25 mL) was added dropwise to a solution of 1,2-diamino-1,4-anthraquinone (0.940 g, 5 mmol) in nitrobenzene (75 mL). The reaction mixture was slowly heated up to 150 °C for 24 h under nitrogen atmosphere. The solution was cooled to room temperature and then the precipitate slowly formed. The precipitate was filtered and washed with diethylether to give a yellow solid of the protecting product (**8**, 70%).

Characterization data for **8** :

^1H -NMR (400 MHz, CDCl_3)

$\delta = 11.35$ (s, 1H, **NH**), 8.35 (dd, 2H, $J = 26, 2.8$ Hz, **ArH**), 8.25(d, 1H, $J = 8.4$ Hz, **ArH**), 8.14(m, 2H, **ArH**), 8.12 (s, 1H, **ArH**), 7.97 (d, 2H, $J = 8.0$ Hz, **ArH**), 7.81 (t, 2H, $J = 3.6$ Hz, **ArH**), 4.21(t, 4H, $J = 5.6$ Hz, OCH_2CH_2), 2.11(t, 2H, $J = 5.6$ Hz, $\text{OCH}_2\text{CH}_2\text{CH}_2\text{O}$) (Figure A.28)

^{13}C -NMR (100.6 MHz, $\text{DMSO-}d_6$)

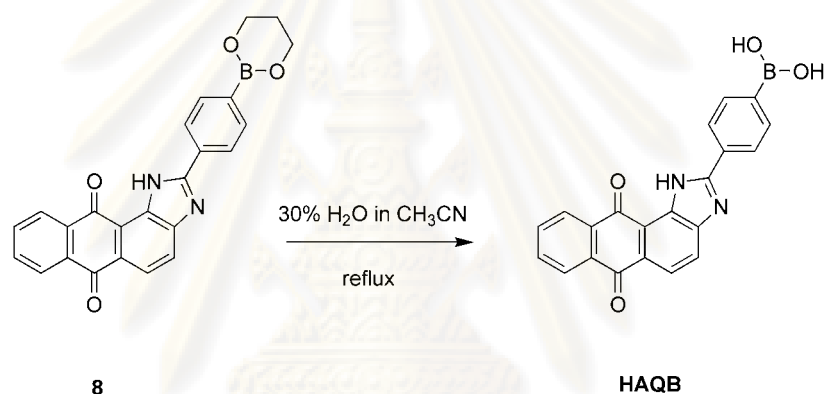
$\delta = 152.8, 152.7, 135.0, 134.4, 134.2, 132.7, 130.7, 130.2, 126.3, 126.1, 62.0, 58.3, 36.2$ (Figure A.29)

Elemental Analysis: Anal. Calcd. for: $\text{C}_{24}\text{H}_{17}\text{BN}_2\text{O}_4$: C, 70.61; H, 4.20; N, 6.86.

Found: C, 62.43; H, 4.26; N, 6.81

MADI-TOF: m/z for $(\text{M} + 2\text{H})^+ = 408.12$ g/mol

2.1.2.8 Preparation 4-(6,11-dioxo-6,11-dihydro-3H-anthra[1,2-d]imidazol-2-yl)phenylboronic acid, HAQB



The protecting group of 2-(4-(1,3,2-dioxaborinan-2-yl)phenyl)-3H-anthra[1,2-d]imidazole-6,11-dione (**8**) (5 mmol) was removed by refluxing in 50 mL of 30% $\text{H}_2\text{O}:\text{CH}_3\text{CN}$. The yellow solid was filtered off and washed with diethylether to give a product in the quantitative yield.

Characterization data for HAQB :

^1H -NMR (400 MHz, $\text{DMSO-}d_6$)

$\delta = 12.97$ (s, 1H, **NH**), 8.34 (d, 1H, $J = 7.6$ Hz, **ArH**), 8.26 (s, 2H, **BOH**), 8.06 (m, 2H, **ArH**), 7.96 (m, 4H, **ArH**), 7.80 (m, 2H, **ArH**) (Figure A.30)

^{13}C -NMR (100.6 MHz, $\text{DMSO-}d_6$)

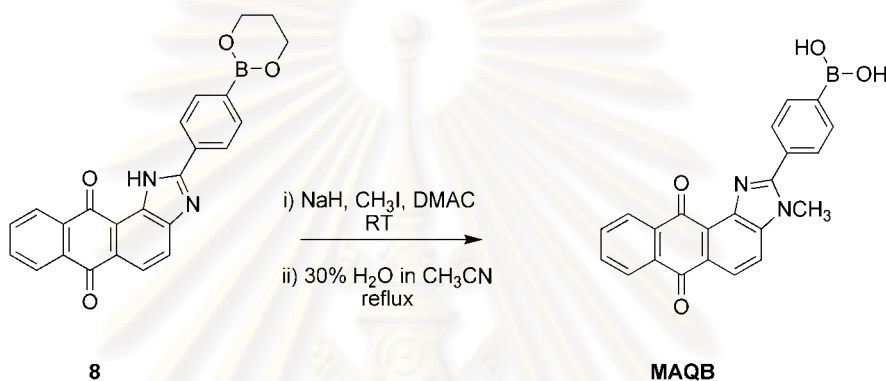
$\delta = 183.37, 182.56, 158.60, 137.53, 134.76, 134.54, 133.36, 133.23, 133.160, 128.33, 127.47, 127.09, 126.50, 125.27, 121.33, 118.91$ (Figure A.31)

Elemental Analysis: Anal. Calcd. for: C₂₁H₁₃N₂O₄: C, 68.51; H, 3.56; N, 7.61

Found: C, 68.57; H, 3.56; N, 7.62

MADI-TOF: m/z for (M + 2H)⁺ = 368.09

2.1.2.9 Preparation of 4-(3-methyl-6,11-dioxo-6,11-dihydro-3H-anthra[1,2-d]imidazol-2-yl)phenylboronic acid, MAQB



2-(4-(1,3,2-dioxaborinan-2-yl)phenyl)-3H-anthra[1,2-d]imidazole-6,11-dione (**8**) (0.5 mmol) and NaH (0.18 g, 0.75 mmol) were charged with 30 mL of *N,N*-dimethylacetamide under nitrogen. Methyl iodide (47 μ L, 0.75 mmol) was added to the reaction mixture via a micro syringe. The reaction mixture was stirred at room temperature for 2 days. The solvent was removed under vacuum to give the solid of methylated products with 45% yield. The protecting group was removed by refluxing in 30% H₂O:CH₃CN. The solution was filtered and washed with diethylether to obtain a yellow solid of the desired product in a quantitative yield.

Characterization data for MAQB:

¹H-NMR (400 MHz, DMSO-*d*₆) δ (in ppm)

δ = 8.31 (s, 2H, BOH), 8.17 (m, 4H, ArH), 8.01 (m, 2H, ArH), 7.90 (m, 4H, ArH), 3.98 (s, 3H, NCH₃). (Figure A.32)

¹³C-NMR (100.6 MHz, DMSO-*d*₆) (in ppm)

δ = 183.62, 183.47, 161.48, 158.88, 149.45, 142.96, 140.97, 135.60, 135.03, 134.95, 134.68, 134.48, 133.14, 131.23, 129.93, 127.26, 125.73, 123.92, 122.65, 117.27, 32.82. (Figure A.33)

Elemental Analysis: Anal. Calcd. for: $C_{22}H_{15}BN_2O_4$: C, 69.40; H, 3.96; N, 7.33.

Found: C, 68.94; H, 4.03; N, 7.34.

MADI-TOF: m/z for $(M + 3H)^+ = 382.11$.

2.2 The complexation studies of the protonated and methylated naphthoquinone imidazole based sensors

2.2.1 The complexation studies of the protonated sensors, *o*-HNQB, *m*-HNQB and *p*-HNQB

2.2.1.1 The complexation studies of sensors using $^1\text{H-NMR}$ techniques

Typically, 5.0 mM solution of sensors in DMSO- d_6 0.5 mL was prepared in NMR tubes (0.6 mL). A 0.05 mol/L stock solutions of various anionic guests including potassium salt of cyanide, acetate, benzoate, chloride, and iodide and tetrabutyl ammonium salt of fluoride in DMSO- d_6 was prepared in a small vial. Solutions of anions were added into NMR tubes according to the desired ratios.

2.2.1.2 The complexation studies of sensors using UV-Vis spectroscopic techniques

a) Screening test with excess anion experiments

Sensors were prepared in spectroscopic grade DMSO at concentrations of 3×10^{-4} mol/L. Eight potassium salts of anions including CN^- , AcO^- , BzO^- , H_2PO_4^- , NO_3^- , Cl^- , Br^- , and I^- and cesium fluoride were weighed as 30 equivalents of sensors (3×10^{-4} mol/L in 3.0 mL) and subsequently added as a solid into the 3.0 mL of sensor solution. The solution mixture was placed in a quartz cuvet with 100 mm path length, and UV-Vis spectra were recorded at 25°C.

b) The complexation studies of the sensor using UV-Vis titration experiments

Sensors were prepared in spectroscopic grade DMSO at concentrations of 3×10^{-4} mol/L. A stock solution of potassium salts of anions including CN^- , AcO^- and BzO^- and cesium fluoride (CsF) were prepared at concentrations of 3×10^{-3} mol/L in spectroscopic grade DMSO. 2.0 mL of sensor solution was placed in a 100.0 mm width quartz cell. The solution of anion was added directly to the sensor solution via microburet in various ratios (0-7 equivalents) and stirred for 30 second. UV-Vis spectra were recorded at 25°C after each addition.

2.2.1.3 The complexation studies of the sensor using fluorescence titration experiments

Sensors were prepared in spectroscopic grade DMSO at concentrations of 3×10^{-4} mol/L. A stock solution of potassium salts of anions including CN^- , AcO^- and BzO^- and cesium fluoride (CsF) were prepared as stock solution at concentrations of 3×10^{-3} mol/L in spectroscopic grade DMSO. 2.0 mL of sensor solution was placed in 100.0 mm width quartz cell. The solution of anions was added directly to the sensor solution via a microburet in various ratios (0-7 equivalents) and stirred for 30 second. Fluorescence spectra were recorded at 25°C after each addition under the following condition:

Start: 356 nm

End: 800 nm

Excitation: 346 nm

Excitation Slit: 5.0

Emission Slit: 5.0

Scan rate: 600 nm/min

2.2.2 The complexation studies of the methylated sensors, *o*-MNQB, *m*-MNQB and *p*-MNQB

2.2.2.1 The complexation studies of sensors using NMR techniques

a) The complexation studies toward F^- and CN^- using 1H -NMR spectroscopy

The solution of sensors in $DMSO-d_6$ was prepared in NMR tubes at concentration of 5×10^{-3} mol/L (0.6 mL) for *m*-MNQB and *p*-MNQB and of 1×10^{-3} mol/L (0.6 mL) for *o*-MNQB. Potassium cyanide and tetraammoniumbutyl fluoride were weighed as 1.95 mg and 9.45 mg (10 equivalents), respectively. The solid of anion salts was added directly to NMR tubes.

b) The fluoride complexation studies of sensor using ^{19}F -NMR spectroscopy

The 5×10^{-2} mol/L of the sensor solutions in $DMSO-d_6$ was prepared in NMR tubes (0.7 mL). The solid of tetraammoniumbutyl fluoride (3 equivalents) was added directly to NMR tubes.

2.2.2.2 The complexation studies using fluorescence spectrophotometry in DMSO

a) Screening test with various anions

Sensor *p*-MNQB was prepared in spectroscopic grade DMSO at concentrations of 3×10^{-4} mol/L. A solid of potassium salts of anions including CN^- , AcO^- and BzO^- and tetrabutylammonium fluoride was added to 3.0 mL of 3×10^{-4} mol/L sensors solution to give 500 equivalents of anions. Solution mixtures stood at room temperature 30 minutes before monitoring the fluorescence spectra under the following conditions:

Start: 360 nm
End: 800 nm
Excitation: 344 nm
Excitation Slit:10.0
Emission Slit:10.0
Scan rate: 120 nm/min

b) The complexation studies of the sensor using fluorescence titration experiments

Sensor *p*-MNQB was prepared in spectroscopic grade DMSO at concentrations of 3×10^{-4} mol/L. A stock solution of tetrabutylammonium fluoride (TBAF) was prepared at concentration of 0.60 mol/L in spectroscopic grade DMSO. 2.0 mL of sensor solution was placed in a 100.0 mm width quartz cell. The solution of TBAF was added to the sensor solution in various ratios (0-1500 equivalents). Fluorescence spectra were recorded at room temperature with 2 minutes stirring time under the following condition:

Start: 360 nm
End: 800 nm
Excitation: 344 nm
Excitation Slit:5.0
Emission Slit:5.0
Scan rate: 600 nm/min

ศูนย์วิทยทรัพยากร
จุฬาลงกรณ์มหาวิทยาลัย

2.2.2.3 The complexation studies by fluorescence spectrophotometry mixture of 1:1; DMSO:H₂O and 1:1; DMSO: HEPES buffer pH 7.4

a) Screening test of anions experiments

Typically, sensors were prepared as stock solution in spectroscopic grade DMSO at concentrations of 1×10^{-4} mol/L. A solid of potassium salts of anions (CN⁻, AcO⁻, BzO⁻, H₂PO₄⁻, NO₃⁻, ClO₄⁻, Cl⁻, Br⁻, SCN⁻ and I⁻) that quantity corresponded to 100 equivalents or 500 equivalents of anions was dissolved in 1.5 mL of 0.2 mol/L NaCl or 0.2 mol/L NaCl in HEPES buffer pH 7.4. The solution of sensors and anions was mixed together to give a final concentration of sensors at 5×10^{-5} mol/L with 100 and 500 equivalents of anions in 1:1; DMSO:H₂O and 1:1; DMSO: HEPES buffer pH 7.4, respectively. In the case of F⁻, a stock solution of sensors and KF were mixed to give a final concentration of sensors (5×10^{-5} mol/L) with 500 equivalent or 100 equivalents of F⁻ in 0.1 mol/L NaCl in 60% HEPES pH 7.4 : DMSO. The mixtures stood at room temperature for 30 minutes before monitoring fluorescence spectra under the following conditions:

Start: 364 nm

End: 800 nm

Excitation: 344 nm

Excitation Slit: 10.0

Emission Slit: 10.0

Scan rate: 120 nm/min

c) The cyanide complexation studies of the sensor using fluorescence titration experiments

Stock solutions of sensors (1.0×10^{-4} mol/L) were prepared in spectroscopic grade DMSO. A stock solution of KCN (0.25 mol/L) was prepared in 0.2 mol/L NaCl as supporting electrolyte in HEPES buffer pH 7.4. In a volumetric flask 5 mL, 2.5 mL of the stock solution of the sensor was mixed with the portion of the KCN stock solution in various ratios and then volume was adjusted with 0.2 M NaCl in H₂O or in HEPES buffer pH 7.4. Solution mixtures stood at room temperature over 10 minutes before monitoring the fluorescence spectra. The mixture was placed in 100.0 mm width quartz cell, and then fluorescence spectra were

recorded at room temperature under the conditions as mentioned in the screening experiment.

2.2.3 The cyanide complexation studies of the methylated sensors, *o*-MNQB, *m*-MNQB and *p*-MNQB in micellar systems using fluorescence spectrophotometry

2.2.3.1 Fluorescence measurements for the optimizing condition of the micellar system

Fluorescence measurements in this section were performed under following condition:

Start: 364 nm

End: 800 nm

Excitation: 344 nm

Excitation Slit: 10.0

Emission Slit: 10.0

Scan rate: 120 nm/min

a) The studies on the effect of surfactant types

Into a 5.0 mL volumetric flask, 1.0 mL of 2.5×10^{-4} mol/L of a sensor in spectroscopic ethanol was mixed with a 1.25×10^{-2} mol/L of a solution of a surfactants (cetyltrimethylammonium bromide (CTAB), sodium dodecyl sulfate (SDS), and Triton X-100 (TX-100)) in MilliQ water. The mixture was shaken gently for 30 second and then the volume was adjusted with MilliQ water to give the final concentration of 5×10^{-5} mol/L for the sensor and 5×10^{-3} mol/L for the surfactant. In the case of KCN sample, 0.1 mL of 2.5×10^{-3} mol/L KCN in MilliQ water was added to the solution mixture of the sensor and the surfactant, and then the volume of the sample was adjusted to 5.0 mL to give the final concentration of 50 μ M for CN⁻, 5×10^{-5} mol/L for the sensor and 5×10^{-3} mol/L for the surfactant. After the sample stood for 30 minutes, the mixture was placed in a 100.0 mm width quartz cell, and then fluorescence spectra were recorded at room temperature.

b) The studies on the effect of cationic surfactants

The procedure for sample preparation and fluorescence measurements were followed those mentioned in previous studies using cetyltrimethylammonium bromide (CTAB), dodecyltrimethyl ammonium bromide (DTAB) and tetradecyltrimethylammonium bromide (TTAB).

c) The studied of CTAB concentration effect

Into a 5.0 mL volumetric flask, 1.0 mL of 2.5×10^{-4} mol/L of a sensor in spectroscopic ethanol was mixed with a 1.25×10^{-2} mol/L cetyltrimethylammonium bromide (CTAB) in various portions according to Table 2.1 Then 100 μ L of 2.5×10^{-3} mol/L KCN in MilliQ water was added to the solution mixture of the sensor and the surfactant and then the volume of sample was adjusted to 5.0 mL to give the final concentration of 50 μ M for CN^- , 5×10^{-5} mol/L for the sensor in various concentration of CTAB. After stood the sample for 30 minutes, the mixture was placed in a 100.0 mm width quartz cell, and fluorescence spectra were then recorded at room temperature.

Table 2.1 Volume of the stock solution of CTAB (1.25×10^{-2} mol/L) and the final concentration of CTAB in 5.0 mL

Volume of CTAB stock solution (mL)	Final concentration of CTAB (mM)
0	0
0.1	0.25
0.4	1
1.2	3
2	5
4	10

d) The studies of sensor concentration effect

Into a 5.0 mL volumetric flask, 5×10^{-4} mol/L of a sensor in spectroscopic ethanol in various portions was mixed with 100 equivalent of CTAB to give the final concentration in 1:4 ethanol:H₂O after volume adjustment with ethanol and water as shown in the Table 2.2. In the presence of cyanide, 50 μ M of 2.5×10^{-3} mol/L KCN in MilliQ water were added to the solution mixture of the sensor and the surfactant and then the volume of sample was adjusted to 5.0 mL with ethanol and water as shown in the Table 2.2 to give the final concentration of 25 μ M for CN⁻ in 1:4 ethanol:H₂O with a variety of sensor concentration in 100 equiv CTAB. After the sample stood for 30 minutes, the solution mixture was placed in a 100.0 mm width quartz cell, and then fluorescence spectra were recorded at room temperature.

Table 2.2 Volume of sensor (5×10^{-4} mol/L) and CTAB (1.25×10^{-2} mol/L) in the stock solution and the final concentration of sensor and CTAB in 5.0 mL of 1:4 ethanol:H₂O

Volume of sensor stock solution (mL)	Final concentration of sensor (μ M)	Volume of CTAB stock solution (mL)	Final concentration of CTAB (mM)
0.05	5.0	0.2	0.50
0.1	10.0	0.4	1.00
0.5	50.0	2	5.00
1	100.0	4	10.00

ศูนย์วิทยทรัพยากร
จุฬาลงกรณ์มหาวิทยาลัย

2.2.3.2 Fluorescence measurement for screening test of anions in optimum condition of the micellar system

Stock solutions of sensors (2.5×10^{-4} mol/L) were prepared in spectroscopic grade ethanol. Stock solutions of anions (KCN, KF, KAcO, KBzO, KH_2PO_4 , KNO_3 , KClO_4 , KCl, KBr, KSCN and KI) and CTAB were prepared in MilliQ water as a concentration of 0.25 mol/L and 1.25×10^{-4} mol/L, respectively. In a 5.0 mL volumetric flask, 1.0 mL of ethanol solution of receptors was mixed with 2.0 mL of the stock solution of CTAB. The mixture was shaken gently for 30 seconds and then the volume was adjusted with MilliQ water to give the final concentration of 5×10^{-5} mol/L for the sensor and 5×10^{-3} mol/L for the surfactant. In the presence of an anion, 10 μM of anionic stock solution was added to the solution mixture of the sensor and the surfactant and then the volume of sample was adjusted to 5.0 mL to give the final concentration as 50 μM for anion, 5×10^{-5} mol/L for the sensor and 5×10^{-3} mol/L for the surfactant. After the sample for stood 30 minutes, the mixture solution was placed in a 100.0 mm width quartz cell, and then fluorescence spectra were recorded at room temperature.

2.2.3.3 Fluorescence titration procedure of sensor with CN^- in optimum condition of the micellar system

Stock solutions of sensors (2.5×10^{-4} mol/L) were prepared in spectroscopic grade ethanol. Stock solutions of anions and CTAB were prepared in MilliQ water as a concentration at 0.25 mol/L and 1.25×10^{-2} mol/L, respectively. In a 5.0 mL volumetric flask, 1.0 mL of ethanol solution of the receptors was mixed with 2.0 mL of the stock solution of CTAB. After shaking for 30 seconds, the mixture was added with portions of the stock solution of potassium cyanide (2.5×10^{-4} mol/L) to give the final concentration of CN^- according to Table 2.3 after the volume adjustment with MilliQ water. Mixtures stood at room temperature for 30 minutes and were placed in a 100.0 mm width quartz cell and then fluorescence spectra were recorded at room temperature.

Table 2.3 Volume of KCN stock solution (2.5×10^{-4} mol/L) and final concentration of CN^- in 5.0 mL of 1:4 ethanol: H_2O

Volume of KCN stock solution (μL)	Final concentration of CN^- in 5.0 mL (μM)
0	0
1	0.5
5	2.5
10	5
20	10
30	15
40	20
50	25
60	30
80	40
100	50
110	55
120	60
150	75
200	100
250	125
300	150
350	175
400	200
500	250

ศูนย์วิจัยทรัพยากร
จุฬาลงกรณ์มหาวิทยาลัย

2.3 The complexation studies of anthraquinone imidazole boronic acid based sensors, HAQB and MAQB with monosaccharides

Fluorescence studies in this section were carried out in a mixture of ethanol:buffer (40% for HAQB and 20% for MAQB). Buffers were prepared according to a procedure of Perrin and Demsey [84] as following: pH 3-5 : 0.2 mol/L phthalate-HCl buffer, pH 6-8 : 0.2 mol/L phosphate buffer, pH 8.5-10 : 0.2 mol/L sodium borate buffer, pH 11-12 : 0.2 mol/L phosphate-NaOH buffer.

2.3.1 The pH dependent experiments

Into a 5.0 mL volumetric flask, 1.0 mL of 2.5×10^{-4} mol/L of a sensor in spectroscopic ethanol was dissolved in a buffer to give the final concentration 5.0×10^{-5} mol/L. In the presence of sugar, 0.2 mL of the stock sugar solution including D-fructose, D-galactose, D-glucose and D-mannose (1.25 mol/L in buffer) was added into 1.0 mL of 2.5×10^{-4} mol/L of stock sensor solution in 5.0 mL volumetric flask. Upon the volume adjustment, the final concentration of the sample was 5.0×10^{-5} mol/L of the sensor in the presence of 50 mM of sugar. After kept standing for 2 minutes, the mixture was placed in a 100.0 mm width quartz cell, and then fluorescence spectra were recorded at room temperature. Fluorescence measurements of HAQB in this section were performed under following condition:

Start: 420 nm

End: 750 nm

Excitation: 395 nm

Excitation Slit: 5.0

Emission Slit: 5.0

Scan rate: 120 nm/min

Fluorescence measurements of **MAQB** in this section were performed under following condition:

Start: 420 nm

End: 750 nm

Excitation: 395 nm

Excitation Slit: 10.0

Emission Slit: 10.0

Scan rate: 120 nm/min

2.3.2 The stoichiometric determination by Job's method

Stock solutions of sensors and sugars were prepared in ethanol:sodium borate buffer pH 8.5 at concentration of 5×10^{-5} mol/L (40% ethanol:sodium borate buffer for sensor **HAQB** and 20% ethanol:sodium borate buffer for sensor **MAQB**). In a 5.0 mL volumetric flask, the portion of ethanol solution of receptors was mixed with portions of the stock solution of sugars to give the final concentration of sugar according to Table 2.4. Mixtures stood at room temperature for 2 minutes and were placed in 10.0 mm width quartz cell, and then fluorescence spectra were recorded at room temperature following the condition mentioned in pH dependent experiments.

ศูนย์วิทยทรัพยากร
จุฬาลงกรณ์มหาวิทยาลัย

Table 2.4 Mole fraction and volume of sensor (5×10^{-5} mol/L) and saccharide stock solution (5×10^{-5} mol/L) for Job's plot method

Sample	mole fraction of sensor	mole fraction of sugar	volume of sensor stock solution (mL)	volume of sugar stock solution (mL)
1	0	1	0	5.0
2	0.1	0.9	0.5	4.5
3	0.2	0.8	1.0	4.0
4	0.3	0.7	1.5	3.5
5	0.4	0.6	2.0	3.0
6	0.5	0.5	2.5	2.5
7	0.6	0.4	3.0	2.0
8	0.7	0.3	3.5	1.5
9	0.8	0.2	4.0	1.0
10	0.9	0.1	4.5	0.5
11	1.0	0	5.0	0

2.3.3 The complexation studies of sensors with saccharides using fluorescence titration

Stock solutions of sensors (2.5×10^{-4} mol/L) were prepared in spectroscopic grade ethanol. 0.25 mol/L stock solutions of sugars were prepared in 0.2 mol/L sodium borate buffer pH 8.5. In a 5.0 mL volumetric flask, 1.0 mL of the ethanolic solution of receptors was mixed with the portions of stock solution sugars to give final concentration of sugar according to Table 2.5. After volume adjustment with sodium borate buffer pH 8.5, the mixtures were stood at room temperature for 2 minutes and placed in a 100.0 mm width quartz cell and then fluorescence spectra were recorded at room temperature following the condition mentioned in pH dependent experiments.

Table 2.5 Volume of the saccharide stock solution (0.25 mol/L) and the final concentration of saccharide in 5.0 mL

Volume of sugar stock solution (mL)	Final concentration of sugar in 5.0 mL (mM)
0.00	0
10.00	0.5
20.00	1
40.00	2
50.00	2.5
80.00	4
100.00	5
120.00	6
150.00	7.5
200.00	10
250.00	12.5
300.00	15
400.00	20
500.00	25
600.00	30
800.00	40
1000.00	50
1200.00	60
1500.00	75

ศูนย์วิทยทรัพยากร
จุฬาลงกรณ์มหาวิทยาลัย

2.4 Determinations of quantum yield [85, 86]

Quantum yield (Φ_f) was obtained by a relative basis with reference to a standard having known quantum yield. Quantum yield of samples were calculated following equation

$$\Phi_x = \Phi_{STD} \left(\frac{A_{STD}}{A_x} \right) \left(\frac{E_x}{E_{STD}} \right) \left(\frac{\eta_x^2}{\eta_{STD}^2} \right)$$

or

$$\Phi_x = \Phi_{STD} \left(\frac{Grad_x}{Grade_{STD}} \right) \left(\frac{\eta_x^2}{\eta_{STD}^2} \right)$$

Φ_x = quantum yield of the unknown

Φ_{STD} = quantum yield of the standard

A = absorbance of solution

E = integrated fluorescence spectra

η = refractive index of solvent

Grad_x = gradient of unknown

Grad_{STD} = gradient of standard

The integrated fluorescence spectra of a sample were plotted versus absorbance at the excitation wavelength to obtain a gradient of sample. The quinine bisulfate in 1N H₂SO₄ was used as a reference sample ($\Phi_f = 0.508$ in 1N H₂SO₄).

ศูนย์วิทยทรัพยากร
จุฬาลงกรณ์มหาวิทยาลัย

CHAPTER III

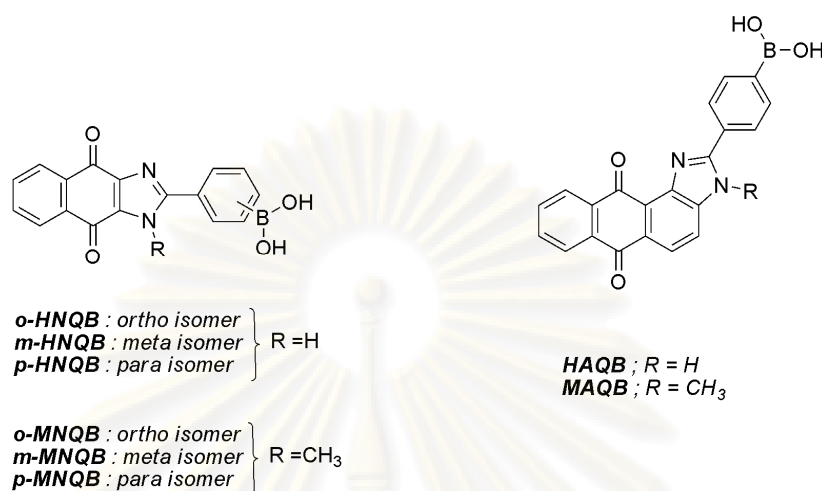
RESULTS AND DISCUSSIONS

3.1 Design and synthesis of quinone boronic-based receptors

Our research has focused on the design and synthesis of the molecules which can act as a desired anion sensor in water. Generally, chemosensors are consisted of binding units and sensory units connecting with the spacer. In the field of supramolecular chemistry, recognition events occur via non-covalent interactions including hydrogen bonding, electrostatic interactions, ion-dipole interactions, cation- π interactions and π - π stacking interactions. [3] It is well known that those interactions played an important role in biological systems due to the selectivity and sensitivity. In natural system, an effective non-covalent recognition of host and guest are derived from complicated molecules or systems that are able to expel or strip the solvated water molecules from the binding site of the host or the guest molecule resulting in perfect recognitions.[5] However, many synthetic receptors based on non-covalent recognition still incapable function in aqueous system because guest molecules are solvated by water consequent to the less effective of synthetic receptors in water. In order to overcome the solvation problem of the synthetic receptors, the higher affinity between host and guest through specific reactions was introduced to sensors. Boronic acids have attracted chemist's attention due to its specific functional group for diol guests such as sugar and their derivatives.[57-61] Recently, they also have been discovered to specifically recognize cyanide [53-56] and fluoride, [87, 88] particularly in aqueous system.

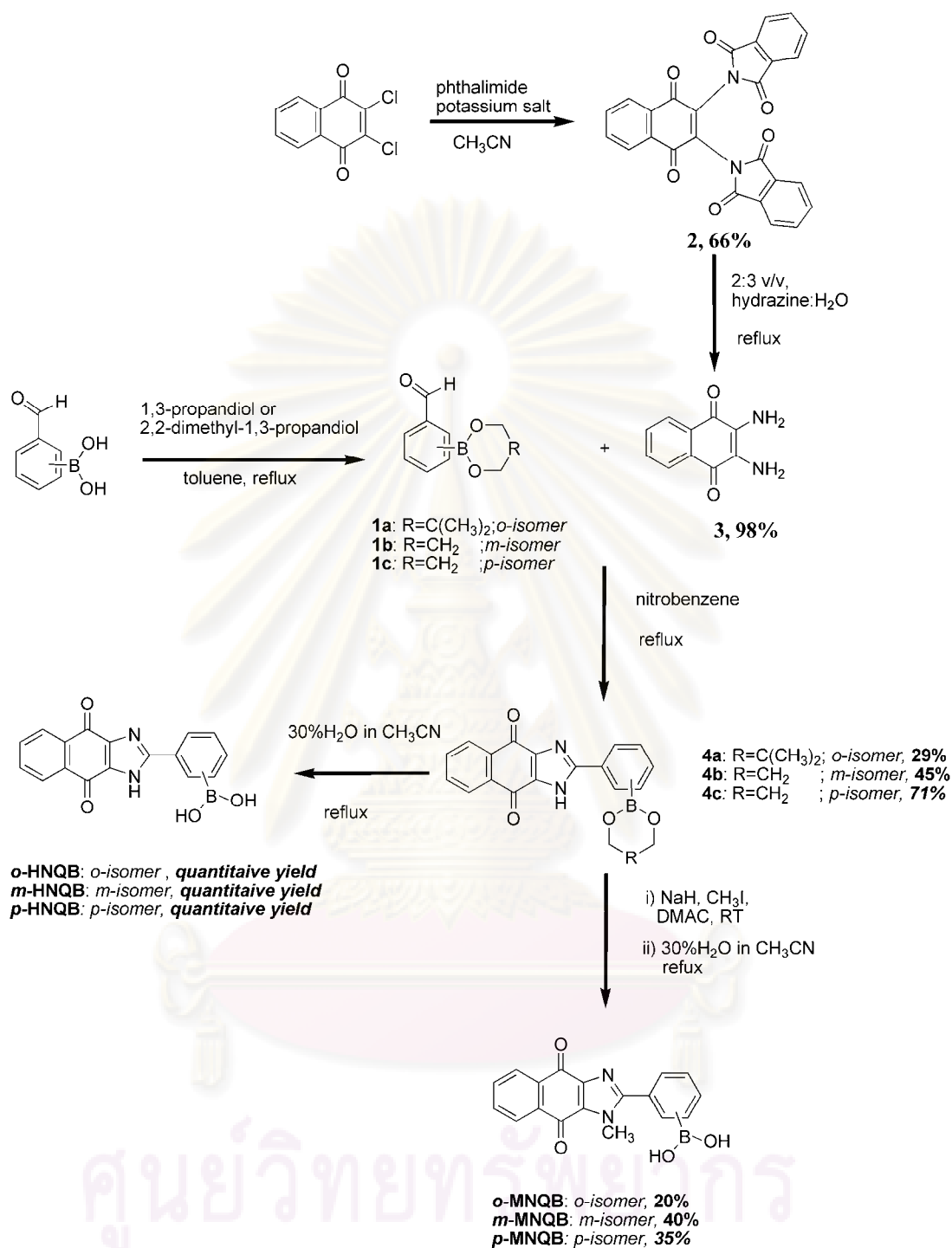
Regarding to sensory systems, optical output such as color, absorption spectra and especially fluorescence spectra was usually due to sensitivity and uncomplicated instrumental readout. Hypothetically, the conjugation of an electron acceptor such a quinone derivative with electron donor such an imidazole as a main acceptor-donor segment (main A-D system) performs intramolecular charge transfer sensory system which is sensitive to a small perturbation. [89-91] Conjugative connecting of anion recognition site as a boronic acid to main A-D site was expected to afford the large

response to the recognition events. Designed receptors based on quinone imidazole boronic acid were depicted in Scheme 3.1.



Scheme 3.1 Structures of designed receptors based on quinone imidazole and boronic acid

Naphthoquinone was chosen to fabricate a main electron acceptor segment of synthesized receptors. Synthetic pathway of receptors, ***o*-HNBQ**, ***m*-HNBQ** and ***p*-HNQB** and ***o*-MNBQ**, ***m*-MNBQ** and ***p*-MNQB** was illustrated in Scheme 3.2. In order to avoid side reaction due to weak Lewis acid properties of boronic acid, synthetic pathway was started by protecting the boronic acid group of appropriated formyl phenylboronic acids using propanediol in refluxing toluene. Dean-Stark apparatus was equipped with the reaction flask in order to remove water from the condensation reaction. After refluxing overnight and removal of toluene, the clear oil of protected formyl phenylboronate products **1a-c** were yielded and were subsequently used in the next steps without purification. The structure of compounds **1a-c** was confirmed by ¹H-NMR spectroscopy by the appearance of ethylene chain as a singlet peak at 3.82 ppm for **1a** and in the case of **1b** and **1c** showing the ethylene chain signal as a triplet peak at 4.20 and 4.18 ppm, respectively.



Scheme 3.2 Synthetic pathway of sensors *o*-HNBQ, *m*-HNBQ and *p*-HNBQ and *o*-MNBQ, *m*-MNBQ and *p*-MNBQ

According to Winkelmann's report, [82] 2,3-diamino-1,4-naphthoquinone, compound **2** was synthesized by a nucleophilic substitution reaction of 2,3-dichloro-1,4-naphthoquinone and phthalimide potassium salt affording a yellow solid of diphtalimide naphthoquinone in 66% yield. The $^1\text{H-NMR}$ spectrum of compound **2** showed a typical two sets of disubstituted aromatic signals. Then, compound **2** was reduced to amine by refluxing in the mixture of hydrazine:water providing a deep violet solid of 2,3-diaminonaphthalene-1,4-dione, **3**, in a quantitative yield. The $^1\text{H-NMR}$ spectrum of compound **3** showed the complete reduction of phthalimide to amine by the appearance of the one set of doublet of doublet at 7.91 and 7.52 ppm assigned to the aromatic protons of naphthoquinone moiety with coupling constants of 5.4 and 3.3 Hz.

The key step of the synthesis is the oxidative condensation [83] of diamine and aldehyde to yield the desired heterocyclic imidazole. Compounds **4a**, **4b** and **4c** were prepared by condensation of 2,3-diamino-1,4-naphthoquinone with an appropriate protected formylphenylboronic acid in refluxing nitrobenzene and the reaction was kept at 150°C . Compounds **4a**, **4b** and **4c** were separated from the reaction mixture by precipitation to obtain the yellow solids of **4a**, **4b** and **4c** in 29%, 45% and 71% yields, respectively. Structures of heterocyclic products **4a**, **4b** and **4c** were assured by $^1\text{H-NMR}$ (Figure 3.1) and $^{13}\text{C-NMR}$ spectroscopy. Interestingly, NH imidazole protons were found at 14.40, 14.42 and 14.39 ppm for **4a**, **4b** and **4c**, respectively. This is indicative of a very high acidic proton due to the intramolecular hydrogen bonding between NH-imidazole and oxygen of naphthoquinone. $^{13}\text{C-NMR}$ spectra showed C=N signal at 155.9 ppm in all isomers. MALDI-TOF mass spectra showed intense peak at 387.15, 359.64 and 358.63 for **4a** ($\text{M}+2\text{H}$) $^+$, **4b** ($\text{M}+2\text{H}$) $^+$ and **4c** ($\text{M}+\text{H}$) $^+$, respectively, corresponded to $\text{C}_{20}\text{H}_{15}\text{BN}_2\text{O}_4$ species. Moreover, elemental analysis of **4a**, **4b** and **4c** showed a good agreement with the desired structures.

จุฬาลงกรณ์มหาวิทยาลัย

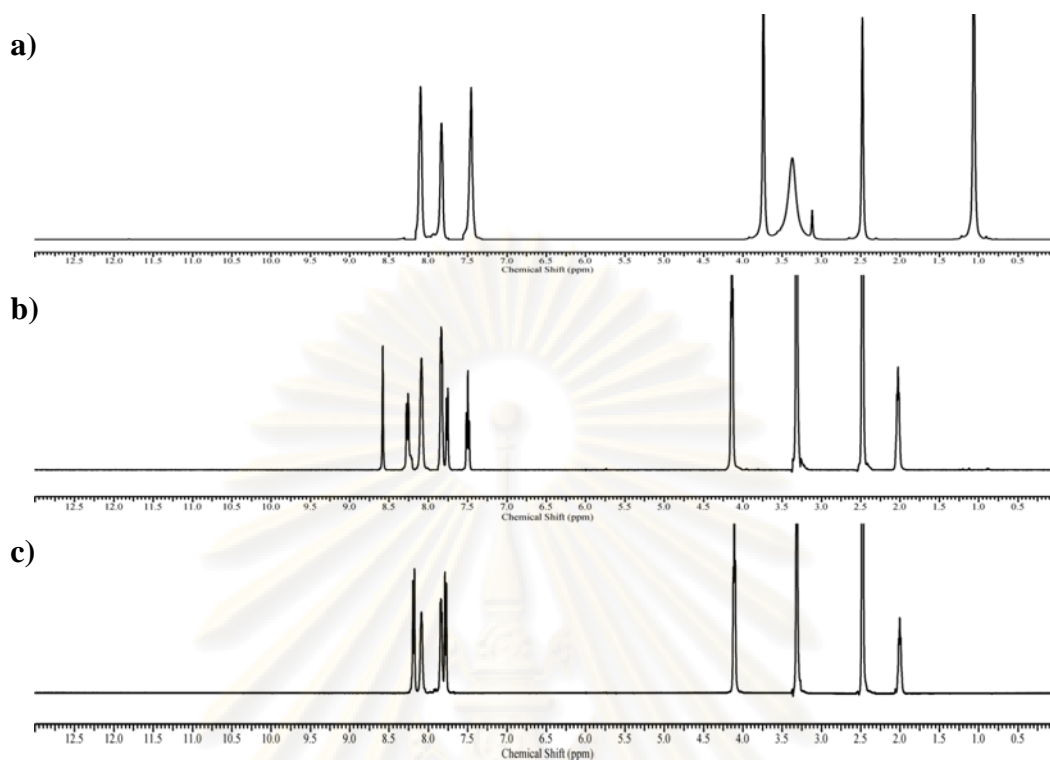


Figure 3.1 $^1\text{H-NMR}$ spectra (400 MHz, $\text{DMSO-}d_6$) of a) **4a**, b) **4b** and c) **4c**

In order to remove the protecting boronate group, compounds **4a-c** were refluxed in 30% H_2O in CH_3CN to give the protonated sensors *o*-**HNbQ**, *m*-**HNbQ** as yellow solid and *p*-**HNbQ** as red-purple solids. Compounds *o*-**HNbQ**, *m*-**HNbQ** and *p*-**HNbQ** were characterized by $^1\text{H-NMR}$, $^{13}\text{C-NMR}$, MADI-TOF mass spectroscopy and elemental analysis. As displayed in Figure 3.2, $^1\text{H-NMR}$ spectra showed that the protecting groups were completely removed by the appearance of hydroxyl signals of the boronic acid moiety at 8.6-8.7 ppm and the vanishing of proton signals of the ethoxy chains. Considering each isomer, the $^1\text{H-NMR}$ spectrum of *o*-**HNbQ** showed three sets of phenyl boronic acid as a doublet, doublet and triplet corresponding to the *ortho* position of the boronic acid (Figure 3.2a). The $^1\text{H-NMR}$ spectrum of *m*-**HNbQ** showed aromatic protons of the phenyl boronic acid as four sets of signals corresponding to the *meta* position of the phenyl boronic acid (Figure 3.2b). The $^1\text{H-NMR}$ spectrum of *p*-**HNbQ** showed doublet of doublet of aromatic protons of phenyl boronic acid at 8.19 and 8.10 ppm corresponding to the *para* position of the phenyl boronic acid (Figure 3.2c). MALDI-TOF mass spectra supported the structures of the designed compounds with intense peak of m/z at 318.0 for *o*-**HNbQ**, 319.0 for

m-HNQB and 319.0 for *p*-HNQB corresponding to C₁₇H₁₁BN₂O₄. Elemental analysis of *o*-HNQB, *m*-HNQB and *p*-HNQB showed a good agreement with the proposed structures.

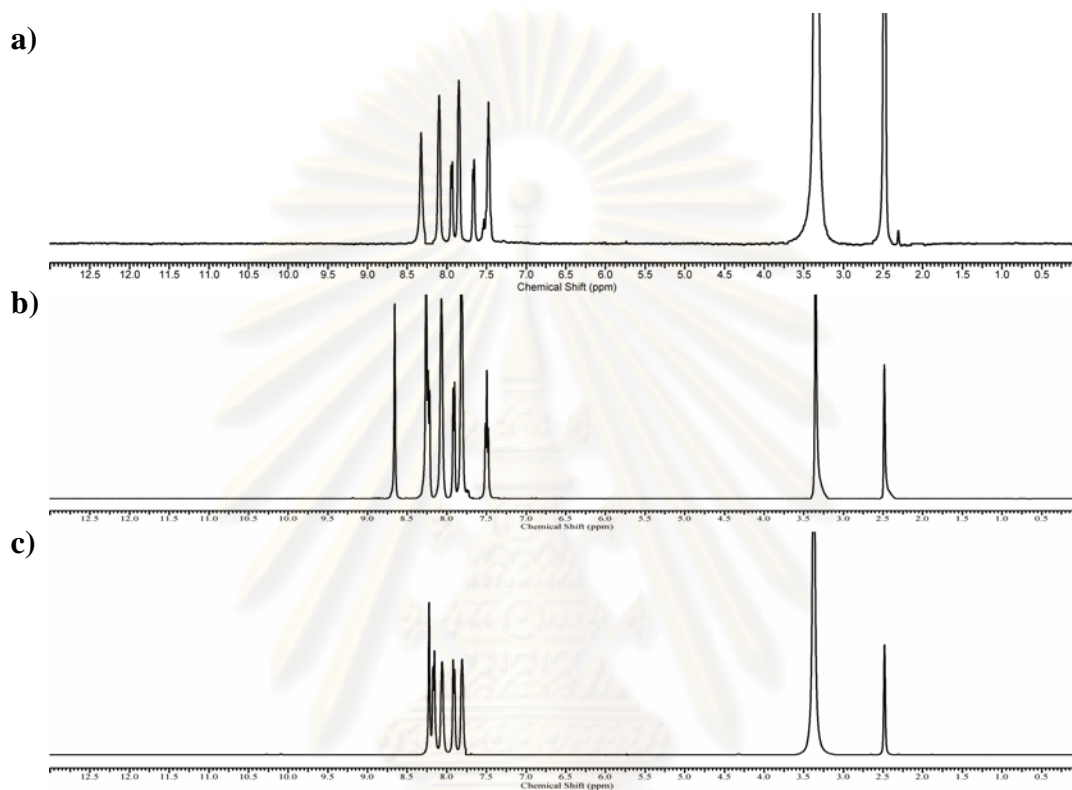


Figure 3.2 ¹H-NMR spectra (400 MHz, DMSO-*d*₆) of a) *o*-HNQB b) *m*-HNQB and c) *p*-HNQB

Methylation of all HNQB isomers were carried out using methyl iodide in *N,N*'-dimethylaminoacetamide (DMAC) in the presence of excess amount of NaH. Poor nucleophilicity of the nitrogen atom on heterocyclic moiety stemmed from strong hydrogen bond of the acidic proton and delocalized electrons of nitrogen atoms. Compounds *o*-MNQB, *m*-MNQB and *p*-MNQB were completely characterized by ¹H-NMR, ¹³C-NMR, MADI-TOF mass spectrometry and elemental analysis. ¹H NMR spectra showed the methyl proton at 3.84 ppm for *o*-MNQB whereas that methyl signals of *m*-MNQB and *p*-MNQB appeared at 4.08 ppm. Considering each isomer, the ¹H-NMR spectrum of each isomer displayed the aromatic signal of phenyl boronic acid corresponding to *ortho*, *meta* and *para*

positions of *o*-MNBQ, *m*-MNBQ and *p*-MNBQ, respectively. The $^1\text{H-NMR}$ spectrum of *o*-MNBQ showed three sets of the phenyl boronic acid as a doublet (Figure 3.3a), doublet and triplet whereas the $^1\text{H-NMR}$ spectrum of *m*-MNBQ showed four sets of the phenyl boronic acid signals as singlet (Figure 3.3b), doublet, doublet and triplet. The $^1\text{H-NMR}$ spectrum of *p*-MNBQ showed doublet of doublet of aromatic protons of the phenyl boronic acid at 7.98 and 7.78 ppm corresponding to *para* position of the phenyl boronic acid (Figure 3.3c). Moreover, all compounds were completely characterized by $^{13}\text{C-NMR}$, MADI-TOF mass spectrometry and elemental analysis. MALDI-TOF mass spectra supported the structures of all the desired compounds with intense peak of m/z at 334.66 m/z for *o*-MNQB, 331.60 m/z for *m*-MNQB and 332.39 m/z for *p*-MNQB corresponding to $[\text{M}+3\text{H}]^+$, $[\text{M}]^+$ and $[\text{M}+\text{H}]^+$, respectively. Elemental analysis of *o*-MNQB, *m*-MNQB and *p*-MNQB showed a good agreement with the proposed structures.

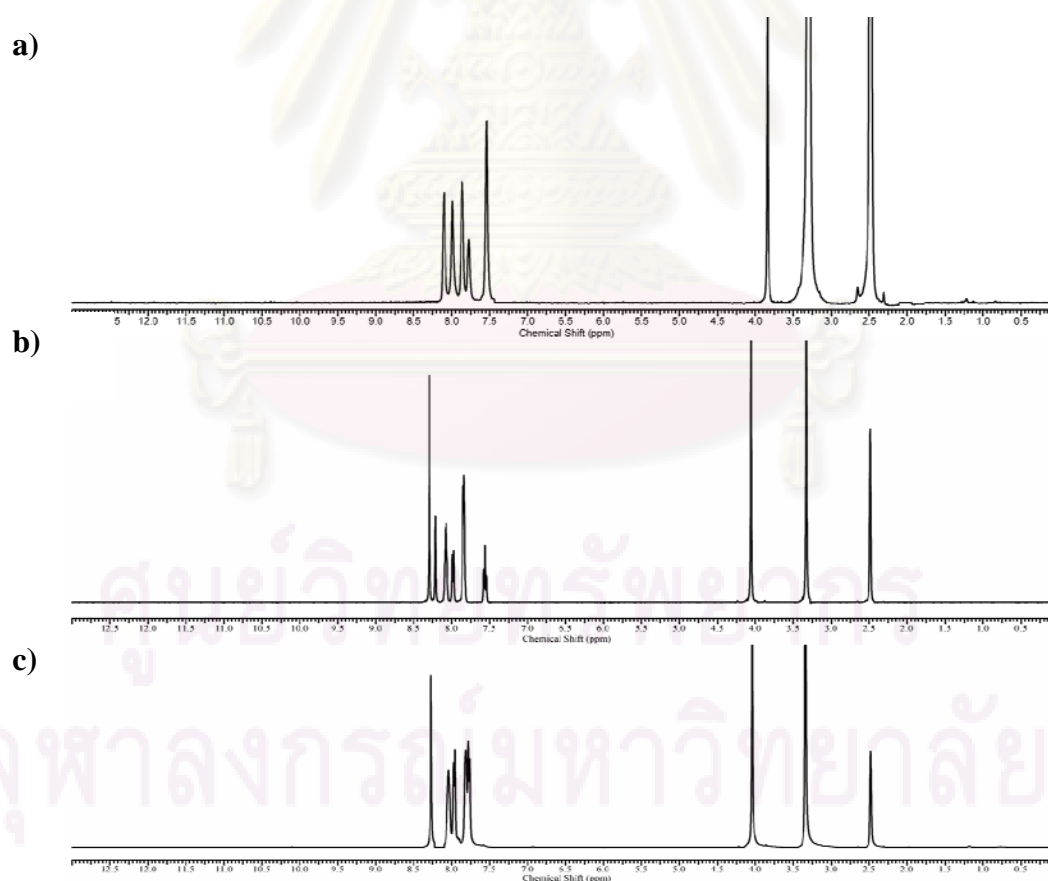
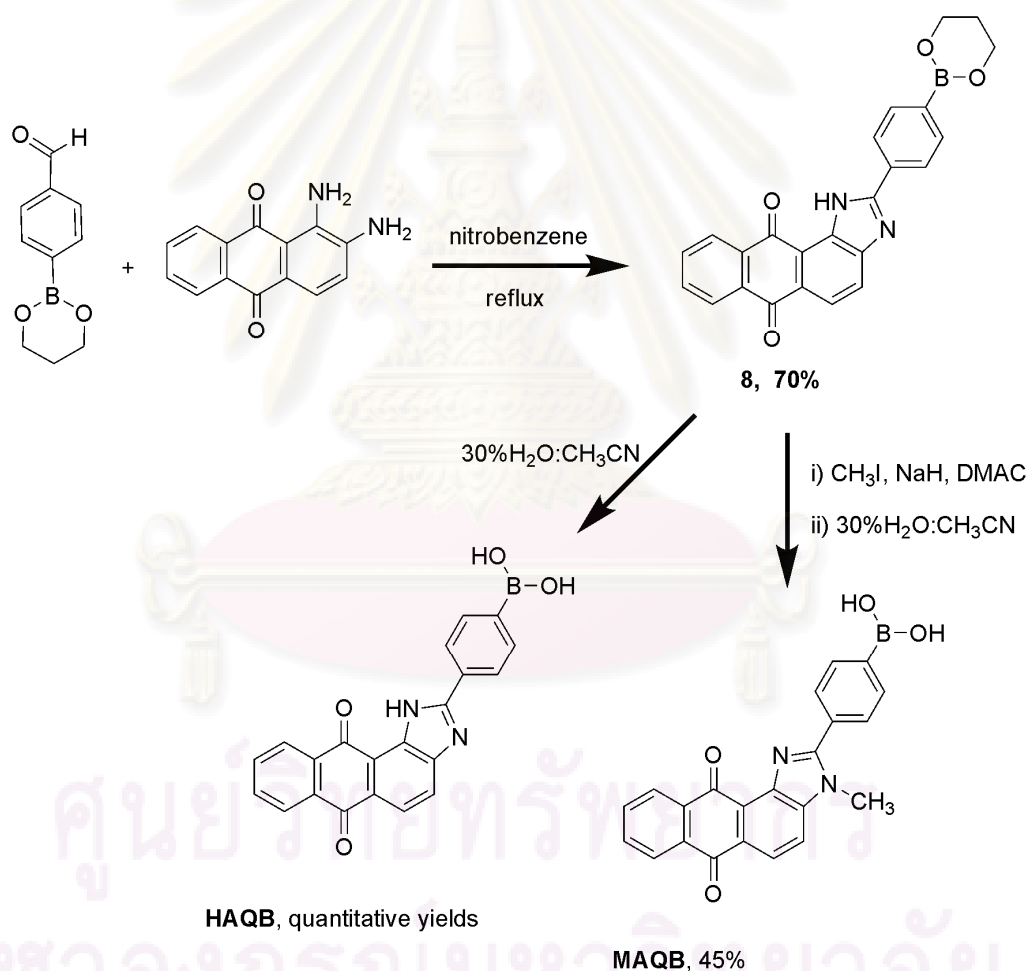


Figure 3.3 $^1\text{H-NMR}$ spectra of (400 MHz, $\text{DMSO-}d_6$) a) *o*-MNQB, b) *m*-MNQB and c) *p*-MNQB

Additionally, control compounds **7a** and **7b** were synthesized in order to prove the signal transductions of the synthesized receptors. Synthesis of compounds **7a** and **7b** were performed similar to that of naphthoquinone boronic based sensors. All characterization data including ^1H NMR, ^{13}C -NMR, MADI-TOF mass spectrometry and elemental analysis were completely supported the structure of compounds **7a** and **7b**.

3.2 Design and synthesis of anthraquinone imidazole boronic acid based receptors **HAQB** and **MAQB**



Scheme 3.3 Synthetic pathway of sensors **HAQB** and **MAQB**

New series of quinone imidazole boronic based sensors, **HAQB** and **MAQB** were designed by extended aromatic conjugation in order to improve the solubility and optical properties of sensors. Anthraquinone compound were synthesized using similar procedure with naphthaquinone receptors as shown in Scheme 3.3. Anthraquinone receptor were prepared using commercial available of 1,2-diamino-1,4-anthraquinone and protected *para*-formylphenylboronate, **1c** refluxed in nitrobenzene. Protecting anthraquinone product were separated by precipitated with diethyl ether to give brown solid of compound **8** in 70%. The $^1\text{H-NMR}$ spectrum of precursor compound **8** showed the imidazole proton at 11.35 ppm due to the hydrogen bonding of this proton with the oxygen atom (Figure 3.4a). Sensors **HAQB** and **MAQB** were prepared by straightforward procedure as mentioned in preparation of naphthoquinone sensors. As shown in Figure 3.4b, the $^1\text{H-NMR}$ spectrum in $\text{DMSO-}d_6$ of **HAQB** showed clearly feature of the desired compound by the appearance of signal of acidic protons of imidazole signal at 12.97 ppm. The $^1\text{H-NMR}$ spectrum of **MAQB** showed a signal of methyl proton at 3.98 ppm with a concomitant of the disappearance of NH proton signals (Figure 3.4c). In additional, all desired products were characterized by $^{13}\text{C-NMR}$, MADI-TOF mass spectrometry and elemental analysis. The results confirmed the existence of structures. MALDI-TOF mass spectra supported the structures compounds showing intense peaks of at 408.12 m/z for compound **8**, 368.09 m/z for **HAQB** and 382.11 m/z for **MAQB** corresponding to $[\text{M}+2\text{H}]^+$, $[\text{M}+2\text{H}]^+$ and $[\text{M}+3\text{H}]^+$, respectively. Elemental analysis of compound **8**, **HAQB** and **MAQB** agree well with the proposed structure.

ศูนย์วิทยทรัพยากร
จุฬาลงกรณ์มหาวิทยาลัย

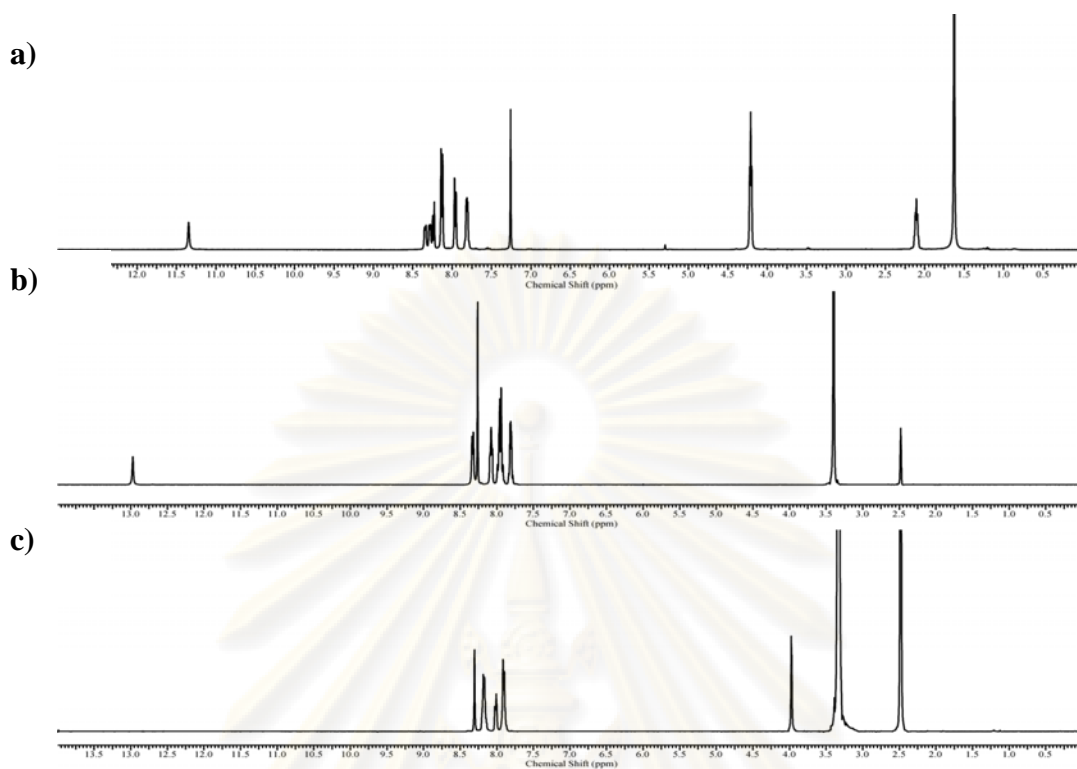


Figure 3.4 ^1H -NMR spectra (400 MHz) of a) **8** in CDCl_3 , b) **HAQB** in $\text{DMSO-}d_6$ and c) **MAQB** in $\text{DMSO-}d_6$

The foregoing ^1H -NMR results showed clearly that NH imidazole of **HAQB** interacted with oxygen atom of anthraquinone moiety in $\text{DMSO-}d_6$ via hydrogen bonding resulting in the high downfield shift of this signal. However, the orientation of methyl group on imidazole ring of **MAQB** must be verified. As expected orientation, ^1H -H NOESY spectra of **MAQB** suggested that the position of the methyl preferred in the outsized of O-N five member ring by the observation of the correlation between methyl group (H_g) and H_d and H_h of aromatic proton as shown in Figure 3.5.

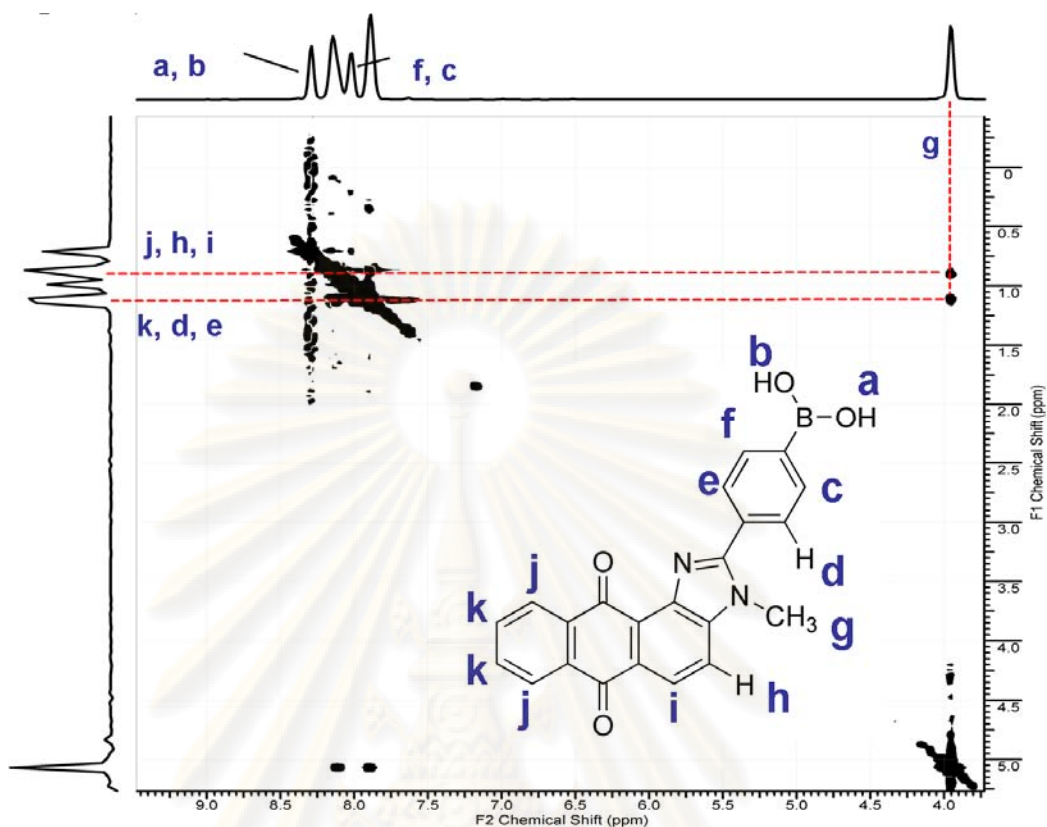


Figure 3.5 ^1H - ^1H NOESY NMR of MAQB (500 MHz) in $\text{DMSO-}d_6$

ศูนย์วิทยทรัพยากร
จุฬาลงกรณ์มหาวิทยาลัย

3.3 Complexation properties of the protonated naphthoquinone sensors *o*-HNQB, *m*-HNQB and *p*-HNQB

3.3.1 Photophysical properties of the protonated sensors

As shown in Figure 3.6 and Table 3.1, DMSO solutions of the protonated naphthoquinone imidazole boronic based sensors *o*-HNQB, *m*-HNQB and *p*-HNQB displayed a light yellow color solution and visible absorption band at 404, 408 and 410 nm, respectively. The light yellow color and the visible absorption bands stemmed from the migration of electron density from electron donating group of amino on imidazole ring to electron acceptor group of naphthoquinone. [7, 92] Compared to the parent compound, 1,4-diamino-2,3-naphthoquinone, compound **3** ($\lambda_{\max} = 585$ nm, $\epsilon = 2161$ mol/L.cm, $E_g \approx 1.55$ eV, Figure A.34), naphthoquinone imidazole boronic based sensors provided a large energy gap ($E_g \approx 2.44$ eV) due to the attachment of electron deficient group (boronic acid) to the structure.

As expected, the protonated naphthoquinone imidazole boronic based sensors exhibit emission properties as listed in Table 3.1, their quantum yield of DMSO was quite low in the attribution of the characteristic of low lying $n-\pi^*$ excited state in quinone compound resulting in dominating of intersystem crossing relaxation pathway. [7]

Table 3.1 Photophysical properties of the protonated sensors in DMSO.

Receptors	λ_{abs} (nm)	Extinction coefficients (ϵ , mol/L.cm)	λ_{em} (nm)	Φ_f^a
<i>o</i> -HNQB	404	1590	550	0.082
<i>m</i> -HNQB	405	1514	551	0.074
<i>p</i> -HNQB	410	2016	551	0.089

^a Quantum yields were determined using quinine sulfate as the standard (Φ_{STD}) 0.508 in 1 N H₂SO₄.

Regarding the position of boronic acid, *o*-HNQB, *m*-HNQB and *p*-HNQB displayed insignificant different feature in absorption and emission spectra suggesting that the position of boronic did not affect the photophysical properties of the free receptors.

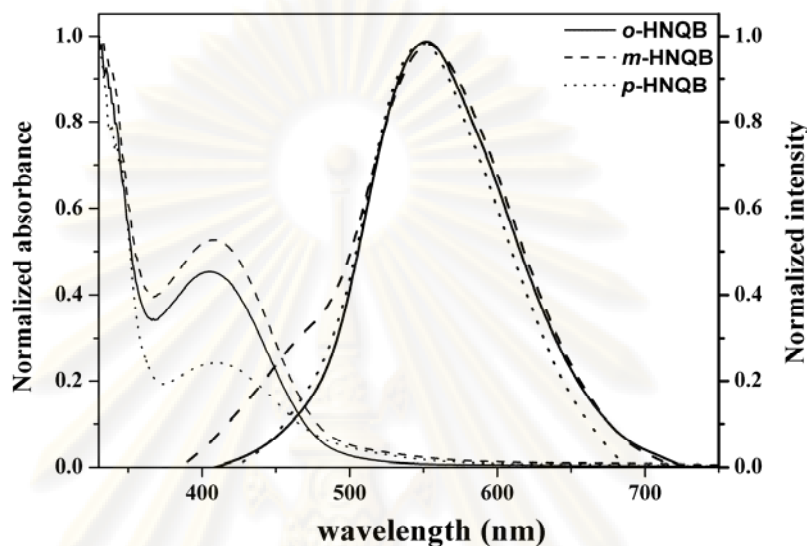


Figure 3.6 Absorption and emission spectra ($\lambda_{\text{excite}} = 344 \text{ nm}$) of *o*-HNQB, *m*-HNQB ($5 \times 10^{-4} \text{ mol/L}$) and *p*-HNQB ($2.5 \times 10^{-4} \text{ mol/L}$) in DMSO.

3.3.2 The complexation studies of sensors *o*-HNQB, *m*-HNQB and *p*-HNQB with various anions using spectrophotometry

The complexation studies of the protonated sensors were carried out using tetrabutylammonium salt of anions in DMSO (F^- , Cl^- , Br^- , I^- , CN^- , AcO^- , BzO^- , H_2PO_4^- and NO_3^-) and potassium salt for CN^- . In the presence of 30 equivalents of anions, color changes from yellow to red and orange of the receptors *p*-HNQB (Figure 3.7) and *m*-HNQB in DMSO were detected by naked eye upon addition of F^- , AcO^- , CN^- and H_2PO_4^- while that of *o*-HNQB showed slightly change. The results suggested that the basicity of anion played as important role of the color changes receptor solution. Complexation abilities of the protonated receptors were also investigated using spectrophotometric technique. UV-Vis spectra (Figure 3.8) clearly showed that basic anions such as F^- , AcO^- , CN^- and H_2PO_4^- caused the bathochromic shift in from 404 nm to 455 nm, 487 nm and 497 nm for *o*-HNQB, *m*-HNQB and *p*-HNQB, respectively.

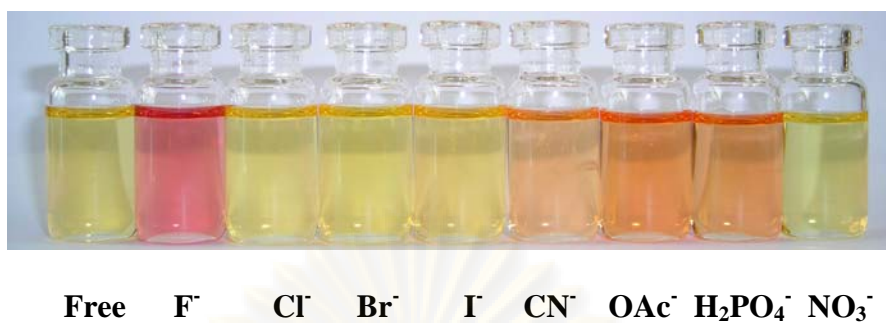


Figure 3.7 Color changes observed upon the addition of 30 equivalents anions into the DMSO solution of *p*-HNQB (3×10^{-4} mol/L).



Figure 3.8 Absorption spectra of a) *o*-HNQB, b) *m*-HNQB and c) *p*-HNQB in the presence of 30 equivalents of various anions in DMSO (3×10^{-4} mol/L of sensors).

In order to evaluate the anion binding properties of each anion and sensor, spectroscopic titrations were performed with anions including F^- , AcO^- , CN^- and $H_2PO_4^-$ in DMSO. As shown in Figure 3.9, the original absorption band at 404 nm gradually decreased and the new absorption band at 481 nm for receptor ***m*-HNQB** and 497 nm for ***p*-HNQB** progressively increased upon increasing CsF concentrations. The well-defined isosbestic point was also observed in both sensors. Although, ***o*-HNQB** gave a slightly change in their color from yellow to pale orange, it exhibited significant red shift (455 nm) upon binding with F^- (Figure 3.9a). In the case of other anions such as AcO^- , CN^- and $H_2PO_4^-$, all sensors showed similar behavior to the CsF titration by producing the new absorption band at a longer wavelength with well-defined isosbestic point. Unfortunately, the stability constant could not be calculated from the UV-vis titration data due to the low dissociation ability of potassium salts or cesium salts in DMSO.



ศูนย์วิจัยทรัพยากร
จุฬาลงกรณ์มหาวิทยาลัย

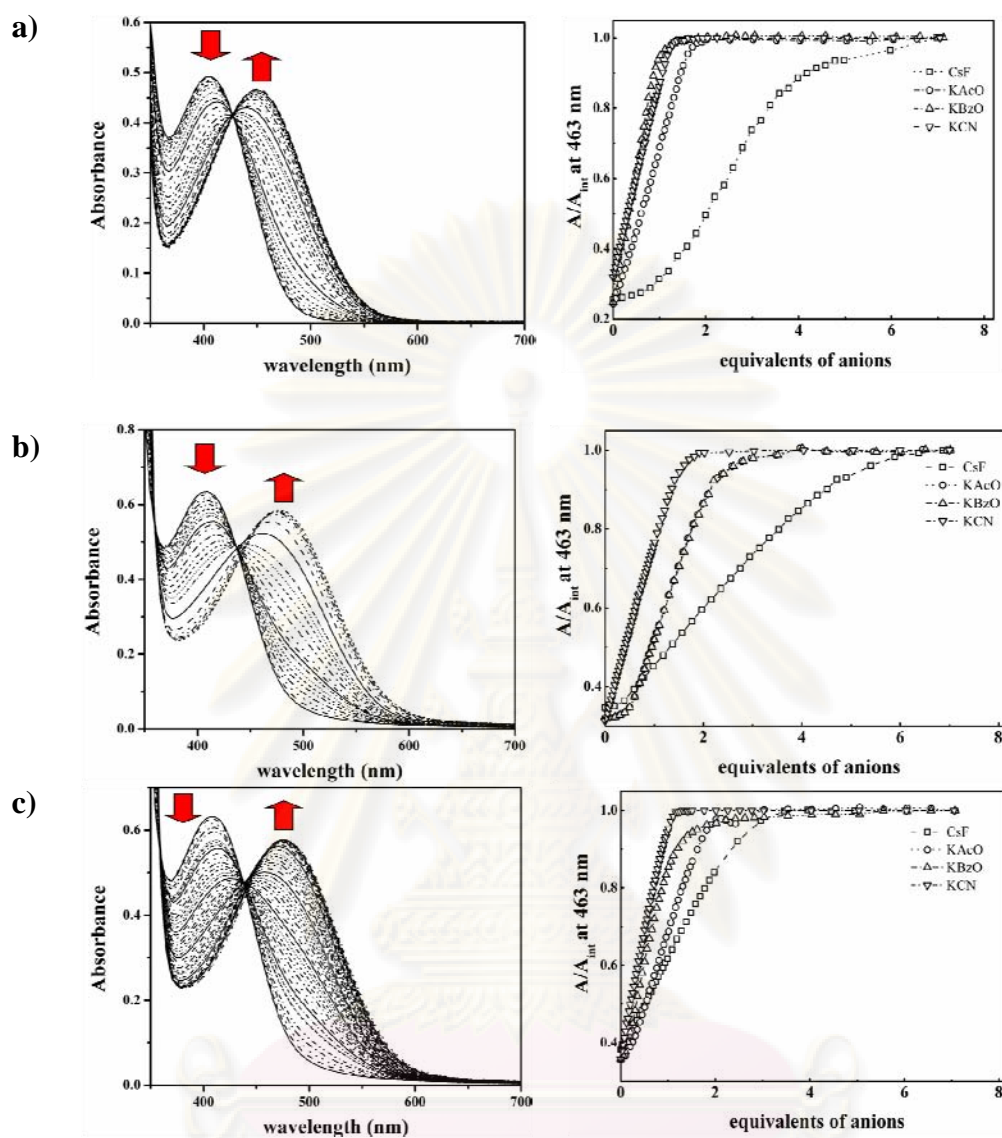


Figure 3.9 Absorption spectra (left) and absorption response at 463 nm (right) toward various anions 0-7 equivalents (A/A_{∞}) of a) *o*-HNQB, b) *m*-HNQB and c) *p*-HNQB upon addition of CsF in DMSO (3×10^{-3} mol/L of sensor in DMSO).

Color and UV spectral changes by the interaction of protonated sensors with anion have been obtained by the deprotonation of NH to N⁻ on imidazole resulting in charge transfer from N⁻ to electron acceptor group (naphthoquinone). [92, 93] To prove this explanation, the anionic complexation properties of methylated compound *p*-MNQB was investigated. As displayed in Figure 3.10, UV-vis spectra and the color changes showed the insignificant changes upon adding anions including F⁻, AcO⁻, CN⁻, H₂PO₄⁻ and BzO⁻. These results supported that the deprotonation on heterocyclic imidazole ring caused a large changes of optical properties for all sensors.

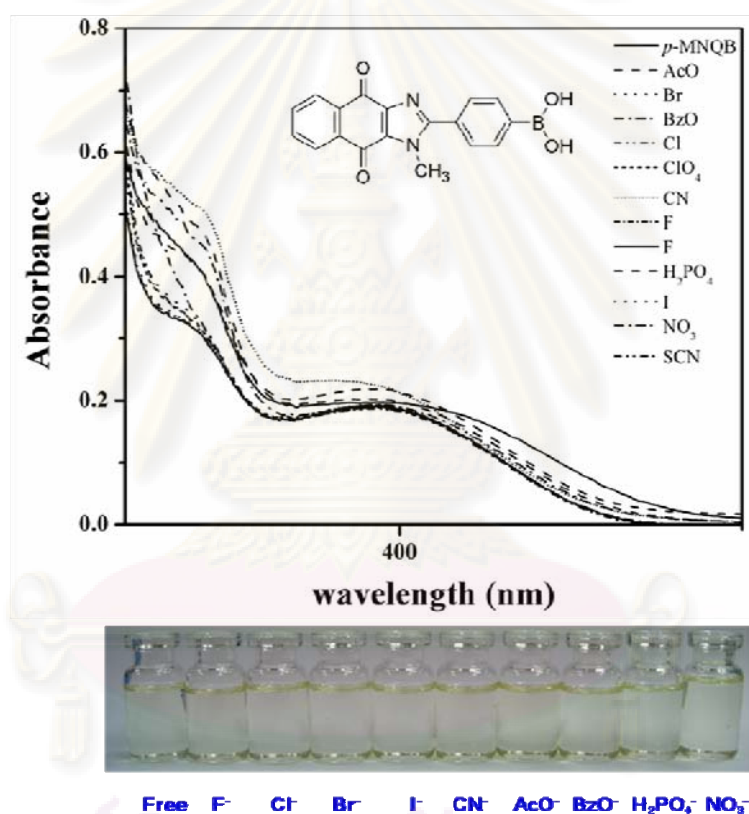


Figure 3.10 Absorption spectra and color changes of control compound *p*-MNQB in the presence of various anions in DMSO (3×10^{-4} mol/L of the sensor in DMSO).

Moreover, UV-vis spectra and color of ***o*-HAQB** showed a slightly change in the presence of anion such as F^- , OAc^- and BzO^- . The deprotonation of NH proton in *ortho* isomer may cause the distorted feature of the *ortho* position and precluded the delocalization of electron in *ortho* isomer consequently revealing in a slight red shift and pale orange color upon the deprotonation.

3.3.3 The complexation studies of sensors *o*-HNQB, *m*-HNQB and *p*-HNQB using 1H -NMR spectroscopy

The protonated sensors, ***o*-HNQB**, ***m*-HNQB** and ***p*-HNQB** possessed two potential sites for the interaction with anions including the acidic proton at imidazole ring and the boronic acid site. In order to clarify the binding mode of the protonated sensors, 1H -NMR experiments were performed in $DMSO-d_6$ to elucidate the binding site of sensors with anions including F^- , AcO^- , CN^- , BzO^- . When the anion was added into the $DMSO-d_6$ solution of sensors, the NH proton in their 1H -NMR spectra completely disappearance, while the hydroxyl signal of boronic acid still remained. It can be rationalized that further binding of anions towards the boron center were blocked by the negative charge of N⁻ atom resulted from deprotonation. These binding modes were further proved by using tetrabutylammonium hydroxide, the same results were observed indicating that the basic anions abstracted proton on the heterocyclic imidazole ring.

Upon the deprotonations of each sensor, 1H -NMR spectra of ***o*-HNQB** displayed dramatically changes in signals of phenyl boronic protons and naphthoquinone protons. As shown in Figure 3.11, H_c and H_e of boronic acid phenyl ring signals were moved to downfield regions whereas H_d signal was moved to upfield region upon the deprotonation. It can be possibly revealed that the boronic phenyl ring plane was distorted perpendicularly to naphthoquinone imidazole plane upon the breaking of N-B interaction caused by the negative charge upon deprotonation. Beside that distortion, the significant upfield shifts of H_f and H_g naphthoquinone protons were also observed due to the increasing of electron density on naphthoquinone imidazole plane upon binding. Interestingly, 1H -NMR spectrum of ***o*-HNQB** in the presence of F^- showed a different pattern with the large downfield shifts of all proton signals as displayed in Figure 3.11. As the results, it can be

rationalized in term of that the high electronegativity and small size of fluoride ion can stabilize the N-B interaction resulting in the existence of planar feature of the deprotonated form of *o*-HNQB. Thus, the negative charges were delocalized through whole molecule via conjugated π -system. These interaction modes were furthermore proved by using tetrabutylammonium hydroxide, the same results were observed. This is indicated that the anions abstracted proton on the heterocyclic imidazole ring.

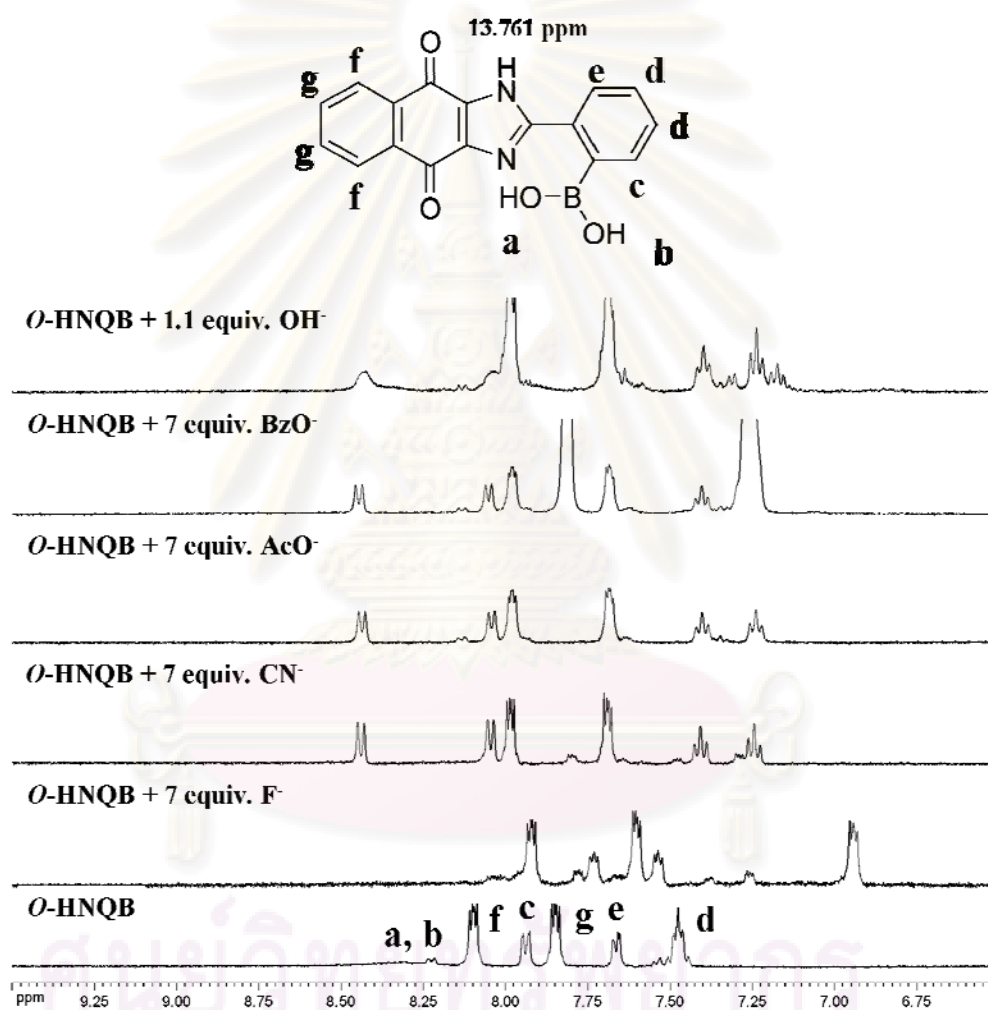


Figure 3.11 ¹H-NMR spectra (400 MHz) of *o*-HNQB upon the addition of 7.0 and 1.1 equiv. of tetrabutylammonium salt of basic anions, F⁻, AcO⁻, CN⁻, BzO⁻ and OH⁻ in DMSO (3×10^{-3} mol/L of sensors in DMSO-*d*₆).

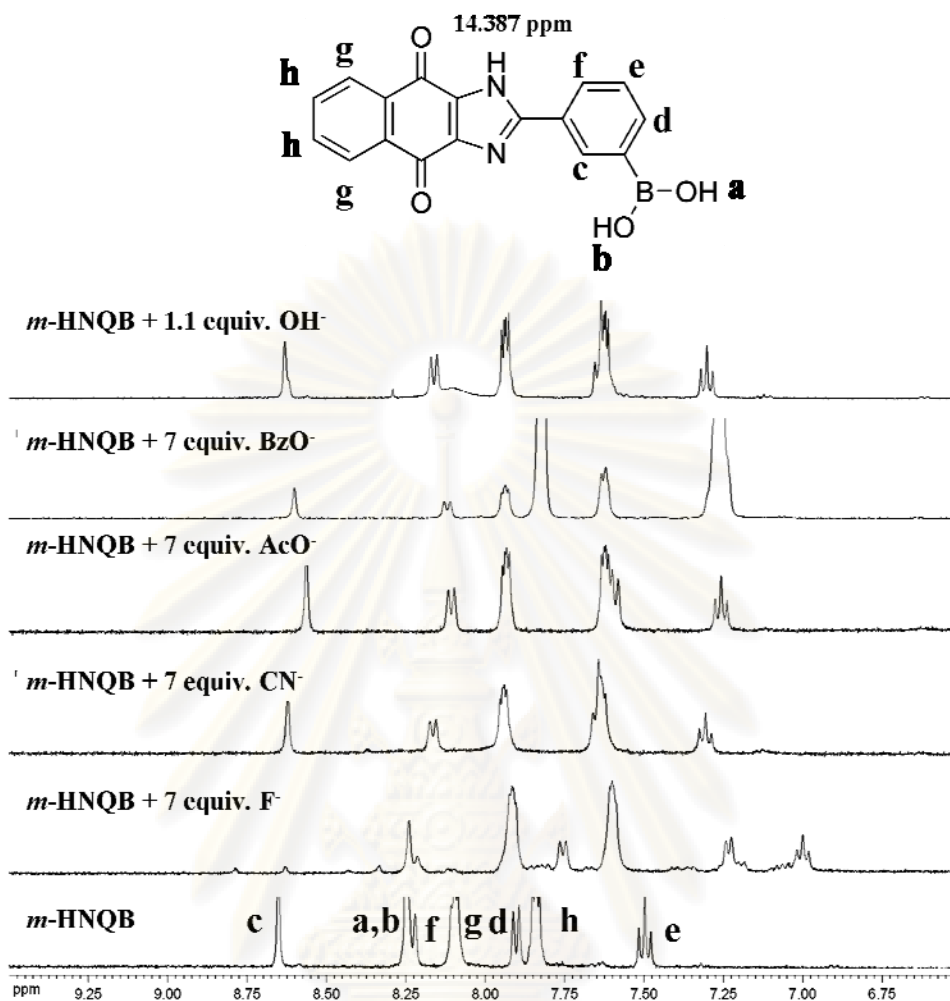


Figure 3.12 $^1\text{H-NMR}$ spectra (400 MHz) of *m*-HNQB upon the addition of 7.0 and 1.1 equiv. of tetrabutylammonium salt of basic anions, F^- , AcO^- , CN^- , BzO^- and OH^- in DMSO (3×10^{-3} mol/L of sensors in DMSO- d_6).

ศูนย์วิทยทรัพยากร
จุฬาลงกรณ์มหาวิทยาลัย

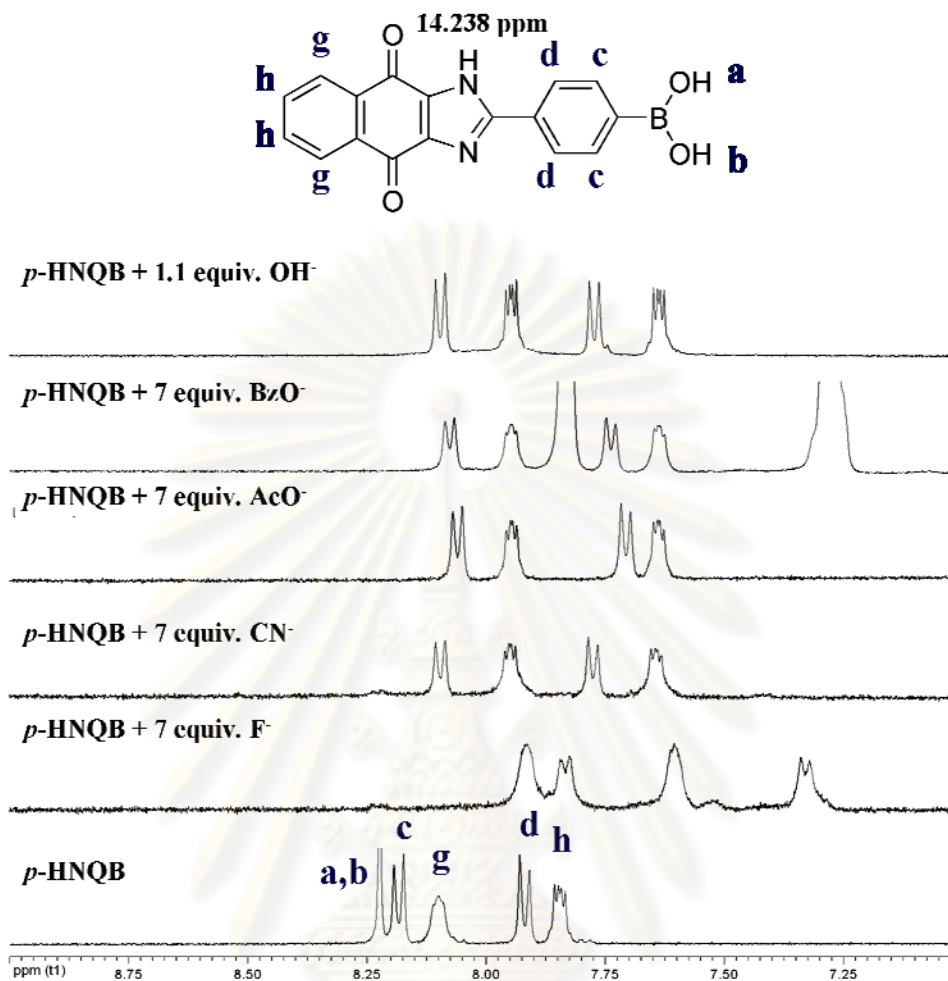


Figure 3.13 $^1\text{H-NMR}$ spectra (400 MHz) of *p*-HNQB upon a addition of 7.0 and 1.1 equiv. of tetrabutylammonium salt of basic anions, F^- , AcO^- , CN^- , BzO^- and OH^- in DMSO (3×10^{-3} mol/L of sensors in $\text{DMSO-}d_6$).

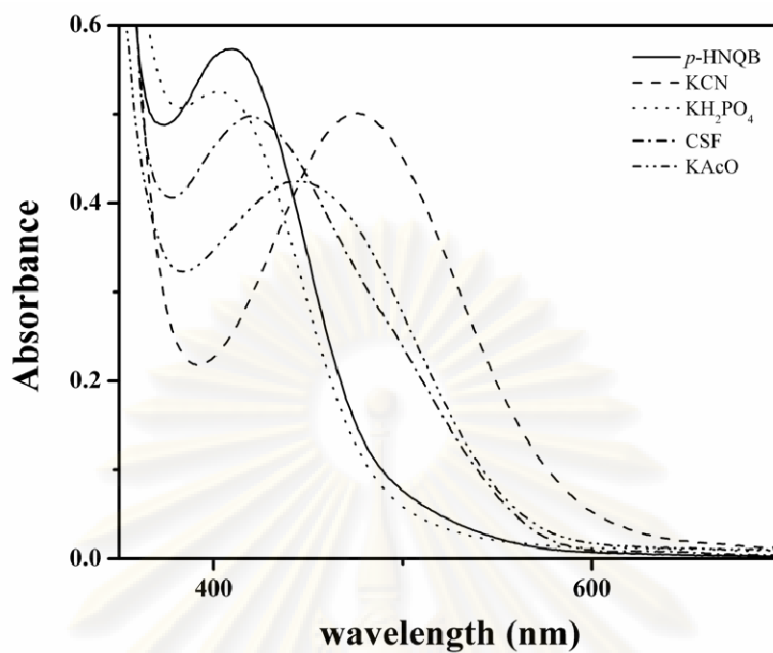
Regarding the effect of deprotonation of *m*-HNBQ and *p*-HNBQ, as displayed in Figures 3.12 and 3.13, slightly upfield shifts of phenylboronic protons were observed while the large upfield shifts were founded in the naphthoquinone proton signal upon the addition of AcO^- , BzO^- and CN^- . Due to the lack of N-B interactions in the *meta* and *para* isomers, the less rigidity in *m*-HNBQ and *p*-HNBQ provided the smaller changes in the phenyl boronic protons. The large upfield shifts of all protons were also found in the presence of F^- due to the high electronegativity of F^- .

Moreover, $^1\text{H-NMR}$ titrations were carried out in $\text{DMSO-}d_6$ using tetrabutylammonium salt of anions except CN^- using potassium salt in order to evaluate the binding properties of the protonated receptor toward anions. $^1\text{H-NMR}$

titration results showed that a slow exchange of protonated and deprotonated forms compared to NMR time scale was observed by the appearance of the new peaks of deprotonated form. Unfortunately, the integration of the protonated and deprotonated form was difficult to measure due to the broad and overlapping signals.

3.3.4 Applications of sensors *o*-HNQB, *m*-HNQB and *p*-HNQB as a CN⁻ naked eye sensor in DMSO:H₂O mixture

Interestingly, *m*-HNQB and *p*-HNQB isomers showed promising application as of naked eye sensors for cyanide ion in aqueous media. In DMSO: water (1:1), the color changed from yellow to red upon addition of cyanide were found, while other anions such as F⁻, OAc⁻, and BzO⁻ still exhibited the original color in this system. These results were interpreted in term of acidity of the conjugate acid of anion in mixture of DMSO:H₂O. HCN is a weak acid in both systems, water ($pK_a = 9.1$) and DMSO ($pK_a = 12.9$) whereas other anions including HF ($pK_a = 3.2$ in water), HBzO ($pK_a = 4.25$ in water) and HAcO ($pK_a = 4.75$ in water) [94] were strong acids in water but there are weak acids in DMSO. Therefore, sensors existed in the deprotonated form in the presence of CN⁻ in the mixture of DMSO:H₂O, whereas sensors returned to the protonated form resulting in recovery of the original color. However, the naked-eye sensing property for cyanide ion in the mixture of DMSO:H₂O could not be found in *o*-HNQB due to the pale orange color of the deprotonated form of this sensor. Therefore, the color change in this sensor could not be detected by eyes. Additionally, UV-vis spectra were observed upon the addition of anions in DMSO:H₂O. As expectation, the red shift was found only in the case of the CN⁻ addition (Figure 3.14) due to the existence of deprotonated form of sensors in this system.



***p*-HNQB** **F⁻** **Cl⁻** **Br⁻** **I⁻** **CN⁻** **OAc⁻** **H₂PO₄⁻** **NO₃⁻**

Figure 3.14 UV-Vis spectra and color change of *p*-HNQB in presence of anions in 1:1 H_2O :DMSO (3×10^{-4} mol/L of *p*-HNQB in presence of 5.0 equiv. anions).

ศูนย์วิทยทรัพยากร
จุฬาลงกรณ์มหาวิทยาลัย

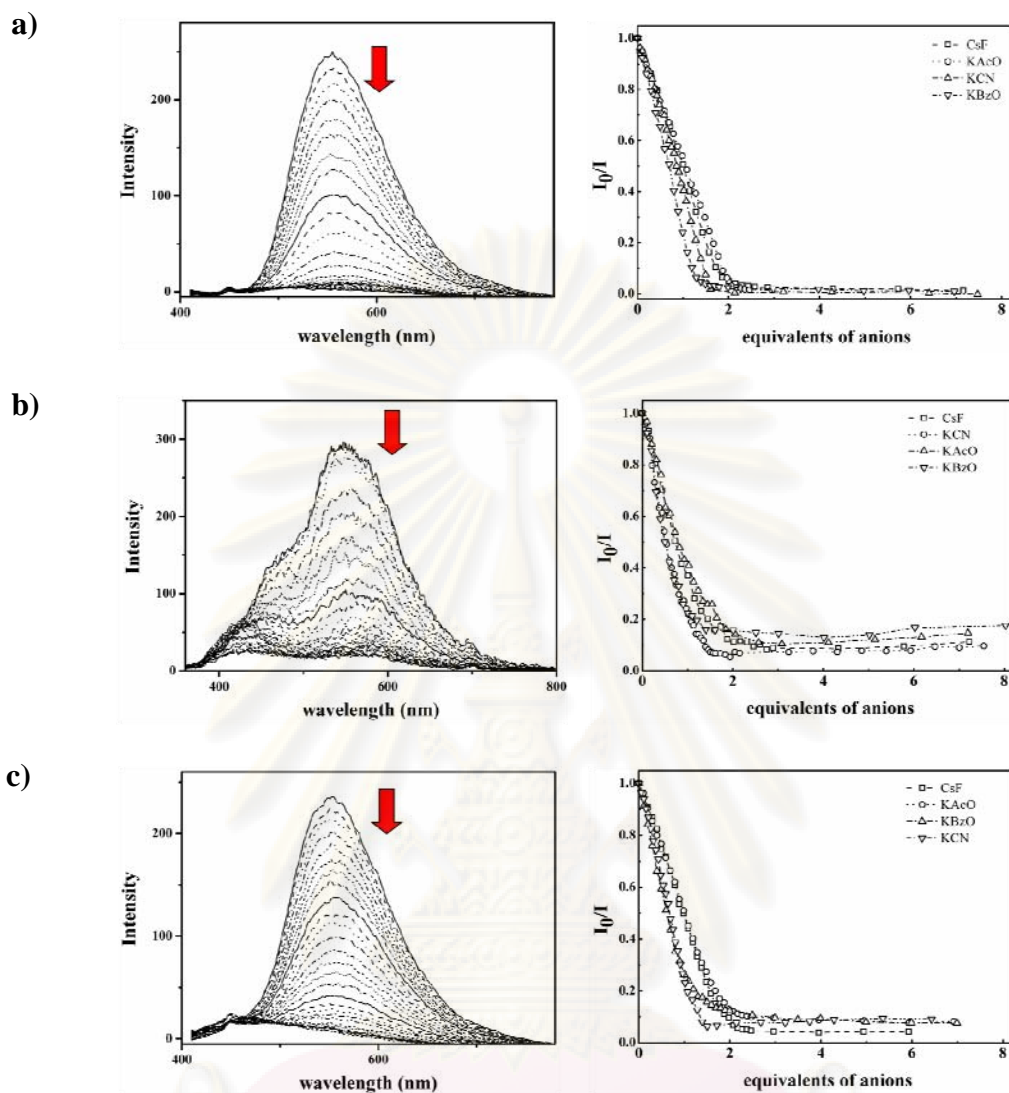
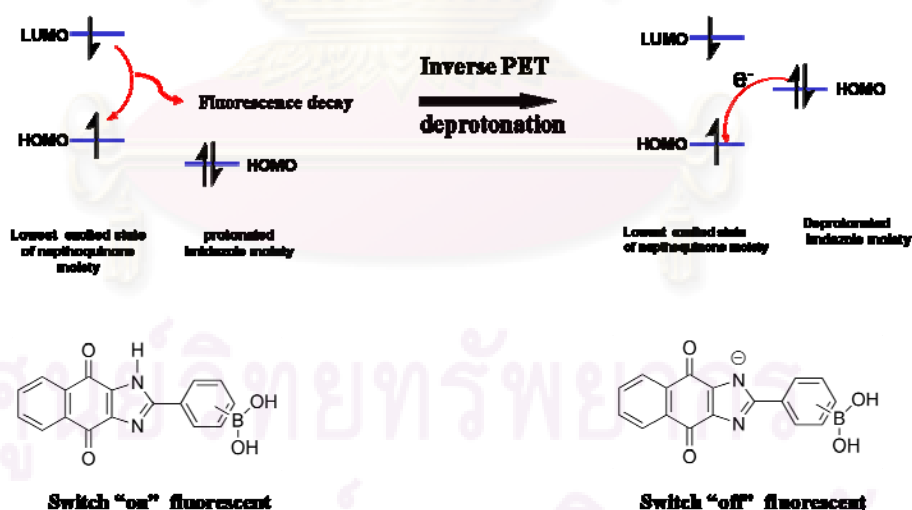


Figure 3.15 Fluorescence spectra of protonated receptors (left) at different aliquots of CsF (0-7 equiv.) and fluorescence responses (I_0/I at 554 nm) (right) upon the addition of 0-7 equiv. of various anions; CsF, KAcO, KBzO and KCN in DMSO, a) *o*-HNQB, b) *m*-HNQB and c) *p*-HNQB (3×10^{-4} mol/L of sensors in DMSO).

3.3.5 Applications of sensors *o*-HNQB, *m*-HNQB and *p*-HNQB as fluorescence anion sensors

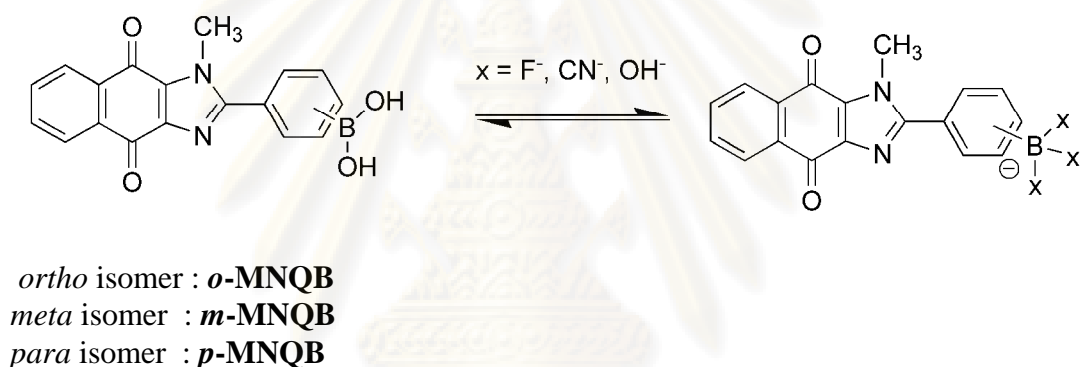
Due to the excellent sensitivity of fluorescence spectrophotometry, we attempted to utilize fluorescence properties of the synthesized sensors for anion detection. Emission spectra of, *o*-HNQB, *m*-HNQB and *p*-HNQB in DMSO solution were recorded in the presence of potassium salts of various anions using the excitation wavelength at 394 nm. Since quinone compound provided low emission properties, the DMSO solution of samples were prepared at high concentration (3×10^{-4} mol/L). Obviously, upon adding anions such as F^- , AcO^- , BzO^- , $H_2PO_4^-$ and CN^- , the emission bands of all sensors at 554 nm were gradually quenched (Figure 3.15). The reduction of quantum yield was possibly ascribed to the occurrence of inverse PET upon the deprotonation on the imidazole ring. As demonstrated in Scheme 3.4, the negative charge possibly moved to the low lying energy level resulting in disruption of emission decay of excited electrons. However, the protonated sensors including *o*-HNQB, *m*-HNQB and *p*-HNQB offered the response toward all anions. Therefore, these sensors gave a poor selectivity for anion detection.



Scheme 3.4 Feasible frontiers orbital energy diagram for the protonated sensors which was represented as the inverse PET (photoinduced electron transfer) upon the deprotonation by anions

3.4 The complexation studies of methylated naphthoquinone imidazole based sensors *o*-MNQB, *m*-MNQB and *p*-MNQB

As mentioned previously, protonated sensors were deprotonation in the presence of anions. The negative charge inhibited the anion substitution of the boron center of sensors and resulted in the poor selectivity of anion detections. The methylation on NH imidazole can inhibited the deprotonation by anions. The covalently anion-substitution on the boron center occurs as shown in Scheme 3.5. Methylated receptors, *o*-MNQB, *m*-MNQB and *p*-MNQB were studied for the effective binding with nucleophilic anions such as CN^- or F^- providing the fluorescence spectral changes.



Scheme 3.5 Equilibrium of nucleophilic substitution on the boron center of the methylated sensors *o*-MNQB, *m*-MNQB and *p*-MNQB

3.4.1 Photophysical properties of the methylated sensors

As shown in Figure 3.16 and Table 3.2, DMSO solutions of the methylated naphthoquinone imidazole sensors; *o*-MNQB, *m*-MNQB and *p*-MNQB offered quite similar optical and photophysical properties to the protonated sensors, *o*-MNQB, *m*-MNQB and *p*-MNQB. The visible absorption band at about 392 nm of all isomers is due to electron transition from electron donating group to acceptor group. Quantum yields of the sensors were as low as those of the protonated sensors.

Table 3.2 Photophysical properties of methylated sensors in DMSO

senors	λ_{abs} (nm)	Extinction coefficients (ϵ , mol/L.cm)	λ_{em} (nm)	$\Phi_{\text{f}}^{\text{a}}$
<i>o</i> -MNQB	391	1652	532	0.019
<i>m</i> -MNQB	393	1690	545	0.065
<i>p</i> -MNQB	394	1970	548	0.052

^a Quantum yields were determined using quinine sulfate as the standard (Φ_{STD}) 0.508 in 1 N H₂SO₄.

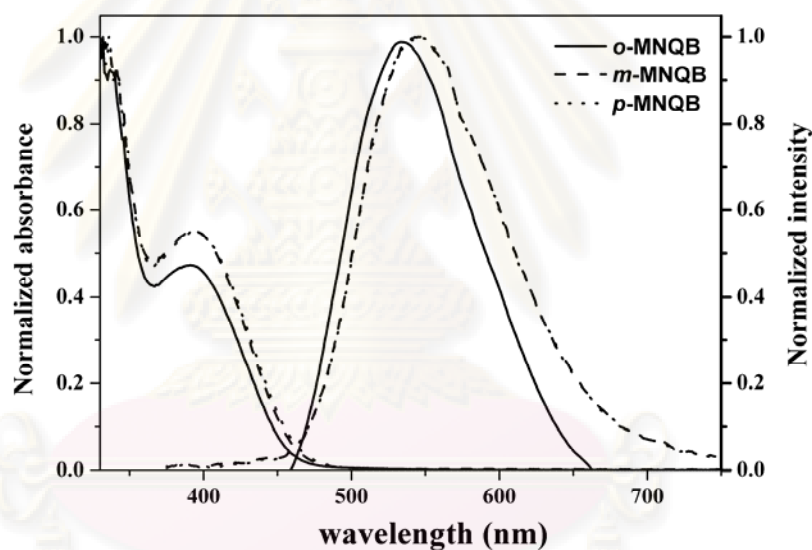


Figure 3.16 Absorption and emission spectra of *o*-MNQB, *m*-MNQB and *p*-MNQB in DMSO (3×10^{-4} mol/L)

3.4.2 The complexation studies of sensors, *o*-MNQB, *m*-MNQB and *p*-MNQB using fluorescence spectrometry

3.4.2.1 Complexation properties of sensors *p*-MNQB using fluorescence spectrophotometry in DMSO system

Complexations studies were studied in DMSO using excess amount of various anions. As shown in Figure 3.17, a large enhancement of emission band at 460 nm was observed upon the addition of 500 equivalents of tetrabutylammonium fluoride into the DMSO solution of *p*-MNQB suggesting that fluoride ion interacted with the boron center of the receptor resulting in the appearance of a new emission band at 460 nm.

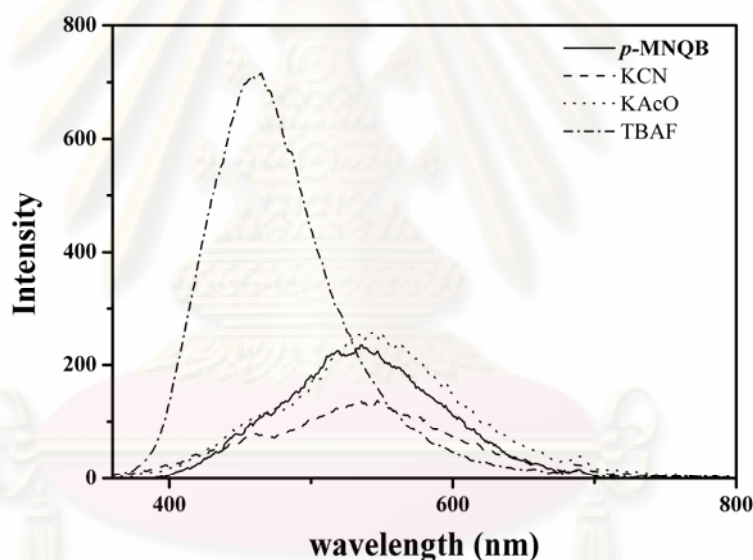


Figure 3.17 Fluorescence spectral change of *p*-MNQB (3×10^{-4} mol/L) in the presence of 500 equivalents of potassium salt for CN^- and AcO^- in DMSO and tetrabutylammonium salt for F^-

The blue shifts of *p*-MNQB upon the fluoride substitution signified to the hybridization changes of boron from sp^2 to sp^3 as shown in Scheme 3.5. Presumably, the large blue shift (*ca.* 100 nm) was derived from the reduction of electron acceptability of boron center upon the anion binding. The existence of anionic fluoride adducts including $\text{RB}(\text{OH})_2\text{F}^-$, $\text{RB}(\text{OH})\text{F}_2^-$ and RBF_3^- in DMSO were observed in $^1\text{H-NMR}$ and $^{19}\text{F-NMR}$ spectra which were described in the next sections.

Fluorescence titration experiments were carried out using 3×10^{-4} mol/L of *p*-MNQB in DMSO and adding F^- for 2 minutes prior to the measurement. As displayed in Figure 3.18, emission band intensities at 460 nm increased upon increasing fluoride concentrations. Concerning of the fluorescence response (I/I_0) at 460 nm, the graph showed gradual increase of the response without the curvature even the 1500 equiv of F^- . It is implied that the reaction between fluoride ion and the sensor was not completed in this condition.

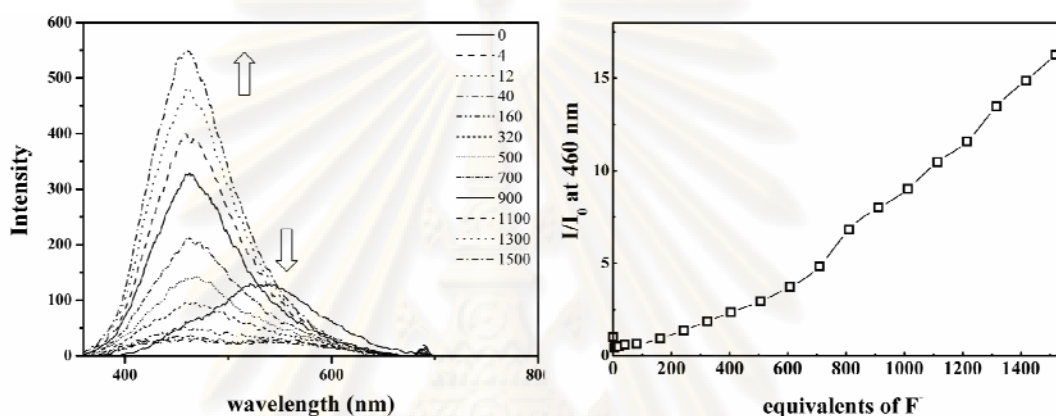


Figure 3.18 Fluorescence spectra (left) and fluorescence response (I/I_0 at 460 nm) (right) of *p*-MNQB (3×10^{-4} mol/L) in the presence of 0-1500 equivalents of tetrabutylammonium fluoride in DMSO

In order to evaluate the complete time of fluoride response, the emission band at 460 nm of *p*-MNQB with 100 equivalents of fluoride were monitored at various times. It was found that the reaction between fluoride and the sensor in DMSO was complete at 320 minutes (Figure 3.19). However, the binding constant for trifluoro-substituted complex could not be deduced by fluorescence titration in these conditions.

จุฬาลงกรณ์มหาวิทยาลัย

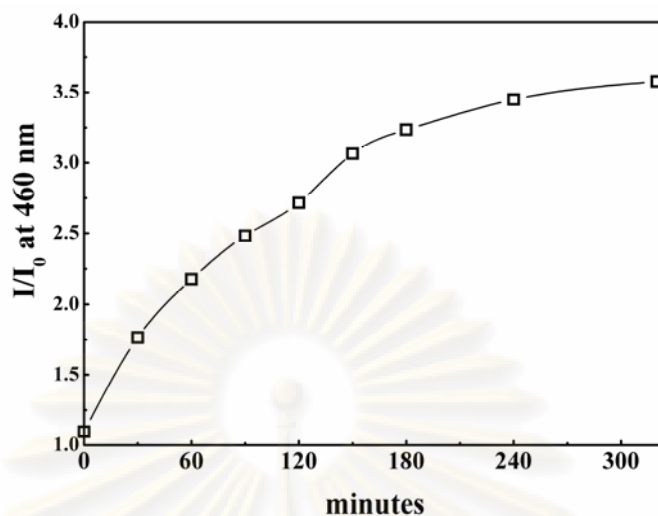


Figure 3.19 Fluorescence responses (I/I_0 at 460 nm) of *p*-MNQB (3×10^{-4} mol/L) in the presence of 100 equivalent of tetrabutylammonium fluoride in DMSO at various times (0-320 minutes).

3.4.2.2 The complexation studies of sensors *o*-MNQB, *m*-MNQB and *p*-MNQB using fluorescence spectrophotometry in DMSO:H₂O system

Although, previous showed that *p*-MNQB was a good characteristic of fluoride by switching “on” the fluorescence band at 460 nm upon fluoride binding, the sensitivity toward fluoride ion of this sensor was not acceptable for practical applications. We intended to study the methylated-sensors for fluoride sensing application in water due to the requirement of an effective fluoride sensor in aqueous system. We expected that the covalent bonding between boron and fluoride could overcome the highly solvation of water molecule toward fluoride anion in aqueous system.

Therefore anion complexation studies of sensors including *o*-MNQB, *m*-MNQB, and *p*-MNQB were examined in the mixture of DMSO: water (1:1) by using NaCl as supporting electrolyte. The selected potassium salts of anions; KCN, KF, KAcO, KBzO, KH₂PO₄, KNO₃, KClO₄, KCl, KBr and KI were tested. In the presence of 100 equiv. of potassium salts of anions, emission spectra of the sensors in the range of 360-750 nm were monitored with excitation at 344 nm to test the selectivity of the sensors.

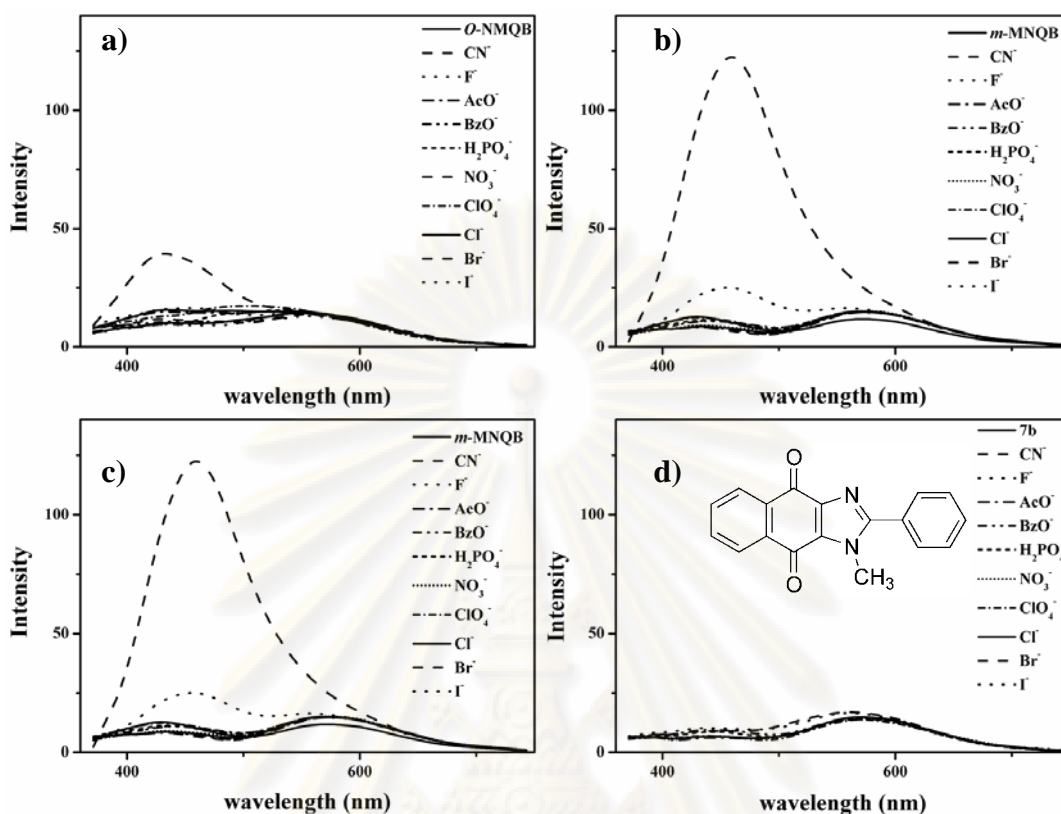


Figure 3.20 Fluorescence spectral changes of a) *o*-MNQB, b) *m*-MNQB c) *p*-MNQB and d) control compound **7b** in presence of 100 equiv. of potassium salt of anions (5×10^{-5} mol/L of receptor in 0.1 mol/L NaCl 1:1, H₂O:DMSO).

As illustrated in Figure 3.20, the enhancements of fluorescence intensities at 460 nm were observed upon the addition of cyanide ion in all receptors. However, *m*-MNQB and *p*-MNQB gave slight responses toward fluoride ion. Since the nucleophilic substitution of cyanide to the carbonyl of naphthoquinone can take place [27, 28] the control compound **7b**, naphthoquinone imidazole derivative without boronic acid, was also synthesized to verify the interaction mode of sensors. The control compound **7b** showed insignificant response toward any anions suggesting that the fluorescence enhancement at 460 nm stemmed from the interaction between cyanide or fluoride ions and the boron center of sensors. Therefore, fluorescence responses at 460 nm upon the cyanide addition were assigned to the anionic substitution on the boron center.

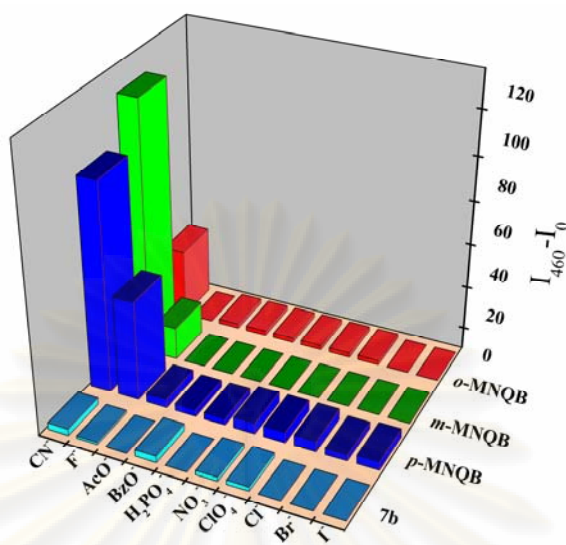


Figure 3.21 Fluorescence response ($I-I_0$ at 460 nm) of *o*-MNQB, *m*-MNQB, *p*-MNQB and control compound **7b** in the presence of 100 equiv. potassium salt of anions (5×10^{-5} mol/L of receptor in 0.1 mol/L NaCl 1:1, H₂O:DMSO).

Considering the selectivity of methylated sensors in DMSO:H₂O system, the high fluorescence responses ($I-I_0$ at 460 nm) illustrated in Figure 3.21 suggested that all methylated sensors preferred cyanide to fluoride. Although it is well known that fluoride was able to bind with the boron center, all isomers gave a high response to CN⁻ over F⁻ in this system. It can be rationalized that fluoride has a high hydration enthalpy and low basicity ($\Delta H_{\text{hyd}}^0 = -504$ kJ/mol, $pK_a = 3.18$) [95] in aqueous system therefore, it is hard to expel the solvated water to undergo the reaction with the boron atom.

To verify the sensitivity of each isomer, fluorescence titrations of methylated compounds were carried out in 0.1 mol/L NaCl 1:1, H₂O:DMSO. Prior to fluorescence measurement, the solution mixture of the sensor and cyanide was stirred for 10 minutes. As displayed in Figure 3.22a, intensities of the emission bands at 460 nm increased as a function of cyanide concentration. As shown Figure 3.22b, the titration curve showed the different ratio of intensity (I/I_0) at 460 nm upon increasing of cyanide. The ratio of I/I_0 of *meta* isomer has higher value than that of *para* and *ortho* isomer. *o*-MNQB showed the fluctuation change of I/I_0 value during the titration. The fluctuated fluorescence results in the case of *o*-MNQB were due to the

weak interaction of cyanide that was arised from two factors, i) the steric on the boron center and ii) the strongest N-B interaction on this isomer. Subsequently, the most effective fluorescence probe for cyanide ion in these studies was the *meta* isomer which possessed a good combination of selectivity, and sensitivity.

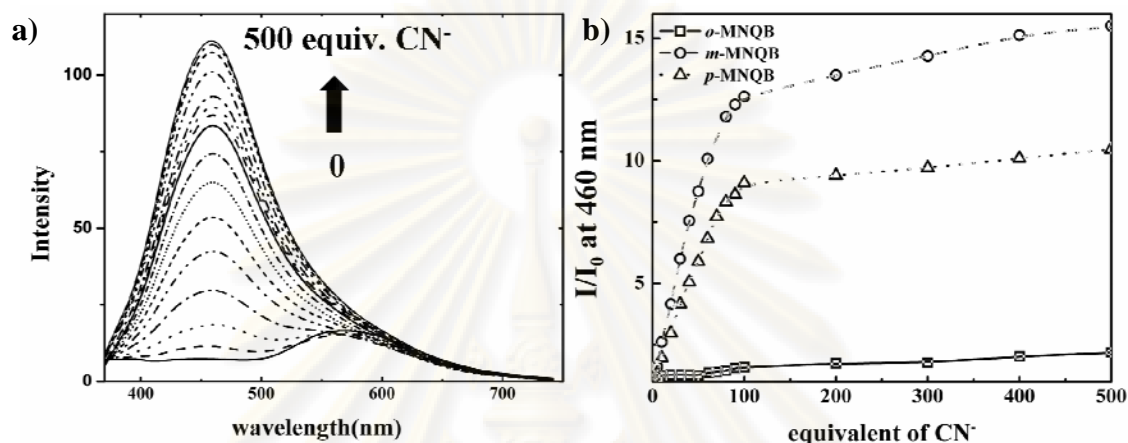


Figure 3.22 A) showed fluorescence spectra changes of *m*-HNQB (5×10^{-5} mol/L) upon the addition of 0-500 equivalents of KCN and right panel b) showed fluorescence responses at 460 nm (I/I_0) of *o*-HNQB, *m*-HNQB and *p*-HNQB in the presence of 0 - 500 equiv. of KCN in 0.1 mol/L NaCl 1:1, $\text{H}_2\text{O}:\text{DMSO}$ (5×10^{-5} mol/L of sensors).

It is well known that hydroxide is able to interact with boronic resulting in the generation of anionic species, $\text{RB}(\text{OH})_3^-$ which has similar electronic properties to RBF_3^- or $\text{RB}(\text{CN})_3^-$. To verify the hydroxide effect, fluorescence titration experiments of *m*-MNQB with potassium hydroxide were performed in 0.1 mol/L NaCl 1:1, $\text{H}_2\text{O}:\text{DMSO}$. As expectation, hydroxide adducts of *m*-MNQB is able to generate the fluorescence response at 460 nm similar to cyanide and fluoride adducts of sensors. As elucidated in Figure 3.23, the results showed that hydroxide response was significantly higher than cyanide response. Therefore, hydroxide concentration must be strongly concerned for boronic based sensors.

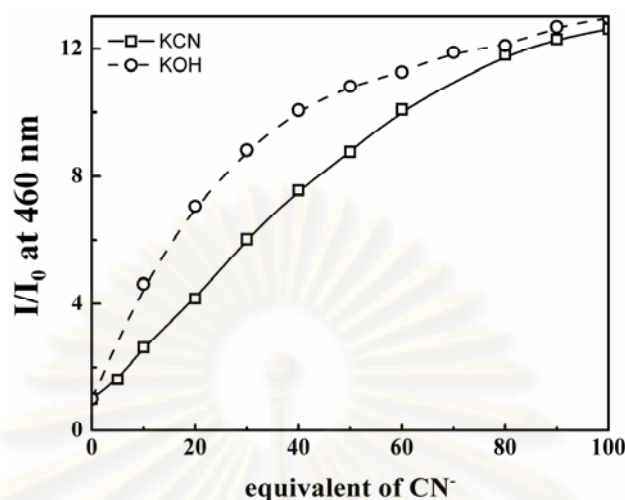


Figure 3.23 Fluorescence responses at 460 nm (I/I_0) of *m*-HNQB in the presence of 0-100 equiv. of KCN and KOH in 0.1 mol/L NaCl 1:1, H₂O:DMSO (5×10^{-5} mol/L of sensors).

3.4.2.3 The complexation studies of sensors, *o*-MNQB, *m*-MNQB and *p*-MNQB by fluorescence spectrophotometry in DMSO:H₂O system in the presence of HEPES as buffering reagent

In order to control hydroxide concentration, HEPES which is organic chemical buffering reagent, is used for maintaining physiological pH change. HEPES not only controlled the pH in the range of pH 6-7, but was also non-coordinating agent. Therefore, complexation studies were carried out in 0.1 mol/L NaCl in 50% HEPES pH 7.4:DMSO using 5×10^{-5} mol/L of sensors. Screening tests were performed in the presence of 500 equivalents of various potassium salts of anions. As presented in Figure 3.24, in the presence of CN⁻ the high response at 460 nm were observed in the case of *m*-MNQB and *p*-MNQB, whereas *o*-MNQB showed a slight response. Furthermore, upon exposing to UV-lamp (365 nm), the solution of *m*-MNQB plus CN⁻ gave a brighter luminescence than that of *m*-MNQB plus F⁻.

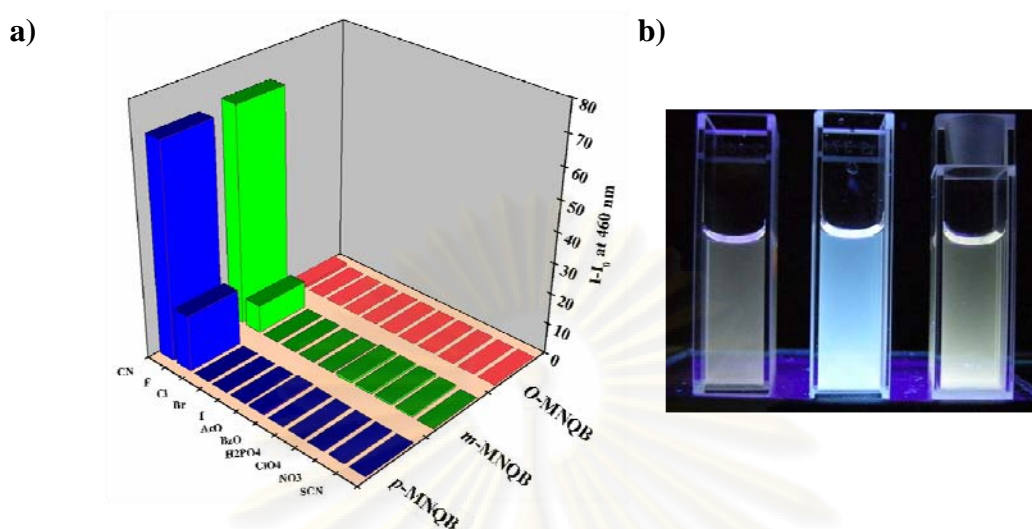


Figure 3.24 A) fluorescence response ($I-I_0$ at 460 nm) of *o*-MNQB, *m*-MNQB and *p*-MNQB in the presence of 500 equiv. of potassium salts of anions and b) fluorescence responses upon irradiated with UV-lamp (256 nm) of solutions of **3b** (left), **3b** + CN⁻ (middle) and **3b** + F⁻ (right) (5×10^{-5} mol/L of sensor in 0.1 mol/L NaCl in 50% HEPES pH 7.4: DMSO)

The cyanide binding properties of the methylated sensors were evaluated by fluorescence titration using DMSO:HEPES buffer system. As shown in Figure 3.24, the similar results were found in all three sensors. As expected, the fluorescence response in this system showed lower response than that of the non-buffer system due to the strong interference of hydroxide concentration generated. However, the methylated sensors provided minimum fluorescence response of cyanide ion over the concentration of 0.5 mM. The saturation of signal was more than 1200 equivalents, which were not appropriate for practical applications.

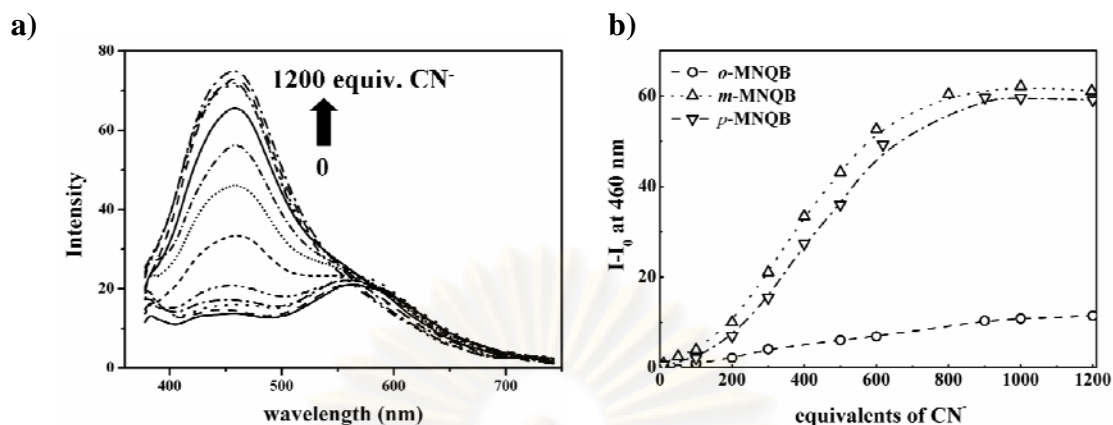


Figure 3.25 A) Fluorescence spectra of *m*-MNQB with increasing of cyanide concentration (5×10^{-5} mol/L of sensor in HEPES buffer pH 7.4, 0.1 mol/L NaCl, 50% H₂O:DMSO) and b) fluorescence response ($I-I_0$ at 460 nm) of *o*-MNQB, *m*-MNQB and *p*-MNQB with increasing of cyanide concentration

It should be noted that hydroxide can be possibly generated by a high concentrations of CN⁻ leading to the increasing of the pH of the solution. High concentration of CN⁻ may be controlled by the buffer capacity. To verify the HEPES buffer capacity, the pH of the solution mixture was measured before and after the addition of 500 equivalent or 25 mM of potassium cyanide in the presence of HEPES. It was found that the pH of the solution was raised from 7.4 to 11. Presumably, at high concentration of potassium cyanide can generate hydroxide ion which was easily substituted on boron center providing R-B(OH)₃⁻ species. Therefore, millimolar level of cyanide ion in water, the intensities of emission band at 460 nm do not reflect to the cyanide recognition only. To clarify this point, the mixture of *p*-MNQB in the presence of 500 equivalent of KCN in HEPES buffer pH 7.4, was tested by ESI mass spectroscopy. The spectrum showed an intense peak at 387.06 m/z which was corresponded to *p*-MNQB-(OH)₃⁻+K⁺ species (Figure 3.26). These phenomena could not occur with other anions because they have a low basicity to generate hydroxide in water.

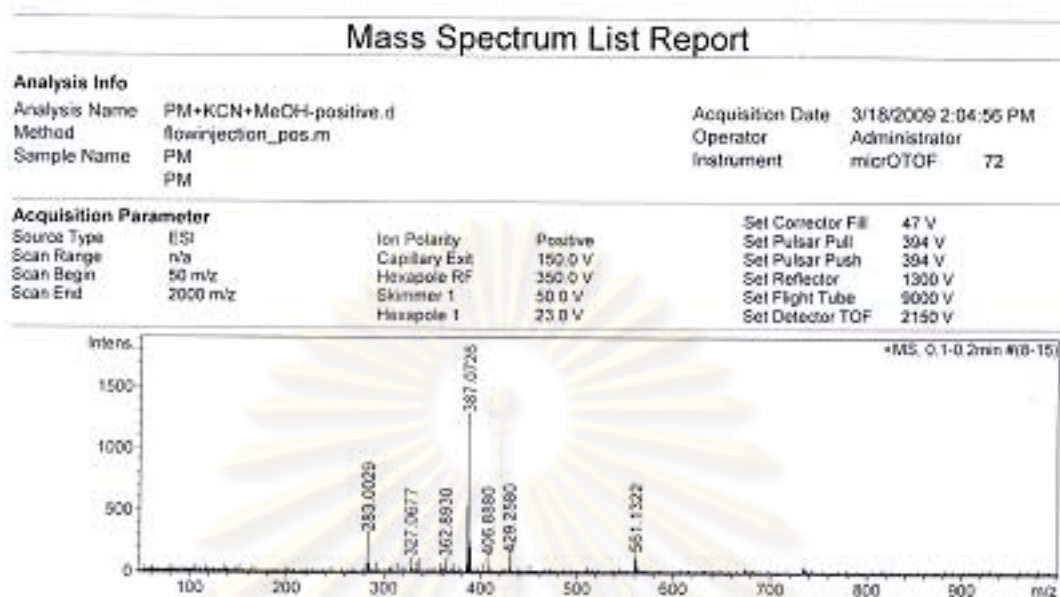


Figure 3.26 The ESI mass spectrum of *p*-MNQB in the presence of 500 equiv. of KCN in HEPES buffer pH 7.4, 0.1 mol/L NaCl, 50% H₂O:DMSO.

The results revealed that the neutral boronic based sensor which lacked of positive charge could not offer the reasonable cyanide detection system regarding response time and working range. However, our synthesized sensors showed the excellent characteristic of the fluorescence sensor in term of a large Stokes shift ($\Delta\lambda_{\text{ex-emiss}} = 120 \text{ nm}$) as well as a large blue shift of *ca.* 100 nm upon the changes in the hybridization of the boron center. Therefore, we intended to develop the methyl naphthoquinone imidazole boronic based sensor for cyanide detection aqueous micellar systems.

ศูนย์วิทยทรัพยากร
 จุฬาลงกรณ์มหาวิทยาลัย

3.4.3 The complexation studies of the sensors, *o*-MNQB, *m*-MNQB and *p*-MNQB using fluorescence spectrophotometry in aqueous micellar systems

We attempted to search for the effective system for cyanide detection using our sensors without the synthetic modifications. In previously reports, a number of the micellar systems were employed in detecting cation [96-105]; anion [108-110]; and neutral analytes. [106, 107] In our approach, the incorporation of the sensors into micellar systems was carried out to increase the solubility of sensors in water and enhance the complexation ability [101, 111-112] of cyanide to the sensor to obtain a good response time and improve the limit of detection down to a micromolar level which could disregard the interference from hydroxide.

3.4.3.1 The micellar optimum condition for the cyanide complexation studies of the sensors *o*-MNQB, *m*-MNQB and *p*-MNQB by fluorescence spectrophotometry.

To optimize the appropriate condition to obtain the highest efficiency of cyanide complexations ability, firstly, three types of surfactants, neutral (Triton X-100), anionic (SDS) and cationic (CTAB) surfactants were examined for the fluorescence responses in the presence of 50 μM cyanide. This cyanide concentration cannot change the pH of the solution resulting in the sustaining of pH at 7 (5×10^{-5} mol/L of receptor in 5 mM of surfactant in 1:4 ethanol:H₂O).

ศูนย์วิทยทรัพยากร
จุฬาลงกรณ์มหาวิทยาลัย

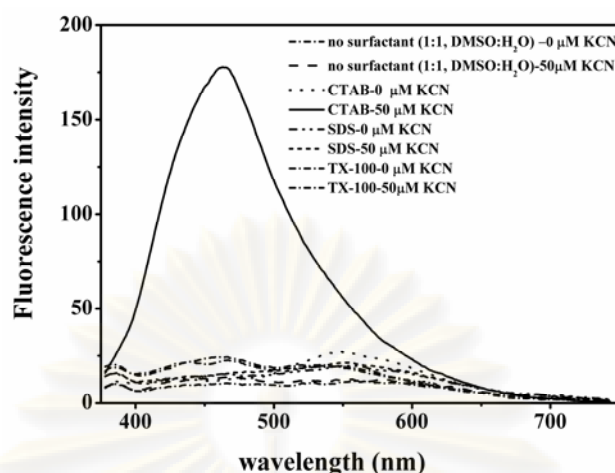


Figure 3.27 Fluorescence spectra of *m*-MNQB and *m*-MNQB + 50 μ M KCN with various types of surfactants (5×10^{-5} mol/L of *m*-MNQB, 5×10^{-3} mol/L of surfactant in 1:4 of ethanol:H₂O)

As expected, all cationic, anionic, and neutral surfactants, offered the improvement of the solubility of the receptors in water by hydrophobic insertion of the sensors into micelles. Emission spectra of free *m*-MNQB in three micellar systems exhibited similar feature with emission maxima at 540 nm. As illustrated in Figure 3.27, in the presence of 50 μ M of cyanide, emission bands at 460 nm of *m*-MNQB which were switched “on” upon the hybridization changes on the boron center from sp^2 to sp^3 was remarkably enhanced in the CTAB system. In the case of TX-100 neutral surfactant system, the receptors showed a slight response upon the addition of 50 μ M cyanide. In SDS anionic surfactant system, the fluorescence response at 460 nm remained unchanged upon the addition of 50 μ M cyanide suggesting no interaction between sensors and cyanide. It implied that complexation ability of sensors toward cyanide was interrupted by electrostatic repulsion between the anionic micellar surface and cyanide. Therefore, neutral and anion surfactants improved only solubility of the sensors in water but not promoted the cyanide-substitution on the boron center. In the case of CTAB micellar system, this system gave remarkable improvement of cyanide detection ability in water by providing a 200-fold fluorescence enhancement at 460 nm in the presence of 50 μ M of potassium cyanide.

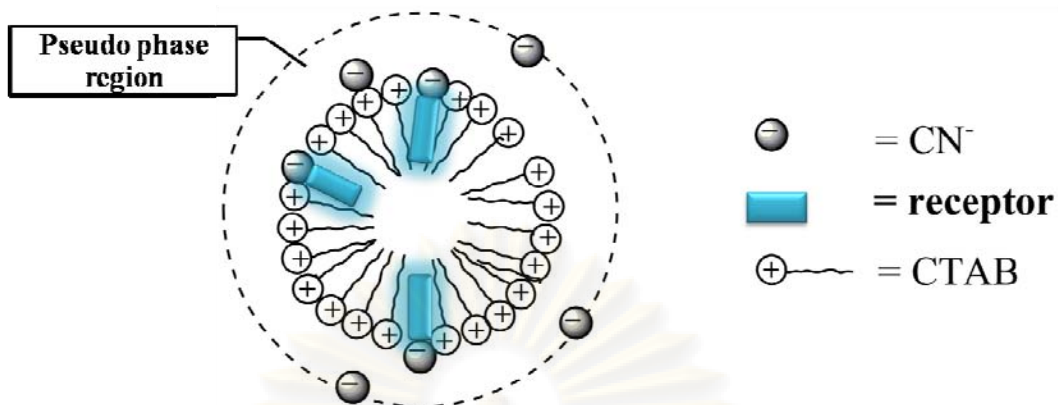


Figure 3.28 The proposed model of the reaction of sensors and cyanide in the CTAB micellar system.

According to the previous reports regarding to the receptors and guests in micellar systems, [111-113] the model of the reaction between sensors and cyanide in the micellar system was proposed in Figure 3.28. The improvement of cyanide detection ability relied largely on the electrostatic interactions between cationic surface of CTAB micelle and the negative charge of cyanide. When CN^- and sensors were brought together on the pseudo-phase region of the micelle, the local concentration of both reactants of the equilibrium increase, subsequently forced the substitution reaction to occur. The emergence of anionic $\text{R-B}(\text{CN})_3^-$ species produced fluorescence enhancement at 460 nm as described in the previous studies. Additionally, this incorporation contributed to the improvement of emission properties of $\text{R-B}(\text{CN})_3^-$ due to good distribution of the sensors in the hydrophobic region of the micelle. This distribution can protect the solvation of the sensors by water and polar solvent, which is probably an important factor of the low quantum yield of the fluorophore in aqueous system due to non-emissive relaxation by a polar solvent.

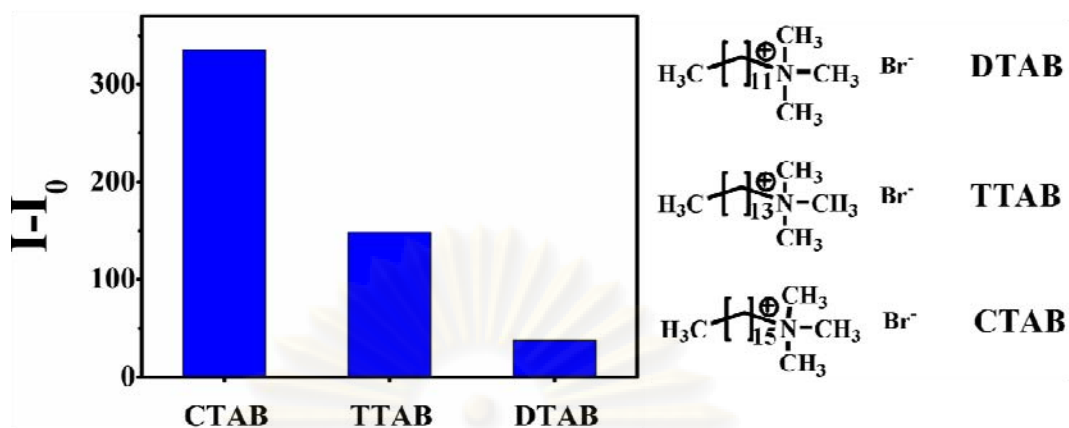


Figure 3.29 Fluorescence responses of *m*-MNQB and *m*-MNQB + 50 μ M KCN with various types of cationic surfactants (5×10^{-5} mol/L of *m*-NQB, 5×10^{-3} mol/L of surfactant in 1:4 ethanol:H₂O)

Moreover, the optimum cationic surfactant with a different chain length were also explored. Figure 3.29 showed the effect of the chain length of cationic surfactants (DTAB, TTAB, and CTAB) versus the cyanide sensing properties of the sensors. In the same conditions, a longer chain micelle such as CTAB provided a complete micelle [113] form resulting in a large response of emission band at 460 nm. It is clearly seen that the incorporating sensors in CTAB remarkably improved the sensitivity of the sensors, CTAB was thus a suitable surfactant for further studies.

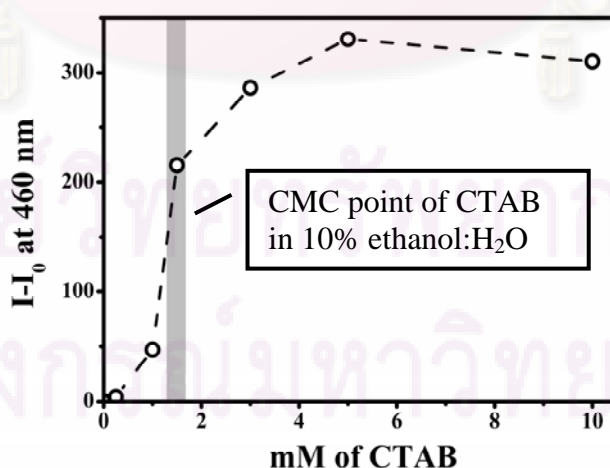


Figure 3.30 Fluorescence response ($I-I_0$) of *m*-MNQB (5×10^{-5} mol/L) + 50 μ M KCN in various concentration of CTAB and CMC of CTAB in 10% ethanol:H₂O shown as gray area.

The effect of CTAB concentrations were also studied as demonstrated in Figure 3.30. The concentration of CTAB at 1.5 mM afforded a large change of fluorescence response in the case of *m*-MNQB and *p*-MNQB. These results agreed well with the critical micelle concentration (CMC) of CTAB in 1:4 ethanol in water reported in the literature. [114] It should be noted that the fluorescence intensity increased with increasing CTAB concentration above the CMC of CTAB (1.5 mM in 1:4 of ethanol in water). These results supported our approach that the reaction between cyanide and the sensors was accelerated at the cationic surface of micelle by means of the encouragement of shift to the right side of equilibrium. However, 5 mM of CTAB was used in all manipulations (100 equivalents compared to the probe)

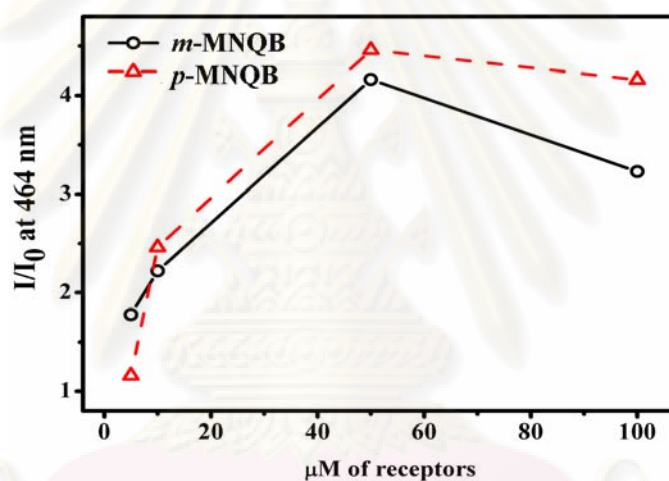


Figure 3.31 Fluorescence responses of *m*-MNQB + 25 μM KCN and *p*-MNQB + 25 μM KCN with various concentration of sensors (100 equivalents of CTAB compared to sensors in 1:4 ethanol:H₂O).

The effect of sensor concentrations was also examined in the presence of 100 equivalents of CTAB compared to sensor concentration and 25 μM of KCN. The fluorescence responses of *m*-MNQB and *p*-MNQB were displayed in Figure 3.31. I/I_0 of the detection system showed the highest response at 50 μM of sensors and 5 mM of CTAB. At low concentration of sensors, the accessibility of the sensor toward cyanide was disturbed by the competitive interaction between CTAB cationic surfaces and cyanide. At high concentration of sensors (100 μM), fluorescence response slightly decreased possibly caused by low amount of cyanide in this system.

For further studies the optimum condition for micromolar cyanide sensing in water is $50 \mu\text{M}$ of sensors and 5.0 mM of CTAB.

3.4.3.2 Selectivity and sensitivity of the sensor in the optimal micellar system

To verify the sensitivity and selectivity of this optimum condition, *m*-MNQB and *p*-MNQB were studied in CTAB micellar system under the optimum conditions in the presence of $50 \mu\text{M}$ of various anions. As illustrated in Figure 3.32, the incorporation of *m*-MNQB and *p*-MNQB into the CTAB micellar system provided the highest fluorescence response for millimolar concentration of cyanide ion. Hence, *m*-MNQB and *p*-MNQB have excellent selectivity for cyanide over other anions in the optimum condition of CTAB micellar system.

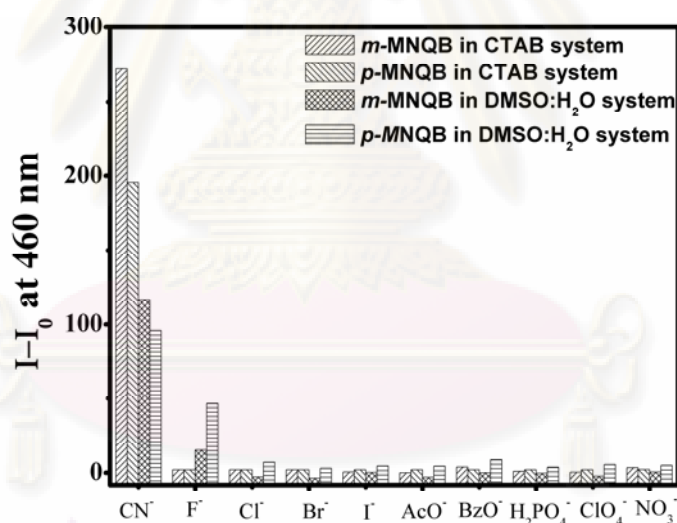


Figure 3.32 Fluorescence responses ($I-I_0$ at 460 nm) of *m*-MNQB and *p*-MNQB in the CTAB micellar system in the presence of $50 \mu\text{M}$ (1 equiv.) of various anions ($5 \times 10^{-5} \text{ mol/L}$ of sensor, $5 \times 10^{-3} \text{ mol/L}$ of CTAB in 1:4 ethanol: H_2O) and fluorescence responses of *m*-MNQB and *p*-MNQB in DMSO: H_2O system with 25 mM (500 equivalents) of various anions ($5 \times 10^{-5} \text{ mol/L}$ of receptor in 0.1 mol/L of NaCl in 50% HEPES pH 7.4:DMSO).

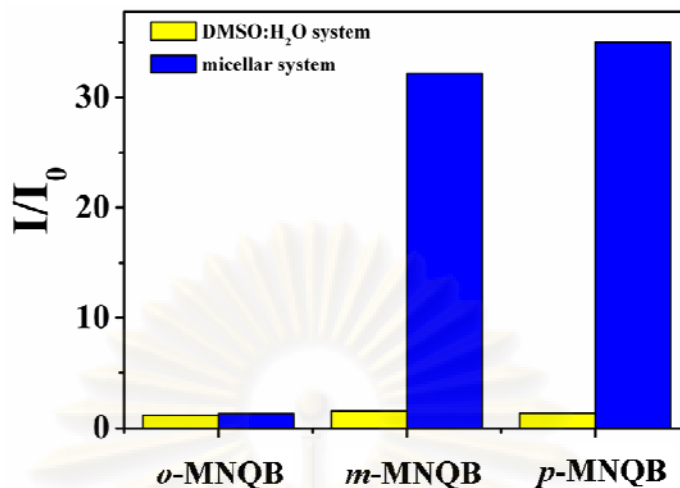


Figure 3.33 Fluorescence response (I/I_0 at 460 nm) of *o*-MNQB, *m*-MNQB and *p*-MNQB with 0.25 mM of cyanide mixing for 30 minutes in the DMSO:H₂O system (5×10^{-5} mol/L of sensor in 0.1 mol/L of NaCl in 50% HEPES pH 7.4:DMSO) and in the micellar system (5×10^{-5} mol/L of sensors, 5×10^{-3} mol/L of CTAB in 1:4 ethanol:H₂O).

To compare the sensitivity of the sensors in the CTAB micellar system and the DMSO:H₂O system, fluorescence responses (I/I_0) at the same amount of KCN were measured after mixing for 30 minutes. The results in Figure 3.33 showed that the incorporation of *m*-MNQB and *p*-MNQB into the CTAB micelle gave remarkably higher sensitivity toward CN⁻ than in the solution of mixed DMSO: H₂O. As described in previous sections, sensors in DMSO:H₂O showed the fluorescence responses in a millimolar level whereas sensors in CTAB micelle afforded the fluorescence response in a micromolar level.

3.4.3.3 The evaluations of stability constants for tricyano-substitution complexes of the sensors in optimum condition of the CTAB micellar system

As describes in previously, we cannot calculate the stability constants (K) of the tricyano-substituted complex of the synthesized sensors in DMSO and DMSO:H₂O system. This probably stemmed from many factors such as i) a poor rate of CN⁻ substitution and ii) the undesired hydroxide interference. However, we found that the reaction between receptors and cyanide was accomplished in the micellar system observing from the saturated fluorescence signal at 460 nm in 30 minutes. Therefore, we take the advantage of the acceleration of the reaction between the sensors and cyanide ion in the CTAB micellar system to evaluate the cyanide complexation abilities of *o*-MNQB, *m*-MNQB and *p*-MNQB.

Fluorescence titrations were carried out in the CTAB optimum conditions by adding aliquots of KCN concentration (5×10^{-5} mol/L of receptors, 0-5 equivalents of KCN in 5×10^{-3} mol/L of CTAB in 1:4 ethanol:H₂O). Fluorescence titration spectra of *o*-MNQB, *m*-MNQB and *p*-MNQB were illustrated in Figure 3.34. Sensors *m*-MNQB and *p*-MNQB showed that emission band at 460 nm were increasing upon the increment of the cyanide concentration. Interestingly, the fluorescence intensity was saturated at 3 equivalents (150 μ M) of KCN. It was indicative of the tri-substitution of cyanide on the boron center of *m*-MNQB and *p*-MNQB. Unfortunately, *o*-MNQB showed a fluctuated titration curve as shown in Figure 3.34a.

ศูนย์วิทยทรัพยากร
จุฬาลงกรณ์มหาวิทยาลัย

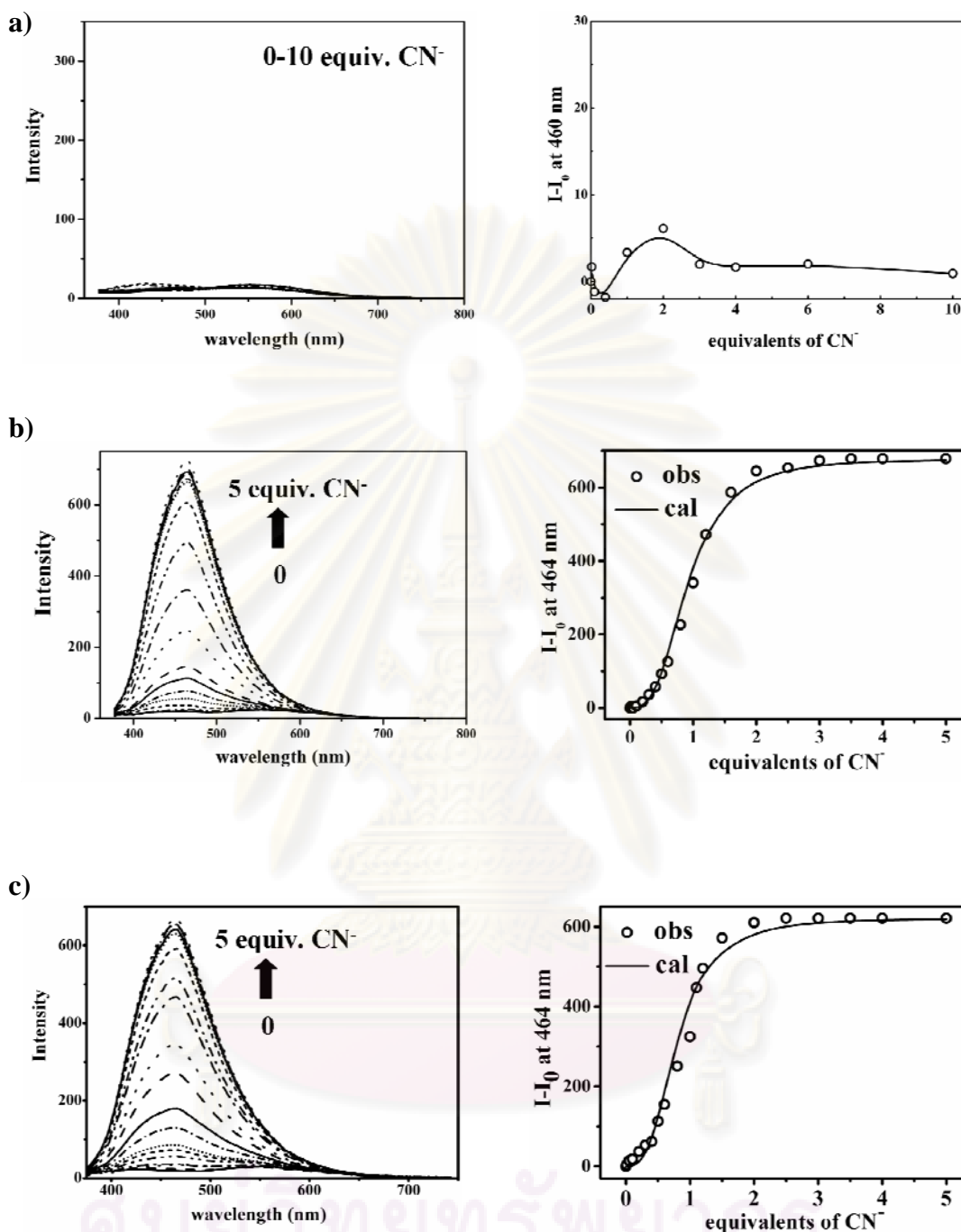
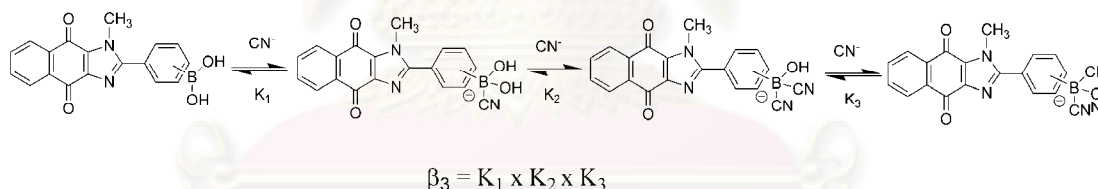


Figure 3.34 Fluorescence titration spectra (left) and the fluorescence titration curves (right) of a) *o*-MNQB, b) *m*-MNQB and c) *p*-MNQB upon the addition of cyanide ion in CTAB micellar system (5×10^{-5} mol/L of sensors, 5×10^{-3} mol/L of CTAB in 1:4 ethanol:H₂O).

Stability constants of *tri*-cyano complexes of the sensors (Scheme 3.9), *m*-MNQB and *p*-MNQB, in CTAB micelle (5×10^{-5} mol/L of sensors, 5×10^{-3} mol/L of CTAB in 1:4 ethanol:H₂O) were calculated by fitting the emission intensity at 460 nm ($\lambda_{\text{ex}} = 344$ nm) versus concentration of potassium cyanide using non-linear relation equation 1 and 2, [58] where I_{min} and I_{max} are the initial and final fluorescence intensities of the titration curves, respectively. Titration data were analyzed using Solver in Microsoft Excel and the regression statistic were determined using SolverStat macro.

$$I = \frac{I_0 + I_{\infty} \beta_n [\text{CN}^-]^n}{1 + \beta_n [\text{CN}^-]^n} \quad (1)$$

$$\beta_n = \frac{[\text{RB}(\text{OH})_{3-n}(\text{CN})_n]}{[\text{RB}(\text{OH})_2][\text{CN}^-]^n} \quad (2)$$



Scheme 3.6 Equilibrium of tricyano-substituted of the methylated sensors *o*-MNQB, *m*-MNQB and *p*-MNQB

From equations 1 and 2, the best fitting of fluorescence intensity at 460 nm versus cyanide concentration corresponded to the n value of 3. As illustrated in Figure 3.34, calculated intensity (I_{cal}) agreed well with the observation data (I_{obs}) which were saturated at three equivalents of cyanide. Unfortunately, the titration data did not well define for the calculations of stepwise stability constants (K_1 , K_2 and K_3). Overall stability constants of tri-cyano substituted complex ($\log \beta_3$) of *m*-MNQB and *p*-MNQB obtained by the best fit were collected in Table 3.3. These results showed that *meta* and *para* isomers have the similar binding abilities towards cyanide in the

CTAB micelle. Therefore, the boronic acids at *meta* and *para* positions has no steric effect on cyanide substitution.

Table 3.3 Overall stability constants for tri-substituted cyanide complex of *o*-MNQB, *m*-MNQB and *p*-MNQB in CTAB micellar condition (5×10^{-5} mol/L of sensors, 5×10^{-3} mol/L of CTAB in 1:4 ethanol:H₂O)

Sensors	$\log \beta_3$
<i>o</i> -MNQB	<i>nd</i>
<i>m</i> -MNQB	4.19 ± 0.09
<i>p</i> -MNQB	3.99 ± 0.05

nd = not determine

Regarding the reactivity of *o*-MNQB toward cyanide, the result showed poor CN-substitution on this isomer. Obviously, the incorporation of *o*-MNQB into CTAB micellar system could not improve the complexation ability toward cyanide ion. Poor substitution of cyanide onto *ortho* position of naphthoquinone imidazole boronic based sensor can be also explained by the calculated structure using density function theory (DFT) at B3LYP/6-31+G(d) level as depicted in Figure 3.35. The calculated structures showed that the dihedral angles of the donor and acceptor planes of *o*-MNQB, *m*-MNQB and *p*-MNQB were 56.5° , 37.5° and 37.7° , respectively. After cyanide substitution, the dihedral angles of CN-substituted *m*-MNQB and *p*-MNQB changed slightly ($\sim 2^\circ$) while that of substituted *o*-MNQB rotated significantly (nearly 12°). The large preorganization of this isomer probably inhibited the substitution of cyanide in the boronic center of *o*-MNQB. The calculated structure thus agreed very well with the experimental results, which showed that the emission spectra of *o*-MNQB before and after cyanide additions were insignificantly different.

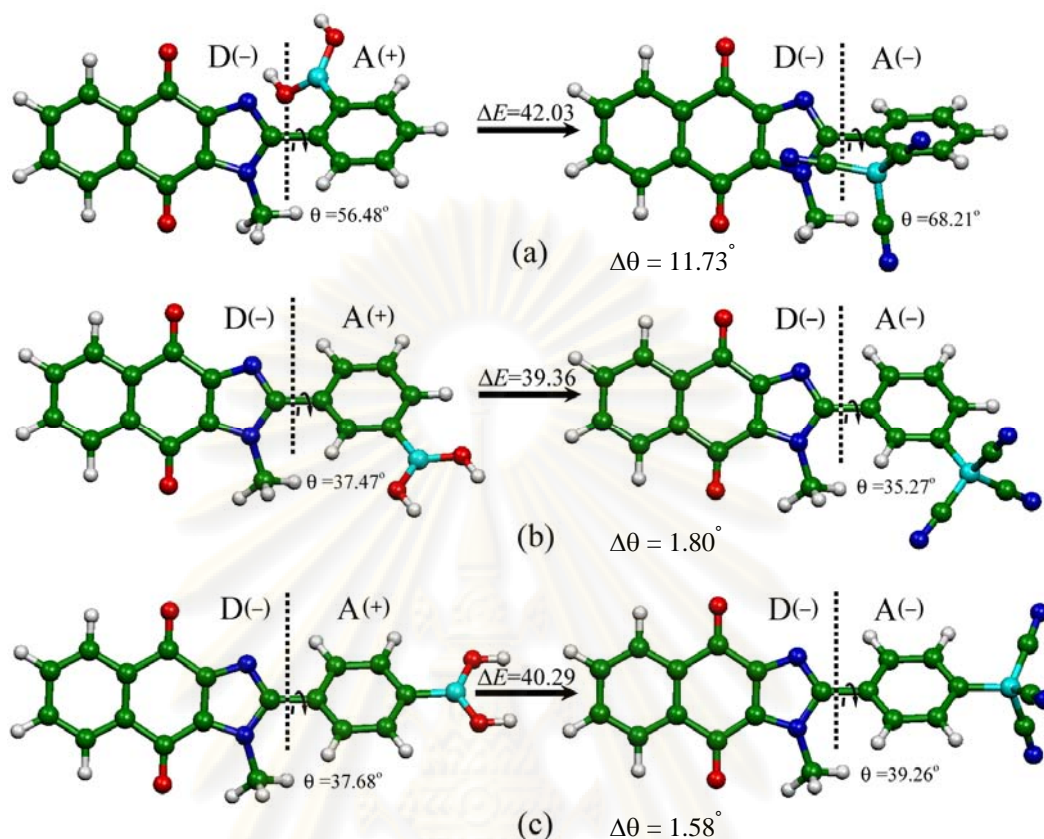


Figure 3.35 B3LYP/6-31+G(d) optimized structures of (a) *o*-MNQB (left), *o*-MNQB-CN₃⁻ (right), (b) *m*-MNQB (left), *m*-MNQB-CN₃⁻ (right) and (c) *p*-MNQB (left), *p*-MNQB -CN₃⁻ (right). Their reaction energies, ΔE are in kcal/mol, interplanar angles, θ are in degrees and D and A represent electron donor and acceptor of their molecular segments, respectively and their charge-signs are in parenthesis.

ศูนย์วิทยทรัพยากร
จุฬาลงกรณ์มหาวิทยาลัย

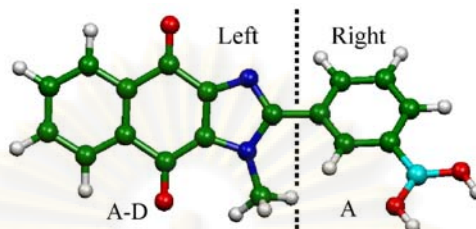
3.4.3.4 Calculated structures of the methylated sensors and their *tri*-cyano adducts using density functions theory (DFT)

As previous discussions, the observation of a high emission band at 460 nm indicated that nucleophilic attacked on boron center to give a sp^3 boron center of anionic adduct, RBX_3^- (X= OH^- , CN^- and/or F^-). On the strategy of design, the sensor was desighed using A-D-A system. Imidazole connecting to naphthoquinone was expected to be main A-D segment. The boronic acid site was expected to be a electron acceptor site. Consequently, the interaction of anion onto boron center was expected to alter the ICT efficiency of the sensor resulting in the large response of their spectra.

For better understanding for photophysical properties, the free methylated sensors and their *tri*-cyano adducts were calculated using density function theory (DFT) at B3LYP/6-31+G(d) level. As collected in Table 3.5, natural bond orbital (NBO) charges of righth segments suggested that segment of free sensor which possessed a negative charge acted as donor site while the righth segment or the boronic segments which possessed a positive charge acted as an electron accptor site. Upon the addition of CN^- , the recognition segment charge turned to negative corresponding to the reduction in acceptability of boronic acid resulting in the pertubation of ICT excited state. It meanted that the dominating of this ICT excited state was swithced “on” by the formation of anionic adduct.

ศูนย์วิจัยทรัพยากร
จุฬาลงกรณ์มหาวิทยาลัย

Table 3.4 NBO charges of segments of *o*-MNQB, *m*-MNQB and *p*-MNQB and of *o*-MNQB(CN)₃⁻, *m*-MNQB(CN)₃⁻ and *p*-MNQB(CN)₃⁻ derived from the B3LYP/6-31+G(d) computations



Species	Charge ^a		Total charge ^a
	Left segment	Right segment	
Free hosts			
<i>o</i> -MNQB	-0.02685	0.02685	0.00
<i>m</i> -MNQB	-0.03985	0.03985	0.00
<i>p</i> -MNQB	-0.02358	0.02358	0.00
Full CN-substituted hosts			
<i>o</i> -MNQB(CN) ₃ ⁻	-0.04235	-0.95762	-1.00
<i>m</i> -MNQB(CN) ₃ ⁻	-0.08330	-0.91670	-1.00
<i>p</i> -MNQB(CN) ₃ ⁻	-0.01968	-0.97892	-1.00

^a The elementary charge unit = 1.602×10^{-19} coulombs

We can conclude that fluorescence modulation of the methylated naphthoquinone imidazole boronic based sensors was attributed to the disturbance of intramolecular charge transfer upon the anion binding. This ICT state was predominant by the poor acceptability on boron center after binding with anions such as OH⁻, F⁻ and CN⁻. [5, 75] A large fluorescence response toward nucleophilic attack of these sensors occurred since the boron center behaved as a complementary acceptor of a standard electron donor-acceptor system (D-A or A-D). The presence of electron donor (imidazole group) and electron acceptor (naphthoquinone group) as a main A-D site caused a prerequisite dipole moment change resulting in a large change in spectral properties. [90, 91]

3.4.3.5 Analytical applications of the sensor in the CTAB micellar system for micromolar cyanide detection in water

From the successful results of the incorporation of sensors in the CTAB micelle, this system can improve the cyanide detection down to micromolar level. For analytical applications, the calibration curves of cyanide ion were carried out using the optimum condition (5×10^{-5} mol/L of sensors and 5×10^{-3} mol/L of CTAB). At below 50 μM cyanide concentration which is the level in practical application, the emission intensities at 460 nm of *m*-MNQB and *p*-MNQB versus the cyanide concentration provided two well linear ranges of cyanide detections, 2.5-15 μM and 20-40 μM (Figure 3.36). Analytical parameters of *m*-MNQB and *p*-MNQB were listed in Table 3.5. The results clearly demonstrated that the synthesized sensors in CTAB micelle gave excellent limits of detection of cyanide at 1.42 and 1.47 μM for *m*-MNQB and *p*-MNQB, respectively.

Table 3.5 Analytical characteristics of *m*-MNQB and *p*-MNQB sensors (5×10^{-5} mol/L of sensors, 5×10^{-3} mol/L of CTAB in 1:4 ethanol:H₂O)

Sensors	Linear range (μM)	Linear regression equation (μM)	Correlation coefficient (R^2)	Detection limit ^a (μM)
<i>m</i> -MNQB	2.5-15	$I = 3.15C_{\text{CN}} + 25.47$	0.9956	1.42
	20-40	$I = 11.22C_{\text{CN}} - 135.12$	0.9920	
<i>p</i> -MNQB	2.5-15	$I = 2.37C_{\text{CN}} - 15.09$	0.9970	1.47
	20-40	$I = 6.84C_{\text{CN}} - 72.46$	0.9963	

[a] Detection limits were calculated from the concentration at which the fluorescence intensity is 3 times of standard deviation of the blank ($n = 10$) [115]

C_{CN} = concentration of KCN in mol/L

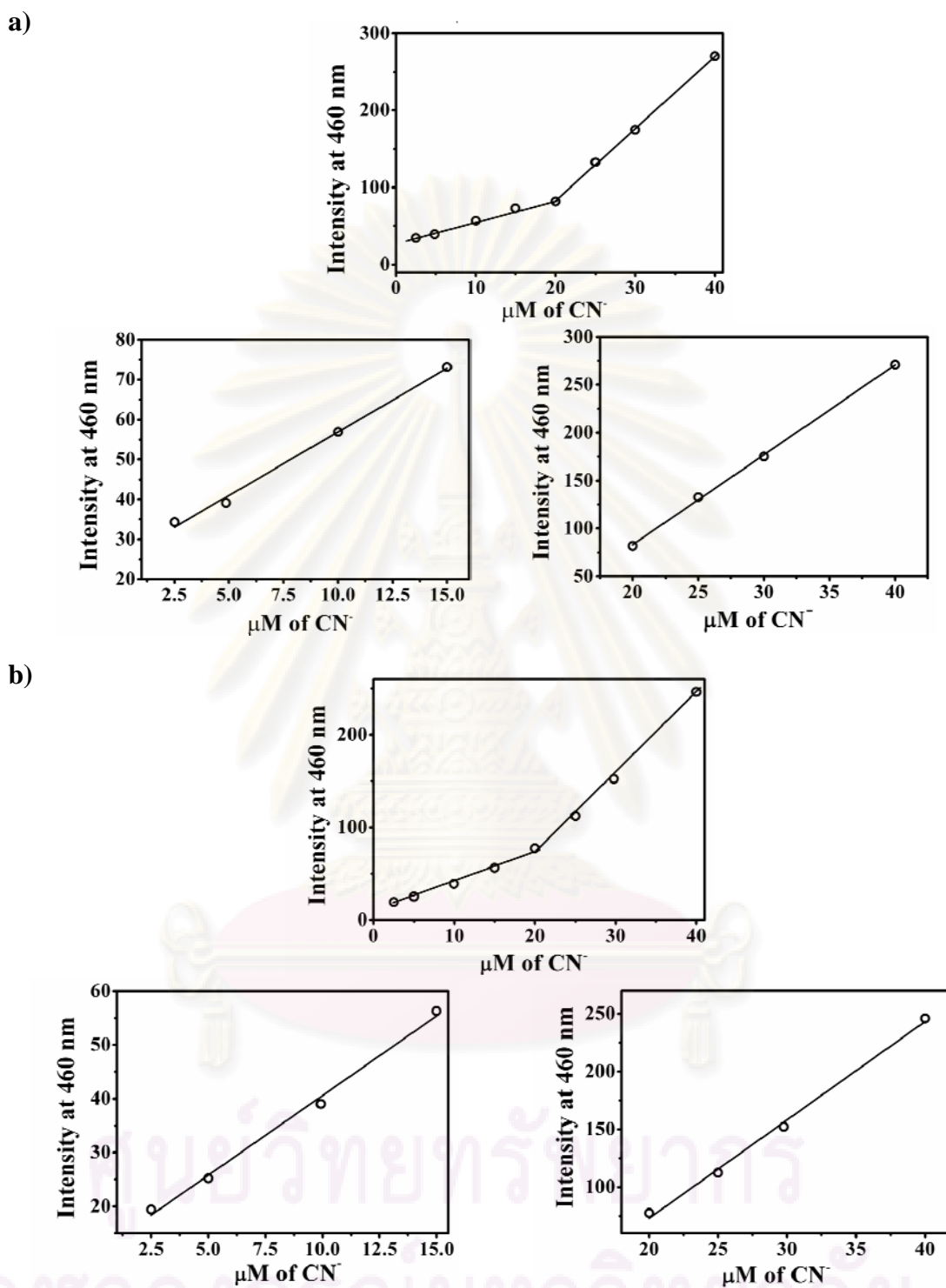


Figure 3.36 Calibration curves of cyanide 2.5-40 μM , 2.5-15 μM and 20-40 μM for a) *m*-MNQB and b) *p*-MNQB in optimum condition (5.0×10^{-5} mol/L of sensors; 5.0×10^{-3} mol/L CTAB in 1:4 ethanol in H_2O).

3.4.4 The electronic properties of the anionic adducts of the sensors

As demonstrated by previously, the methylated naphthoquinone imidazole boronic based receptors showed excellent fluorescence response toward hybridization changes of boron center upon the nucleophilic substitution by OH^- , F^- and CN^- . A large stoke shift ($\Delta\lambda_{\text{ex-emiss}} = 120 \text{ nm}$) as well as enhancement of large blue shift (*ca.* 100 nm) of new emission band at 460 nm of sensor corresponded to the existence of RBX_3^- species. Henceforth, the existences of RBX_3^- species of each system were characterized using several techniques such as $^1\text{H-NMR}$, $^{19}\text{F-NMR}$, and cyclic voltammetry.

3.4.4.1 $^1\text{H-NMR}$ spectroscopy of fluoride and cyanide adducts of the sensors

$^1\text{H-NMR}$ spectra of fluoride and cyanide adducts of the methylated receptors were measured in $\text{DMSO-}d_6$ using tetrabutylammonium fluoride and potassium cyanide, respectively. After the addition of anions (3 days), we found that $^1\text{H-NMR}$ spectra of *m*-MNQB and *p*-MNQB showed the complete vanishing of hydroxyl signals of *m*-MNQB and *p*-MNQB at 8.29 ppm and 8.23 ppm, respectively. The signals of all aromatic proton shifted upfield due to the existence of the anionic adducts upon the binding (Figure 3.38 and Figure 3.39). As shown in Figure 3.37, *o*-MNQB showed the incomplete changes by the remaining of free sensor signals due to the poor substitution of nucleophiles to the boron center. Therefore, the poor fluorescence response of *o*-MNQB caused by the low concentrations of its RBX_3^- (X = F, CN) species.

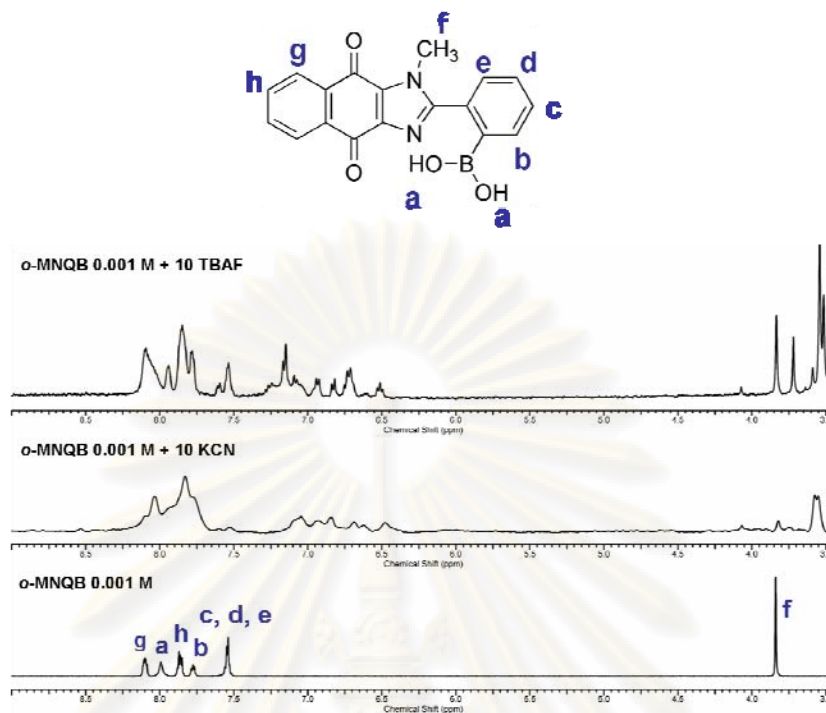


Figure 3.37 The ^1H -NMR spectrum (400 MHz) of *o*-MNQB (0.001 mol/L) in presence of 10 equiv. of potassium cyanide and tetrabutylammonium fluoride in $\text{DMSO-}d_6$.

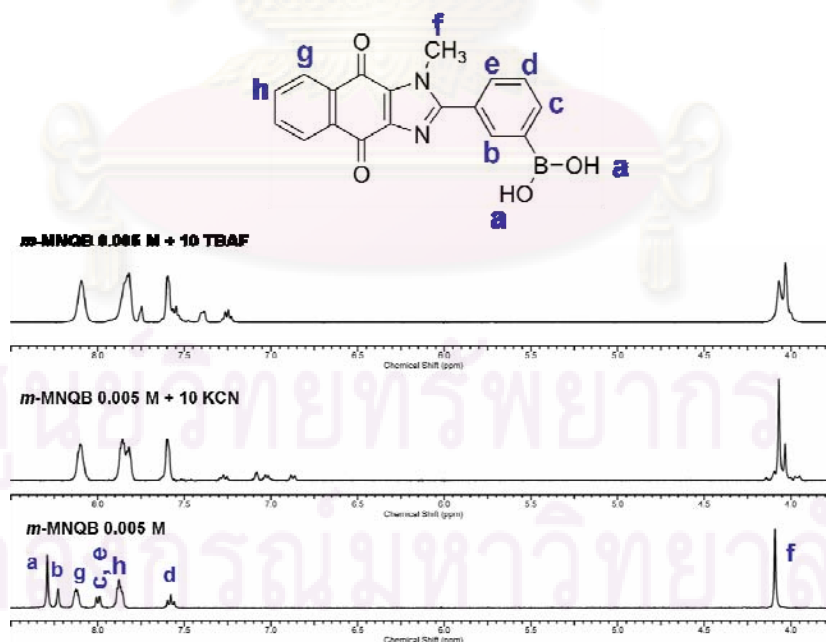


Figure 3.38 The ^1H -NMR spectrum (400 MHz) of *m*-MNQB (0.005 mol/L) in presence of 10 equiv. of potassium cyanide and tetrabutylammonium fluoride in $\text{DMSO-}d_6$.

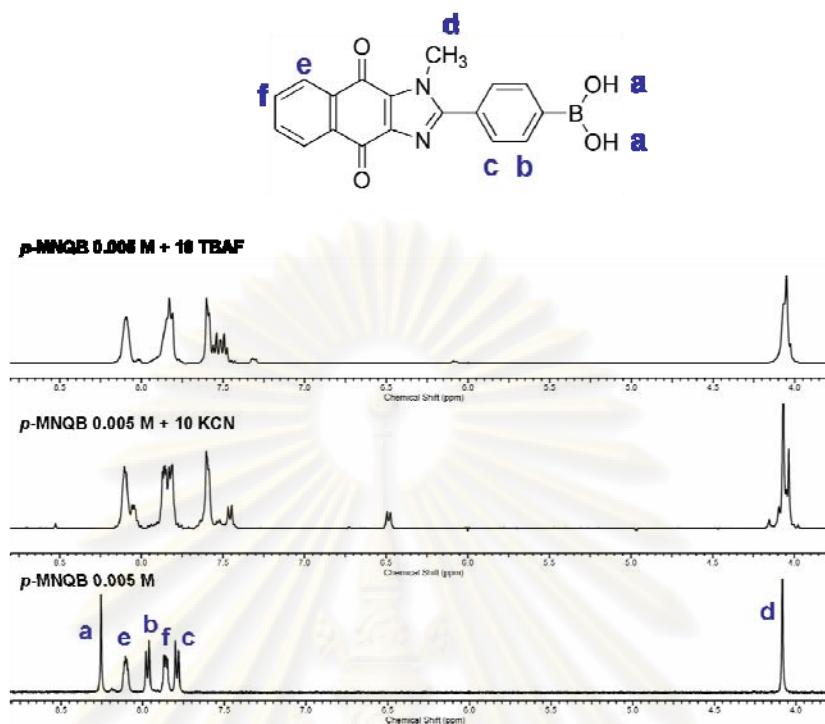


Figure 3.39 The ^1H -NMR spectrum (400 MHz) of *p*-MNQB (0.005 mol/L) in presence of 10 equiv. of potassium cyanide and tetrabutylammonium fluoride in $\text{DMSO-}d_6$.

3.4.4.2 ^{19}F -NMR spectroscopy of fluoride adducts of the sensors

Interactions of fluoride ion toward the boron center of the methylated receptors were clarified using ^{19}F -NMR spectroscopy in $\text{DMSO-}d_6$ by the addition of 3 equivalents of tetrabutylammonium fluoride. ^{19}F -NMR spectra of *m*-MNQB upon adding showed the signals at 128.86 ppm for $\text{RB(OH)}_2\text{F}^-$, 134.67 ppm for RB(OH)F_2^- and 143.22 ppm for RBF_3^- (Figure 3.40), whereas *o*-MNQB showed only signal of monosubstituted fluoride ($\text{RB(OH)}_2\text{F}^-$) at 129.89 ppm [89] (Figure 3.41) due to the steric hindrance in this isomer.

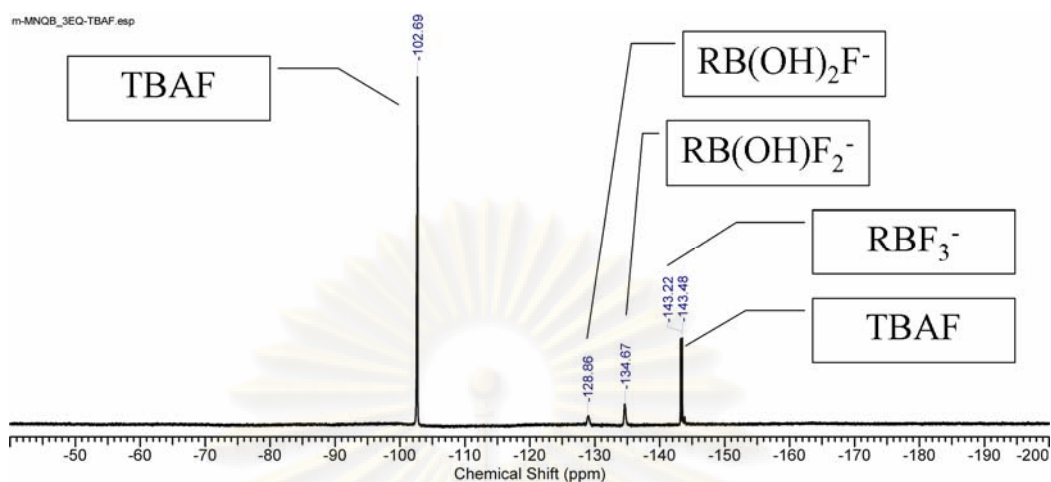


Figure 3.40 The ^{19}F -NMR spectrum (470 MHz) of *m*-MNQB in presence of 3 equiv. of tetrabutylammonium fluoride in $\text{DMSO-}d_6$

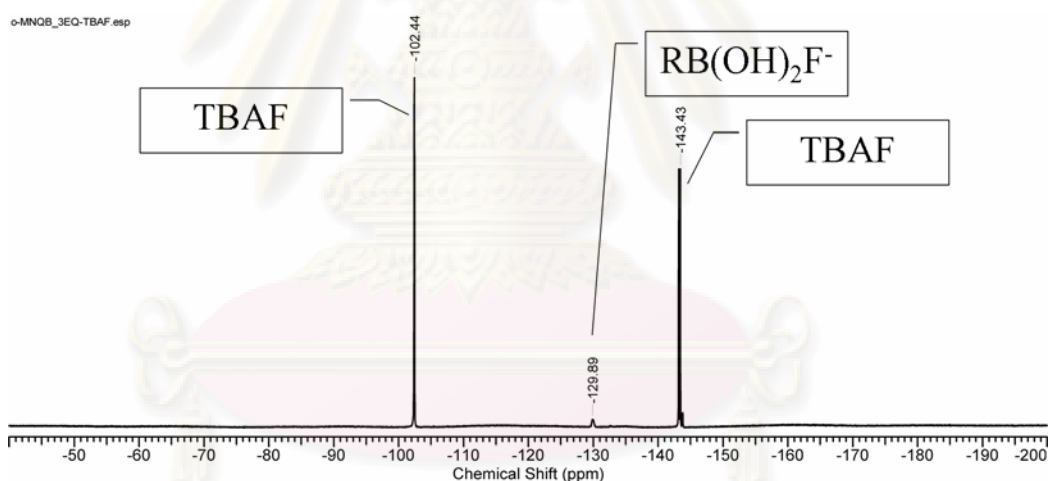


Figure 3.41 The ^{19}F -NMR spectrum (470 MHz) of *o*-MNQB in presence of 3 equiv. of tetrabutylammonium fluoride in $\text{DMSO-}d_6$

3.4.4.3 Electrochemical studies of the sensors in the presence of cyanide in the mixture of DMSO:H₂O system

Cyclic voltammograms of *o*-MNQB, *m*-MNQB and *p*-MNQB were recorded in 0.1 mol/L NaCl (1:1, DMSO:H₂O) as the supporting electrolyte. At the scan rate of 200 mV s⁻¹, the CV response of free sensor, *m*-MNQB and *p*-MNQB showed similar feature. Upon the addition of CN⁻ in the solution of sensors, the CV responses showed the cathodic shift of reduction waves of both sensors. It was assumed that the anionic adduct (RBX₃⁻) was obtained in the solution. Consequently, quinone was hard to be reduced to dianion. As expected, *o*-MNQB showed slightly changes of cyclic voltammograms upon the addition of 5 equiv CN⁻. The CV results supported the result from fluorescence spectrophotometry.

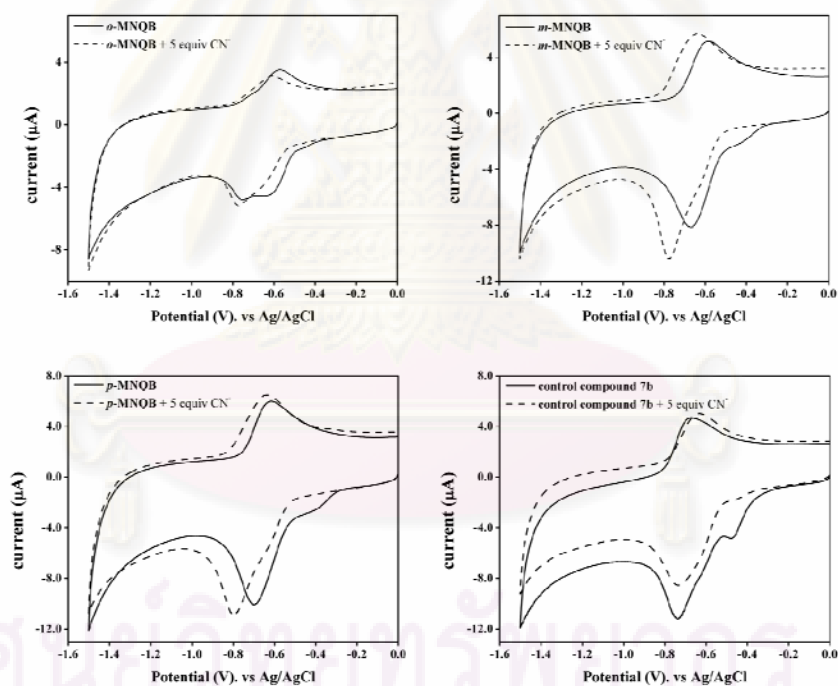


Figure 3.42 Cyclic voltammograms of sensors in the absence (solid line) and the presence 5 equivalent of KCN (dash line) (2×10^{-4} mol/L of sensor in 0.1 mol/L NaCl 1:1; H₂O:DMSO for *m*-MNQB, *p*-MNQB and control compound **7b**, 1×10^{-4} mol/L for *o*-MNQB in 0.1 mol/L NaCl 1:1; H₂O:DMSO)

3.5 The sensing properties of the anthraquinone sensors towards monosaccharides

The previous results showed that naphthoquinone imidazole boronic based sensors gave an excellent characteristic of the fluorescence sensor for anions in terms of a large Stokes shift and a large blue shift upon the formation of anionic adducts. Accordingly, the quinone boronic based sensor was expected to use the alternation of the ICT process to induce the spectral shift and fluorescence intensity changes upon binding saccharides. Due to poor solubility of the naphthoquinone sensors in organic solvent and water, the modification of the quinone based sensors are required. More extended aromatic systems in anthraquinone sensors were synthesized and the complexation ability toward several simple monosaccharides was studied. Considering the extended conjugated π -system, it is expected that the anthraquinone sensors would show a better solubility in organic solvents and also provide stronger emission spectra.

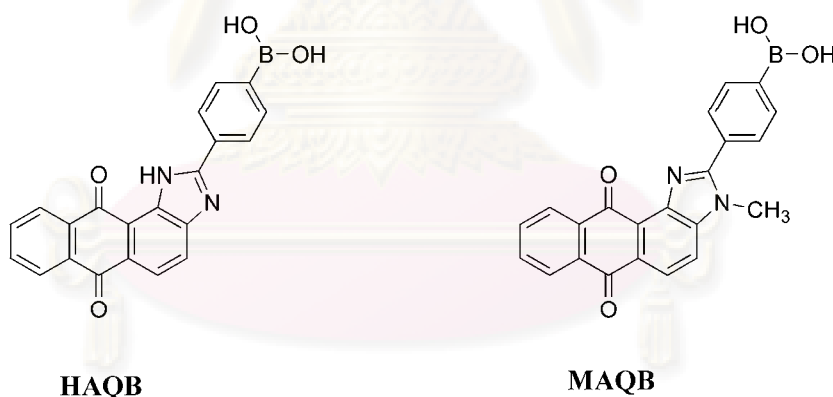


Figure 3.43 Structures of the anthraquinone imidazole boronic based sensors, **HAQB** and **MAQB**

3.5.1 Photophysical properties of the anthraquinone sensors, HAQB and MAQB.

As listed in Table 3.6, photophysical properties of the **HAQB** and **MAQB** offered better optical properties than those of naphthoquinone sensors including extinction coefficients and quantum yield due to the better conjugative π -system. Similar to naphthoquinone derivatives, electronic transition of anthraquinone involves the migration of electron density from electron donating group to electron acceptor group. [7, 92, 93] Due to H-bonding of **HAQB**, more extended π -conjugative system of this sensor provided better emissive properties than that of the methylated anthraquinone sensor in DMSO and EtOH.

Table 3.6 Photophysical properties of **HAQB** and **MAQB** in DMSO and EtOH

Sensors/solvent	λ_{abs} (nm)	Extinction coefficients (ϵ , mol/L.cm)	λ_{em} (nm)	$\Phi_{\text{f}}^{\text{a}}$
HAQB				
DMSO	408	19280	535	0.225
EtOH	395	10380	542	0.323
MAQB				
DMSO	395	23020	525	0.027
EtOH	384	7540	536	0.051

^a Quantum yields were determined using quinine sulfate as the standard (Φ_{STD}) 0.508 in 1 N H₂SO₄.

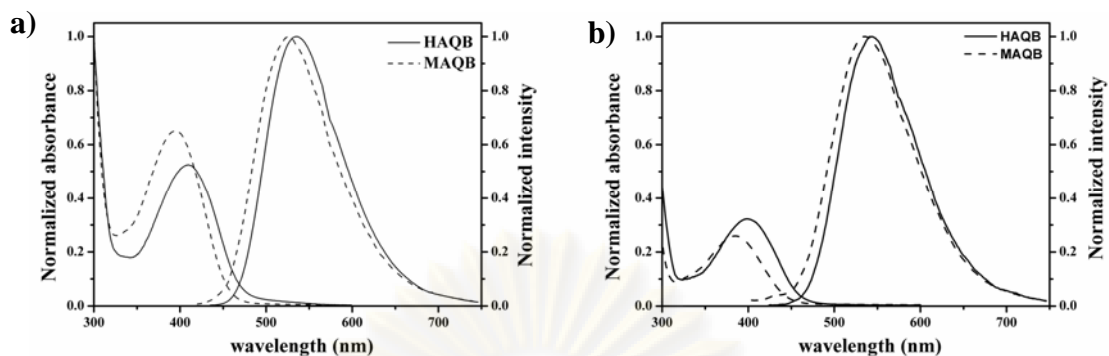
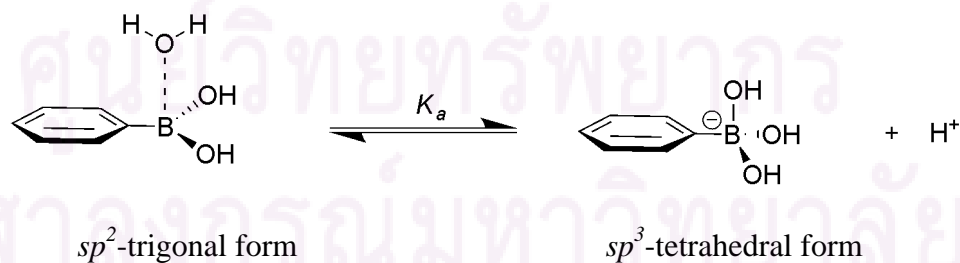


Figure 3.44 Absorption and emission spectra of **HAQB** and **MAQB** (5×10^{-5} mol/L) in a) DMSO and b) EtOH

3.5.2 The complexation studies of the anthraquinone sensors, HAQB and MAQB towards several monosaccharides using fluorescence spectrophotometry

The aim of this work focused on the evaluation of the new ICT sensor based on anthraquinone imidazole boronic acid as a saccharide fluorescence probe. Due to the solubility limit, the complexation studies were carried out in the mixture of ethanol:water. Previous reports showed that the reaction of boronic acid and diol was fastest in aqueous basic media where the boron existed in a tetrahedral anionic form (Scheme 3.7). [5] Due to the lack of appropriate donor atom such as nitrogen for self-coordination, the complexation studies of sensors with saccharides must be performed where the pH is larger than the pK_a of boronic acid at which most of boron centers existed in the tetrahedral form. [62-66]



Scheme 3.7 The acid-conjugate base equilibrium for phenylboronic acid in water

According to Figure 3.45, fluorescence-pH titration of **HAQB** and **MAQB** in 20% EtOH:H₂O and 40% EtOH:H₂O, respectively, displayed fluorescence quenching in a basic pH condition.

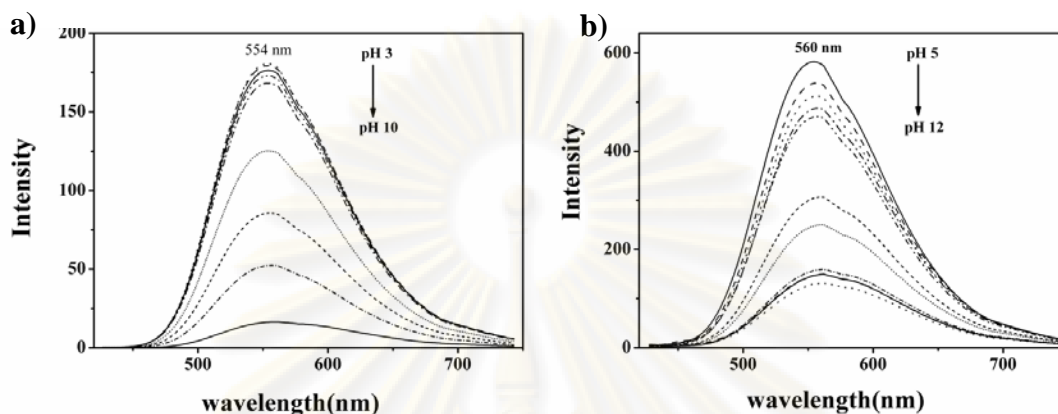


Figure 3.45 Fluorescence spectra of **HAQB** (5×10^{-5} mol/L in 40% ethanol: buffer) at pH 3-10 buffer and **MAQB** (5×10^{-5} mol/L in 20% ethanol: buffer) at pH 5-12 buffer (pH 3-5 : 0.2 mol/L phthalate-HCl buffer, pH 6-8 : 0.2 mol/L phosphate buffer, pH 8.5-10 : 0.2 mol/L sodium borate buffer, pH 11-12 : 0.2 mol/L phosphate-NaOH buffer)

The pK_a values of **HAQB** and **MAQB** can be estimated by fitting emission intensities versus pH using a non-linear relation equation 3, [75] where I_{acid} and I_{base} are fluorescence intensities of the complete acid form and the complete base form, respectively. Titration data were analyzed using Solver in Microsoft Excel.

$$I = \frac{10^{-pH} I_{acid} + K_a I_{base}}{K_a + 10^{-pH}} \quad (3)$$

The fitting of the pH profiles yielded pK_a of sensors **HAQB** and **MAQB**, 8.45 and 8.14, respectively (Figure 3.46). These pK_a values corresponded to typical pK_a values of phenylboronic acid without intramolecular N-B interactions. [5]

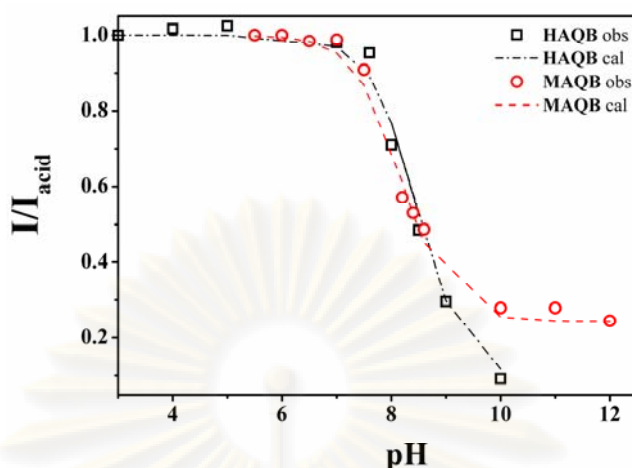


Figure 3.46 pH-Dependent fluorescence response (I/I_{acid} at 555 nm) of **HAQB** (5×10^{-5} mol/L in 40% ethanol: buffer) at pH 3-10 buffer and **MAQB** (5×10^{-5} mol/L in 20% ethanol: buffer) at pH 5-12 (pH 3-5 : 0.2 mol/L phthalate-HCl buffer, pH 6-8 : 0.2 mol/L phosphate buffer, pH 8.5-10 : 0.2 mol/L sodium borate buffer, pH 11-12 : 0.2 mol/L phosphate-NaOH buffer)

The 1:1 stoichiometry of complexes was validated by the continuous variation method or Job's method [7] using D-fructose as a representative of the simple monosaccharide. The plot of $I - I_0(1 - X_{\text{fructose}})$ versus X indicated that the stoichiometry of complexes was 1:1 for both sensors (Figure 3.47).

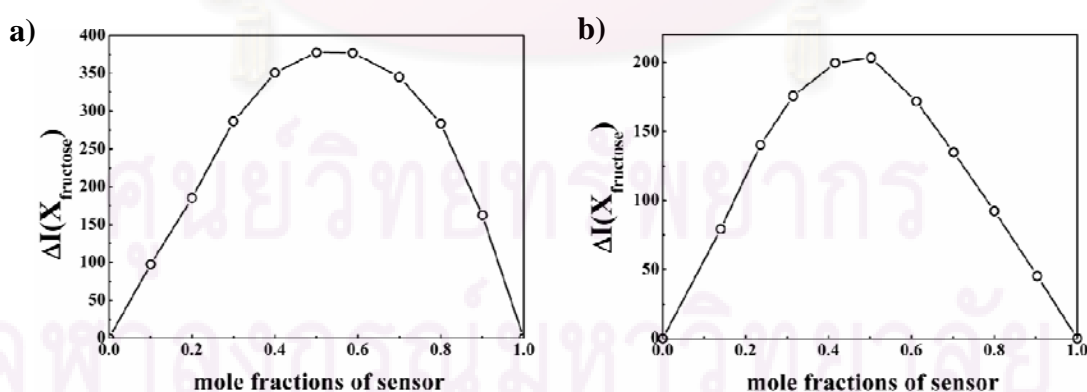


Figure 3.47 Job's plots for 1:1 complexes of a) **HAQB** and b) **MAQB** with D-fructose at pH 8.5 (5×10^{-5} mol/L in 40% EtOH:buffer pH 8.5 for **HAQB** and 5×10^{-5} mol/L in 20% EtOH:buffer pH 8.5 for **MAQB**)

To explore the general applications of sensors **HAQB** and **MAQB**, the effect of sugars on the fluorescence responses of **HAQB** and **MAQB** was examined at pH = 8.5 in the mixture of 40% EtOH:buffer and 20% EtOH:buffer, respectively. As shown in Figure 3.48, the addition of D-fructose resulted in significant fluorescence intensity changes in both sensors and a slightly red shift (*ca.* 30 nm) in the case of **MAQB**.

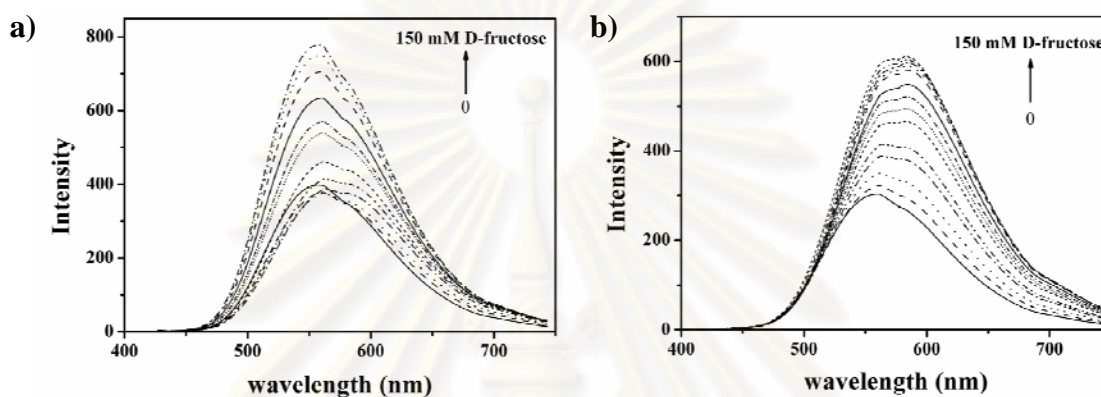


Figure 3.48 Fluorescence spectra of a) **HAQB** (5×10^{-5} mol/L in 40% ethanol:buffer pH 8.5, $\lambda_{\text{ex}} = 410$ nm) and b) **MAQB** in the presence of 0-150 mM of D-fructose (5×10^{-5} mol/L in 20% ethanol:buffer pH 8.5, $\lambda_{\text{ex}} = 395$ nm)

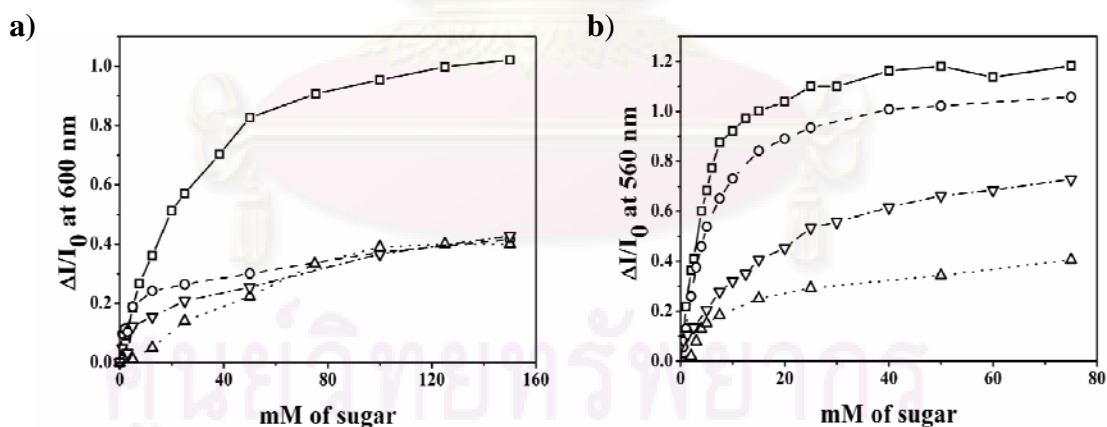


Figure 3.49 Fluorescence response ($\Delta I/I_0$) at 600 nm of a) **HAQB** (5×10^{-5} mol/L in 40% ethanol:buffer pH 8.5) and b) at 560 nm of **MAQB** (5×10^{-5} mol/L in 20% ethanol: buffer pH 8.5) in the presence of 0-150 mM of various saccharides ; \square = D-fructose, \circ = D-galactose, ∇ = D-glucose, \triangle = D-mannose

Furthermore, the effect of other saccharides including D-galactose, D-glucose and D-mannose were also studied at pH 8.5. As displayed in Figure 3.49, when fluorescence intensities were monitored at 600 nm for **HAQB** and 560 nm for **MAQB**, the results clearly showed that the binding of other simple monosaccharides with the sensors effected fluorescence intensities. It seems that the binding affinity toward simple monosaccharide of the sensor followed in the order of D-fructose > D-galactose > D-mannose > D-glucose. For more quantitative results, the stability constants K_s between the sensors and saccharides were determined using the non-linear fitting of intensities at 554 nm versus saccharide concentrations as expressed in equation 4. [75] Stability constants were calculated on the basis of 1:1 sensor and sugar interactions.

$$I = \frac{I_0 + I_\infty K_s [\text{Sugar}]}{1 + K_s [\text{Sugar}]} \quad (4)$$

As summarized in Table 3.7, the affinity trend of both sensors followed the preliminary results. Indeed, the affinity trends were similar to those observed in phenylboronic acid reported previously. [59-61]

Table 3.7 Stability constants (K_s) of complexes of **HAQB** and **MAQB** and different monosaccharides at pH 8.5 in 40% ethanol: sodium borate buffer and in 20% ethanol: sodium borate buffer, respectively

Sugar	Stability constants (K_s , M^{-1})	
	HAQB	MAQB
D-fructose	51.15	454.70
D-galactose	*	246.26
D-glucose	*	98.63
D-mannose	*	115.21

* not determined

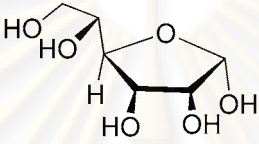
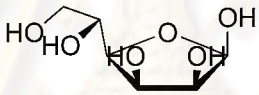
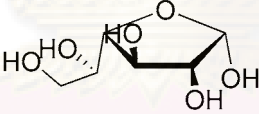
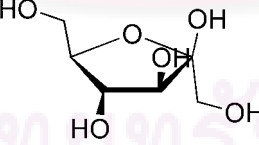
Unfortunately, fluorescence titration experiments for **HAQB** cannot provide the stability of all sugars due to the small fluorescence change upon the addition of D-galactose, D-glucose and D-mannose. However, the fluorescence spectral changes ($\Delta I/I_0$) showed that affinity trend of **HAQB** belonged in order of D-fructose > D-galactose > D-glucose > D-mannose the same as observed in the case of **MAQB**. The titration results and stability constants of **HAQB** indicated a high selectivity of **HAQB** toward D-fructose.

The apparent of the stability constants (K_s) of the simple mono-boronic acid depended on the available of vicinal diol of a saccharide to arrange a *syn*-periplanar orientation which was the most stable form of boronic-diol complexes. [5] As listed in Table 3.8, D₂O equilibrium of monosaccharides showed that D-fructose has an enormous percentage of *syn*- periplanar β -D-fructofuranose whereas those values of the other monosaccharide were quite low.[5] Therefore, the monoboronic based sensor remarkably preferred binding with D-fructose to other monosaccharides.



ศูนย์วิทยทรัพยากร
จุฬาลงกรณ์มหาวิทยาลัย

Table 3.8 Equilibrium percentages of *syn*-periplanar anomeric hydroxyl pair of furanose form in D₂O of simple monosaccharides [5]

Monosaccharides	Structure of furanose form (with <i>syn</i> -periplanar anomeric hydroxyl pair)	Percentage of furanose form (with <i>syn</i> -periplanar anomeric hydroxyl pair) in D ₂ O (%)
D-Glucose	 <p>α-D-glucofuranose</p>	0.14 ^a
D-Mannose	 <p>β-D-mannofuranose</p>	0.3 ^b
D-Galactose	 <p>α-D-galactofuranose</p>	2.5 ^b
D-Fructose	 <p>β-D-fructofuranose</p>	25 ^b

^a Following equilibrium in D₂O at 27 °C

^b Following equilibrium in D₂O at 31°C

3.5.3 The correlation of ionization state of the boron center and fluorescence properties of sensor MAQB

According to pH-dependent experiments in the absence and the presence of sugars, the correlation of the fluorescence properties and the feature of the sensors could be deduced. Firstly, to understand the structural features associated with the fluorescence properties changes, the pH-profile of **MAQB** in the absence of sugar was re-considered.

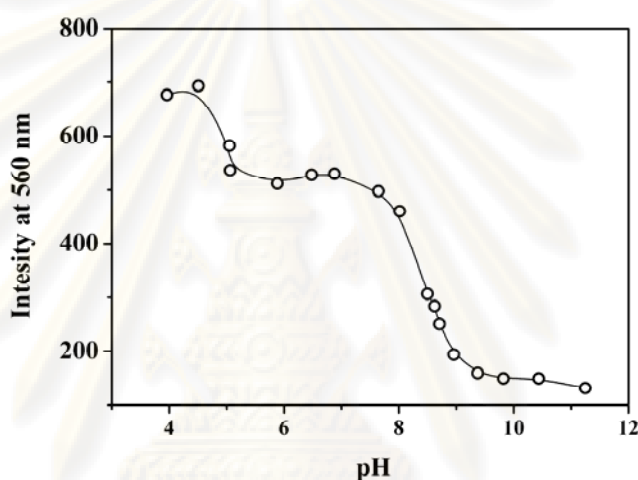
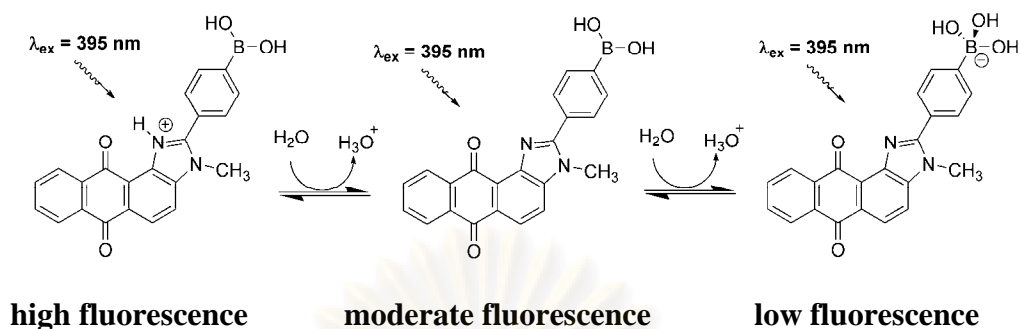


Figure 3.50 pH-Profiles of the fluorescence intensities 560 nm of **MAQB** (5×10^{-5} mol/L, 20%EtOH:buffer) in various pH (pH 3-5 : 0.2 mol/L phthalate-HCl buffer, pH 6-8 : 0.2 mol/L phosphate buffer, pH 8.5-10 : 0.2 mol/L sodium borate buffer, pH 11-12 : 0.2 mol/L phosphate-NaOH buffer)

As displayed in Figure 3.50, at pH 4, the strong emission band with fluorescence maxima at 555 nm was observed that peak possibly corresponded to the protonated at nitrogen of trigonal planar boronic acid species. At the pH range 4-6.5, the fluorescence intensity decreased as increasing of pH due to the formation of neutral form of **MAQB** with sp^2 hybridization boron center. The fluorescence intensity decreased dramatically when the pH changed from 6 to 9 and show a slightly changes beyond 9. Besides the quenching of fluorescence intensity at upon the increasing of pH, the slightly red shift to 587 nm was also observed. the These changes possibly correlated with the hybridization changes of boronic acid from sp^2 to sp^3 upon the hydroxide binding as illustrated in Scheme 3.8.



Scheme 3.8 Association of fluorescence properties and ionization states of **MAQB** in the absence of sugar

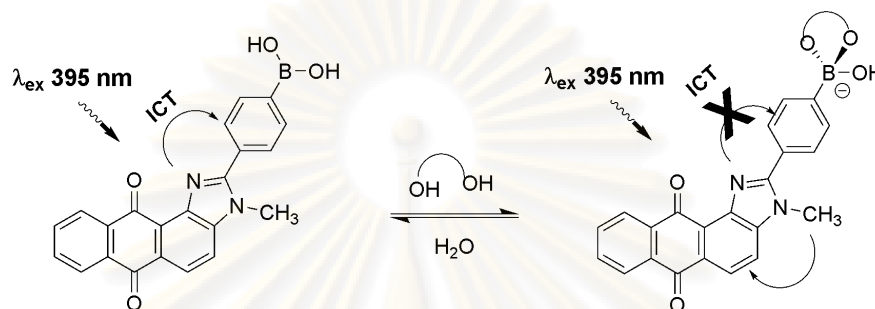
Moreover, we also studied the pH influence on fluorescence behavior of the sensor in the presences of 50 mM of saccharides such as D-fructose, D-galactose, D-glucose and D-mannose (Figure A.35). The result showed the fluorescence enhancement and red shift upon the addition of saccharide as represent in FE values (I/I_0 at 560 nm) in Table 3.9. Interestingly, slightly fluorescence enhancements and red shifts were observed at the acidic pH 4-6. It is implied that the interactions between the sensor and sugar could occur even acidic media.

Table 3.9 Fluorescence enhancement values (FE) at 560 nm of **MAQB** in presence of 50 mM of various saccharides at pH 4-12

pH	FE values (I/I_0 at 560 nm)			
	D-Fructose	D-Galactose	D-Glucose	D-Mannose
4	1.24	1.34	1.37	1.18
5	1.30	1.08	1.10	1.05
6	1.43	1.23	1.04	1.17
7	1.47	1.53	0.99	1.32
8	1.75	1.92	0.83	1.44
8.5	2.70	3.07	2.17	2.45
9	4.24	5.04	3.91	4.00
10	3.66	5.22	4.53	4.16
11	6.17	6.72	-*	4.89
12	6.78	7.49	-*	5.45

-* not determined

The increasing of the fluorescence quantum yield of the sensor upon binding with saccharides was attributed to the switching “off” ICT transition upon the reduction of electron acceptability of the boron center as illustrated in Scheme 3.9. [79]



Scheme 3.9 The model of signal transductions of **MAQB** upon the hybridization changes of boron center

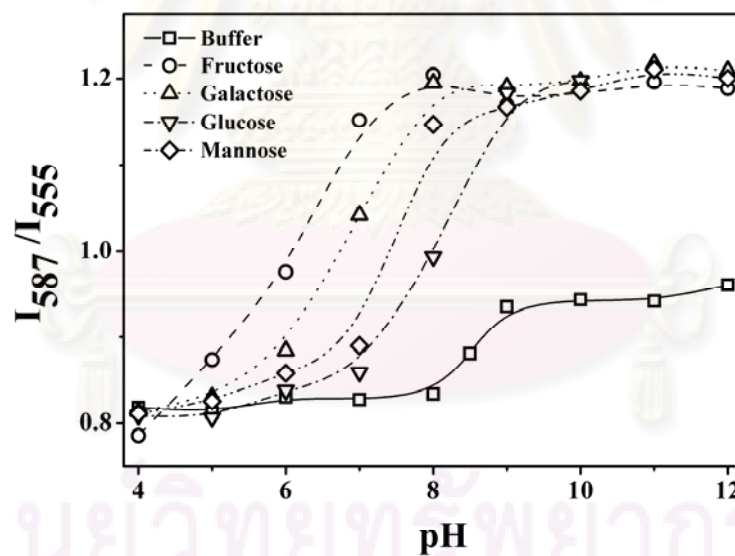


Figure 3.51 pH-Profiles of the fluorescence intensities ratio at 587 nm and 555 nm (I_{587}/I_{555}) of **MAQB** in the absence (-□-) and the presence of 50 mM of sugars: D-fructose (-○-), D-galactose (-△-), D-glucose(-▽-) and D-mannose (-◇-) (5×10^{-5} mol/L in 20% EtOH in various buffer; pH 3-5 : 0.2 mol/L phthalate-HCl buffer, pH 6-8 : 0.2 mol/L phosphate buffer, pH 8.5-10 : 0.2 mol/L sodium borate buffer, pH 11-12 : 0.2 mol/L phosphate-NaOH buffer)

Regarding to the ionization changes, the pH-profile of **MAQB** was re-plotted between the ratio of I_{587}/I_{555} (indicative of sp^3/sp^2) against pH in order to track the ionization state changes of the boron center. As illustrated in Figure 3.51, the pH-profile in the absence of sugars showed that the ratio of I_{587}/I_{555} remarkably increased where the pH of the solution was larger than pK_a . These results indicated that anionic tetrahedral of boron was formed at $pH \geq pK_a$ as described previously. Furthermore, in the presence of saccharides, the results were similar to those in the absence of saccharides. The sp^3 form of the sugar-**MAQB** adduct increased as increasing the pH. The ionization changes in the presence of saccharides were observed at lower pH than that in the absence of sugars (the shifted to the left of the pH-profile). It can be rationalized that the pK_a of saccharide-boronic complex are lower than the uncomplexed boronic acid in other words the boronic ester is more acidic than the boronic acid. The higher acidity of saccharide-sensor adduct can be explained by that the formation of tetrahedral boronate-saccharide complex or the rehybridization from sp^2 to sp^3 of the boron reduced ring strain and lowers the energy of the product. Consequently, the equilibrium between the neutral boronic acid -saccharide complex and the boronate anion-saccharide complex shifted to the right resulting in the lower pK_a of saccharide-boronic complex. [5]

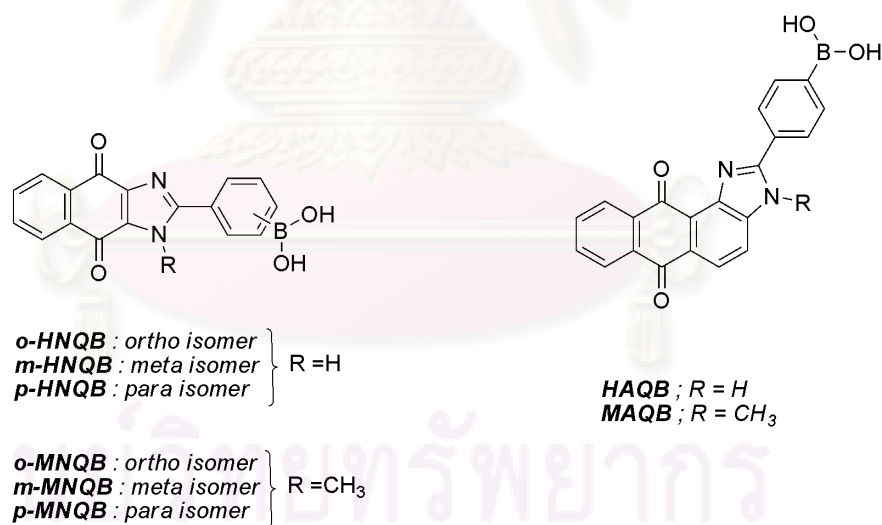
According to Table 3.8 and Figure 3.51, besides the correlation of the hybridization of the boron center and emission maxima, the fluorescence intensity of the saccharide-sensor adduct seems to be much stronger than that of free sensors, although, they were possessed the same ionization state especially at high pH (11 and 12). This result indicated that it was not only the effect of the ionization state or the hybridization of the boron changes that corresponded to the fluorescence signal changes, changes in electronic structures also influenced the fluorescence intensity. Regarding ICT properties of the sensors, the fast internal conversion (IC) mainly causes low quantum yield in polar solvents. [116] Presumably, the internal conversion pathway was prohibited upon the saccharide binding resulting in the increasing of the fluorescence intensity.

CHAPTER IV

CONCLUSIONS

4.1 Naphthoquinone imidazolidione boronic acid based fluorescence sensors for cyanide detection in water

Naphthoquinone imidazolidione boronic acid fluorescence sensors have been synthesized from heterocyclic precursors by using the oxidative condensation of 2,3-diamino-1,4-naphthoquinone and the corresponding protected formylphenylboronate yielded the ester-protected products in 29 %, 45% and 71% yields, respectively. The protonated forms of sensors, *o*-HNQB, *m*-HNQB and *p*-HNQB can be accomplished upon the removal of the protecting groups in quantitative yields. The methylated sensors, *o*-MNQB, *m*-MNQB and *p*-MNQB can be accomplished by the reaction of the corresponding protected derivative with methyl iodide to give desired products upon the deprotection of the ether group in 20%, 40%, and 45% yields for *o*-MNQB, *m*-MNQB and *p*-MNQB, respectively.



Scheme 4.1 Structures of all synthesized sensors

Spectrophotometric investigations of *o*-HNQB, *m*-HNQB and *p*-HNQB in DMSO with various anions exhibited the red shift of absorption spectra concomitant with the color changes from yellow to red upon the addition of basic anions including F^- , OAc^- , BzO^- and $H_2PO_4^-$. Color and UV spectral changes can be explained by means of the deprotonation of NH to N^- on the imidazole moiety resulting in charge transfer from the donor to the electron acceptor group. Besides the color changes by basic anions in DMSO, *m*-HNQB and *p*-HNQB showed the naked-eye sensor character for cyanide in the mixture of DMSO:H₂O due to the weak acid properties of HCN in DMSO and H₂O. However, all protonated sensors showed poor characteristic of a fluorescence sensor in terms of selectivity. They offered the quenching of fluorescence intensities upon the addition of basic anions including F^- , OAc^- , BzO^- and $H_2PO_4^-$ due to the inverse of PET process upon the deprotonation. The binding mode of anion recognition was clarified by the control compound **7**. The ¹H-NMR and UV-vis techniques revealed that the anion such as F^- , CN^- and OH^- could not interact with boronic acid in deprotonation form sensors due to the repulsion of the negative charge.

Complexation studies of methylated sensors *o*-MNQB, *m*-MNQB and *p*-MNQB were carried out using the fluorescence spectrophotometry in four solvent systems including DMSO, DMSO:H₂O, DMSO:HEPES pH 7.4 and CTAB micelle. In DMSO system, *m*-MNQB and *p*-MNQB showed the appearance of a new emission band at 460 nm in the presence of excess amount of fluoride. However, fluorescence responses of this band did not provide saturated signal even in the addition of an excess amount of fluoride in DMSO system. The complexation studies with anions of all sensors in the DMSO:H₂O (1:1) system showed the high intensity fluorescence band at 460 nm upon the addition of cyanide and fluoride. Regarding to fluorescence response ($I-I_0$) of the new emission band at 460 nm, it suggested that all methylated compound sensors preferred to bind with cyanide over fluoride and others anions in this system. However, the sensors also responded to OH^- resulting in the significant increasing of the fluorescence intensity at 460 nm. The fluorescence properties of the sensors were also studied in the mixture of DMSO:HEPES pH 7.4 (1:1) in order to control the hydroxide concentration. Results showed that sensor *m*-MNQB and *p*-MNQB in this system still gave unpromising results including the slow rate of cyanide response and the limit of cyanide detection because the pH or hydroxide

concentration of this cyanide detection system could not be controlled by the HEPES buffer. Therefore, the neutral boronic acid based sensor could not provide a reasonable anion or cyanide detection system due to the lack of positive charge for driving the anion recognition.

The optimum condition for cyanide detection using the assistance of a surfactant was investigated in a micromolar level of cyanide concentration in water. The optimum condition for micromolar cyanide detection in water using the incorporation of *m*-MNQB or *p*-MNQB into a cationic micellar system is 5×10^{-5} mol/L of sensors and 5×10^{-3} mol/L of cetyltrimethyl ammonium bromide (CTAB) in 1:4 ethanol:H₂O. Compared to cyanide detection studies in the solution of DMSO:H₂O, the CTAB micellar system provided significant improvement in sensitivity and selectivity resulting in 1000-fold enhancement of the detection limits for *m*-MNQB and *p*-MNQB. At below 50 μ M of KCN under optimal condition of CTAB, fluorescence intensities at 460 nm of *m*-MNQB and *p*-MNQB provided two sets of linear ranges, 2.5-15 μ M and 20-40 μ M and the limit of cyanide detection at 1.4 μ M. Furthermore, the stability constant of tricyano complex of *m*-MNQB and *p*-MNQB under optimum condition of the CTAB micellar system showed similar affinities for both sensor, $\log \beta_3 = 4.19 \pm 0.09$ and 3.99 ± 0.05 for *m*-MNQB and *p*-MNQB, respectively. However, *o*-MNQB showed a poor response toward any anions even cyanide in any systems including DMSO, DMSO:H₂O, DMSO:HEPES pH 7.4 and CTAB micellar system due to the steric hindrance on the binding site of this sensor.

As described previously, the blue band corresponded to the existence of anionic form of RBX_3^- when X represented F⁻ or CN⁻ and OH⁻. Regarding to their natural bond orbital (NBO) charge, the naphthoquinone imidazole acted as main donor site and boronic acid acted as acceptor site of the free sensor. The fluorescence enhancement at 460 nm corresponded to the perturbation of ICT efficiency by the decreasing of electron acceptability properties of a acceptor site upon anion binding. The new blue band was ascribed to the destabilization of charge transfer at the excited state of sensors resulting in large energy band gap of anionic forms of sensors.

4.2 Anthraquinone imidazolidione boronic acid based sensors for saccharide detection

Anthraquinone imidazolidione boronic acid based sensors were designed using the ICT concept. **HAQB** and **MAQB** were synthesized using similar procedure to the naphthoquinone based sensor to give the desired products in quantitative yields at the last step. Complexation properties of **HAQB** and **MAQB** were studied using various simple monosaccharides as a particular guest. According to pH variation experiments, pK_a of both sensors were estimated to be 8.45 and 8.14 for **HAQB** and **MAQB**, respectively. At pH=8.5, both sensors showed fluorescence enhancement upon the addition of monosaccharides and the slightly red shift (*ca.* 30 nm) was observed in the case of **MAQB**. According to the stability constants K_s of the 1:1 complex, results clearly showed that the binding affinity toward simple monosaccharides of both sensors was in order of D-fructose > D-galactose > D-glucose > D-mannose. Besides the similar binding affinity trends of both sensors, **HAQB** showed remarkable selectivity toward D-fructose.

Furthermore, the correlation of fluorescence properties and hybridization changes of **MAQB** was explored in the presence of and in the absence of saccharides by pH variation experiments. Emission bands at 555 nm and 587 nm were ascribed to sp^2 and sp^3 hybridization of the boron center, respectively. Fluorescence intensities of saccharide-sensor adducts were stronger than that of free sensor at the studied pH (4-12). It can be concluded that not only the effect of ionization state or changes in hybridization of the boron center resulted in the fluorescence signal changes, but that changes in electronic structures also influenced the fluorescence intensity.

ศูนย์วิจัยทรัพยากร
จุฬาลงกรณ์มหาวิทยาลัย

4.3 Suggestions for future works

Future works will focus on:

- i) characterization of cyanide-sensor adducts using ^{11}B -NMR spectroscopy
- ii) evaluation of *m*-**MNQB** and *p*-**MNQB** in the CTAB micellar system for the analytical applications of cyanide detection in real samples such as drinking water
- iii) pH dependent studies of **HMQB** in the presence of monosaccharides using spectroscopic techniques
- iv) complexation and pH dependent studies of **HAQB** and **MAQB** with monosaccharides using ^{11}B -NMR spectroscopy.



ศูนย์วิจัยทรัพยากร
จุฬาลงกรณ์มหาวิทยาลัย

REFERENCES

- [1] Lehn, J.-M. Cryptates : inclusion complex of macropolycyclic receptor molecules. *Pure Appl. Chem.* 50 (1978): 871-892.
- [2] Lehn, J.-M. Supramolecular chemistry-scope and perspective molecules supramolecules and molecule device (Nobel Lecture). *Angew. Chem. Int. Ed.* 27 (1988): 89-122.
- [3] Lehn, J.-M. *Supramolecular Chemistry, Concepts and Perspectives*. Weinheim: VCH, 1995.
- [4] Steed, J. W., and Atwood, J. L. *Supramolecular Chemistry*. London: Wiley & sons, 2000.
- [5] James, T. D. Saccharide-selective boronic acid based photoinduced electron transfer (PET) fluorescent sensors. *Top. Curr. Chem.* 277 (2007): 107-152.
- [6] Lakowicz, J. R. *Principle of Fluorescence Spectroscopy*. New York: Springer, 2006.
- [7] Value, B. *Molecular fluorescence principle and application*. New York: Wiley-VCH, 2001.
- [8] Schmidtchem, F. P., and Berger, M. Artificial organic host molecules for anions. *Chem. Rev.* 97 (1997): 1609-1646.
- [9] Value, B., and Leray, I. Design principle of fluorescent molecular sensors for cation recognition. *Coor. Chem. Rev.* 205 (2000): 3-40.
- [10] Czarnik, A. W. Chemical communication in water using fluorescent chemosensors. *Acc. Chem. Res.* 27 (1994): 302-308.
- [11] Martínez-Máñez, R., and Sancenón, F. Fluorogenic and chromogenic chemosensors and reagents for anions. *Chem. Rev.* 103 (2003): 4419-4476.
- [12] Xu, Z., Chen, X., Kim, H. N., and Yoon, J. Sensors for the optical detection of cyanide ion. *Chem. Soc. Rev.* 39 (2010): 127-137.
- [13] Hathaway, G. J., and Proctor, N. H. *Chemical Hazards of the Workplace*, 5th, Hoboken: John Wiley & Son Inc, 2004.
- [14] Patnaik, P. *A Comprehensive Guide to the Hazardous Properties of Chemical Substance*. New York: van Nostrand Reinhold, 1992.

- [15] Ishii, A., Seno, H., Watanabe-Suzuki, K., Suzuki, O., and Kumazawa, T. Determination of cyanide in whole blood by capillary gas chromatography with cryogenic oven trapping. *Anal. Chem.* 70 (1998): 4873-4876.
- [16] Moriya, F., and Hashimoto, Y. Potential for error when assessing blood cyanide concentration in fire victims. *J. Forensic Sci.* 46 (2001): 1421-1425.
- [17] Nelson, L. Acute cyanide toxicity: mechanisms and manifestations. *J. Emerg. Nurs.* 32 (2006): S8-S11.
- [18] Larson, J. W., and McMahon, T. B. Hydrogen bonding in gas-phase anions. The energetic of interaction between cyanide ion and Brønsted acids determined from ion cyclotron resonance cyanide exchange equilibria. *J. Am. Chem. Soc.* 109 (1987): 6230-6236.
- [19] Djebra-Belmessaoud, N., Nail Achour, M., Bethier, G., and Savinelli, R. A comparative theoretical study of the hydrogen bonding between cyanide or isocyanide hydrides and water. *J. Mol. Struct. (THEOCHEM)*, 941 (2010): 85-89.
- [20] Sun, S.-S., and Lees, A. J. Anion recognition through hydrogen bonding: a simple yet highly sensitive luminescent metal-complex receptor. *Chem. Commun.* (2000): 1687-1688.
- [21] Anzenbacher, P. Jr., Tyson, D. S., Jursíková, K., and Castellano, F.N. Luminescence lifetime-based sensor for cyanide and related anions. *J. Am. Chem. Soc.* 124 (2002): 6232-6233.
- [22] Gimeno, N., Li, X., Durrant, J. R., and Vilar, R. Cyanide sensing with organic dyes: Studies in solution and on nanostructured Al_2O_3 surfaces. *Chem. Eur. J.* 14 (2008): 3006-3012.
- [23] Kim, Y.-H., and Hong, J.-I. Ion pair recognition by Zn-porphyrin/crown ether conjugates: visible sensing of sodium cyanide. *Chem. Commun.* (2002): 512-513.
- [24] Liu, H., Shao, X.-B., Jia, M.-X., Jia, X.-K., Li, Z.-T., and Chen, G.-J. Selective recognition of sodium cyanide and potassium cyanide by diaza-crown ether-capped Zn-porphyrin receptors in polar solvents. *Tetrahedron* 61 (2005): 8095-8100.

- [25] Li, Z., Lou, X., Yu, H., Li, Z., and Qin, J. An imidazole-functionalized polyfluorene derivative as sensitive fluorescent probe for metal ions and cyanide. *Macromolecules* 41 (2008): 7433-7439.
- [26] Lou, X., Zhang, L., Qin, J., and Li, Z. An alternative approach to develop a highly sensitive and selective chemosensor for the colorimetric sensing of cyanide in water. *Chem. Commun.* (2008): 5848-5850.
- [27] Guibault, G. G., and Kramer, D. N. Specific detection and determination of cyanide using various quinone derivatives. *Anal. Chem.* 37 (1965): 1395-1399.
- [28] Reynolds, G. A., and Vanallan, J. A. The reactions of 2,3-dichloro-1,4-naphthoquinone with alkali metal cyanides. *J. Org. Chem.* 29(1964): 591-593.
- [29] Kim, Y. K., Lee, Y.-H., Lee, H.-L., Kim, M. K., Cha, G. S., and Ahn, K. H. Molecular recognition of anions through hydrogen bonding stabilization of anion-ionophore adducts: a novel trifluoroacetophenone-based binding motif. *Org. Lett.* 5(2003): 4003-4006.
- [30] Kim, D.-S., Miyaji, H., Chang, B.-Y., Park, S.-M., and Ahn, K. H. Selective recognition and electrochemical sensing of dicarboxylates with a ferrocene-based bis(*o*-trifluoroacetylcarboxanilide) receptor. *Chem. Commun.* (2006) 3314-3316.
- [31] Chung, Y. M., Raman, B., Kim, D.-S., and Ahn, K. H. Fluorescence modulation in anion sensing by introducing intramolecular H-bonding interaction in host-guest adducts. *Chem. Commun.* (2006): 186-188.
- [32] Miyaji, H., Kim, D.-S., Chang, B.-Y., Park, E., Park, S.-M., and Ahn, K. H. Highly cooperative ion-pair recognition of potassium cyanide using a heteroditopic ferrocene-based crown ether trifluoroacetylcarboxanilide receptor. *Chem. Commun.* (2008): 753-755.
- [33] Lee, H., Chung, Y. M., and Ahn, K. H. Selective fluorescence sensing of cyanide with an *o*-(carboxamido)trifluoroacetophenone fused with a cyano-1,2-diphenylene fluorophore. *Tetrahedron Lett.* 49(2008): 5544-5547.

- [34] Ekmekci, Z., Yılmaz, M. D., and Akkaya, E. U. A monostyrylboradiazaindacene (BODIPY) derivative as colorimetric and fluorescent probe for cyanide ions. *Org. Lett.* 10(2008): 461-464.
- [35] Lee, K. S., Lee, J. T., Hong, J. -I., and Kim, H. -J. Visual Detection of Cyanide through Intramolecular Hydrogen Bond. *Chem. Lett.* 46(2007): 816-819.
- [36] Lee, K. -S., Kim, H. -J., Kim, G. -H., Shin, I., and Hong, J. -I. Fluorescent chemodosimeter for selective detection of cyanide in water. *Org. Lett.* 10(2008): 49-51.
- [37] Kwon, S. K., and others. Sensing cyanide ion via fluorescent change and its application to the microfluidic system. *Tetrahedron Lett.* 49(2008): 4102-4105.
- [38] Cho, D. -G., Kim, J. -H., and Sessler, J. L. The benzil-cyanide reaction and its application to the development of selective cyanide anion indicator. *J. Am. Chem. Soc.* 130(2008): 12163-12167.
- [39] Sessler, J. L., and Cho, D. -G. The benzil rearrangement reaction: trapping of a hitherto minor product and its application to the development of a selective cyanide anion indicator, *Org. Lett.* 10(2008): 73-75.
- [40] Chen, C. -L., Chen, Y. -H., Chen, C. -Y., and Sun, S. -S. Dipyrrole carboxamide derived selective ratiometric probes for cyanide ion. *Org. Lett.* 8(2006): 5053-5056.
- [41] Tomasulo, M., and Raymo, F. M. Colorimetric detection of cyanide with a chromogenic oxazine. *Org. Lett.* 7(2005): 4633-4636.
- [42] Tomasulo, M., Sortino, S., White, A. J. P., and Raymo, F. M. Chromogenic oxazine for cyanide detection. *J. Org. Chem.* 71(2006): 744-753.
- [43] Ren, J., Zhu, W., and Tian, H. A highly sensitivity and selective chemosensor for cyanide. *Talanta* 75(2008): 760-764.
- [44] Hong, S. -J., Yoo, J., Kim, S. -H., Kim, J. S., Yoon, J., and Lee, C. -H. β -Vinyl substituted calix[4]pyrrole as a selective ratiometric sensor for cyanide anion. *Chem. Commun.* (2009): 189-191.
- [45] Yang, Y. -K., and Tae, J. Acridinium salt based fluorescent and colorimetric chemosensor for the detection of cyanide in water. *Org. Lett.* 8(2006): 5721-5723.

- [46] Ros-Lis, J. V., Martínez-Mañes, R., and Soto, J. A selective chromogenic reagent for cyanide determination. *Chem. Commun.* (2002): 2248-2249.
- [47] Zhang, X., Li, C., Cheng, X., Wang, X., and Zhang, B. A near-infrared croconium dye-based colorimetric chemodosimeter for biological thiols and cyanide anion. *Sens. Actuators B* 129(2008): 152-157.
- [48] Quian, G., Li, X., and Wang, Z. Y., Visible and near-infrared chemosensor for colorimetric and ratiometric detection of cyanide. *J. Mater. Chem.* 19(2009): 522-530.
- [49] Ros-Lis, J. V., Matínez-Mañez, R., and Soto, J. Subphthalocyanines as fluorochromogenic probes for anions and their application to the highly selective cyanide detection. *Chem. Commun.* (2005): 5260-5262.
- [50] Palomarez, E., Matínez-Días, M. V., Torres, T., and Coronado, E. A highly sensitive hybrid colorimetric and fluorometric molecular probe for cyanide sensing based on a subphthalocyanine dye. *Adv. Funct. Mater.* 16(2006): 1166-1170.
- [51] Huh, J. O., Do, Y., and Lee, M. H. A BODIPY-borane dyad for the selective complexation of cyanide ion. *Organometallic.* 27(2008): 1022-1025.
- [52] Hudnall, T. W., and Gabbai, F. P., Ammonium boranes for the selective complexation of cyanide and fluoride ion in water. *J. Am. Chem. Soc.* 129(2007): 11978-11986.
- [53] Badugu, R., Lakowicz, J. R., and Geddes, C. D. Excitation emission wavelength ratiometric cyanide-sensitive probes for physiological sensing. *Anal. Biochem.* 327(2004): 82-90.
- [54] Badugu, R., Lakowicz, J. R., and Geddes, C. D. Cyanide sensitive fluorescent probes. *Dyes Pigment* 64(2005): 49-55.
- [55] Badugu, R., Lakowicz, J. R., and Geddes, C. D. Fluorescence intensity and lifetime-based cyanide sensitive probes for physiological safeguard. *Anal. Chem. Acta.* **2004**, 522, 9-17.
- [56] Badugu, R., Lakowicz, J. R., and Geddes, C. D. Enhanced fluorescence cyanide detection at physiologically lethal levels: reduced ICT-based signal transduction. *J. Am. Chem. Soc.* 127(2005): 3635-3641.
- [57] Hall, G. D. *Boronic acid*. Weinheim: Wiley-VCH Verlag GmbH&Co. KGaA, 2005.

- [58] James, T. D., Phillips, M. D., and Shinkai, S. *Boronic acid in saccharide recognition*. Cambridge: RSC Publishing, 2006.
- [59] Yan, J., Fang, H., and Wang, B. Boronlectins and fluorescent boronlectins : an examination of the detailed chemistry issues important for the design. *Med. Res. Rev.* 25(2005): 490-520.
- [60] Cao, H., and Heagy, M. D. Fluorescent chemosensors for carbohydrates : A decade's worth of bright spies for saccharides in review. *J. Fluoresc.* 14(2004): 569-584.
- [61] Fang, H., Kaur, G., and Wang, B. Progress in boronic acid-based fluorescent glucose sensors. *J. Fluoresc.* 14(2004): 481-489.
- [62] Springsteen, G., and Wang, B. A detailed examination of boronic acid-diol complexation. *Tetrahedron* 58(2002): 5291-5300.
- [63] Bosch, L. I., Fyles, T. M., and James, T. D. Binary and ternary phenylboronic acid complexes with saccharide and Lewis bases. *Tetrahedron* 60(2004): 11175-11190.
- [64] Miyamoto, C., Suzuki, K., Iwatsuki, S., Inamo, M., and Takagi, H. D. Kinetic evidence for high reactivity of 3-nitrophenylboronic acid compared to its conjugate boronate ion in reactions with ethylene and propylene glycols. *Inorg. Chem.* 47(2008): 1417-1419.
- [65] Wiskur, S. L., and others. pKa values and geometries of secondary and tertiary amines complexed to boronic acid-implications for sensor-design. *Org. Lett.* 3(2001): 1311-1314.
- [66] Nicholls, M. P., and Paul, P. K. C. S. Structure of carbohydrate-boronic acid complexes determined by NMR and molecular modelling in a aqueous alkaline media. *Org. Biomol. Chem.* 2(2004): 1434-1441.
- [67] James, T. D., Sandanayake, K. R. A. S., and Shinkai, S. Novel photoinduced electron-transfer sensor for saccharides based on the interaction of boronic acid and amine. *Chem. Commun.* (1994): 477-478.
- [68] James, T. D., Sandanayake, K. R. A., Igarashi, R., and Shinkai, S. Novel saccharide photoinduced electron transfer sensors based on the interaction of boronic acid and amine. *J. Am. Chem. Soc.* 117(1995): 8982-8987.

- [69] Trupp, S., Schweitzer, A., and Mohr, G. J. A fluorescent water-soluble naphthalimide-based for saccharide with highest selectivity in the physiological pH range. *Org. Biomol. Chem.* 4(2006): 2965-2968.
- [70] James, T. D., and Sandanayake, K. R. A. A glucose-selective molecular fluorescence sensor. *Angew. Chem. Int. Ed. Engl.* 33(1994): 2207-2209.
- [71] Bielecki, M., Eggert, H., and Norrild, J. C. A fluorescent glucose sensor binding covalent to all five hydroxy groups of α -D-glucopyranose. A reinvestigation. *J. Am. Chem. Soc. Perkin Trans.* 2(1999): 449-455.
- [72] Zhao, J., Davidson, M. G., Mahon, M. F., Kociok-Köhn, G., and James, T. D. An enantioselective fluorescent sensor for sugar acids. *J. Am. Chem. Soc.* 126(2004): 16179-16186.
- [73] Zhao, J., and James, T. D. Chemoselective and enantioselective fluorescent recognition of sugar alcohols by a bisboronic acid receptor. *J. Mater. Chem.* 15(2005): 2896-2901.
- [74] Shinmori, H., Takeuchi, M., and Shinkai, S. Spectroscopic sugar sensing by a stilbene derivative with Push(Me₂-N)-Pull(-(OH)₂B-) type substituent. *Tetrahedron* 51(1995): 1893-1902.
- [75] Dicesare, N., and Lakowicz, J. R. Spectral properties of fluorophores combining the boronic acid group with electron donor or withdrawing groups. Implication in the development of fluorescence probes for saccharides. *J. Phy. Chem. A* 105(2001): 6834-6840.
- [76] Dicesare, N., and Lakowicz, J. R. Wavelength-ratiometric probes for saccharides based donor-acceptor diphenylpolyene. *J. Photochem. Photobiol. A Chem.* 143(2001): 143, 39-47.
- [77] Dicesare, N., and Lakowicz, J. R. A new highly fluorescent probes for saccharides based on donor-acceptor diphenyloxazole. *Chem. Commun.* (2001): 2022-2023.
- [78] Dicesare, N., and Lakowicz, J. R. Fluorescent probes for monosaccharide based on a functionalized boron-dipyrromethane with a boronic acid group. *Tetrahedron Lett.* 42(2001): 9105-9108.

- [79] Gao, X., Zhang, Y.; and Wang, B. Naphthalene-based water-soluble fluorescent boronic acid isomers suitable for ratiometric and off-on sensing of saccharides at physiological pH. *New J. Chem.* 29(2005): 579-586.
- [80] Gao, X., Zhang, Y., and Wang, B. New boronic acid fluorescent receptor compounds. 2. A naphthalene-based On-off sensor functional at physiological pH. *Org. Lett.* 5(2003): 4615-4618.
- [81] Zhang, Y., Gao, X., Hardcastle, K., and Wang, B. Water soluble fluorescent boronic acid compound for saccharide sensing: substituent effect on their fluorescence properties. *Chem. Eur. J.* 12(2006): 1377-1384.
- [82] Winkelmann, E. 2,3,5,6-Tetra-amino-1,4-benzochinon (TABC): Darstellung, eigenschaften und reaktionen. *Tetrahedron* 25(1969): 2427-2454.
- [83] Kim, S. J., and Kool, E. T. Sensing metal ions with DNA building blocks: fluorescent pyridobezimidazole nucleosides. *J. Am. Chem. Soc.* 128(2006): 6164-6171.
- [84] Perrin, D. D., and Dempsey, B. *Buffer for pH and metal ion control*. London: Chapman and Hall, 1974.
- [85] Melhuish, W. H. Quantum efficiencies of fluorescence of organic substances effect of solvent and concentration of the fluorescent solute. *J. Chem. Phys.* 65(1961), 65, 229-235.
- [86] Dawson, W.R., and Windsor, M. W. Fluorescence yields of aromatic compounds. *J. Phys. Chem.* 72(1968): 3251-3260.
- [87] Cooper, C. R., Spencer, N., and James, T. D. Selective fluorescence detection of fluoride using boronic acids. *Chem. Commun.* (1998), 1365-1366.
- [88] Badugu, R., Lakowicz, J. R., and Geddes, C. D. A wavelength-ratiometric fluoride-sensitive probe based on the quinolinium nucleus and boronic acid moiety. *Sens. Actua. B* 104(2005): 103-110.
- [89] Valeur, B., Pouget, J., Bourson, J., Kachke, M., and Ernsting, N. P. Tuning of photoinduced energy transfer in a bichromophoric coumarin supermolecule by cation binding. *J. Phys. Chem.* 96(1992): 6545-6549.

- [90] Fery-Forgues, S., Le Bris, M.-T., Guetté, J.-P., and Valeur, B. Ion-responsive fluorescent compound. I. Effect of cation binding on photophysical properties of a benzoxazinone derivative linked to monoaza-15-crown-5¹. *J. Phy. Chem.* 92(1988): 6233-6237.
- [91] Marcotte, N., Plaza, P., Lavabre, D., Fery-Forgues, S., and Martin, M. M. Calcium photorelease from a symmetrical donor-acceptor-donor bis-crown-fluoroionophore evidenced by ultrafast absorption spectroscopy. *J. Phy. Chem. A* 107(2003): 2394-2402.
- [92] Chu, K.-Y., and Griffiths, J. Naphthoquinone colouring matters. Part 1. Synthesis and electronic absorption spectra of 1,4-naphthoquinone derivatives with electron donating group in the quinonoid ring. *J. Chem. Soc. Perkin Trans. I* (1978): 1083-1087.
- [93] Batista, R. M. F., Oliveira, E., Costa, S. P. G., Lodeiro, C., and Raposo, M. M. M. Synthesis and ion sensing properties of properties of new colorimetric and fluorimetric chemosensor for bi-thienyl-imidazo-anthraquinone chromophores. *Org. Lett.* 9(2007): 3201-3204.
- [94] Brodwell, F. G. Equilibrium acidities in dimethyl sulfoxide solution. *Acc. Chem. Res.* 21(1988): 456-463.
- [95] Boiocchi, M., Del Boca, L., Gomez, D. E., Fabbrizzi, L., Licchelli, M., and Monzani, E. Nature of urea-fluoride interaction: incipient and definition proton transfer. *J. Am. Chem. Soc.* 126(2004): 16507-16514.
- [96] Bhattacharya, S., and Gulyani, A. First report of Zn²⁺ sensing exclusively at mesoscopic interfaces. *Chem. Commun.* (2004): 224-225.
- [97] Nakahara, Y., Kida, T., Naktsuji, Y., and A kashi, M. A novel fluorescent indicator for Ba²⁺ in a aqueous micellar solution. *Chem. Commun.* (2002): 224-225.
- [98] Vargas, L. V., Sand, J., Brandão, T. A. S., Fieldler, H. D., and Quina, F. H. Determination of environmentally important metal ions by fluorescence quenching in anionic micellar solution. *Analyst* 130(2005): 242 -246.

- [99] Fernandez, Y. D., and others. Using micelles for a new approach to fluorescent sensors for metal cations. *Chem. Commun.* (2004): 1650-1651.
- [100] Mèallet-Renault, R., Pansu, R., Amigoni-Gerbier, S., and Larpent, C. Metal-chelating nanoparticles as selective fluorescent sensor for Cu^{2+} . *Chem. Commun.* (2004): 2344-2345.
- [101] Mallick, A., Mandal, M. C., Haldar, B., Chakrabarty, A., Das, P., and Chattopadhyay, N. Surfactant-induced modulation of fluorosensor activity : a simple way to maximize the sensor efficiency, *J. Am. Chem. Soc.* 126(2006): 3126-3127.
- [102] Nakahara, Y., Kida, T., Nakatsuji, Y., and Akashi, M. Fluorometric sensing of alkali metal and alkaline earth metal cations by novel photosensitive monoazacryptand derivatives in aqueous micellar solutions, *Org. Biomol. Chem.* 3(2005): 1787-1794.
- [103] Avirah, P. R., Jyothish, K., and Ramaiah, D. Dual-mode semisquaraine-based sensor for selective detection of Hg^{2+} in a micellar medium. *Org. Lett.* 9(2007): 121-124.
- [104] Pallavicini, P., Dias-Fernandez, Y. A., Foti, F., Mangano, C., and Patroni, S. Fluorescent sensors for Hg^{2+} in micelles : a new approach that transforms an ON-OFF into an OFF-ON response as a function of the lipophilicity of the receptor. *Chem. Eur. J.* 13(2007): 178-187.
- [105] Das, P., Mallick, A., Sarkar, D., and Chattopadhyay, N. Application of anionic micelle for dramatic enhancement in the quenching-based metal ion fluoresensing. *J. Coll. Inter. Sci.* 320(2008): 9-14.
- [106] Yu, F., Ding, Y., Gao, Y., Zhen, S., and Chen, F. Fluorescence enhancement effect for the detection of DNA with calcein-cetyltrimethyl ammonium bromide system. *Anal. Chem. Acta.* 625(2008): 195-200.
- [107] Shen, Y., Yang, X.-F., Wu, Y., and Li, C. Sensitive spectrofluorimetric determination of cytochrome C with spirocyclic rhodamine B hydrazide in micellar medium. *J. Fluoresc.* 18(2008): 163-168.
- [108] Hayakawa, K., Kanda, M., and Satake, I. The determination of the formation constant of triiodide ion in micellar solution of dodecyltrimethyl ammonium chloride. *Bull. Chem. Soc. Jpn.* 52(1979): 3171-3175.

- [109] Coccovla, I. M., and Chaimovich, H. Determination of micromolar concentrations of iodine with a aqueous micellar hexadecyltrimethyl ammonium bromide. *Anal. Chem.* 54(1982): 789-791.
- [110] Kunda, S., Ghosh, S. K., Mandal, M., and Pal, T. Micelle bound redox dye marker for nanogram level arsenic detection promoted by nanoparticles. *New J. Chem.* 26(2002): 1081-1084.
- [111] Mallick, K., Jewrajka, S., Pradhan, N., and Pal, T. Micelle-catalysed redox reaction. *Curr. Sci.* 80(2001): 1408-1412.
- [112] Button, C. A., Nome, F., Quina, F. H., and Romsted, L. S. Ion binding and reactivity at charged aqueous interfaces. *Acc. Chem. Res.* 24(1991): 357-364.
- [113] Matzinger, S., Hussey, D. M., and Fayer, M. D. Fluorescent probe solubilization in the headgroup and core regions of micelles : fluorescence lifetime and orientational relaxation measurements. *J. Phy. Chem. B* 102(1998): 7216-7224.
- [114] Wei, L., Ming, Z., Jinli, Z., and Yongcai, H. Self-assembly of cetyl trimethylammonium bromide in ethanol-water mixtures. *Front. Chem. China.* 4(2006): 438-442.
- [115] Ingle, J. D. Jr., and Wilson, R. L. Difficulties with determining the detection limit with nonlinear calibration curves in spectrometry. *Anal. Chem.* 48(1976): 1641-1642.
- [116] Sun, X.-Y., and Liu, B. The fluorescence sensor for saccharide based on internal conversion. *Luminescence* 20(2005): 331-333.



APPENDIX

ศูนย์วิทยทรัพยากร
จุฬาลงกรณ์มหาวิทยาลัย

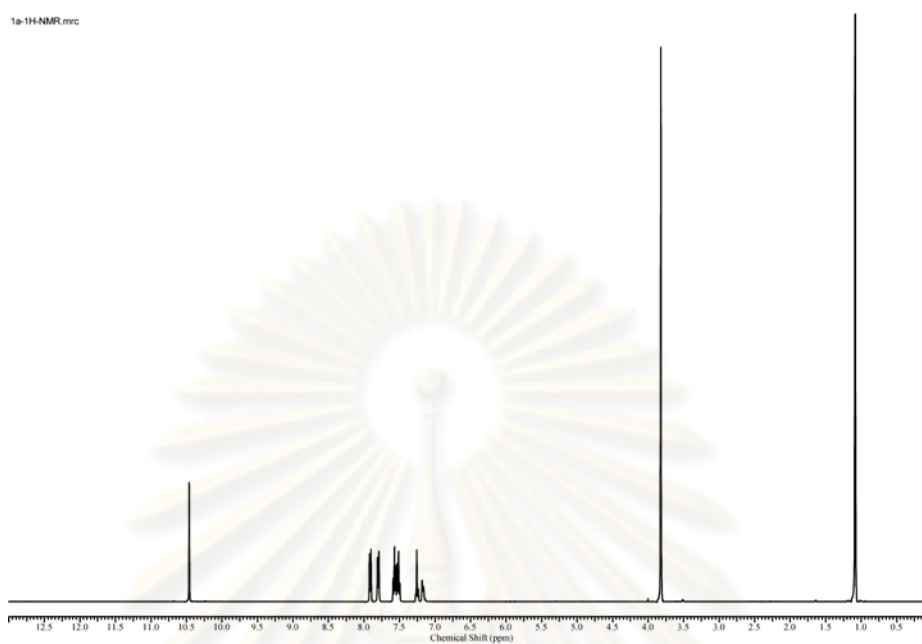


Figure A.1 The ¹H-NMR spectrum (400 MHz) of 2-(5,5-dimethyl-1,3,2-dioxaborinan-2-yl)benzaldehyde (**1a**) in CDCl₃.

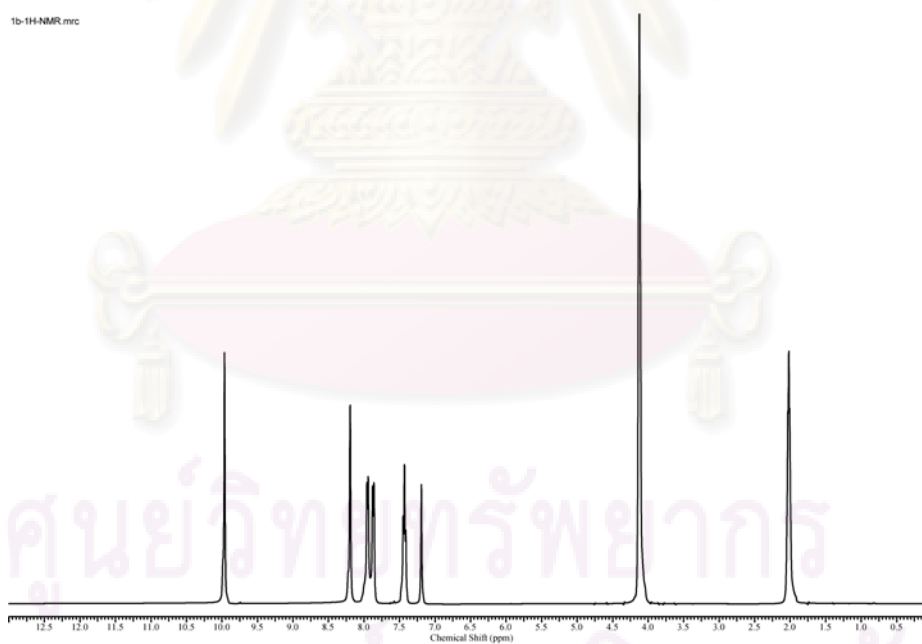


Figure A.2 The ¹H-NMR spectrum (400 MHz) of 3-(1,3,2-dioxaborinan-2-yl)benzaldehyde (**1b**) in CDCl₃.

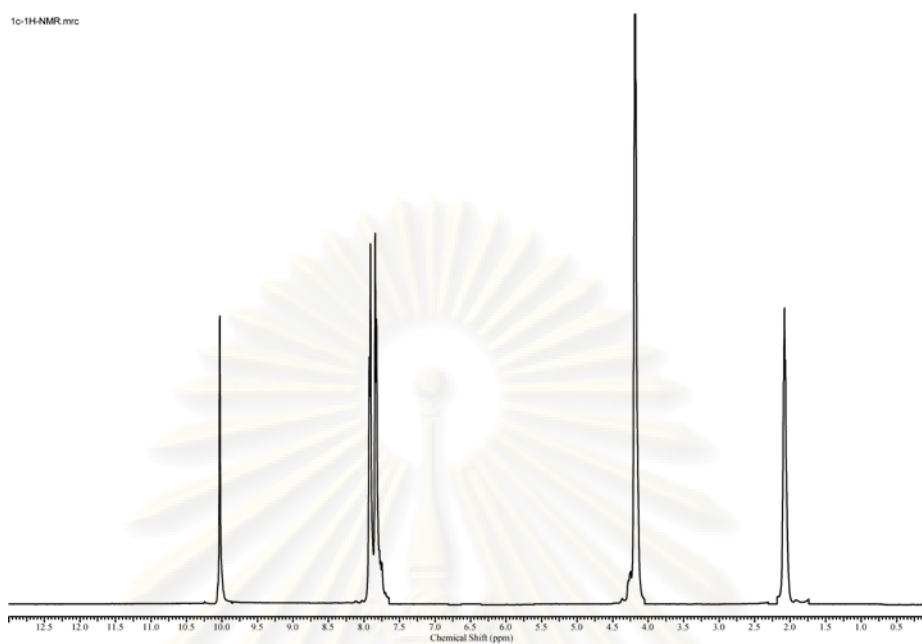


Figure A.3 The ¹H-NMR spectrum (400 MHz) of 4-(1,3,2-dioxaborinan-2-yl)benzaldehyde (**1c**) in CDCl₃.

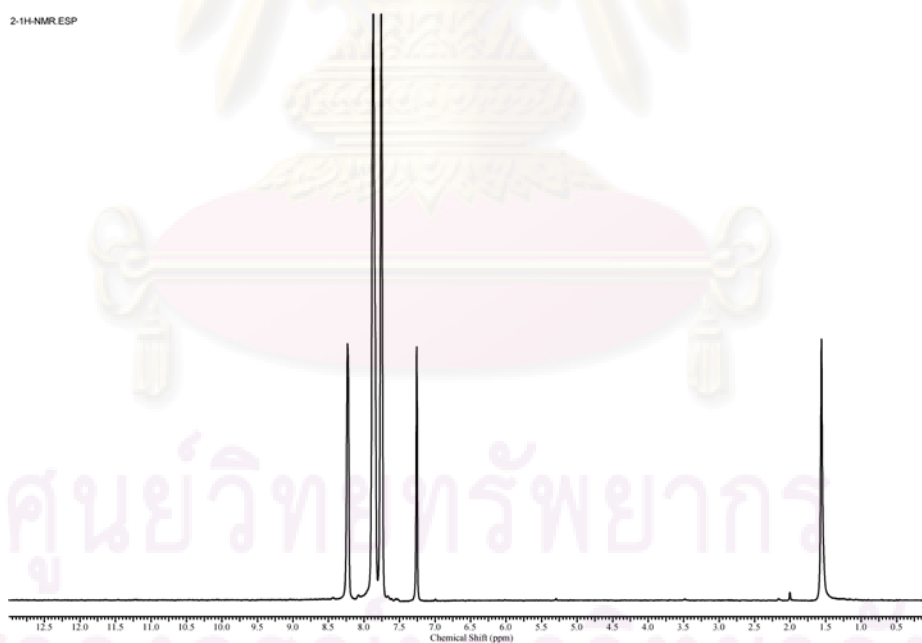


Figure A.4 The ¹H-NMR spectrum (400 MHz) of dipthalimide naphthaquinone (**2**) in CDCl₃.

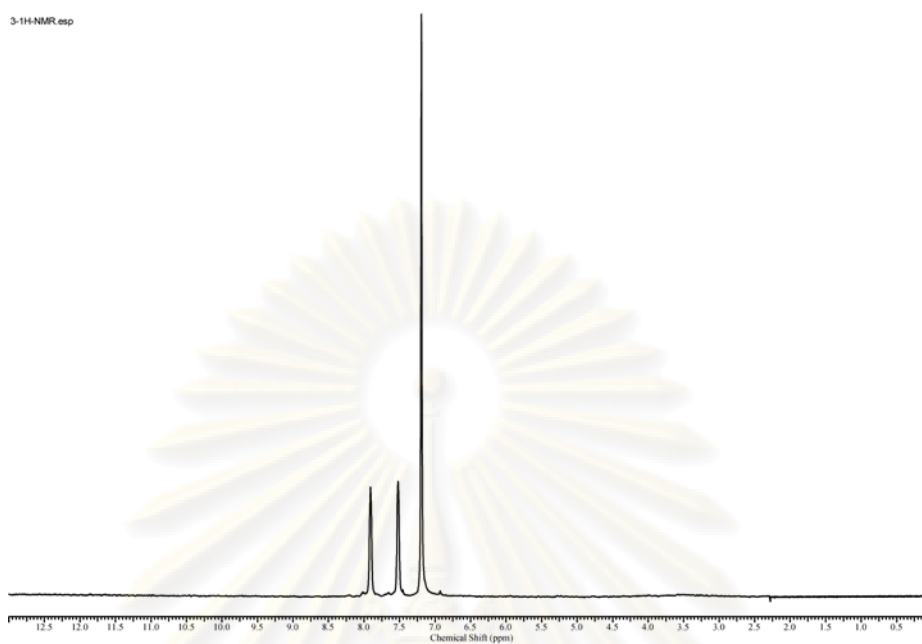


Figure A.5 The ¹H-NMR spectrum (400 MHz) of 2,3-diaminonaphthalene-1,4-dione (**3**) in CDCl₃.

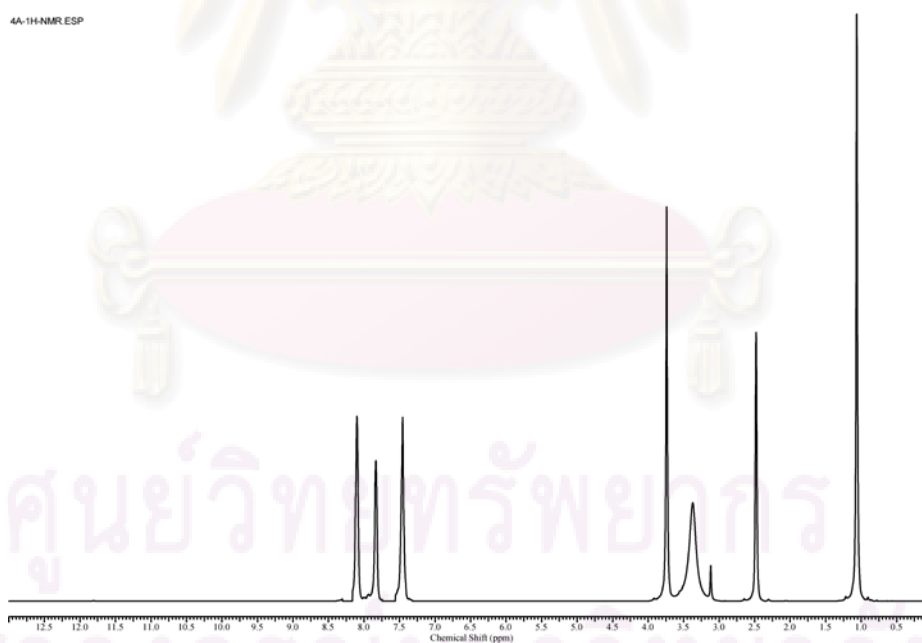


Figure A.6 The ¹H-NMR spectrum (400 MHz) of 2-(2-(5,5-dimethyl-1,3,2-dioxaborinan-2-yl)phenyl)-1H-naphtho[2,3-d]imidazole-4,9-dione (**4a**) in DMSO-*d*₆.

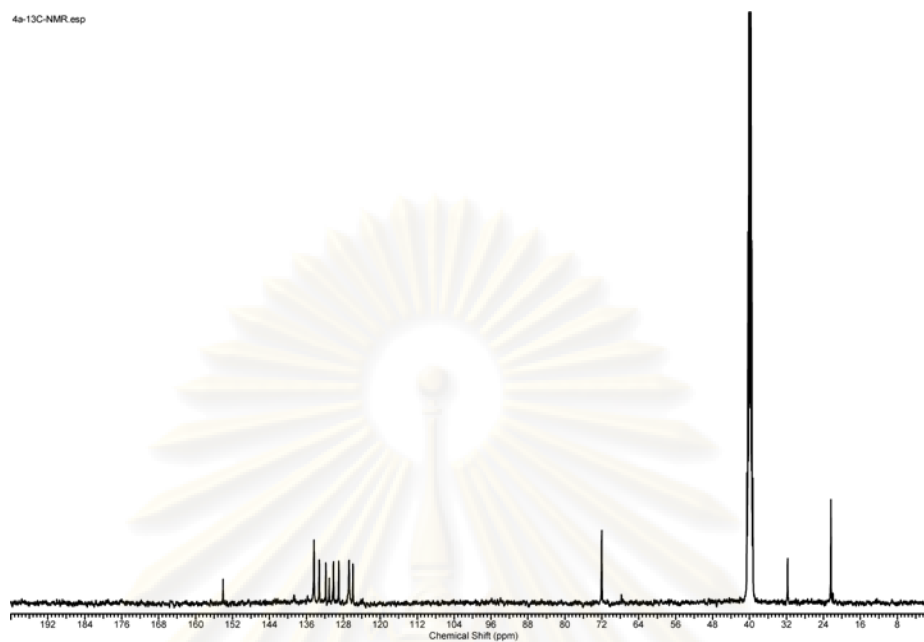


Figure A.7 The ^{13}C -NMR spectrum (100.6 MHz) of 2-(2-(5,5-dimethyl-1,3,2-dioxaborinan-2-yl)phenyl)-1H-naphtho[2,3-d]imidazole-4,9-dione (**4a**) in $\text{DMSO-}d_6$.

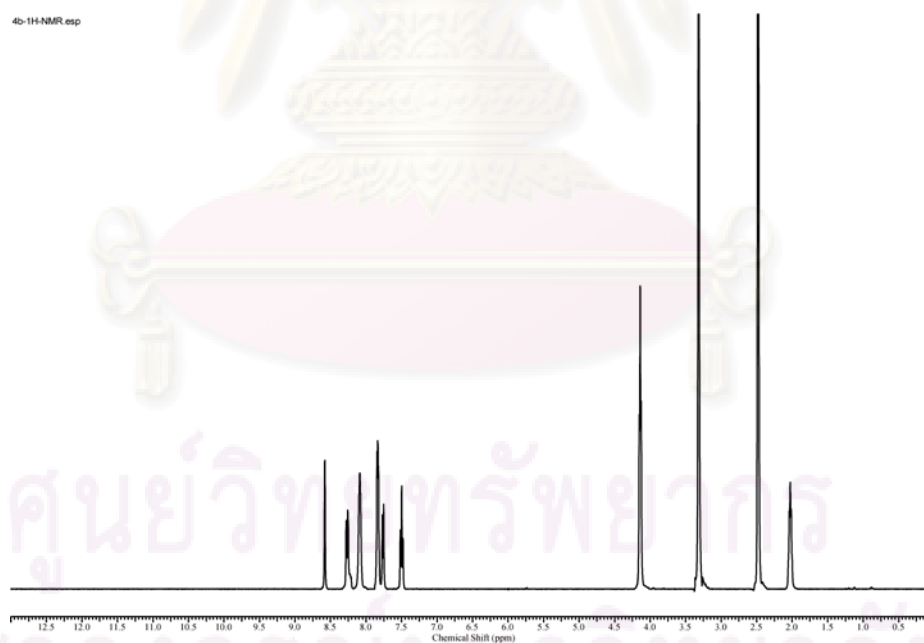


Figure A.8 The ^1H -NMR spectrum (400 MHz) of 2-(3-(1,3,2-dioxaborinan-2-yl)phenyl)-1H-naphtho[2,3-d]imidazole-4,9-dione (**4b**) in $\text{DMSO-}d_6$.

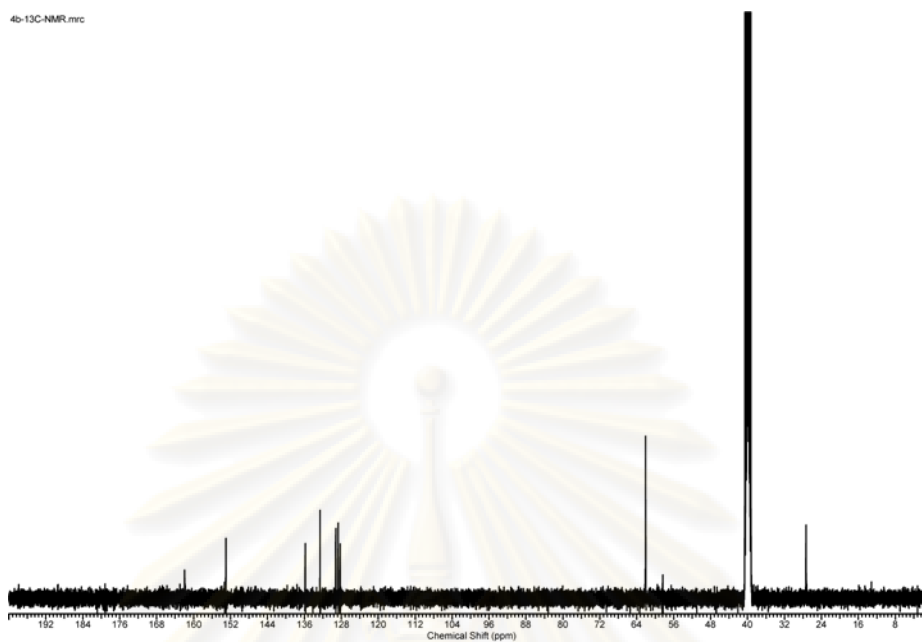


Figure A.9 The ^{13}C -NMR spectrum (100.6 MHz) of 2-(3-(1,3,2-dioxaborinan-2-yl)phenyl)-1H-naphtho[2,3-d]imidazole-4,9-dione (**4b**) in $\text{DMSO-}d_6$.

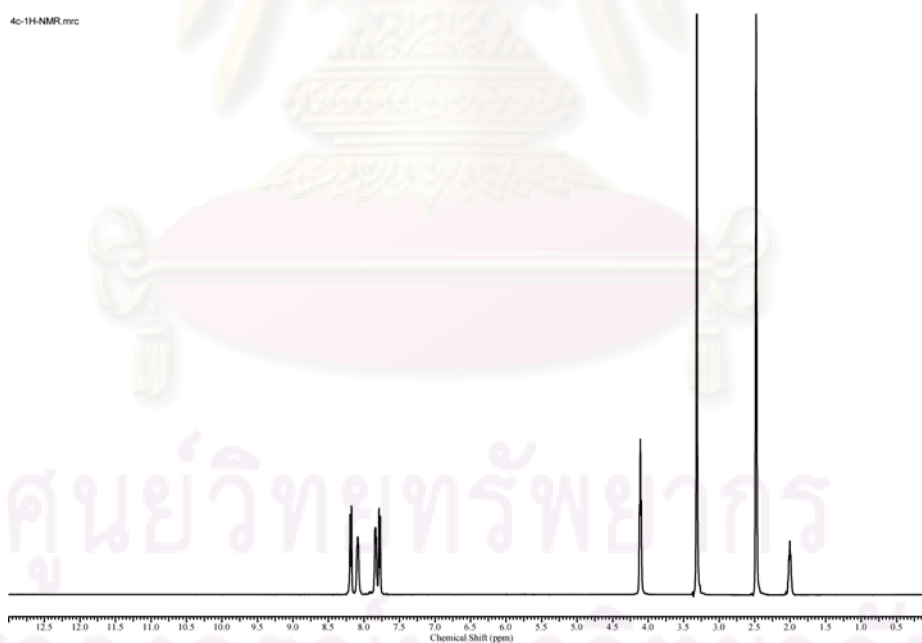


Figure A.10 The ^1H -NMR spectrum (400 MHz) of 2-(4-(1,3,2-dioxaborinan-2-yl)phenyl)-1H-naphtho[2,3-d]imidazole-4,9-dione (**4c**) in $\text{DMSO-}d_6$.

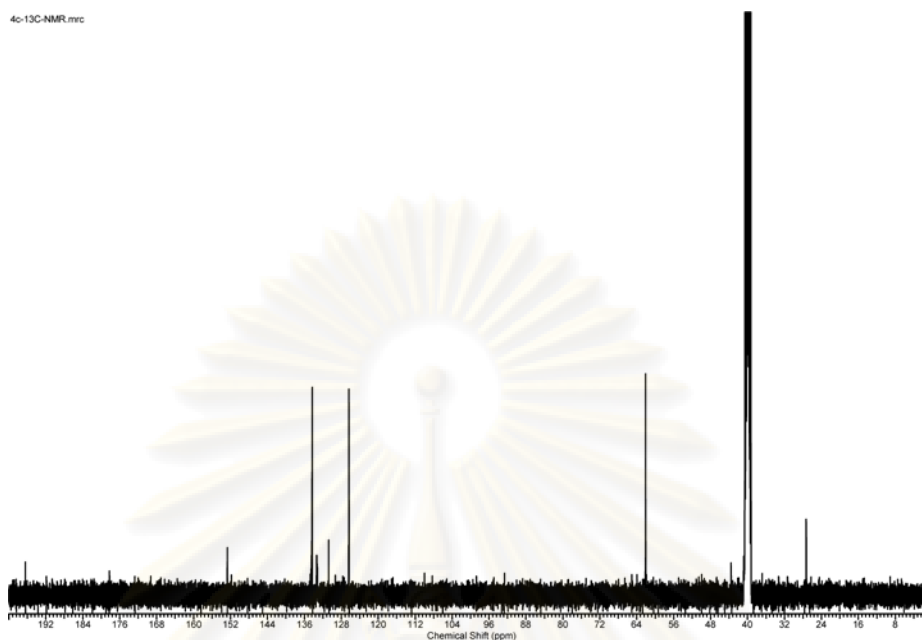


Figure A.11 The ¹³C-NMR spectrum (100.6 MHz) of 2-(4-(1,3,2-dioxaborinan-2-yl)phenyl)-1H-naphtho[2,3-d]imidazole-4,9-dione (**4c**) in DMSO-*d*₆.

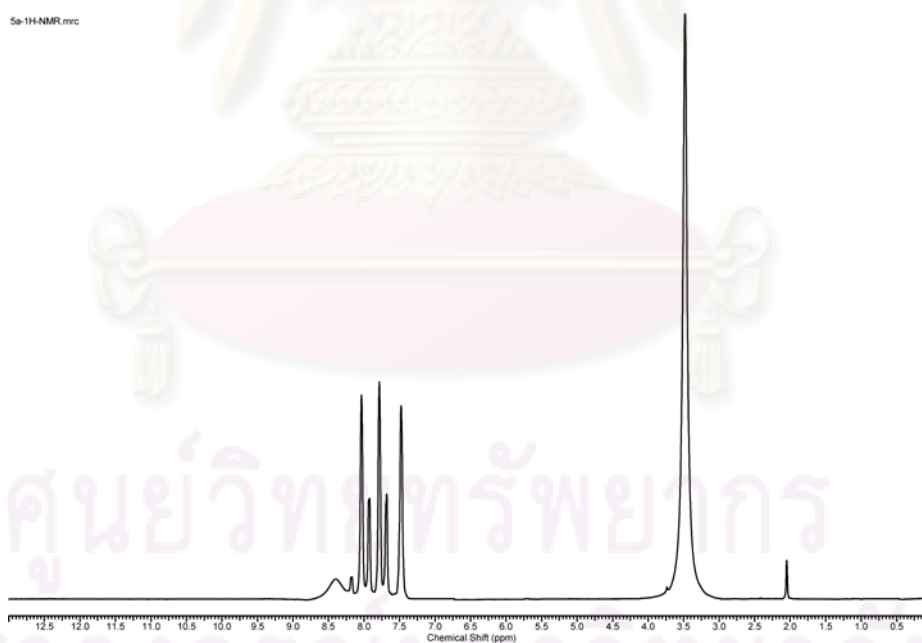


Figure A.12 The ¹H-NMR spectrum (400 MHz) of 4,9-dioxo-4,9-dihydro-1H-naphtho[2,3-d]imidazol-2-yl)phenylboronic acid (***o*-HNQB**) in DMSO-*d*₆.

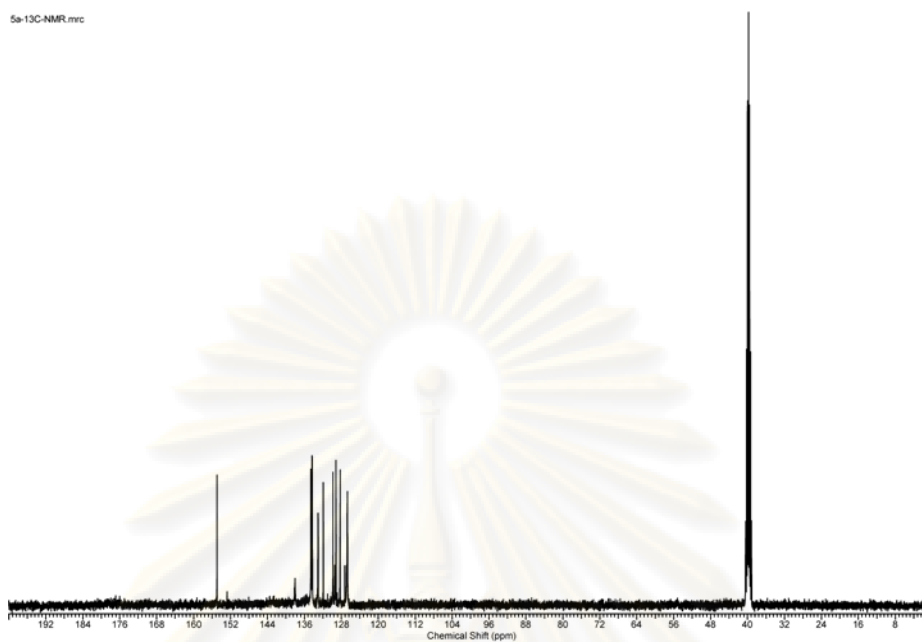


Figure A.13 The ^{13}C -NMR spectrum (100.6 MHz) of 4,9-dioxo-4,9-dihydro-1H-naphtho[2,3-d]imidazol-2-yl)phenylboronic acid (*o*-HNQB) in $\text{DMSO-}d_6$.

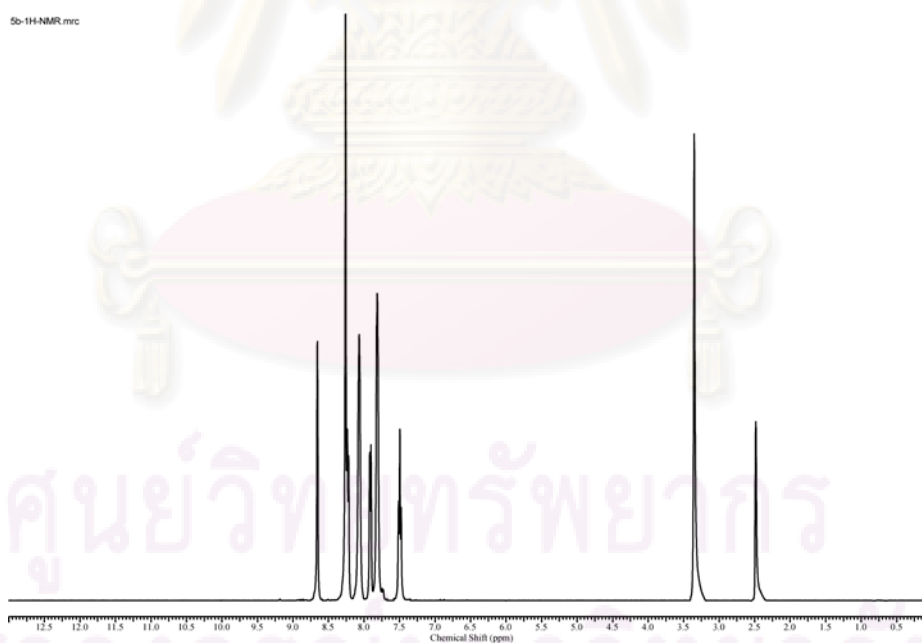


Figure A.14 The ^1H -NMR spectrum (400 MHz) of 4,9-dioxo-4,9-dihydro-1H-naphtho[2,3-d]imidazol-2-yl)phenylboronic acid (*m*-HNQB) in $\text{DMSO-}d_6$.

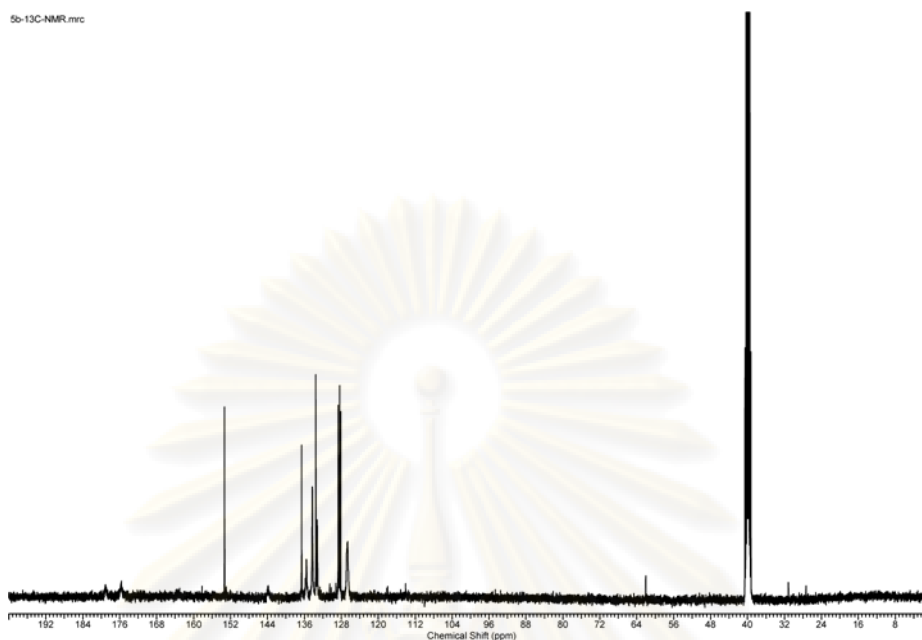


Figure A.15 The ^{13}C -NMR spectrum (100.6 MHz) of 4,9-dioxo-4,9-dihydro-1H-naphtho[2,3-d]imidazol-2-yl)phenylboronic acid (*m*-HNQB) in $\text{DMSO-}d_6$.

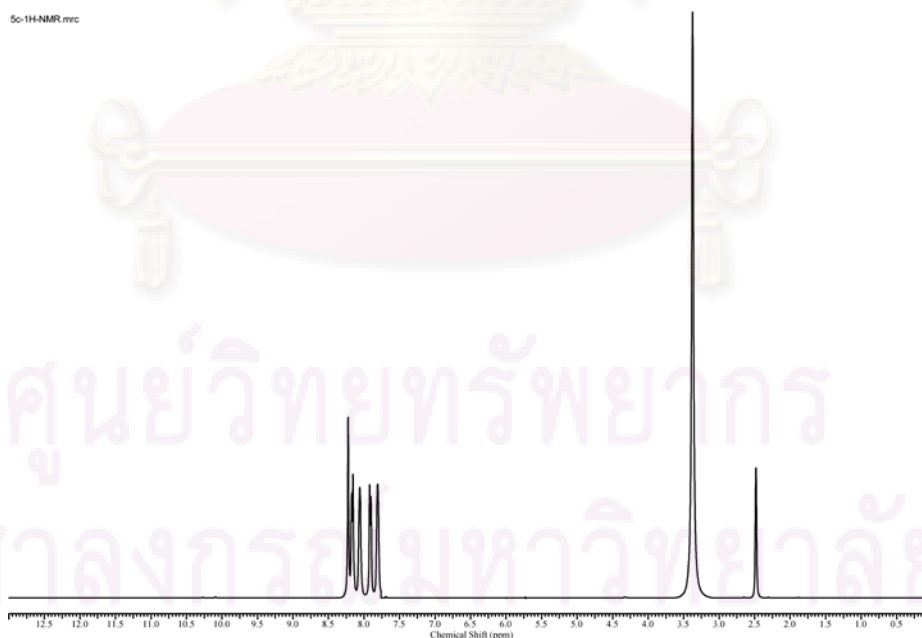


Figure A.16 The ^1H -NMR spectrum (400 MHz) of 4,9-dioxo-4,9-dihydro-1H-naphtho[2,3-d]imidazol-2-yl)phenylboronic acid (*p*-HNQB) in $\text{DMSO-}d_6$.

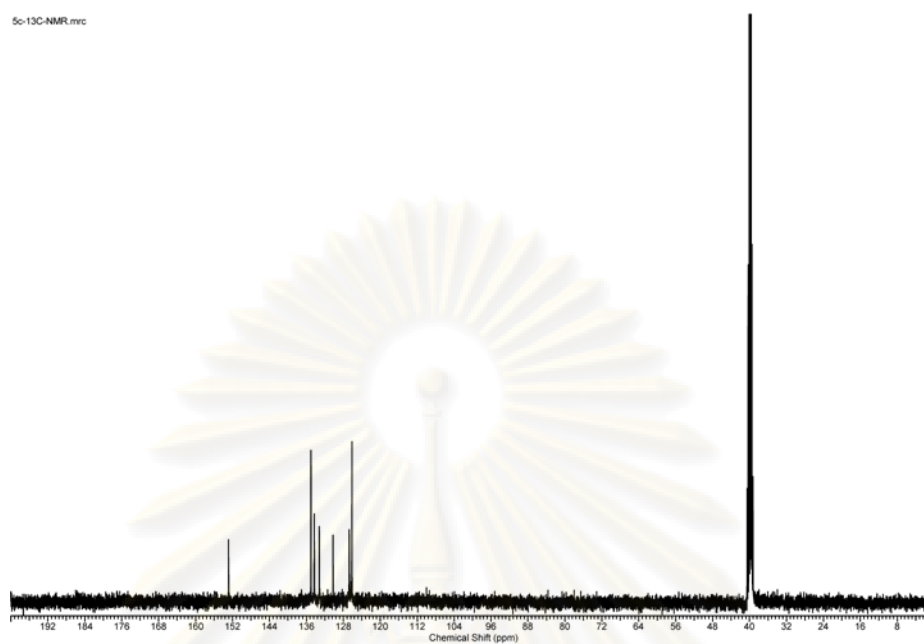


Figure A.17 The ^{13}C -NMR spectrum (100.6 MHz) of 4,9-dioxo-4,9-dihydro-1H-naphtho[2,3-d]imidazol-2-yl)phenylboronic acid (***p*-HNQB**) in $\text{DMSO-}d_6$.

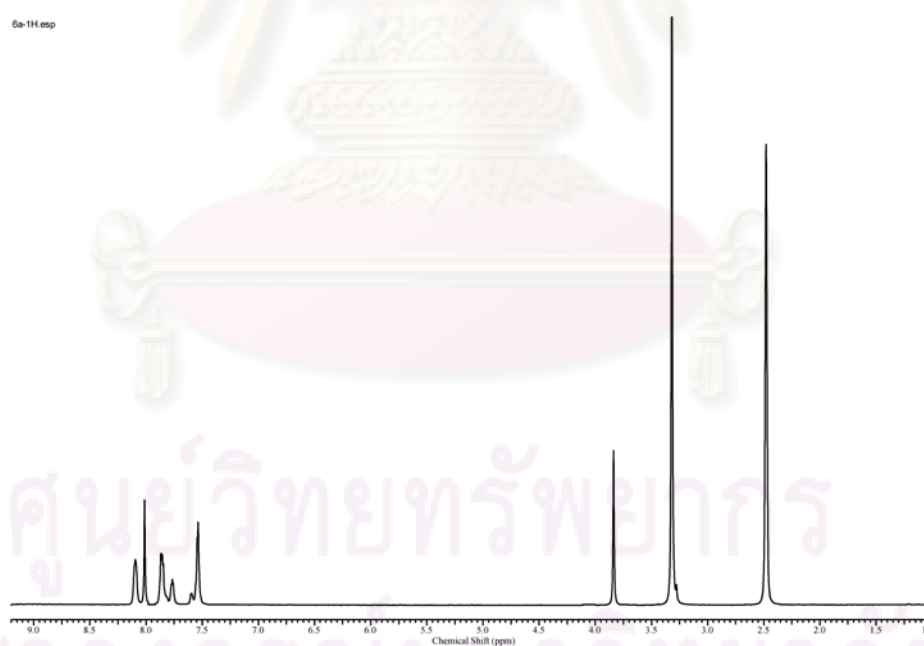


Figure A.18 The ^1H -NMR spectrum (400 MHz) of 4-(1-methyl-4,9-dioxo-4,9-dihydro-1H-naphtho[2,3-d]imidazol-2-yl) phenylboronic acid (***o*-MNQB**) in $\text{DMSO-}d_6$.

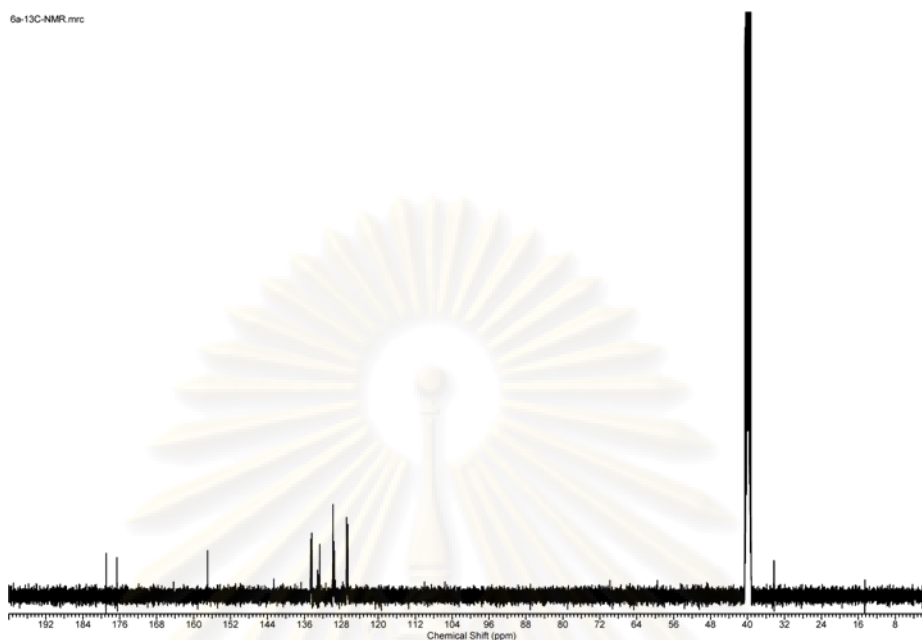


Figure A.19 The ^{13}C -NMR spectrum (100.6 MHz) of 4-(1-methyl-4,9-dioxo-4,9-dihydro-1H-naphtho[2,3-d]imidazol-2-yl) phenylboronic acid (*o*-MNQB) in $\text{DMSO-}d_6$.

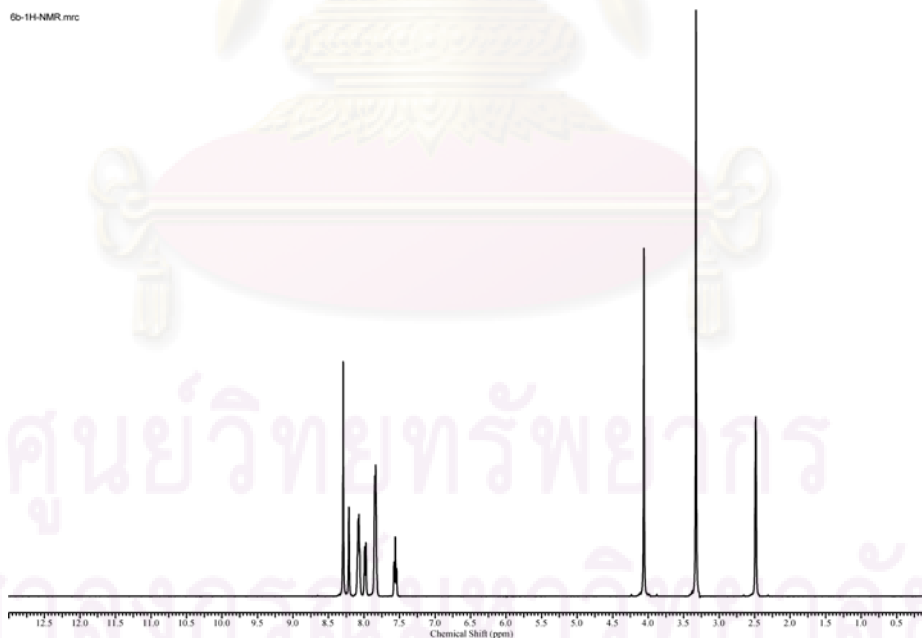


Figure A.20 The ^1H -NMR spectrum (400 MHz) of 4-(1-methyl-4,9-dioxo-4,9-dihydro-1H-naphtho[2,3-d]imidazol-2-yl) phenylboronic acid (*m*-MNQB) in $\text{DMSO-}d_6$.

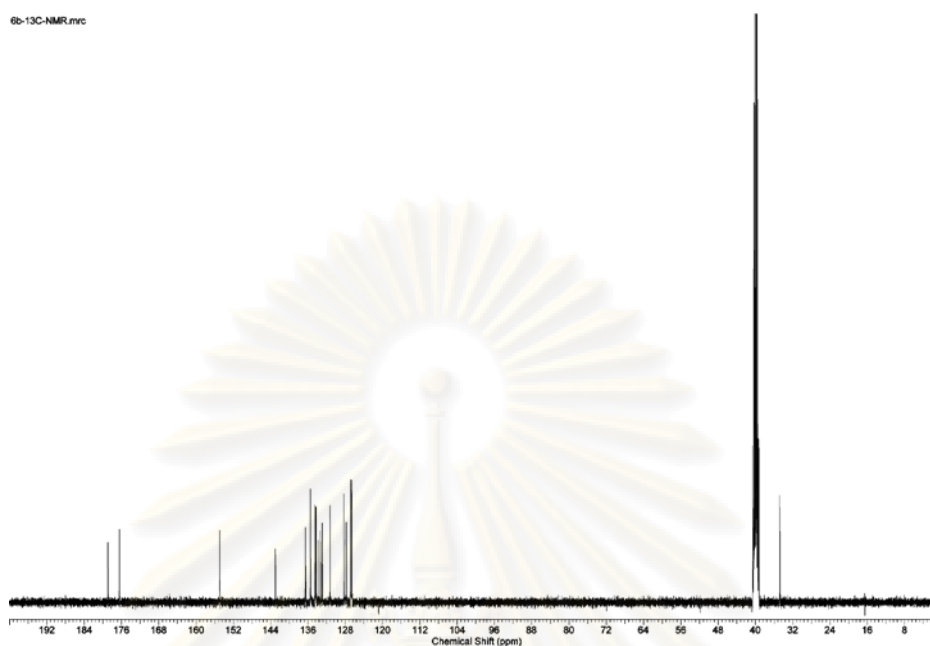


Figure A.21 The ¹³C-NMR spectrum (100.6 MHz) of 4-(1-methyl-4,9-dioxo-4,9-dihydro-1H-naphtho[2,3-d]imidazol-2-yl) phenylboronic acid (*m*-MNQB) in DMSO-*d*₆.

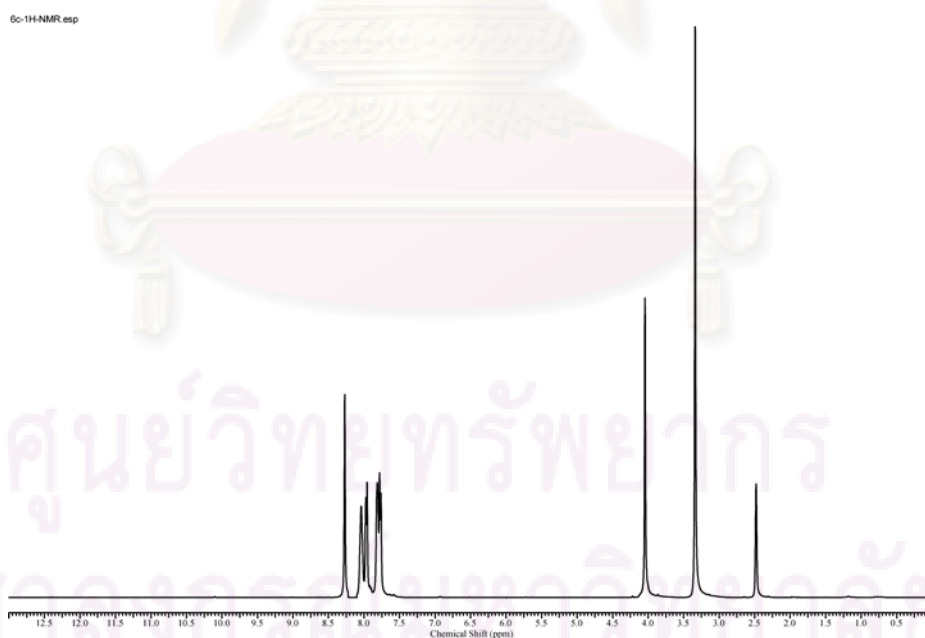


Figure A.22 The ¹H-NMR spectrum (400 MHz) of 4-(1-methyl-4,9-dioxo-4,9-dihydro-1H-naphtho[2,3-d]imidazol-2-yl) phenylboronic acid (*p*-MNQB) in DMSO-*d*₆.

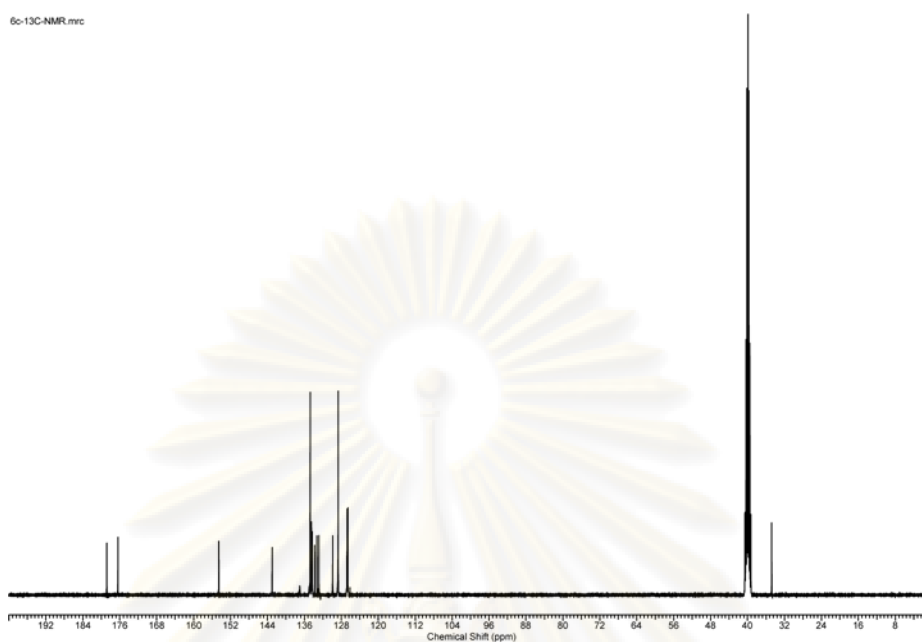


Figure A.23 The ^{13}C -NMR spectrum (100.6 MHz) of 4-(1-methyl-4,9-dioxo-4,9-dihydro-1H-naphtho[2,3-d]imidazol-2-yl) phenylboronic acid (*p*-MNQB) in $\text{DMSO-}d_6$.

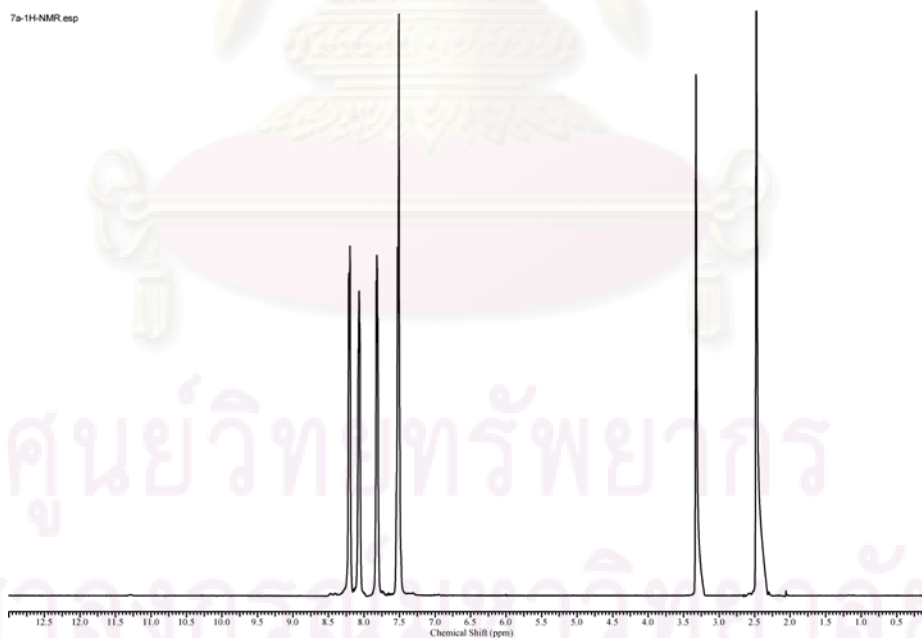


Figure A.24 The ^1H -NMR spectrum (400 MHz) of 2-phenyl-1H-naphtho[2,3-d]imidazole-4,9-dione (**7a**) in $\text{DMSO-}d_6$.

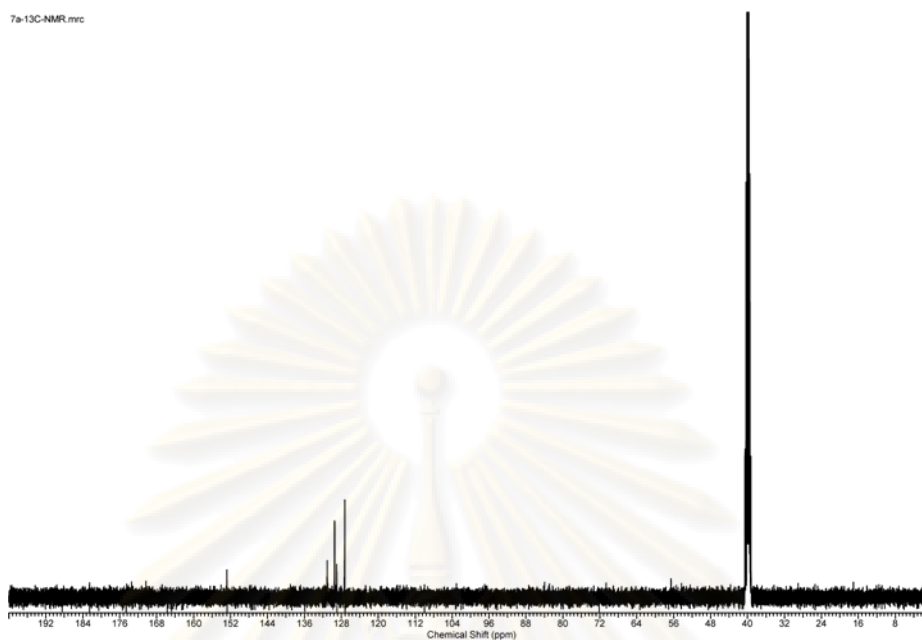


Figure A.25 The ^{13}C -NMR spectrum (100.6 MHz) of 2-phenyl-1H-naphtho[2,3-d]imidazole-4,9-dione (**7a**) in $\text{DMSO-}d_6$.

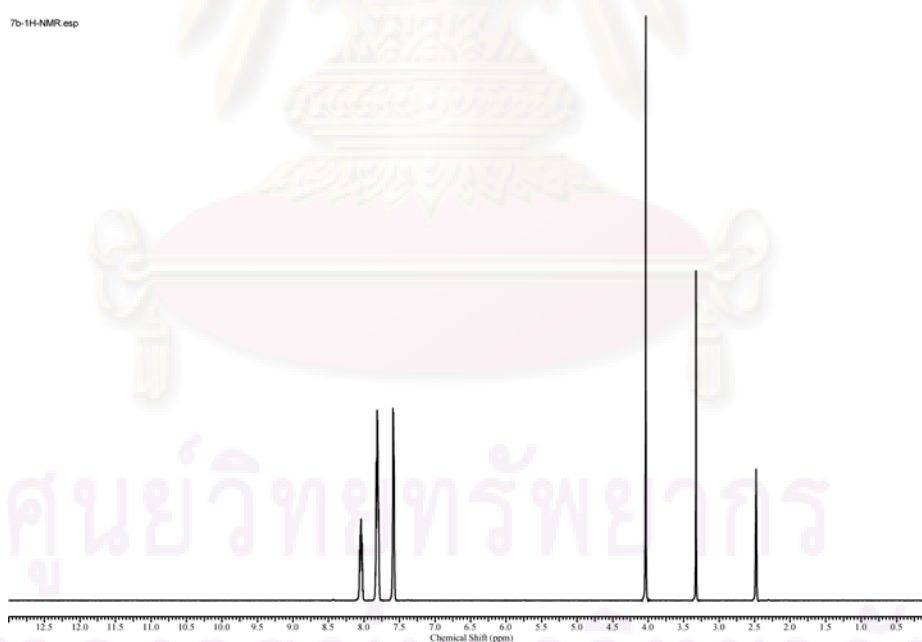


Figure A.26 The ^1H -NMR spectrum (400 MHz) of 1-methyl-2-phenyl-1H-naphtho[2,3-d]imidazole-4,9-dione (**7b**) in $\text{DMSO-}d_6$.

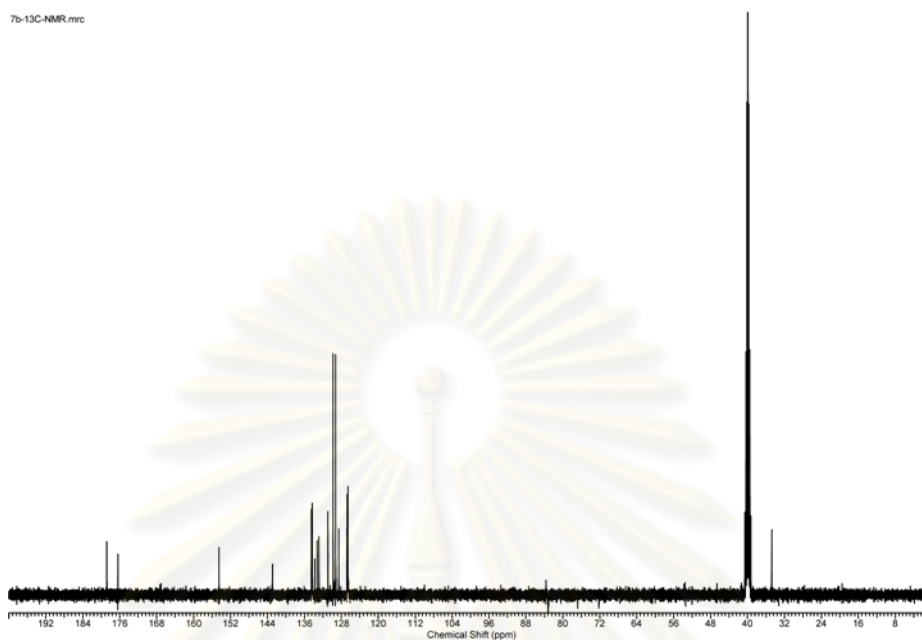


Figure A.27 The ^{13}C -NMR spectrum (100.6 MHz) of 1-methyl-2-phenyl-1H-naphtho[2,3-d]imidazole-4,9-dione (**7b**) in $\text{DMSO-}d_6$.

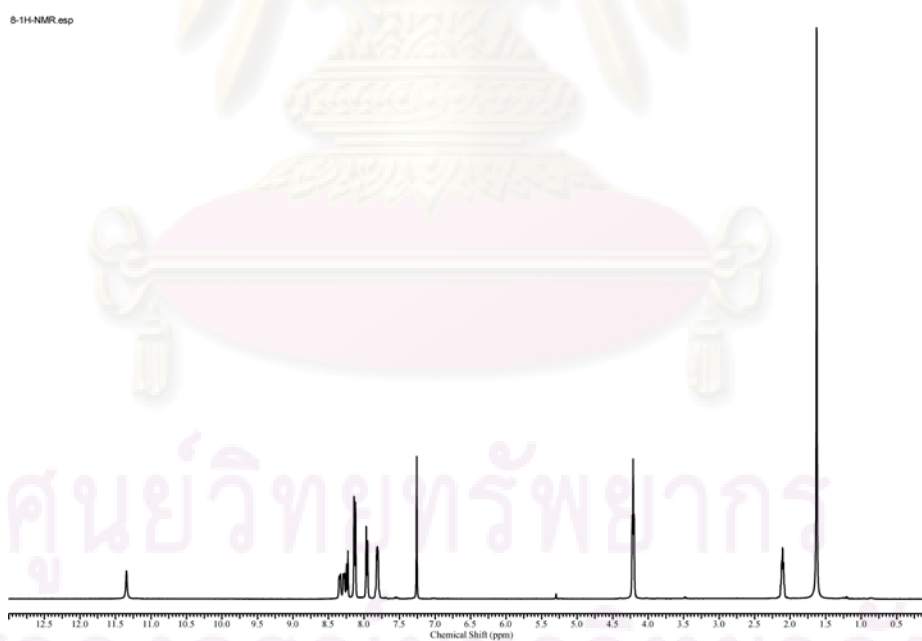


Figure A.28 The ^1H -NMR spectrum (400 MHz) of 2-(4-(1,3,2-dioxaborinan-2-yl)phenyl)-3H-anthra[1,2-d]imidazole-6,11-dione (**8**) in CDCl_3 .

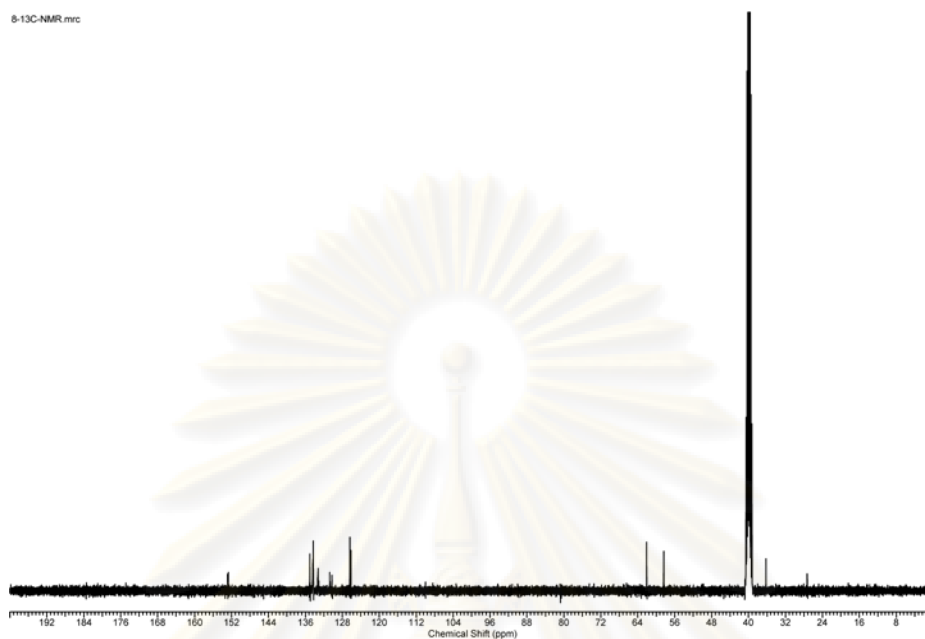


Figure A.29 The ¹³C-NMR spectrum (100.6 MHz) of 2-(4-(1,3,2-dioxaborinan-2-yl)phenyl)-3H-anthra[1,2-d]imidazole-6,11-dione (**8**) in DMSO-*d*₆.

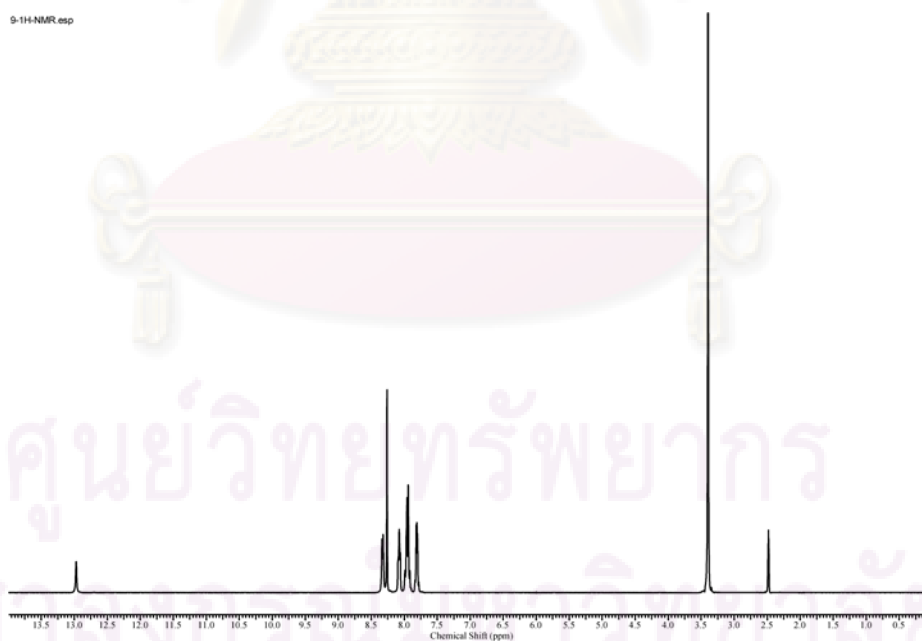


Figure A.30 The ¹H-NMR spectrum (400 MHz) of 4-(6,11-dioxo-6,11-dihydro-3H-anthra[1,2-d]imidazol-2-yl)phenylboronic acid (**HAQB**) in DMSO-*d*₆.

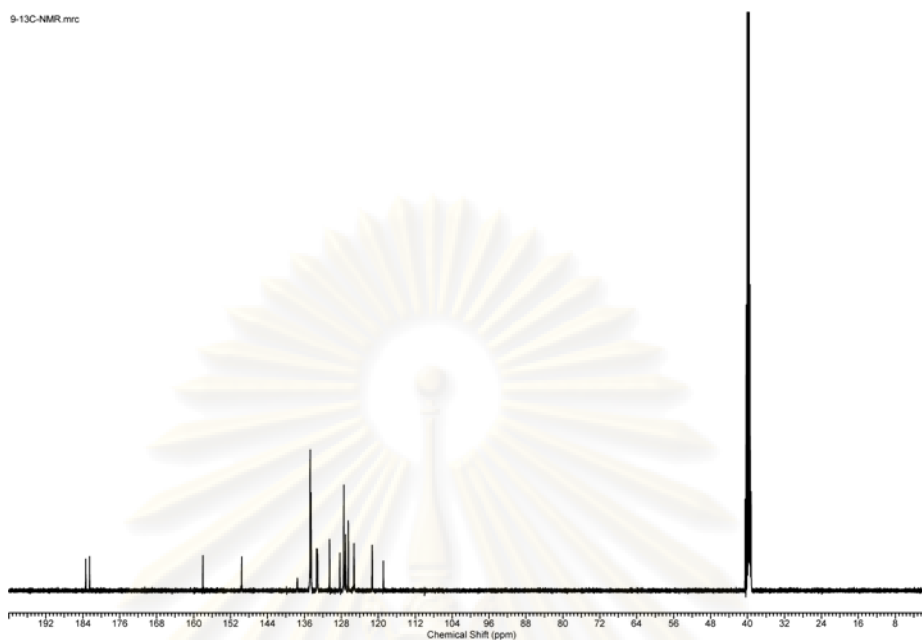


Figure A.31 The ^{13}C -NMR spectrum (100.6 MHz) of 4-(6,11-dioxo-6,11-dihydro-3H-anthra[1,2-d]imidazol-2-yl)phenylboronic acid (**HAQB**) in DMSO- d_6 .

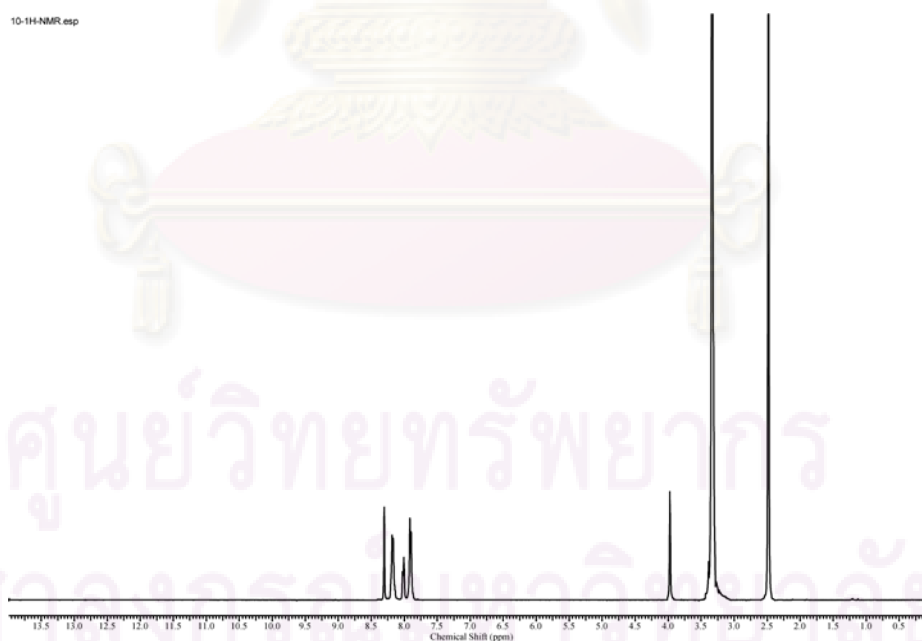


Figure A.32 The ^1H -NMR spectrum (400 MHz) of 4-(3-methyl-6,11-dioxo-6,11-dihydro-3H-anthra[1,2-d]imidazol-2-yl)phenylboronic acid (**MAQB**) in DMSO- d_6 .

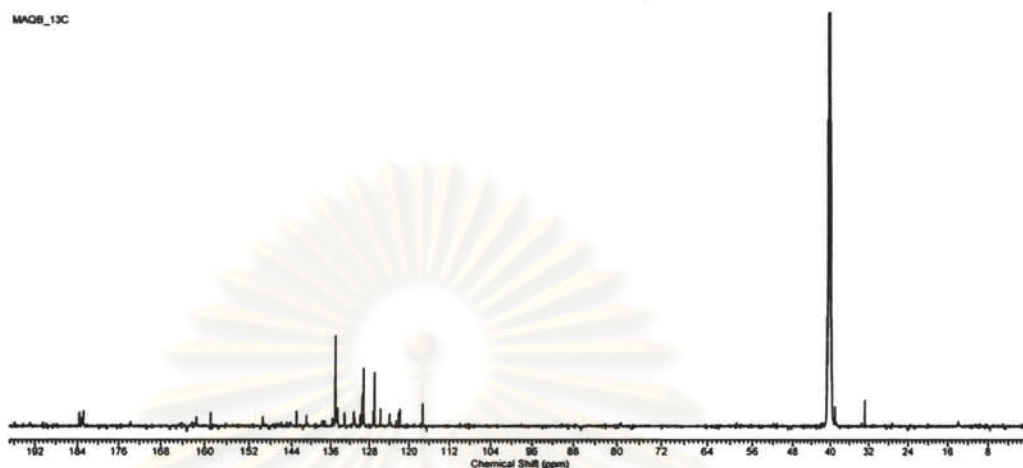


Figure A.33 The ^{13}C -NMR spectrum (100.6 MHz) of 4-(3-methyl-6,11-dioxo-6,11-dihydro-3H-anthra[1,2-d]imidazol-2-yl)phenylboronic acid (MAQB) in DMSO-d_6 .

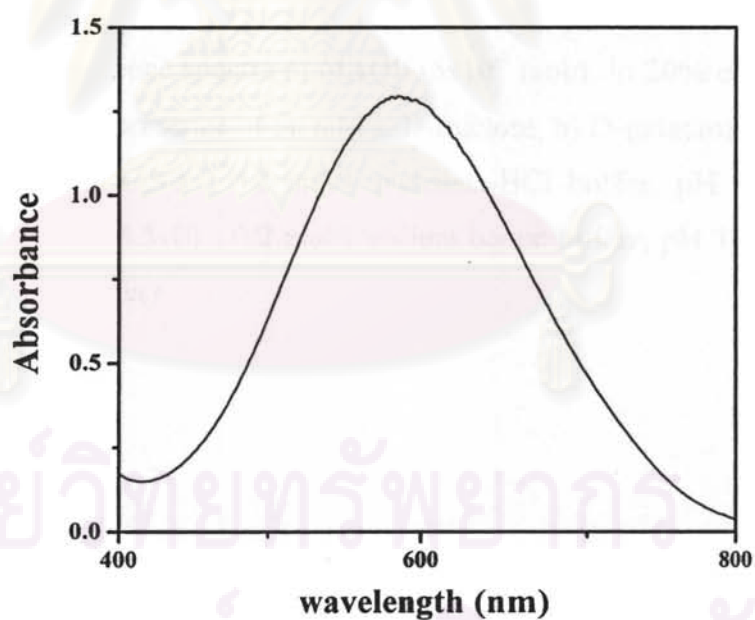


Figure A.34 The UV-vis spectrum of diaminonaphthoquinone 6×10^{-4} mol/L in DMSO

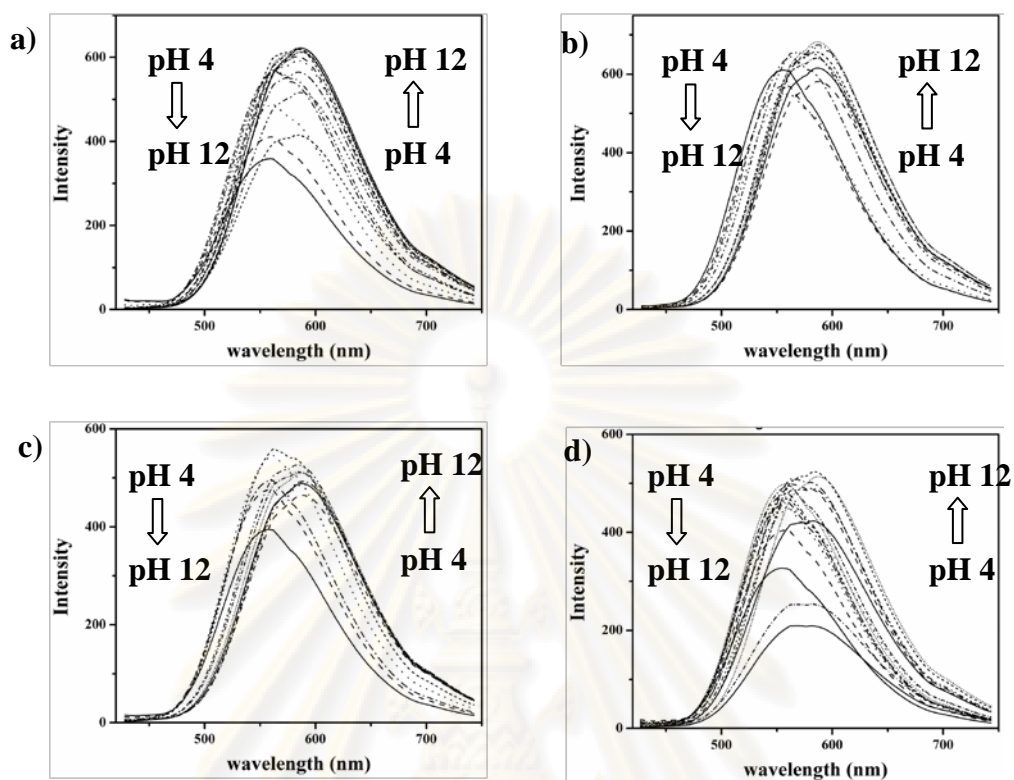


Figure A.35 Fluorescence spectra of MAQB (5×10^{-5} mol/L in 20% ethanol: buffer) at pH 4-12 buffer in the presence of 50 mM a) D-fructose, b) D-galactose, c) D-mannose and d) D-glucose (pH 3 -5 : 0.2 mol/L phosphate-HCl buffer, pH 6 -8 : 0.2 mol/L phosphate buffer, pH 8.5-10 : 0.2 mol/L sodium borate buffer, pH 11-12 : 0.2 mol/L phosphate-NaOH buffer)

ศูนย์วิทยทรัพยากร
จุฬาลงกรณ์มหาวิทยาลัย

Table A.1. Relative energies (ΔE_{rel}) of *o*-MNQB, *m*-MNQB and *p*-MNQB and of *o*-MNQB(CN)₃⁻, *m*-MNQB(CN)₃⁻ and *p*-MNQB(CN)₃⁻ computed at the B3LYP/6-31+G(d) level

Species	$E_{\text{total}}^{\text{a}}$	$\Delta E_{\text{rel}}^{\text{b}}$
<i>Non CN-substituted ligand</i>		
<i>o</i> -MNQB	-1129.1705186	3.42
<i>m</i> -MNQB ^c	-1129.1759608	0.00
<i>p</i> -MNQB	-1129.1753226	0.40
<i>Full CN-substituted ligand</i>		
<i>o</i> -MNQB(CN) ₃ ⁻	-1256.1064595	6.08
<i>m</i> -MNQB(CN) ₃ ^{-d}	-1256.1161552	0.00
<i>p</i> -MNQB(CN) ₃ ⁻	-1256.1140361	1.33

^a In hartree. ^b In kcal/mol. ^c The most stable isomer of non cyanide-substituted ligands. ^d The most stable isomer of full cyanide-substituted ligands

A.1 Molecular structures and total energies of *o*-MNQB, *m*-MNQB and *p*-MNQB and their cyanide adducts.

Compound: *o*-MNQB

Total energy: -1129.1705186 au

Table A.2 Cartesian coordinates (in angstrom) of *o*-MNQB:

Atoms	x	y	z
C	5.78100200	-0.29040300	0.22409400
C	4.63942300	-1.05472400	0.47168800
C	3.37104800	-0.55322900	0.16061300
C	3.24717000	0.73721900	-0.40837300
C	4.39797600	1.49311500	-0.65207000
C	5.65997200	0.98401500	-0.33879500
C	2.17338200	-1.41435600	0.44205400
C	1.90743700	1.33376800	-0.76156300
C	0.75389000	0.46043100	-0.48587700
C	0.90393200	-0.80082300	0.07831900
C	-1.21762000	-0.34385800	-0.29738400
H	6.76229000	-0.68841700	0.46870000
H	4.71111900	-2.04679500	0.90693100
H	4.28266000	2.48023800	-1.08931600
H	6.54728700	1.58061000	-0.53392300
O	1.80737200	2.46043300	-1.23051100
O	2.27138600	-2.54046600	0.93343100
N	-0.55862200	0.73331200	-0.71533500
N	-0.36985200	-1.31140000	0.19828900
C	-0.73406800	-2.57749500	0.83646800
H	-0.46493800	-3.42041700	0.19406800
H	-0.19397300	-2.67598000	1.77874000
H	-1.80856900	-2.57757700	1.01820900
C	-2.68663600	-0.48501100	-0.38036400
C	-3.52682400	0.51484000	0.16306600
C	-3.23690700	-1.56713500	-1.08439200
C	-4.91080600	0.39609300	-0.04937500
C	-4.61760200	-1.67408100	-1.25841800

H	-2.57969400	-2.31108900	-1.52819900
C	-5.45830800	-0.68601400	-0.74222400
H	-5.56888700	1.16684900	0.34288700
H	-5.02992500	-2.51473100	-1.81050900
O	-1.97814200	1.47782300	1.92541200
H	-1.62906800	2.25000500	2.39344100
O	-3.64730400	2.91596200	0.90186100
H	-3.33930500	3.63544500	1.47166200
B	-2.99220800	1.71569500	1.02893200
H	-6.53388200	-0.75413100	-0.88436800

Compound: *o*-MNQB(CN)₃⁻

Total energy: -1256.1064595 au

Table A.3 Cartesian coordinates (in angstrom) of *o*-MNQB(CN)₃⁻:

Atoms	x	y	z
C	-6.06658300	-0.96241900	-0.11246100
C	-4.82735600	-1.29593700	-0.66149900
C	-3.69618000	-0.52307400	-0.37905200
C	-3.81195000	0.60441800	0.46510500
C	-5.05891300	0.93218000	1.00662900
C	-6.18239500	0.15340600	0.72306000
C	-2.38161700	-0.92432800	-0.99571100
C	-2.62654900	1.48026800	0.80074600
C	-1.35239800	1.03363900	0.22407600
C	-1.26434100	-0.08415200	-0.60243200
C	0.70961100	0.84932300	-0.31351800
H	-6.93911300	-1.57256800	-0.33361400
H	-4.71221200	-2.15777400	-1.31188800
H	-5.12409200	1.80296600	1.65214100
H	-7.14587200	0.41514600	1.15412900
O	-2.75639600	2.48230400	1.49532300
O	-2.29811300	-1.87853500	-1.77204700

N	-0.13302700	1.61115900	0.38355200
N	0.05935500	-0.18000900	-0.95748400
C	0.64747800	-1.19085700	-1.83596800
H	0.67676800	-2.15779800	-1.32959000
H	0.04105800	-1.28049700	-2.73835300
H	1.66196500	-0.88453300	-2.08804600
C	2.15272900	1.16099800	-0.11246100
C	2.42049100	2.39402600	-0.66149900
C	3.20994300	0.34104900	-0.37905200
C	3.72546500	2.82237300	0.46510500
H	1.58241600	3.01427300	1.00662900
C	4.51785700	0.80714800	0.72306000
C	4.78379800	2.01244300	-0.99571100
H	3.91259000	3.77564700	0.80074600
B	3.09281900	-1.09375600	0.22407600
C	4.15937800	-1.12191000	-0.60243200
N	4.94578100	-1.13343900	-0.31351800
C	3.46625700	-2.28367600	-0.33361400
N	3.73793500	-3.11462700	-1.31188800
C	1.66286100	-1.41704100	1.65214100
N	0.63617700	-1.69384700	1.15412900
H	5.81366300	2.32458800	1.49532300
H	5.35576000	0.20725400	-1.77204700

ศูนย์วิทยทรัพยากร
จุฬาลงกรณ์มหาวิทยาลัย

Compound: *m*-MNOB

Total energy: -1129.1759608 au

Table A.4 Cartesian coordinates (in angstrom) of *m*-MNOB:

Atoms	x	y	z
C	6.11267200	-1.05051500	-0.10254400
C	4.84295500	-1.57929800	0.13552000
C	3.71007700	-0.76177700	0.05869600
C	3.85601900	0.60859300	-0.26399500
C	5.13281700	1.12698500	-0.50057700
C	6.25763800	0.30353500	-0.42073500
C	2.36705100	-1.37876400	0.32472400
C	2.67343600	1.53776500	-0.36109300
C	1.36949500	0.90317700	-0.09614600
C	1.25224500	-0.44480300	0.22140000
C	-0.72269800	0.54044100	0.17915300
H	6.98674600	-1.69337200	-0.04004500
H	4.70880900	-2.62756700	0.38401200
H	5.22334900	2.18058700	-0.74667800
H	7.24521000	0.71753600	-0.60664500
O	2.80424900	2.72371100	-0.63328300
O	2.23856300	-2.57303100	0.60247200
N	0.15087900	1.50222500	-0.11676000
N	-0.09594200	-0.67037100	0.40686800
C	-0.69637200	-1.92409200	0.87148100
H	-0.95358100	-2.56758600	0.02461300
H	0.02693800	-2.44750200	1.49452900
H	-1.59694400	-1.69528000	1.44238200
C	-2.17321500	0.77822300	0.26127100
C	-2.61559000	2.02691500	0.73632900
C	-3.12470500	-0.16102600	-0.16454900

C	-3.97842600	2.30904900	0.80526700
H	-1.87916600	2.76419700	1.04044300
C	-4.50252700	0.10826500	-0.10225100
H	-2.80404100	-1.10938000	-0.58311600
C	-4.91512000	1.35664900	0.39558800
H	-4.30939800	3.27464100	1.17894700
O	-5.06418900	-2.16212900	-1.04546700
H	-5.72136200	-2.80294700	-1.35128000
O	-6.87755300	-0.62863800	-0.52669500
H	-7.50510500	-1.30101100	-0.82675200
B	-5.54250600	-0.95444300	-0.58699100
H	-5.97657000	1.58168400	0.45233100

Compound: *m*-MNBQ(CN)₃⁻

Total energy: -1256.1161552 au

Table A.5 Cartesian coordinates (in angstrom) of *m*-MNBQ(CN)₃⁻:

Atoms	x	y	z
C	6.71590600	1.25453200	0.17880200
C	5.42159000	1.70728600	-0.08344000
C	4.33916700	0.82213700	-0.04126800
C	4.56153800	-0.53892800	0.26851600
C	5.86196200	-0.98253600	0.52856400
C	6.93651100	-0.09214200	0.48536700
C	2.96270200	1.36309700	-0.32983200
C	3.43217600	-1.53820700	0.32577000
C	2.10023600	-0.97758100	0.05218100
C	1.90546300	0.36932000	-0.24892600
C	-0.00965700	-0.73774500	-0.24772300
H	7.55011200	1.95098200	0.14478800
H	5.22639400	2.74810600	-0.32301400
H	6.00880900	-2.03235900	0.76407300

H	7.94323600	-0.44775700	0.69083600
O	3.63890900	-2.71974400	0.57691000
O	2.78804400	2.55228800	-0.60849300
N	0.92320500	-1.64914500	0.04800000
N	0.54831200	0.51166600	-0.45083100
C	-0.12419600	1.73417400	-0.90823600
H	-0.47427500	2.32822500	-0.05961900
H	0.58810500	2.32598900	-1.48036200
H	-0.97936000	1.45755100	-1.52520600
C	-1.43980700	-1.05625300	-0.35943300
C	-1.80439500	-2.32793400	-0.83477700
C	-2.44768900	-0.15102100	0.02136100
C	-3.15386800	-2.65600500	-0.94844400
H	-1.02912000	-3.03716200	-1.10794200
C	-3.81009800	1.25453200	-0.08976900
H	-2.17212900	1.70728600	0.43628800
C	-4.14089100	0.82213700	-0.59048500
H	-3.43934100	-0.53892800	-1.32474000
B	-4.97492600	-0.98253600	0.36925600
C	-5.57837000	-0.09214200	1.78908500
N	-5.99871200	1.36309700	2.81917900
C	-6.15967800	-1.53820700	-0.70964100
N	-7.00643200	-0.97758100	-1.50933300
C	-4.36648700	0.36932000	0.49591600
N	-3.86466300	-0.73774500	0.57470000
H	-5.18808900	1.95098200	-0.70224700

ศูนย์วิจัยทรัพยากร
จุฬาลงกรณ์มหาวิทยาลัย

Compound: *p*-MNOB

Total energy: -1129.1753226 au

Table A.6 Cartesian coordinates (in angstrom) of *p*-MNOB:

Atoms	x	y	z
C	-6.41817700	0.42167700	0.02967200
C	-5.24163500	1.16780600	0.11618100
C	-3.99570600	0.53454100	0.04978000
C	-3.93177800	-0.87083400	-0.10696600
C	-5.11703900	-1.60761000	-0.19226500
C	-6.35576500	-0.96686900	-0.12466400
C	-2.76000500	1.38177400	0.14716100
C	-2.61999900	-1.60866200	-0.18361800
C	-1.42509900	-0.75023800	-0.08651800
C	-1.51399900	0.62809400	0.06810500
C	0.59066100	-0.03311600	-0.00843500
H	-7.38127400	0.92247400	0.08252200
H	-5.26844100	2.24651100	0.23568300
H	-5.04663500	-2.68448400	-0.31142200
H	-7.27055500	-1.54981100	-0.19217600
O	-2.56876900	-2.82451400	-0.31130600
O	-2.81309600	2.60622700	0.27951200
N	-0.12781000	-1.14885100	-0.12848500
N	-0.21360200	1.08359800	0.12640500
C	0.19569600	2.46283400	0.40543400
H	0.28080800	3.03647000	-0.52274200
H	-0.56186800	2.93324300	1.03013800
H	1.15788000	2.44979100	0.91838000
C	2.06234900	-0.02923500	-0.01211800
C	2.73199600	-1.11970100	0.57230700
C	2.82248700	0.98546000	-0.62025000
C	4.12294100	-1.17512400	0.56778500

H	2.14633600	-1.91657500	1.01971700
C	4.21506800	0.91764000	-0.62138500
H	2.33151500	1.81144700	-1.12581900
C	4.89581100	-0.15733400	-0.02297500
H	4.62364900	-2.02225900	1.02824200
H	4.78593000	1.70643100	-1.10358600
O	7.14993200	0.79939600	-0.63071200
H	8.11527100	0.73517400	-0.62560600
O	7.05830600	-1.30942900	0.57426500
H	8.02521800	-1.33774800	0.55799500
B	6.45884400	-0.22679200	-0.02684300

Compound: *p*-M_NQ_B(CN)₃⁻

Total energy: -1256.1140361 au

Table A.7 Cartesian coordinates (in angstrom) of *p*-M_NQ_B (CN)₃⁻:

Atoms	x	y	z
C	-7.21572900	-0.47946000	-0.04824800
C	-6.02548700	-1.20733800	-0.09971800
C	-4.79116300	-0.55151800	-0.04279300
C	-4.75263600	0.85751300	0.06896300
C	-5.95061300	1.57680200	0.11980100
C	-7.17833200	0.91427100	0.06162400
C	-3.53640600	-1.38156300	-0.10041800
C	-3.45066500	1.61930500	0.13421200
C	-2.24308000	0.77972600	0.07600400
C	-2.31055100	-0.60693700	-0.03794300
C	-0.21143000	0.09277000	0.04527000
H	-8.16994900	-0.99853600	-0.09363500
H	-6.03065000	-2.28978800	-0.18416500
H	-5.89698000	2.65799200	0.20489200

H	-8.10349300	1.48391100	0.10190100
O	-3.43071400	2.84061700	0.22301700
O	-3.58056700	-2.61242600	-0.18988100
N	-0.95524800	1.20080000	0.12417300
N	-1.00042600	-1.03895400	-0.06906500
C	-0.56212700	-2.41300400	-0.32436600
H	-0.50539300	-2.98183300	0.60877200
H	-1.28602300	-2.89684700	-0.97878600
H	0.42147600	-2.38577000	-0.79388100
C	1.25558600	0.08956100	0.06136300
C	1.94747600	1.12990200	-0.58221800
C	2.00405700	-0.89601300	0.73172100
C	3.34213600	1.15462300	-0.58692600
H	1.38070200	1.91304800	-1.07769600
C	3.39626800	-0.85145600	0.72510600
H	1.50121200	-1.67977400	1.29242400
C	4.10443800	0.16181100	0.05347100
H	3.84994000	1.96775400	-1.09958800
H	3.94702600	-1.61919200	1.26376000
B	5.74136600	0.12948700	-0.00118900
C	6.33863800	-0.23869700	1.43970700
N	6.73975900	-0.52185000	2.49594700
C	6.33898700	1.53694800	-0.47149100
N	6.74307100	2.57057400	-0.82438000
C	6.19719200	-1.00085200	-1.04602800
N	6.48658600	-1.83375800	-1.80749000

ศูนย์วิจัยทรัพยากร
จุฬาลงกรณ์มหาวิทยาลัย

VITAE

Name: Miss Matinee Jamkratoke

Born: September 2nd 1976

Education:

1997 B.Sc. (Chemistry), Burapha University, Chonburi, Thailand

2000 M.Sc. (Chemistry),
Chulalongkorn University, Bangkok, Thailand

2010 Ph.D. (Chemistry), Chulalongkorn University,
Bangkok, Thailand

Professional Career: 2001-2005: Lecturer, Faculty of Science & Arts, Burapha University Chanthaburi Campus, Chanthaburi, Thailand

Publication:

- 1) Pulpoka, B., Jamkratoke, M., Tuntulani, T., and Ruangpornvisuti, V. Synthesis of 1,3-alternate calix[4]-cyclen-benzo-crown-6 as a hard-soft receptor. *Tetrahedron Lett.* 41(2000): 9167-9171.
- 2) Jamkratoke, M., Ruangpornvisut, V., Tumcharern, G., Tuntulani, T., and Tomapatanaget, B. A-D-A Sensors Based on naphthoimidazoledione and boronic Acid as Turn-On Cyanide Probes in Water *J. Org. Chem.* 74(2009): 3919-3922.